Non-perturbative approaches to transport in nanostructures and granular arrays

A thesis presented

by

Pablo San José Martín

to

The Department of Condensed Matter Physics

in partial fulfillment of the requirements

for the degree of

Doctor of Philosophy

in the subject of

Physics

Universidad Autónoma de Madrid

Madrid

September 2004

Thesis advisor
Francisco Guinea

Author
Pablo San José Martín

Non-perturbative approaches to transport in nanostructures and granular arrays

Abstract

Universal interaction effects in electronic nanostructures are analyzed by means of auxiliary phase field dynamics. Simple analytical non-perturbative approximations are discussed, and are found to capture all expected physical phenomena arising from interactions. Transport through metallic nano-grains and few-level quantum dots in linear response are analyzed in detail. The formal techniques are extended to include exchange interactions and superconductivity in nanostructures. Finally nanostructured arrays, such as granular systems, are discussed with these techniques to explore the interaction-induced metal-insulator transition.

Contents

Citations to Previously Published Work

Part of the contents of this work can be found in the following publications.

- D. P. Arovas, F. Guinea, C. P. Herrero and P. San Jose (2003). *Granular systems in the Coulomb blockade regime.* Physical Review B **68**(8).
- S. Florens, P. San-Jose, F. Guinea and A. Georges (2003). *Coherence and Coulomb blockade in single-electron devices: A unified treatment of interaction effects.* Physical Review B **68**(24).
- P. San-Jose, C. P. Herrero, F. Guinea, and D. P. Arovas (2004). *Interplay between exchange interactions and charging effects in metallic grains.* Preprint archive cond-mat/0401557, to appear in Physical Review B.

Other publications by the author of this thesis are [1]

- M. Rabinovich, A. Volkovskii, P. Lecanda, R. Huerta, H. D. I. Abarbanel and G. Laurent (2001). *Dynamical encoding by networks of competing neuron groups: Winnerless competition.* Physical Review Letters 8706(6).
- R. Gomez-Medina, P. San-Jose, A. Garcia-Martin, M. Lester, M. Nieto-Vesperinas and J. J. Saenz (2001). *Resonant radiation pressure on neutral particles in a waveguide.* Physical Review Letters **86**(19): 4275-4277.
- P. San-Jose, F. Guinea, T. Martin (2004). *Electron backscattering from dynamical impurities in a Luttinger liquid.* Preprint archive cond-mat/0409515, sent to Physical Review B.

[1] In the first reference of this list the author chose, for reasons unclear even to himself, to sign it under the alias of P. Lecanda (great-grandfather surname). This was obviously fruit of the tender years of youth, in the time before he had become aware of the convenience of people in this business to know one by name.

Acknowledgments

I would like to express my deepest gratitude to my wife Elsa, who has helped me enormously through the process of developing this thesis, with constant support, inspiration and insights. She manages to make every burden light, and every effort worthwhile. I also want to sincerely thank my advisor Prof. Francisco Guinea for his invaluable help, without whose razor-sharp intuition and knowledge I might never have put this work together. There goes my deepest admiration for his talent. Additionally, of course, a big, big Thanks! to 'La Piarilla', my friends and colleagues in the Institute, which were like a family in this journey and taught me so much. Ramón, Geli, Ana, Rafa, Simone, Alberto, César, María, Juan Luis, Rafa Sánchez and Alberto Pequeño. You were all great to me, and certainly the best part of my stay in the ICMM. And finally I would like to thank my family for their support, specially my brother, for his undeniable talent to make us folk laugh. Great fuel. Thank you all.

To Elsa.

Chapter 1

Introduction and Outline

1.1 Interactions in solid state physics

The modeling of physical systems is at the roots of physical science as we know it. There is a whole universe of implicit assumptions about reality that must be made to arrive at this way of thinking, which is the floor where physics stands. In this process the physical world is objectified (separated from the thinker), ordered and decomposed into certain ingredients, such as elementary particles or fields, that are endowed with a set of properties and mutual relations. A conceptual framework is set up, and physicists are left to play with the ingredients, to work out their 'correct' relations and the phenomenological manifestations that can arise from them according to the rules of the game. Philosophers are left with the daunting task of making sense of the world without all these assumptions. Luckily for us (and for me!) we are officially allowed to disregard questions such as "What *is* a field?", or "What *are* interactions?". That certainly is a heavy load off our shoulders! In this introduction we will rather concentrate on merely illustrating the role of electronic interactions in solid state matter, which is the essential subject of this work, and on classifying some of the different phenomena for which these interactions are directly responsible.

Let us therefore shut ourselves away in our minds for a while, and take a walk starting with one of the simplest systems in the game called 'Non-relativistic Quantum Mechanics', the Ideal Fermi Gas, i.e. a set of non interacting fermions (such as electrons) in a box. We can think of it as one of the *ingredients* of the game, unrelated yet by any interactions. It is a convenient starting point, since the present work focuses precisely on some of the situations where an almost similarly simple model, the Fermi Liquid, is no longer valid to describe an electronic system.

The Fermi Liquid

One would expect this non-interacting Fermi Gas model to be of no use in real world electronic systems, since we know that an essential property of electrons is that they interact with any other charged particle through electromagnetic fields. And this interaction is strong. At any given moment a typical conduction band electron in bulk gold suffers an acceleration twenty orders of magnitudes greater than that of the Earth's gravity, due to

its electromagnetic interactions with neighboring electrons. Even if it could be tracked as a distinguishable classical particle, its trajectory would be very different from that of a free-flying non-interacting electron. Nevertheless its fermionic nature is responsible for a very remarkable result applicable to many realistic electronic systems without strong disorder and reasonably high density: an extra electron injected into a low temperature metal, if considered together with the electronic cloud of positive background charge it excites around itself due to electron-electron repulsion, can be quantized and is an almost non-interacting entity perfectly similar to a free electron[1]. It is called a quasiparticle. This is admittedly a loose way of speaking for a mathematically oriented reader, but the precise fact is that expressed in certain basis of states (no longer a single particle one, but a superposition of many, the quasiparticle), the Hamiltonian of a realistic metallic system often resembles (at least in what concerns the asymptotically low energy excitation spectrum) that of the Fermi Gas in spite of the strong electronic interactions, albeit with a different particle mass in the dispersion relation called effective mass m^*. This 'interaction triviality' happens to be closely related to the fermionic statistics of electrons, and to the fact that they form a 'Fermi sea' in order to satisfy Pauli's exclusion principle. For excitations of finite energy E though, their mutual effective interactions increase like E^2 within the Fermi Liquid theory.

This is the basis of what is known as the Fermi Liquid theory for metals, which was conceived by the brilliant intuition of the Russian physicist and nobel price Lev Davidovich Landau in the fifties [61]. A very elegant derivation of this theory and its leading corrections can be performed by Renormalization Group (RG) techniques, see for example [88].

This thesis work deals with some of the most relevant cases where the Fermi Liquid paradigm breaks down, and interactions show up as an essential ingredient of the system's mechanics. We will now proceed to give a quick overview of some of the mechanisms responsible for this break down.

Screening

From a microscopic point of view an intuitive explanation for the irrelevant character of electron-electron interactions in metals is the mechanism of 'screening', which underlies the Fermi Liquid theory. The electronic cloud that we mentioned above which 'dresses' a bare electron injected into the metal, is said to screen the electronic potential the electron creates by decreasing the surrounding electron density. If one calculates, within certain approximations, the potential felt by any other electron induced by the new screened electron, it happens to go like $V(r) \sim e^{-r/\xi}/r$ instead of $V(r) \sim 1/r$, so it is suppressed at distances greater than a certain screening length ξ.

So, why aren't interactions altogether irrelevant in practice? Well, such screening is only effective in appropriate circumstances. For example, screening would only be efficient if the interaction energy scale is smaller than the typical kinetic energy, so that electrons remain mobile in spite of the interactions. Otherwise electrons could get localized at fixed positions (Wigner's crystallization), which is predicted to happen for extremely low electronic density in the absence of background charge modulations (see below). Another requirement is that the system must be large enough so that the relaxation of the

[1] 'Almost' here means a vanishing interaction strength between two such entities at vanishing excitation energy scales

system electrons caused by the newly injected one is more or less complete. If the system is small the relaxation of its electrons due to the presence of the new electron is not complete because of the constraint imposed by the boundaries, hindering the complete screening of the electron's electrostatic potential. Therefore the presence of physical boundaries or low dimensionality can make interactions a very relevant ingredient of the physics of a system, even (specially!) at low energy scales.

Zero dimensional systems

A typical case of this boundary effect is a small metallic island or a quantum dot. A metallic island is basically a metallic droplet, maybe capacitively coupled to some gate, and connected by metal oxide tunnel junctions to a bulk metal. A quantum dot is generally a small region in a 2D electron gas (2DEG) where electrons get confined by electrostatic gates set atop of the heterojunction, and can tunnel to and from the 2DEG through tunable barriers. Other equivalent realizations are also possible.

Both these systems are classed as 'zero dimensional' as opposed to wires, sheets or bulky systems, and each has specific characteristics that make them specially suited to study different effects of interaction effects. In a first approximation both can be seen as a small spatial region, connected (or not) in some way to a bulk metal, where electrons get confined by some boundaries. The electrostatic energy associated to the addition of a single electron in such region is bigger the smaller the region. This is simply the concept of capacitance C. A small piece of metal has lower capacitance, so a small increment in charge generates a large potential energy. Hence, a finite charging energy $E_C = e^2/(2C)$ is required to add the minimum charge possible e, a single electron [2], which can be of the order of 10-100 mK for $C \lesssim 10^{-15}F$, which for 2D quantum dots means sizes in the order of $100nm$. Such technical feat of microfabrication became possible at the beginning of the 90's [36, 51] For 3D metallic grains the required size is a good order of magnitude smaller, but this too was achieved in the mid 90's [81] In bigger systems the temperature required for these discrete charge effects not to be washed out decreases beyond current experimental feasibility, so that the electrons that traverse the system can be considered (once screened) as free quasiparticle for all practical purposes without further complications if the rest of the Fermi Liquid theory requirements are met.

One dimensional systems

Another typical case of ineffective screening and quasiparticle buildup is the 1D electron system. The problem in this case is that the concept of quasiparticle itself breaks down in purely 1D systems, since two quasiparticles would never be able to avoid a collision with each other and therefore act as non-interacting, since the available scattering phase space is too small. Intuitively, two quasiparticles would always collide head to head and invade each other screening cloud, therefore interacting directly as free electrons when the distance is small enough, even taking into account their quantum nature. Furthermore, it

[2] An important simplifying assumption is made when C is taken as a constant independent of the total number of electrons in the system, but it is good enough in all but extreme regimes, and this simplification will be made in the rest of this work.

can be seen that since the bare potential in 1D is linear with distance, there cannot be a complete screening no matter how the other electrons readjust themselves. The low energy dynamics is therefore very unlike the Fermi Gas. It is rather known as the Luttinger Liquid, which will be explored in a later section of this work.

Other common scenarios for the breakdown of the Fermi Liquid theory

The basic assumptions in the Fermi Liquid theory for metallic systems are the following

- There is a one to one correspondence of excitations with and without interactions.
- There system will not undergo any phase transitions if we were to adiabatically switch on the interactions (there is no 'level crossing').
- The interacting ground state is non-degenerate.

Both the zero and one dimensional electron systems break the first assumption, but there are other very common systems that do not behave like a Fermi Liquid for one reason or another. A non-comprehensive list of some such situations follows, intended to serve simply as a context summary.

- **Zero and one dimensional systems.**

  As explained above, both of these have an excitation spectrum that does not flow continuously from the excitations of the non-interacting system. Rather, a different family of quantum numbers must be used to classify excitations.

- **Disordered systems.**

  Anderson Localization theory shows how a certain amount of disorder (such as crystalline dislocations or defects) in an initially metallic 3D electron system can drive it to an insulating state even without interactions. Initially extended particle or quasiparticle eigenstates (as those in a conduction band) get localized due to the competition between the kinetic energy and the energy mismatch of different sites. In 2D a non-interacting system becomes insulating with an arbitrarily small disorder density [1]. The question of disorder plus interactions in 2D is still an open problem. In 3D the situation gets quite complicated in that certain portions of the bands (beyond certain 'mobility edges') get localized while the rest don't, but a satisfactory theory exists for this case. In one dimensional systems even the weak localization correction to conductance (leading high temperature correction which appear with any amount of disorder density) would also lead to an insulating phase as long as the quasiparticle coherence length exceeds the size of the system.

  Although disorder can break down the Fermi Liquid, it is a complication altogether different from interactions. It doesn't involve many body effects, it is rather the breakdown of coherent one-particle transport taking place, due to non-constructive interference of extended paths along a sample, which is the reason behind the existence

of bands themselves. Lattice randomness breaks this coherent band formation, which in its turn makes the low energy excitations unconnected from those of a Fermi Gas.

In this work we will merely hint at the possibilities of applying the formalisms we will be presenting to the problem of disorder in metals, since a deeper analysis of these problems would escape the scope of the thesis.

- **Superconductivity**

  Any kind of effective attractive interaction between electrons, be it due to retarded phonon exchange or due to more complicated collective processes can be proven to make the ground state unstable, leading to a spontaneous breaking of the local gauge symmetry. This is nothing but a superconducting phase transition. In a finite size system, the ground state can be thought to suffer a level crossing with the first excitations, beyond which the continuity of the excitation spectrum is broken. A gap is developed and new physical properties arise. Nevertheless, at least in the BCS superconductors, an effective analogue of the Fermi Liquid excitations can be recovered in certain basis of 'Bogolons' or 'BCS quasiparticles', although with a different (gapped) dispersion relation.

  Many of the techniques to be presented in this work have their origin in the microscopic theory of Josephson junctions (weak links between superconductors), and therefore they are very well suited to including BCS superconductors in the analysis. We will briefly touch on this in the chapter dealing with Quantum Rotors.

- **Mott-Hubbard metal-insulator transitions**

  Another very common scenario for the departure from a Fermi Liquid is the Mott-Hubbard metal-insulator transition. It is a transition predicted in particular for the Hubbard model, which was itself designed as an extremely simplified model for real metals but involving also many body effects. It essentially substitutes the wild variety of electronic orbitals in a real atom of the metal by a single orbital, able to host up to two electrons with opposite spin. The Hamiltonian is composed of a familiar hopping interaction between neighboring atoms, plus an on-site intereaction that penalizes occupancies other than a fixed average N_0[3] The general formulation has the form

$$H = E_C \sum_i (n_i - N_0)^2 + t \sum_i c_i^+ c_{i+1} + H.c \tag{1.1}$$

  where $n_i = c_i^+ c_i$.

  As we will see in detail in the second part of this work, this model has a Fermi Liquid-type phase for low enough E_C/t. Recall that in the continuum limit t takes on the role of a typical kinetic energy. E_C represents Coulomb interactions between electrons, taken only within the same site for simplicity (other extensions have also been studied, such as the extended Hubbard model) [9,27,92]. If the normalized temperature T/E_C is below certain critical value, a critical boundary shows up at certain values of E_C/t between the Fermi Liquid phase and an insulating phase, in which the concept of

[3]The equilibrium population N_0 is tunable by gate potentials.

coherent quasiparticle holds no more. This phase transition, which we will show to be first order in character, is very physical, since it merely reveals the fact that a certain minimum amount of typical kinetic energy is necessary for an electron to develop into an extended quasiparticle traveling through the system, since the on-site repulsion must be overcome in order to allow for the site charge fluctuations that a extended state involves. If t is too low, electrons will remain localized at a given atom, giving way to an insulating state (a finite voltage is necessary to wake a finite current). For high enough temperatures this phase transition gives way to a smooth crossover. This phase transition is held responsible for the essential phase diagram features of various correlated electron materials such as Vanadates like $(V_{1-x}Cr_x)_2O_3$ [66–68] or quasi-2D organic compounds of the $\kappa - BEDT$ family [52, 55].

- **Wigner crystallization**

  Wigner crystallization is the analogue of this phase transition but applied to the model of free electrons (in the sense that no underlying lattice is favoring certain points in space) mutually interacting through long range Coulomb potentials. In this model also, when the electron density is low enough so that the typical kinetic energy E_F is not able to overcome the Coulomb repulsion the screening and quasiparticle paradigm breaks down, leading to a peculiar phase in which electrons remain localized [97] forming a triangular lattice (in 2D). The predicted density at which this is expected to happen is extremely low, such that the average electron distance is about 40 times the Bohr radius ($a_0 \approx 0.53$Å), which as far as I know is still quite beyond current technology in solid state electronic systems. Certain observations on the surface of liquid helium do suggest a direct measurement of this phase [79].

  Although it is very interesting in itself and it is directly related to interaction effects in metallic systems, we will not discuss this topic further in this work.

- **Exchange interactions and the Kondo effect**

  We have made no mention of the magnetic properties of the Fermi Liquid. In the absence of interactions and in the case of an even number of electrons, the ground state of an electron system is a singlet, since each state gets occupied by two electrons. This also holds for the Fermi Liquid, since its spectrum is adiabatically derived from the Fermi Gas. However when interactions begin to play a dominant role a whole new range of possibilities opens up. However, the dominant mechanism responsible for a magnetic ground state is not dipolar magnetic or spin-orbit interactions [11]. It turns out that Coulomb interactions plus fermionic statistics are enough to conjure non-trivial affects like magnetic ordering. The mechanism is called exchange interactions (or variations like superexchange) and it is the one behind the familiar Hund rules, by which electron-electron repulsion tends to maximize total spin, orbital momentum and total momentum in a given electronic system. Why does Coulomb repulsion do this? Two electrons will in general minimize their Coulomb energy by minimizing their spatial wavefunction overlap, in particular making $\Psi(\mathbf{r_1} \approx \mathbf{r_2})$ very small. Fermion statistics on its part requires the total wavefunction to be antisymmetric. This implies that the minimum energy will be achieved in a triplet configuration (parallel spins), since a triplet is symmetric, and therefore the spatial Ψ is antisymmetric

spatial wavefunction with much less electron-electron overlap than a symmetric one. Therefore repulsive interactions drive a tendency to parallel spins in the ground state, while attractive interactions favor antiparallel singlet ground states. This reasoning holds in the case of many electrons too, and it cannot be described naturally within the Fermi Liquid theory.

One particularly celebrated case of non-trivial exchange effects is known as the Kondo problem. We will extensively discuss this effect in the course of this work, so for now we will just note that the Kondo physics due to a finite concentration of magnetic impurities in a metal, together to the "multichannel assumption" (by which a certain quantum number other than spin - for example angular momentum in the $\hat{z}$ - is conserved in electron scattering on the impurities) is enough to rigourously guarantee that the ground state will no longer be that of the Fermi Liquid, and strong correlations will survive between electrons due to residual exchange interactions.

1.2 Structure of this thesis

This is only a portion of the great diversity of behaviors and phases possible in electronic systems due to interaction that are clearly beyond the Fermi Liquid paradigm. We will be discussing some of this subjects with a variety of techniques that were developed in many cases specifically to tackle these situations, such as DMFT or Slave rotor techniques. We have divided the discussion in four parts. Chapter 2 serves as a detailed introduction to part of the techniques to be used. The phase-only action will be introduced and will be shown to give a suitable description of Coulomb blockade in metallic grains. Most of this material is not new, and the fundamental aspects of the techniques were already known back in the eighties, but it is a necessary starting point for a self contained exposition. In Chapter 3 we extend the concepts of the preceding chapter to include fermion dynamics, which opens the path to the discussion of few-level quantum dots and Kondo effect. Most of the results there were published in [31]. In Chapter 4 we explore the effects of exchange interactions and superconductivity, and demonstrate how they can be very elegantly included in the proposed formalism. We discuss the case of a superconducting grain in particular. The results presented there can be found in [85]. Finally in Chapter 5 we depart from the study of single nanostructures and ask about the effects associated to the addition of many coupled nanostructures, or in other words in nanostructured materials such as granular arrays. We discuss two kinds of metal-insulator transitions by means of several techniques. Part of these results were published in [10], but the last part of the chapter has not yet been sent for publication.

Moreover, I have transferred to the appendices some of the more lengthy discussions and computations that could have otherwise distracted from the main discourse. They include however, as is often the case, some of the bits that some readers (myself included) might find more interesting, but they can be safely skipped in a quick reading.

Chapter 2

The Quantum Rotor approach to Coulomb Blockade

As briefly described in the introduction, quantum dots and metallic grain[1] are very apt systems in which to study the interesting effects that can arise due to electrostatic interactions between electrons. There are several energy scales that one must keep in mind in such systems. We will give an overview of these before proceeding to the definition of the 'orthodox model' for metallic grains that we will be using in most of this work. The material in these first section is rather basic, so a reader acquainted with Coulomb Blockade and transport in nanostructures might want to skip straight to section 2.3.

2.1 Energy scales and definitions

The existence of geometrical boundaries makes the energy of the system jump by a finite amount $E_C = e^2/2C$ when an extra electron is added to it. The capacitance C is the sum of the different parallel capacitances coupling the system to the outer world, such as the gate and the electrode capacitances. C scales roughly as R^2, where R is the size of the system, just as in the case of planar capacitors, so $E_C \sim R^{-2}$.

Another important scale, mean level spacing scales as the inverse volume, $\delta \sim R^{-3}$ in 3D. E_C is much larger than δ in all but really tiny 3D grains (with $R \sim 2$Å).

The third relevant scale Γ, the elastic level width, measures the strength of the coupling of the grain to its environment (the leads, or the bulk of the metal), through hopping terms. In the orthodox model to be described below certain single particle levels are still defined in spite of the interactions, and their coupling to L metal leads gives them typically a low energy finite lifetime $\tau = \hbar/\Gamma$ with $\Gamma = L\pi\rho(0)t^2$ where $\rho(0)$ is the metal density of states at the Fermi energy, L is the number of leads and t is the hopping between that level and a low energy state in the bulk (assuming a constant hopping here for simplicity). Further relaxation rates due to other couplings such as electron-phonon (Γ_{ph}^{inel}) or electron-electron (Γ_{e}^{inel}) scattering can also be defined.

[1] We will use the term 'grain' sometimes to refer to quantum dots or metallic grains indistinctively, considered as effectively zero dimensional systems with certain spectral properties.

The Thouless energy E_{Th} is also a relevant scale to get an idea of the range of validity for the existence of the above single particle levels, which are actually quasiparticle states. E_{Th} is defined as the inverse time a particle takes to traverse the system once, and it goes like D_{diff}/r^2 and v_F/r for diffusive and ballistic systems respectively. It turns out that if the system is too *large* (the quasiparticle states get too close together) electron-electron interactions will endow them with a $\Gamma_e^{inel} > \delta$ for energies $\varepsilon \gtrsim E_{Th}$, so that the levels blur into each other and the orthodox model breaks down. The criterion to know when this begins to happen is that the 'intrinsic dimensionless conductance' $g_I \equiv E_{Th}/\delta$, which goes like r^2 (r) in 3D ballistic (diffusive) systems, is $g_I \gg 1$ [6, 95]. This is equivalent to saying that the quasiparticle decay rate is smaller than the mean level spacing, which is a mesoscopic requirement for the validity of the quasiparticle concept. The effects associated with this decay can be seen as corrections to the orthodox model, just as quasiparticle decay are corrections to the low energy limit of the Fermi Liquid in macroscopic metals, and we will ignore them in most of the following, focusing only on the universal interaction effects due to electrostatic charging. In chapter 5 we will cover some of the effects expected beyond this Fermi-liquid type of approximation in connection with the tunneling quasiparticle redressing problem.

External voltages V, as usual, will naturally affect also the state of the system, inducing charge transport. One of the new feature is that at low enough temperatures, the I-V response of the system will be extremely non-linear, showing sharp plateaus and jumps whenever V is large enough to overcome the charging energy of the system induced by injecting a new particle. This 'Coulomb staircase' gets blurred when Γ or T increase.

Finally, of course, one has temperature T as an essential energy scale, that blurs any effect at energy scales below T.

Dynamically developed energy scales like the Kondo temperature T_K and the renormalized charging energy E_C^* will be discussed later, since they involve a more elaborate discussion.

Regimes and techniques

The most interesting regime to unveil non trivial interaction effects is $T \ll E_C$. In this regime, experimentally reachable for one decade now, [19, 81–83], new correlations become apparent in transport measurements (linear conductance, I-V characteristic, noise...). The new features, such as the suppression of conductance for $n_g \neq 1/2$, cotunneling signatures, Coulomb staircase, etc. are known as the Coulomb blockade scenario [2]. The essential hallmark of this regime is that particle number fluctuations get suppressed to some extent due to the charging barrier, and therefore the quantum dynamics of the system gets constrained about a subspace with fixed number of particles. The rest of the scales provide a wealth of different regimes and features, from Kondo to the 'inverse crossover regime' to be discussed in the next chapter.

The development of a simple technique to deal with the complexity of all these phenomena is still a difficult challenge. Many different (and sometimes really tough) techniques have been and are still being developed to deal with the most difficult aspects of this

[2] Or in a more advanced context also dynamical Coulomb blockade if the coupling to the environment is strong.

problems, like the effects of disorder [20, 76], the quasiparticle decay regime [6], the open grain limit [32], the far from equilibrium limit, etc. The traditional starting point for the study of transport for example within most of the techniques is perturbative techniques and partial infinite summations, in the line of the rate equation techniques, which we sketch in Appendix G.

One technique, developed in the 80's [7, 17], that takes on a somewhat more abstract route proved to be very useful and instructive to access a large portion of the phase diagram, and also to be very generalizable to treat other systems, as this thesis will demonstrate. It is known as the 'Quantum Rotor' technique, and it builds on work done on Josephson junctions, non-linear sigma models from Nuclear Physics and on its extension to the orthodox model defined below [38]. We will give an account of the method adapted to our subsequent work on the field of transport through nanostructures.

2.2 The orthodox model

Ignoring electronic level reshuffling and population-dependent capacitance, a useful simplified hamiltonian for a metallic grain coupled by tunnel barriers to a metallic bulk is

$$\begin{aligned} H &= H_G + H_L + H_T + H_C \\ H_G &= \sum_{\alpha s} \epsilon_\alpha d^+_{\alpha s} d_{\alpha s} \\ H_L &= \sum_{rks} \epsilon_k c^+_{rks} c_{rks} \\ H_T &= \sum_{r\alpha ks} t_{rk\alpha} c^+_{rks} d_{\alpha s} + \text{H.c} \\ H_C &= E_C \left(\sum_{\alpha s} d^+_{\alpha s} d_{\alpha s} - N_0 - n_D \right)^2 \end{aligned} \tag{2.1}$$

Some words on notation: N_0 is the average number of particles in the ground state *without* interactions

$$N_0 = \sum_{\alpha s} \langle d^+_{\alpha s} d_{\alpha s} \rangle_0 \tag{2.2}$$

L and G subindices denote 'lead' (or 'bulk') and 'grain'; the extra index 'r' can denote different terminals (such as right and left lead) coupled to the system; hopping is described as usual by overlap integral $t_{rk\alpha}$, and an extra intra-grain interaction term H_C ('C' for 'charging') is considered; the sum over spin represents a channel doubling for all processes, since nothing depends on spin. Therefore we say this is an $N = 2$ channel model. It can also be formally extended to arbitrary N as we will do later; $n_D = \sum_r C_r \mu_r / e$ represents an external effective charge accumulating in nearby gates, to which a certain voltage μ_r is applied. This contribution takes into account the electrostatic energy that the system loses when the electrodes or gates relax in order to screen the charge in the grain. In equilibrium situations, as the ones we will be studying throughout this work, only capacitively coupled gates should be considered, so that $n_D = n_g = C_g \mu_g / e$. This is known the orthodox model for Coulomb blockade.

Note that H_C has the form of a classical electrostatic charging energy kind of term $((Q-Q_g)^2/2C)$. This is the essential physical assumption of the model, which is equivalent to saying that the electrostatic potential in the system is spatially uniform. From that point the form of H_C is very straightforwardly derived by electrostatic arguments [14]. The validity of this description for mesoscopic systems has been extensively discussed [2, 20–22], the criterion for applicability being $g_I \gg 1$ (typically it fails for system sizes smaller that the screening cloud dimensions). This was also shown to be the correct universal low energy interaction model for chaotic grains within the Random Matrix Theory [4].

The orthodox model action

We will be working in the imaginary time path integral formulation of quantum mechanics, since it is simpler at describing the effective dynamics of a subsystem at finite temperature, such as a metallic grain, that is coupled to a certain electronic bath, the bulk or leads. The action version of (2.1) is

$$\begin{aligned} S &= S_G + S_L + S_T + S_C \qquad (2.3)\\ S_G &= \sum_{\alpha s} \int d\tau d^+_{\alpha s}(\partial_\tau + \epsilon_\alpha - \mu) d_{\alpha s} \\ S_L &= \sum_{rks} \int d\tau c^+_{rks}(\partial_\tau + \epsilon_k - \mu_r) c_{rks} \\ S_T &= \sum_{r\alpha ks} \int d\tau t_{rk\alpha} c^+_{rks} d_{\alpha s} + \text{c.c} \\ S_C &= E_C \int d\tau \left[\sum_{\alpha s} d^+_{\alpha s} d_{\alpha s} - N_0 - n_G \right]^2 \end{aligned}$$

We have denoted by $\tau = it$ the imaginary time coordinate, and c, c^+, d, d^+ are now conjugate Grassmann variables instead of operators.

Let us examine the model (2.3) in some detail. The essential difficulty lies in S_C due to its quartic nature. The identifications ['quadratic'⇔'free propagation' ⇒ 'easy'] and ['quartic' ⇔ 'interaction' ⇒ 'tough'] have a very definite mathematical manifestation within the path integral formalism. Observable expectation values under an arbitrary quadratic action can be trivially calculated since they merely involve gaussian integrals or cumulants thereof, which just amounts to the diagonalization of the kernel matrix in the action. Just by looking at a Hamiltonian then, one can know if the physics to expect is trivial (single body, quadratic actions) or not. The form of H_C is immediately suggesting that one will have to work harder to get the physics of the system right. Furthermore, some non-perturbative effects can also be expected already at this point. Note that eqs. (2.3) are a generalization of the Anderson model, albeit with a certain spectrum structure in the impurity. It is known that such a model develops a Kondo resonance around the impurity under appropriate circumstances (localized moment regime, low temperature $T < T_K$).

The strategy therefore will be to reduce the term S_C to a tractably quadratic form (which is essentially what a self-energy perturbative approximation is about) in such a way

that this effects are approximately retained. At different stages of this process one can stop the chain of approximations and try to do some numbers, or rather take the final quadratic form and perform analytical calculations.

2.3 The Quantum rotor in a 'toy model'

Instead of following the standard perturbation theory path, we are going to show how any quartic interaction term can be decoupled exactly by the introduction of an extra bosonic field, also known as an 'auxiliary field', and how one obtains the Quantum Rotor model in general. This will not make life any easier in itself (we have one more field to deal with), but it opens up new types of approximation schemes. Let us demonstrate this in a simplified version of the orthodox model. We will analyze the fermionic toy action

$$S = \int d^+(\partial_\tau + \epsilon - \mu)d + E_C(d^+d - N_0 - n_G)^2 \tag{2.4}$$

which is a pretty silly model since it can only have zero or one electrons, so the interaction term is quite trivial. For this reason, despite being a quartic action, its partition function is exact [3],

$$Z = e^{-\beta E_C(N_0+n_G)^2} + e^{-\beta(\epsilon-\mu+E_C(1-N_0-n_G)^2)} \tag{2.5}$$

In the slightly more general case of an N degenerate level, we would have

$$Z = \sum_{k=0}^{N} \binom{k}{N} e^{-\beta(\epsilon-\mu)k-\beta E_C(k-N_0-n_G)^2)} \tag{2.6}$$

Note the binomial factor, due to the fact that the degeneracy of the level carries a distinguishable quantum number.

In this section we will treat this trivial model as if it were non-trivial, and use it to illustrate the techniques that we will employ in the more complicated orthodox model (2.3) later.

We will denote for simplicity the free action kernel by

$$G^{-1} = -(\partial_\tau + \epsilon - \mu)\delta_{\tau\tau'} \tag{2.7}$$

which can be thought of as a (continuous) matrix $G^{-1}(\tau,\tau') = G^{-1}(\tau-\tau')$, which is non-diagonal in the imaginary time basis due to the time derivative. The action of the model can therefore be rewritten as

$$S = -\int d\tau d\tau' d^+_\tau G^{-1}_{\tau,\tau'} d_{\tau'} + \int d\tau E_C(d^+_\tau d_\tau - N_0 - n_G)^2 \tag{2.8}$$

Note the minus sign in front of G^{-1}. This is the definition compatible with the usual convention for the fermionic free Green's function, whereby $G_{i\omega} = 1/(i\omega - \epsilon + \mu)$ for a single level at energy ϵ, see section 2.4 later.

[3] Another 'philosophical reason' being that the equations of motion for the Green functions can be closed for the orthodox model in the atomic limit, which is what our toy model essentially is.

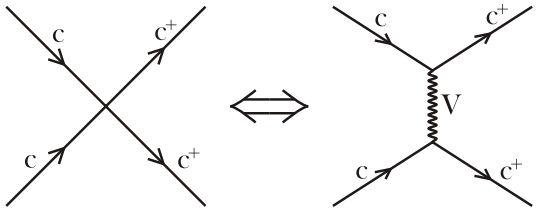

Figure 2.1: Diagramatic representation of the Hubbard-Stratonovich decoupling. The quartic (left) vertex in the action turns into a three field vertex, so that a diagram made of two such vertex (right) is equivalent to the initial one.

2.3.1 The Hubbard - Strattonovich transformation

The essential object for thermal equilibrium calculations, such as linear response theory (through fluctuation-dissipation theorem), charge fluctuations and other thermodynamic averages, is the partition function, defined in this case in the path integral formalism as follows

$$Z = \int \mathcal{D}[dd^+]\ e^{-S} = \int \mathcal{D}[dd^+]\ \exp\left[\int d^+_\tau G^{-1}_{\tau\tau'} d_{\tau'} - E_C(d^+_\tau d_\tau - N_0 - n_G)^2\right] \tag{2.9}$$

We will now show that it can be reexpressed identically as

$$Z = \int \mathcal{D}[V dd^+]\ \exp\left[\int d^+_\tau G^{-1}_{\tau\tau'} d_{\tau'} - \frac{1}{4E_C} V^2_\tau - iV_\tau(d^+_\tau d_\tau - N_0 - n_G)\right] \tag{2.10}$$

This operation, known as a Hubbard - Strattonovich transformation, essentially converts the initial four-field vertex into a three-field one by the introduction of a new auxiliary field V, see Fig. 2.3.1. Upon integration of this new field we would identically recover the original action with a four-legged vertex.[4]

This relation comes about very naturally if we take an infinitesimal slicing of the time axis into N intervals of width ϵ. Using the following integral identity at each slice

$$e^{-\epsilon E_C(d^+_\tau d_\tau - N_0 - n_G)(d^+_\tau d_\tau - N_0 - n_G)} = \sqrt{\frac{\epsilon}{4\pi E_C}} \int dV_\tau\ e^{-\frac{\epsilon}{4E_C} V^2_\tau + i\epsilon V_\tau (d^+_\tau d_\tau - N_0 - n_G)} \tag{2.11}$$

and defining the proper measure for V we arrive immediately at eq. (2.10).

A very important subtlety must be noted, however. V is not a usual bosonic field at this point. All physical fields in an imaginary time path integral approach have a definite periodicity condition, so that for fermions for example $d(\tau + \beta) = -d(\tau)$. The integral identity that leads to eq. (2.10) involves no periodicity constraint of any kind on $V(\tau)$. This must be kept in mind in the following discussion.

[4] The measure of the new field V involves a $(\epsilon/4\pi E_C)^{N/2}$ factor as usual in path integral definition. This is only important when taking derivatives of the Free Energy $F = -K_B T \ln Z$ respect to β or E_C.

2.3.2 Gauge transformations

We now take a hard look at our new action in imaginary time

$$S = \int -d_\tau^+ G^{-1}_{\tau\tau'} d_{\tau'} + \frac{1}{4E_C} V_\tau^2 + iV_\tau (d_\tau^+ d_\tau - N_0 - n_G) \tag{2.12}$$

It still is not a quadratic action, of course, due to the last term. It might seem we haven't advanced much. But neglecting the subtlety stated in the preceding paragraph the last term might remind us of the three-legged QED coupling of electrons and electromagnetic fields (see also Fig. (2.3.1)), $A^\mu \bar{\psi} \gamma_\mu \psi$, only that here instead of a four-vector A^μ we have a scalar V. We also know that local gauge transformations can modify the vector potential A^μ. With this inspiration we will perform a local gauge transformation on the fermions c with the hope of ridding ourselves of the non-trivial three-legged vertex.

$$f_\tau = e^{i\phi_\tau} d_\tau \tag{2.13}$$

To retain the anti-periodicity constraint on the f's, it is essential that ϕ_τ itself obey a periodicity constraint $\phi_{\beta+\tau} = \phi_\tau + 2\pi m$ (with arbitrary τ-independent integer m, known as the 'winding number' of the phase).

Plugging the canonical transformation (2.13) in the action (2.12), and taking the usual $G^{-1} = -(\partial_\tau + \epsilon - \mu)\delta_{\tau\tau'}$ kernel, a new term appears, $-if_\tau^+ f_\tau \partial_\tau \phi_\tau$, so that

$$S = \int -f_\tau^+ G^{-1}_{\tau\tau'} f_{\tau'} + \frac{1}{4E_C} V_\tau^2 + iV_\tau (f_\tau^+ f_\tau - N_0 - n_G) - if_\tau^+ f_\tau \partial_\tau \phi_\tau \tag{2.14}$$

If, given a field configuration V_τ, we could simply choose $\partial_\tau \phi_\tau = V_\tau$, the modified three-legged vertex would vanish, giving us an action that would be the sum of two uncoupled quadratic terms. The problem would then be exactly solvable! Note that all operations we have used are exact. Where is the catch then (if there is one)? The answer is in the subtlety pointed out at the end of the previous subsection. The periodicity constraint on ϕ_τ makes it impossible to build the corresponding $\partial_\tau \phi_\tau$ than cancels an arbitrary unconstrained V_τ. Only the V_τ's which satisfy the condition $\phi_\beta - \phi_0 = \int V_\tau = 2\pi m$ can be 'gauged away' by choosing $V_\tau = \partial_\tau \phi_\tau$. Let us identify the extra 'non-gaugeable' part of V_τ as

$$\tilde{V_0} = \frac{1}{\beta} \int_0^\beta V_\tau \quad \mod \ 2\pi/\beta \in [0, 2\pi/\beta) \tag{2.15}$$

which is distributed uniformly in the $[0, 2\pi/\beta)$ interval. We can now choose β-periodic ϕ_τ so that

$$V_\tau = \partial_\tau \phi_\tau + \tilde{V_0} \tag{2.16}$$

since $V_\tau - \tilde{V_0}$ will be completely arbitrary but it will satisfy the constraint $\frac{1}{\beta}\int_0^\beta (V_\tau - \tilde{V_0}) = 2\pi m/\beta$ with arbitrary integer m, just like $\partial_\tau \phi_\tau$. By construction $\tilde{V_0}$ here is an unconstrained time-independent real field that takes values in $[0, 2\pi/\beta)$, and ϕ_τ is a periodic (modulus 2π) field, so that

$$\phi_\beta - \phi_0 = 2\pi m \tag{2.17}$$

Making the above choice for the gauge transformation, we obtain the following transformed action

$$S = \int -f_\tau^+ G^{-1}_{\tau\tau'} f_{\tau'} + \frac{1}{4E_C}\left(\partial_\tau \phi_\tau + \tilde{V_0}\right)^2 + i\tilde{V_0}(f_\tau^+ f_\tau - N_0 - n_G) - i\partial_\tau\phi_\tau(n_G + N_0) \quad (2.18)$$

There is an alternative decomposition of V_τ that can also prove useful. We can define

$$V_0 = \frac{1}{\beta}\int_0^\beta V_\tau \in (-\infty, \infty) \quad (2.19)$$

and

$$V_\tau = \partial_\tau \tilde{\phi}_\tau + V_0 \quad (2.20)$$

In this case V_0 is a real unbounded field, but $\tilde{\phi}_\tau$ has the additional constraint of having zero winding number

$$\tilde{\phi}_\beta - \tilde{\phi}_0 = 0 \quad (2.21)$$

This turns eq. (2.18) into the totally equivalent form

$$S = \int -f_\tau^+ G^{-1}_{\tau\tau'} f_{\tau'} + \frac{1}{4E_C}\left[\left(\partial_\tau \tilde{\phi}_\tau\right)^2 + V_0^2\right] + iV_0(f_\tau^+ f_\tau - N_0 - n_G) \quad (2.22)$$

What we have really done here is a mere change of variables in the path integral sense: we have rewritten the auxiliary field V_τ in a new parametrization $\phi_\tau, \tilde{V_0}$ (or $\tilde{\phi}_\tau, V_0$) that spans the same Hilbert space of the original V_τ. The jacobian for this change of variables is one, and we can now consider them as merely as two independent fields. ϕ is a 'quantum rotor' field (since it moves in a unit circle, like a 2D rotor), hence the name of this technique, and $\tilde{V_0}$ is a 'projector field', as will be shown in the next subsection.

2.3.3 Projection field

We will now try to shed some light on the physical meaning of this new field V_0. We will call it a projection field, since we will show how the integration over V_0 is equivalent in the Hamiltonian representation to projecting all operators onto the subspace in which

$$Q = d^+ d - N_0 \quad (2.23)$$

Q being the conjugate of the ϕ variable.

The slave boson technique takes a different approach that leads to a very similar chain of transformations. The connection is quite remarkable and gives a physical interpretation of V_0. Retaking the hamiltonian description of our toy model

$$H = \epsilon d^+ d + E_C(d^+ d - N_0 - n_G)^2 \quad (2.24)$$

we could have thought of making $Q = d^+ d - N_0$ a new charge operator initially independent of d's (which would now be called pseudofermions f's), therefore writing

$$H = \epsilon f^+ f + E_C(Q - n_G)^2 \quad (2.25)$$

and then implementing an exact constraint in Fock space so that all states and operators are projected to the subspace $Q = f^+f - N_0$. This projection $\mathcal{P}_Q$ should be applied on all Q dependent operators $A \to P_Q A P_Q$ such that $P_Q(f^+f - N_0 - Q)P_Q = 0$, including the density matrix $\rho = \exp[-\beta H]$ whereby $Z = \mathrm{Tr}[\mathcal{P}\rho\mathcal{P}] = \mathrm{Tr}[\rho\mathcal{P}]$ is defined. Doing this we would be describing the same system, it would be exact. One useful implementation of the projection operator is the delta function of operators $\mathcal{P}_Q = \int_0^{2\pi/\beta} d\tilde{V}_0 \exp(-i\beta\tilde{V}_0(f^+f - N_0 - Q))$ (note that these are operators, not Grassmann variables). Therefore the projection of the density matrix ρ is performed by adding $i\tilde{V}_0(f^+f - N_0 - Q)$ to the Hamiltonian[5], and performing an extra integral over time-independent scalar $\tilde{V}_0$ at the end.

Translating this to the action representation of Z (inserting closure relations $\int |c\rangle |Q\rangle |\phi\rangle \langle\phi| \langle Q| \langle c|$ in each imaginary time slice) we would get

$$Z = \int_0^{2\pi/\beta} d\tilde{V}_0 \sum_{Q_\tau} \int \mathcal{D}[\phi f^+ f] e^{-S} \tag{2.26}$$

with

$$S = \int d\tau f_\tau^+(\partial_\tau - \mu) f_\tau - iQ_\tau \partial_\tau \phi_\tau + \epsilon f_\tau^+ f_\tau + E_C(Q_\tau - n_G)^2 + i\tilde{V}_0(f_\tau^+ f_\tau - N_0 - Q_\tau) \tag{2.27}$$

where the last term is the piece we have added to the Hamiltonian that implements the projection. Summation over the field Q_τ would take us back to eq. (2.18). ϕ, the conjugate of Q would now take its place by the following imaginary time relation

$$\partial_\tau \phi_\tau = 2iE_C(Q_\tau - n_G) - \tilde{V}_0 = [\phi, H] \tag{2.28}$$

$$Q = n_G - i\frac{\partial_\tau \phi_\tau}{2E_C} - i\tilde{V}_0 \tag{2.29}$$

It is clear now that the last term of (2.27),

$$i \int d\tau \tilde{V}_0 (f_\tau^+ f_\tau - N_0 - n_G - i\frac{\partial_\tau \phi_\tau}{2E_C}) \tag{2.30}$$

which is identical to what we had in (2.18), is the one that implements the projection over the desired subspace (2.23).

2.3.4 Exact solution for the toy model

Let us see how the present auxiliary field formulation enables us to recover the exact partition function of our toy model cf. the discussion at the beginning of this section. This illustrates the exact nature of all the above transformations, and the importance of the projection field if one is to recover the previously known exact results for Z.

Take eq. (2.22). Instead of integrating V_0 first, which would restore the quartic terms that we have decoupled, we can integrate the fermionic fields, using the general property

$$\int \mathcal{D}[c^+ c] e^{-\int c_\tau^+ A_{\tau,\tau'} c_{\tau'}} = \det A \tag{2.31}$$

[5]The Hamiltonian should in principle commute with Q and the total number of pseudofermions.

together with $\det(\partial_\tau + \epsilon - \mu + iV_0) = 1 + e^{-\beta(\epsilon-\mu+iV_0)}$ (see appendix H). We obtain

$$\begin{aligned} Z &= \int_\infty^\infty dV_0 (1 + e^{-\beta(\epsilon-\mu+iV_0)}) e^{-\frac{\beta V_0^2}{4E_C} + iN_0\beta V_0} \times \int \mathcal{D}[\tilde{\phi}] \exp\left[- \int \frac{\left(\partial_\tau \tilde{\phi}_\tau\right)^2}{4E_C} \right] \\ &= \left(e^{-\beta E_C (N_0+n_G)^2} + e^{-\beta(\epsilon-\mu+E_C(1-N_0-n_G)^2)} \right) \times \int \mathcal{D}[V_0\tilde{\phi}] \exp\left[- \int \frac{\left(V_0 + \partial_\tau \tilde{\phi}_\tau\right)^2}{4E_C} \right] \end{aligned}$$

This is exactly the expected result for Z. The extra factor to the right of the second line is identically one, since the measure for the Hubbard - Strattonovich was defined that way (see subsection 2.3.1 and footnote therein).

2.3.5 Saddle point approximation in the constraint field

In more elaborate models which include some coupling to the bulk, like the orthodox model, the previous calculation cannot be performed exactly. The chain of transformations we have introduced are tailored to be useful in such systems, by the application of appropriate approximation procedures. We will illustrate those procedures on the present toy model first.

The decoupling of the original quartic term has led to a three-legged vertex that remains troublesome to work with. The whole idea is to perform a saddle point approximation on the slave field V_0. This is the philosophy that lead to the BCS theory, where the Δ order parameter was finally understood [7] to represent a Hubbard - Strattonovich decoupling field that was treated in a mean field approximation. The approach we will present here is somewhat more elaborate, since a largest part of the Hubbard - Strattonovich field, the phase ϕ, will be treated beyond mean field, and only $\tilde{V_0}$ will be approximated by a mean field value. We choose the $\tilde{V_0}$ representation, eq. (2.18), instead of the V_0 one, eq. (2.22), since we want to approximate as much of the original Hubbard - Strattonovich field as possible.

The saddle point in this case amounts to substituting $\tilde{V_0}$ in (2.18) by a constant

$$-i\tilde{V_0} = \delta\mu \tag{2.32}$$

$$\delta n \equiv \frac{\delta\mu}{2E_C} \tag{2.33}$$

so that

$$S = \int f_\tau^+ (\partial_\tau + \epsilon - \mu - \delta\mu) f_\tau + \frac{1}{4E_C} (\partial_\tau \phi_\tau)^2 - i\partial_\tau\phi_\tau (n_G + N_0 - \delta n) + 2E_C \delta n (N_0 + n_G - \delta n/2) \tag{2.34}$$

The value of $\delta n, \delta\mu$ will be chosen so that the exact constraint (2.23), which will no longer be satisfied, is at least preserved in average

$$\langle Q \rangle = \langle f^+ f \rangle - N_0 \tag{2.35}$$

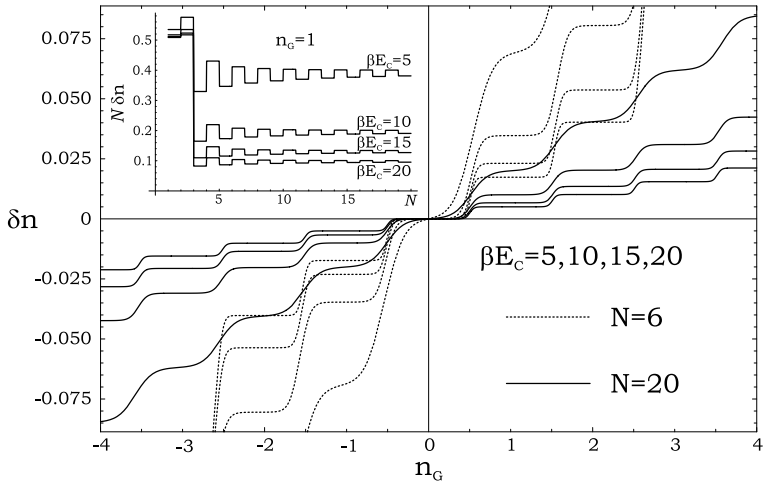

Figure 2.2: This is the saddle point value of δn for different values of the gate voltage, and various temperatures $\beta E_C = 5, 10, 15, 20$, as derived from condition (2.35). We also plot in the inset how δn decays like $1/N$ for large N.

Starting from the original Hamiltonian (2.25) we see that $\langle Q \rangle$ should in general be defined as follows

$$\begin{aligned} \langle Q \rangle &= n_G - \frac{1}{2E_C}\frac{\partial F}{\partial n_G} = n_G - \delta n + \frac{\langle i\partial_\tau \phi \rangle}{2E_C} = n_G - \delta n + \frac{\langle 2\pi i m \rangle}{2\beta E_C} = \\ &= n_G - \delta n + \frac{\pi}{\beta E_C}\frac{\sum_{m=-\infty}^{\infty} m \sin\left[2\pi i(n_G + N_0 - \delta n)m\right] e^{-\frac{(2\pi m)^2}{4\beta E_C}}}{\sum_{m=-\infty}^{\infty} \cos\left[2\pi i(n_G + N_0 - \delta n)m\right] e^{-\frac{(2\pi m)^2}{4\beta E_C}}} \end{aligned} \tag{2.36}$$

Here we have made use of equation (2.17) and the fact that $\langle i\partial_\tau\phi\rangle = \langle i\int_0^\beta \partial_\tau\phi\rangle/\beta$. The last equality is only valid for the present toy model case, and it will be different in the more realistic orthodox model.

Furthermore, since for a constant $-i\tilde{V}_0 = \delta\mu$ and in the particular case of the toy model the fermions f behave just as free fermions, we also have

$$\begin{aligned} \langle f^+ f \rangle - N_0 &= N\left[f^+(\epsilon - \mu - \delta\mu) - f^+(\epsilon - \mu)\right] \\ &= N\frac{\sinh\left[\beta E_C \delta n\right]}{\cosh\left[\beta E_C \delta n\right] + \cosh\left[\beta(\epsilon - \mu - E_C\delta n)\right]} \end{aligned} \tag{2.37}$$

We have generalized this expression to the case of an N-degenerate level, and used $f^+(\omega) = 1/(e^{\beta\omega}+1)$ as usual.

The solution to equation (2.35) cannot be given in a closed form, since it is a transcendental equation. We give a numerical solution in Fig. 2.2. Note the following essential features: it has the same sign as n_G, so that the effective value of n_G gets reduced; it is smaller at lower temperatures, and also for higher values of N; it is fairly constant at low temperatures within the Coulomb blockade plateau; for a given n_G the value of δn falls like $1/N$ for all temperatures and high enough N.

In Fig. 2.3 we present a comparison of the saddle point to the exact solution for $\langle Q \rangle$, which is analytical in the toy model, since the exact free energy is known from (2.6). The difference between the saddle point and exact value for $\langle Q \rangle$ is one possible benchmark for the validity of the approximation. It is interesting to note that the deviation of the saddle point solution increases as n_G approaches $\pm N/2$, see left of Fig. 2.3. This is linked to the fact that one essential property of the saddle point approximation for the rotor dynamics is that the Coulomb staircase becomes unbounded, instead of being truncated at the zero and N values of the total charge. Therefore, the closer we get to such totally empty and totally full grain, the saddle point deviation grows correspondingly. Therefore if $N \to \infty$ we can expect the approximation to become increasingly good. This is verified by comparing the left and right sides of Fig. 2.3. We see that increasing N reduces the saddle point deviation. This is a systematic tendency throughout this work. However, even for finite N it is encouraging to note that even for very large values of n_G the region around the center of each plateau is very precisely described, the deviation approximating zero exponentially at low temperatures, at least in what concerns the value of $\langle Q \rangle$. Additionally we note that the most important breakdown of the approximation occurs around the half integer values of n_G, i.e. the transparency points (lifting of the Coulomb Blockade), also known as sequential tunneling regimes (although interestingly enough precisely at transparency the saddle point solution again yields a correct answer). Close to such regions it is known by non-perturbative techniques [32] that peculiar logarithmic behaviors linked to a pseudospin Kondo mechanism are to be expected, where the two degenerate charge states play the role of the fluctuating spin. To finish with Fig. 2.3, we have added a comparison of the charge deviation within the saddle point approximation to the case $\delta n = 0$, where the constraint eq. (2.35) is ignored. The saddle point approximation is obviously superior in a wider range of n_G values.

2.4 The fermion-phase form of the orthodox model

Let us retake the orthodox model (2.3). We are going to apply the transformations we have introduced in the toy model to this more useful model, and then discuss the physical information this technique provides.

Notation

First of all let us introduce the notation we will be using. To avoid excessive indexing we will employ a partial matrix notation for fermion fields

$$\mathbf{c}_\tau = c_{l\tau} \qquad \textit{lead electrons} \tag{2.38}$$

$$\mathbf{d}_\tau = d_{g\tau} \qquad \textit{grain electrons} \tag{2.39}$$

$$\mathbf{f}_\tau = e^{i\phi_\tau}\mathbf{d}_\tau \qquad \textit{grain 'non-interacting' fermions} \tag{2.40}$$

$$\mathbf{t} = t_{gl} = \delta_{ss'}t_{rk\alpha} \tag{2.41}$$

Indexes l stand for lead quantum numbers, $l = (k, r, s)$. Likewise $g = (\alpha, s)$ is a shorthand for grain quantum numbers. $\mathbf{f}$ is the equivalent to $\tilde{c}$ in (2.13), but we will keep the distinction

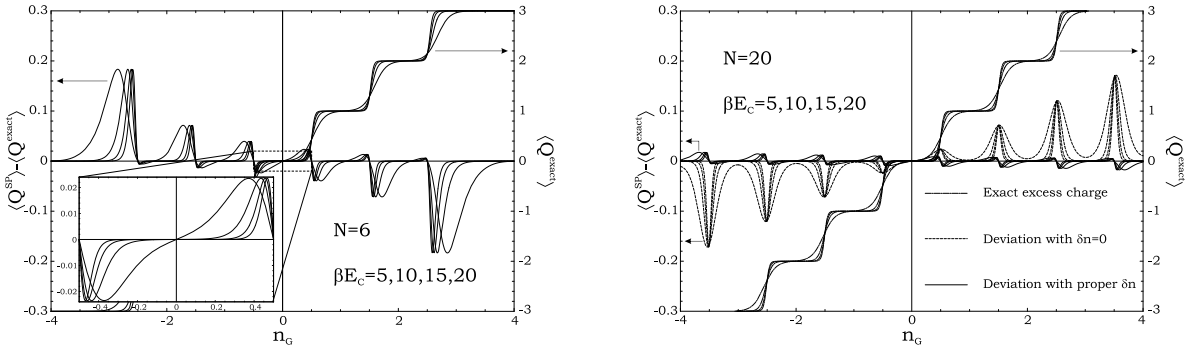

Figure 2.3: The deviation of this saddle point solution from the exact one is represented in the figure on the left for $N = 6$ and on the right for $N = 20$. Different curves correspond to different values of $\beta E_C = 5, 10, 15, 20$, starting from the smoothest curve. On both left and right we plot the Coulomb staircase as is obtained exactly from (2.6) over which the saddle point error must be added. Note the factor 10 difference in scale. The error goes to zero a) at zero temperature, b) when $N \to \infty$ or c) when we stay close to the center of the plateaus. For comparison purposes we also plot the deviation in $\langle Q \rangle$ one would obtain if we were to simply set $\delta n =$, thus neglecting the saddle point condition (2.35).

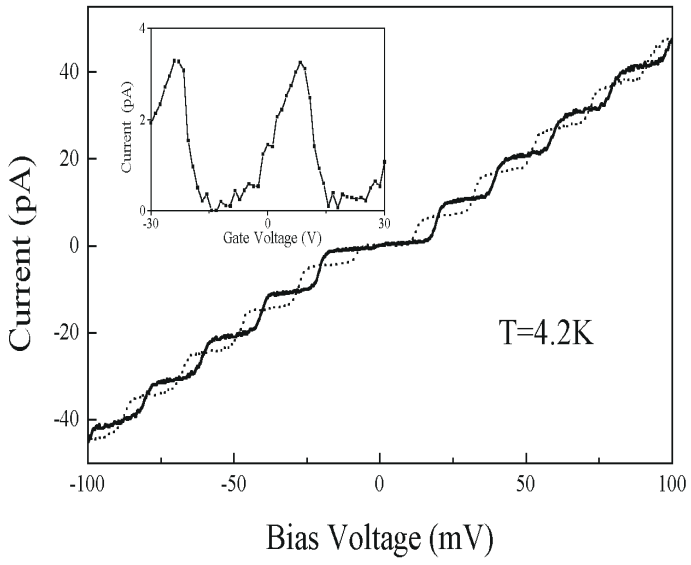

Figure 2.4: Typical experimental Coulomb staircase of a metallic grain, as demonstrated in [44] by means of an STP tip plus gate setup.

between $\mathbf{f}$ and $\mathbf{d}$ for future convenience. Note that hopping $\mathbf{t}$ is not a square matrix, since it connects the leads quantum number subspace to the grains subspace, and that it is spin independent like everything else.

Fourier transforms are defined following the usual convention

$$\mathbf{c}_{\omega_n} = \int_0^\beta d\tau e^{i\omega_n \tau} \mathbf{c}_\tau \tag{2.42}$$

$$\mathbf{c}_\tau = \frac{1}{\beta} \sum_{\omega_n} e^{-i\omega_n \tau} \mathbf{c}_{\omega_n} \tag{2.43}$$

The (free causal) correlation functions in imaginary time (in the absence of grain-lead coupling, $\mathbf{t} = 0$) are defined as follows

$$\bar{\mathbf{G}}_{\tau\tau'} = -\langle \mathbf{c}_\tau \mathbf{c}^+_{\tau'} \rangle \tag{2.44}$$

$$\bar{\mathbf{G}}^{-\mathbf{1}}_{\tau\tau'} = G^{-1}_{l\tau, l'\tau'} = -\delta_{kk'}\delta_{rr'}\delta_{ss'}(\partial_\tau + \epsilon_k - \mu_r)\delta_{\tau\tau'} \tag{2.45}$$

$$\bar{\mathbf{G}}_\omega = -\frac{1}{\beta}\langle \mathbf{c}_\omega \mathbf{c}^+_\omega \rangle = \frac{1}{i\omega - \epsilon_k + \mu} \tag{2.46}$$

$$\mathbf{G}_{\tau\tau'} = -\langle \mathbf{f}_\tau \mathbf{f}^+_{\tau'} \rangle \tag{2.47}$$

$$\mathbf{G}^{-\mathbf{1}}_{\tau\tau'} = \bar{G}^{-1}_{g\tau, g'\tau'} = -\delta_{\alpha\alpha'}\delta_{ss'}(\partial_\tau + \epsilon_\alpha - \mu - \delta\mu)\delta_{\tau\tau'} \tag{2.48}$$

$$\mathbf{G}_\omega = -\frac{1}{\beta}\langle \mathbf{f}_\omega \mathbf{f}^+_\omega \rangle = \frac{1}{i\omega - \epsilon_\alpha + \mu + \delta\mu} \tag{2.49}$$

The saddle point value for $\tilde{V_0}$ has been written as an effective chemical potential following 2.3.5, since it appears just in this form. We have denoted

$$-i\,\tilde{V_0}\Big|_{\text{saddle point}} = \delta\mu \tag{2.50}$$

$$\delta n \equiv \frac{\delta\mu}{2E_C} \tag{2.51}$$

In the particle-hole symmetric cases, $\delta\mu = 0$ as discussed in 2.3.5.

We also define the following correlation functions for future use

$$\mathcal{G}_{\tau\tau'} = \langle \cos(\phi_\tau - \phi_{\tau'}) \rangle \tag{2.52}$$

$$\mathbf{G^d}_{\tau\tau'} = -\langle \mathbf{d}_\tau \mathbf{d}^+_{\tau'} \rangle = -\langle e^{-i(\phi_\tau - \phi_{\tau'})} \mathbf{f}_\tau \mathbf{f}^+_{\tau'} \rangle \tag{2.53}$$

Whenever we use the explicit index notation, equal indexes are implicitly summed (Einstein's convention). Likewise, when we use the matrix and vector notation we assume the usual rules for vector and matrix multiplication. In particular we take $\mathbf{f}$ to be a *vertical* vector, so that $\langle \mathbf{f}^+ \mathbf{f} \rangle$ and $\mathbf{f}^+ \mathbf{G}^{-\mathbf{1}} \mathbf{f}$ are scalars, but $\langle \mathbf{f}\, \mathbf{f}^+ \rangle$ is a matrix, since it is a tensor product of two vectors, vertical times horizontal.

The fermion-phase action

Recall the transformations described in the toy model: identification of quartic Q^2 term in the action where $Q = \sum \mathbf{d}^+ \mathbf{d}$; introduction of auxiliary field V_τ to decouple Q^2

into iVQ terms; gauge transformation of $\mathbf{d}$'s into $\mathbf{f}$'s so that $\partial_\tau \phi_\tau = V_\tau - \tilde{V}_0$; saddle point approximation of $\tilde{V}_0$, thereby absorbing it as a constant contribution to the effective chemical potential in the dot. Repeating this chain on (2.3), the resulting $S = S_G + S_C + S_T + S_L$ is

$$\begin{aligned} S &= \int \Big[-\mathbf{f}^+_\tau \mathbf{G}^{-\mathbf{1}}_{\tau\tau'} \mathbf{f}_{\tau'} + \frac{1}{4E_C} (\partial_\tau \phi)^2 - \mathbf{c}^+_\tau \bar{\mathbf{G}}^{-\mathbf{1}}_{\tau\tau'} \mathbf{c}_{\tau'} + e^{i\phi_\tau} \mathbf{f}^+_\tau \mathbf{t} \mathbf{c}_\tau + \text{c.c.} && (2.54) \\ & \quad -i\partial_\tau \phi_\tau (n_G + N_0 - \delta n) + 2E_C \delta n (N_0 + n_G - \delta n/2)] && (2.55) \end{aligned}$$

Recall that $\int$ stands for integration over $\tau\tau'$ if the integrand depends on both, or over τ if it only depends on one time coordinate. Note the presence of the effective potential shift $\delta\mu = 2E_C \delta n$ in (2.48) and also its peculiar coupling to the phase in the above equation. It becomes of interest when exploring the 'Coulomb Blockade staircase' $\langle Q \rangle(\mu_g)$, see Fig. 2.4 and the various derivatives of the Free energy with gate voltage. We will however be concerned mainly with the particle-hole symmetric case, for which $\delta\mu = \delta n = 0$ exactly: it is simpler and it is in in this region that the saddle point approximation behaved best.

Now we are going to see one reason why the action formulation of quantum mechanics is so useful. We are going to perform and exact integration of the lead fermions $\mathbf{c}$, which is one of the integrals that appear in the full $Z = \int \mathcal{D}[\mathbf{c}^+ \mathbf{c} \mathbf{f}^+ \mathbf{f} \phi] e^{-S}$, so as to obtain an *effective action* for the remaining degrees of freedom, which are the ones we will want to evaluate observables on. To do so we use a particular case of the Cumulant Expansion theorem (see Appendix I),

$$\langle e^{-\int \mathbf{a}^+_\tau \mathbf{c}_\tau + \text{c.c.}} \rangle_c = \frac{\int \mathcal{D}[\mathbf{c}^+ \mathbf{c}] e^{-\int \mathbf{a}^+_\tau \mathbf{c}_\tau + \text{c.c.}} e^{-S[\mathbf{c}^+ \mathbf{c}]}}{\int \mathcal{D}[\mathbf{c}^+ \mathbf{c}] e^{-S[\mathbf{c}^+ \mathbf{c}]}} = e^{\frac{1}{2} \iint \langle \mathbf{a}^+_\tau \mathbf{c}_\tau \mathbf{c}^+_{\tau'} \mathbf{a}_{\tau'} \rangle + \langle \mathbf{c}^+_\tau \mathbf{a}_\tau \mathbf{a}^+_{\tau'} \mathbf{c}_{\tau'} \rangle} \tag{2.56}$$

which is exact as long as the average over $\mathbf{c}$ follows a centered multigaussian distribution $S[\mathbf{c}^+ \mathbf{c}]$. We can use this relation to perform the integration of the lead fermions in Z by identifying $\mathbf{a}^+_\tau = e^{i\phi_\tau} \mathbf{f}^+_\tau \mathbf{t}$, and $S[\mathbf{c}^+ \mathbf{c}] = \int \mathbf{c}^+_\tau \bar{\mathbf{G}}^{-\mathbf{1}}_{\tau\tau'} \mathbf{c}_{\tau'}$. Taking into account eq. (2.44) we arrive at the following effective action for grain fermions plus phase (in the absence of gate voltages, $\delta n = 0$)

$$S = \int -\mathbf{f}^+_\tau \mathbf{G}^{-\mathbf{1}}_{\tau\tau'} \mathbf{f}_{\tau'} + \frac{1}{4E_C} (\partial_\tau \phi_\tau)^2 + \mathbf{f}^+_\tau \mathbf{\Delta}_{\tau\tau'} \mathbf{f}_{\tau'} \cos(\phi_\tau - \phi_{\tau'}) \tag{2.57}$$

We will use the action (2.57) in a later chapter for the analysis of Kondo physics and other phenomena. Assuming zero bias ($\mu_r = 0$), the 'bath function' is defined as

$$\begin{aligned} \mathbf{\Delta}_{\tau\tau'} &= \Delta_{g\tau, g'\tau'} = \mathbf{t} \bar{\mathbf{G}}_{\tau\tau'} \mathbf{t}^+ = L t^2 \delta_{s,s'} \frac{1}{\beta} \sum_{\omega_n k} \frac{e^{-i\omega_n(\tau - \tau')}}{i\omega_n - \epsilon_k} \\ &= L t^2 \delta_{s,s'} \rho_l(0) \frac{\pi/\beta}{\sin[\pi(\tau - \tau')/\beta]} \overset{\beta \to \infty}{\longrightarrow} L t^2 \delta_{s,s'} \rho_l(0) \frac{1}{\tau - \tau'} \end{aligned} \tag{2.58}$$

Recall that here ω_n are fermionic Matsubara frequencies. See (A.20) for a useful identity in deriving the above equation. The last equalities are the expressions in the particular case of a constant hopping amplitude $t_{gl} = \delta_{ss'} t$ (local hopping approximation), which will be common throughout this text. It merely means that hopping of electrons occurs locally,

from a spatially resolved point in the leads to a point in the grain, which is a very sensible and generally valid model for the hopping. We have also denoted by L the number of identical metallic leads to which the grain is connected (sum over the r index). $\rho(\epsilon)$ will stand for a density of states *per channel*, so it doesn't include the N multiplicity of states. In the second line of (2.58) we have also assumed a slowly varying density of states $\rho_l(\epsilon)$ on the scale of the temperature. Note that under these conditions we have an algebraic decay for the bath function in the low temperature limit. This will have physical consequences later on related to cotunneling and the low temperature survival of Coulomb blockade at large couplings.

2.5 The large N limit and the phase-only action

There is a whole family of physical questions about a metallic grain that involves only transitions between different real charge states, and in which the detailed fermion configuration given a total charge does not matter. An example of this is the effective capacitance of a grain, in which we are interested in the average charge of the grain versus an external gate voltage in the presence of leads. A related question is the size of charge fluctuations in the grain when the coupling to the leads grow. Also, the form of the charge oscillations between two grains (like in the Josephson effect, where these techniques were born) only depend on the total charge states of the grains. Another very important one, as we will see later, is the Coulomb blockade correction to the linear conductance of a grain. To answer this class of questions it would suffice to compute an effective total charge action, or equivalently a phase-only action, by integrating out the grain fermion fields $\mathbf{f}$ in (2.57), just as we did with $\mathbf{c}$, which would give us the minimum possible model to calculate such quantities. But unlike in the case of lead fields, this cannot be done exactly, and further approximations are involved. We will devote the remaining part of this chapter to analyze the aspects of this so-called phase-only approach.

Now, recall that the orthodox model has a sum over $N = 2$ spin states. As we mentioned earlier, since nothing depends on spin in this model, the s quantum number represents a degenerate channel index. This degeneracy turns out to be a very powerful handle for approximations. As in the case of the toy model we will keep N an indefinite number, thereby extending the dimension of the representation of the SU(2) symmetry of the model, and considering fermions with arbitrary spin. Alternatively, since N really represents number of degenerate channels respect to tunneling, it does not have to involve an N-spin, but also orbital quantum numbers are allowed. In this sense, Large-N also means large number of conserved transverse tunneling channels, a condition found in broad contacts between metals and metallic grains, the canonical systems to look for Coulomb blockade.

There is a powerful approximation scheme, born in the field of nuclear physics, that consists of performing an expansion of observables or action in orders of $1/N$, so that they become exact in the limit of $N \to \infty$. This will be our strategy now. The results of the leading large-N expansion [18] are found to be qualitatively correct even in the $N = 2$ case [48, 56]. Further corrections of order $1/N$ can also be included in the study, as in the NCA approximation [3, 41, 45, 53, 75] and will be discussed in a later chapter.

In order for the $N \to \infty$ limit to be well defined it is essential to scale the hopping amplitude of each of those channels by $N^{-1/2}$, so that $t = \bar{t}/\sqrt{N}$, otherwise the lifetime of a fermion in one of these N-degenerate levels, which is a measure of the resistance of the grain, would vanish as we increase the number of exit channels $N \to \infty$.

The large-N limit will allow us to integrate out the grain fermions. The trick is in the cumulant expansion again. From Appendix I we know that formally

$$\langle e^{-ta} \rangle_{P_a} = \exp\left(\sum_n^{\infty} \frac{(-1)^n}{n!} t^n \langle\langle a^n \rangle\rangle_{P_a} \right) \tag{2.59}$$

where a is a random variable with distribution $P_a(a)$, and $\langle\langle a^n \rangle\rangle_{P_a}$ is the n-th cumulant (or the n-th irreducible momentum) of a, which is a certain combination of averages of a. For example, $\langle\langle a \rangle\rangle_{P_a} = \langle a \rangle_{P_a}$ (the average), $\langle\langle a^2 \rangle\rangle_{P_a} = \langle a^2 \rangle_{P_a} - \langle a \rangle_{P_a}^2$ (the variance), etc. A general definition can be found in Appendix I.

The reason that enabled us to integrate the lead electrons exactly before is that all cumulants except the second are zero for a centered Gaussian distribution. In eq. (2.57) however, the variable in the exponent to be averaged is $\int e^{i\phi_\tau} \mathbf{f}^+ \mathbf{\Delta_l} \mathbf{f} e^{-i\phi'_\tau}$, which unlike $\mathbf{f}^+$ does not have a Gaussian distribution, and in principle all cumulants should be summed.

First of all let us calculate the first cumulant contribution to the effective phase-only action

$$\begin{aligned} S_D &= \int \langle \mathbf{f}^+_\tau \mathbf{\Delta}_{\tau\tau'} \mathbf{f}_{\tau'} \rangle \cos(\phi_\tau - \phi_{\tau'}) = \int \langle f^+_{g\tau} f_{g'\tau'} \rangle \Delta_{g\tau g'\tau'} \cos(\phi_\tau - \phi_{\tau'}) \\ &= \int G_{g'\tau' g\tau} \Delta_{g\tau g'\tau'} \cos(\Delta\phi_{\tau\tau'}) = \int \mathrm{Tr}\left[\mathbf{G}_{\tau'\tau} \mathbf{t} \bar{\mathbf{G}}_{\tau\tau'} \mathbf{t}^+ \right] \cos(\Delta\phi_{\tau\tau'}) \end{aligned} \tag{2.60}$$

We will define in the case of a smooth grain density of states $\rho_g(\epsilon)$ (see next subsection for detailed calculations)

$$\alpha = LNt^2 \rho_l(0) \rho_g(0) \tag{2.61}$$

$$K_{\tau\tau'} = -\frac{1}{\alpha} \mathrm{Tr}\left[\mathbf{G}_{\tau'\tau} \mathbf{t} \bar{\mathbf{G}}_{\tau\tau'} \mathbf{t}^+ \right] = -\frac{LNt^2}{\alpha} \mathrm{Tr}\left[\mathbf{G}_{\tau'\tau} \right] \mathrm{Tr}\left[\bar{\mathbf{G}}_{\tau\tau'} \right] \tag{2.62}$$

where we have again assumed a momenta-independent hopping for simplicity $t_{gl} = \delta_{ss'} t$, and denoted the number of leads by L and the number of channels by N. Correspondingly, the factorized trace of the propagators does not include the sum over the channel and lead indices. We can write, up to an unimportant constant the following first-cumulant contribution to the effective dissipation action

$$S_D = \alpha \int K_{\tau\tau'} \left[1 - \cos(\phi_\tau - \phi_{\tau'}) \right] \tag{2.63}$$

Note that according to the arguments given some paragraphs above, the quantity $Nt^2 = \bar{t}$ in α does not scale with N, while K is independent of N and t, so this first cumulant contribution is finite in the $N \to \infty$ limit.

Large-N approximation

Now let's go for the other cumulants. In Appendix I the reader may also find the demonstration of a very important property of cumulants. For an 'N-degenerate' random variable $b = \sum_s^N a_s$, with probability $P_b(b[a_s]) = \prod_s^N P_a(a_s)$, we have the important property

$$\langle\langle b^m \rangle\rangle_{P_b} = N \langle\langle a^m \rangle\rangle_{P_a} \tag{2.64}$$

independently of m. In our case this means that the contribution to the action from the n-th cumulant will have a coefficient $Nt^{2n} = \bar{t}^{2n}/N^{n-1}$ times an N, t-independent function, so that all those contributions will vanish in the large-N limit, except of course for the first one $n = 1$.

Therefore, in the large-N limit (i.e. large degeneracy per level, small per-channel conductance) the phase-only action

$$S = \int \frac{1}{4E_C} \left(\partial_\tau \phi_\tau\right)^2 + \alpha \int K_{\tau\tau'} \left[1 - \cos(\phi_\tau - \phi_{\tau'})\right] \tag{2.65}$$

gives an exact description of charge dynamics (within the validity of the saddle point approximation for the projection field).

True electron Green's function

To finish with the large-N introduction, let us ask the following question: is it possible to recover the full grain electron's Green function from this action within this approximation?

It is indeed possible to obtain imaginary time Green's functions in an alternative way, through generating functionals. If one adds to the original action S a term of the form $S_{\text{source}} = \int \mathbf{d}^+{}_\tau \mathbf{W}_{\tau\tau'} \mathbf{d}_{\tau'}$, where $\mathbf{W}_{\tau\tau'}$ is a bi-local external (*source*) field. Building Z out of this new action (now formally called a generating functional), one has the following identity

$$G^d_{g\tau,g'\tau'} = \left.\frac{\delta \ln Z}{\delta W_{g'\tau',g\tau}}\right|_{\mathbf{W}_{\tau\tau'}=0} \tag{2.66}$$

Now, if the mathematical transformations described above are performed while keeping the source term (and also scaling $\mathbf{W}$ with N in a similar way to the hopping $\mathbf{t}$), one ends up with $S_{\text{source}} = \int \text{Tr}\left[\mathbf{W}_{\tau'\tau}\mathbf{G}_{\tau\tau'}\right] \cos(\phi_{\tau'} - \phi_\tau)$. If one then performs the functional derivation above on the final Z, one obtains the following result, which is exact in the large-N limit

$$G^d_{g\tau,g'\tau'} = \left.\frac{\delta \ln Z}{\delta W_{g'\tau',g\tau}}\right|_{\mathbf{W}_{\tau\tau'}=0} = G_{g\tau,g'\tau'} \mathcal{G}_{\tau',\tau} \tag{2.67}$$

This means that (2.53) factorizes into two independent Green's functions within this approximation. This relation even holds to order $1/N$ as will be demonstrated in future chapters, and it will have useful applications in what follows. This decomposition is said to neglect 'vertex corrections' since an exact (to all orders in $1/N$) expression would involve further terms, as depicted in Fig. 2.5.

Figure 2.5: The full electronic propagator is composed, according to the particular case of the Bethe-Salpeter equation depicted above, to the factorized term (2.67) plus some vertex corrections which involve the vertex function Γ, which are neglected in the large-N limit.

2.5.1 Kernel zoo

To calculate the kernel $K_{\tau\tau'}$ we can consider various situations depending on the grain spectrum. Using again (A.20), a continuous grain spectrum of infinite bandwidth yields

$$K_{\tau\tau'} = -\frac{1}{\alpha}\mathrm{Tr}\left[\mathbf{G}_{\tau'\tau}\mathbf{t}\bar{\mathbf{G}}_{\tau\tau'}\mathbf{t}^{+}\right] = \left[\frac{\pi/\beta}{\sin\left[\pi(\tau-\tau')/\beta\right]}\right]^{2} \overset{\beta\to\infty}{\longrightarrow} \frac{1}{|\tau-\tau'|^{2}} \tag{2.68}$$

Alternatively one can consider a continuous band of width $2D$. To give the integral over $\epsilon_\alpha \in [-D, D]$ in a closed form we have to take the low temperature limit. This gives

$$K_{\tau\tau'} \overset{\beta\to\infty}{\longrightarrow} \frac{1-e^{-D|\tau-\tau'|}}{|\tau-\tau'|^{2}} \tag{2.69}$$

Another interesting case is the first correction to the orthodox model that one can consider, namely the many body character associated with an electron jump into the dot. Such event can indeed cause a physical redistribution of electrons not captured by the charging energy model. Orthogonality catastrophe arguments [8,64,93], see chapter 5, show that these so called 'excitonic effects'[6] can be taken into account approximately simply by taking

$$K_{\tau\tau'} = E_C^{\varepsilon}\left[\frac{\pi/\beta}{\sin\left(\pi(\tau-\tau')/\beta\right)}\right]^{2-\varepsilon} \overset{\beta\to\infty}{\longrightarrow} \frac{E_C^{\varepsilon}}{|\tau-\tau'|^{2-\varepsilon}} \tag{2.70}$$

where ε (not to be confused by energy ϵ) is a parameter for the strength of the excitonic effects associated to the phase shift in the scattering of an electron going into and out of the grain. In can be either positive (for repulsive interactions as is the case of electrons) or negative (for attractive interactions).

To finish our comparison we can also take the single level case, which in the low temperature limit yields

$$K_{\tau\tau'} \overset{\beta\to\infty}{\longrightarrow} \frac{1}{\beta|\tau-\tau'|} \times \begin{cases} \frac{1}{2}\mathrm{sign}(\tau-\tau') & \text{if } \beta\epsilon \ll 1 \\ \theta_{\tau-\tau'}e^{-\epsilon(\tau-\tau')} & \text{if } \beta|\epsilon| \gg 1,\ \epsilon > 0 \\ -\theta_{\tau'-\tau}e^{-\epsilon(\tau-\tau')} & \text{if } \beta|\epsilon| \gg 1,\ \epsilon < 0 \end{cases} \tag{2.71}$$

In this case α is defined as $\alpha = LN\beta t^2\rho_l(0)$, since $\rho_g(0)$ has no relevant meaning.

[6]The name comes from the fact that an electron in the tip of one lead and a hole in the edge of the grain (or viceversa) can form a bound state known as an exciton when these type of localized interaction effects are taken into account.

The crucial difference between all these cases is the long time behavior of the kernel. As we will show now, this behavior is responsible for the transport properties in linear response of our system. A kernel that decays 'slowly enough' is a signature of conducting behavior at low temperature, while if it decays 'fast enough' the system will be insulating. Let us see how.

2.5.2 Kosterlitz transition and Griffiths Theorem

In this section we will analyze the influence of the behavior of $K_{\tau\tau'}$ on the phase-phase correlation function $\mathcal{G}_{\tau\tau'}$, see eq. (2.52). The relevance of this analysis to linear transport properties will become clear in the next section.

Kosterlitz demonstrated, using Renormalization Group (RG) analysis in the context of ferromagnetic chains, that a 1-D chain of n-component spins with long range interactions analogous to (2.65) (where $K_{\tau\tau'}$ represents the long range interactions in coordinate τ) can lead to an ordered or disorder ground state depending on how fast $K_{\tau\tau'}$ decays [58]. In the original paper instead of imaginary time τ the author dealt with spatial coordinate x along the chain, but the result he obtained is exactly applicable to our case, where ϕ_τ substitutes the spin orientation for the special case of $n = 2$ component spins. It all boils down to the RG flow equation for $z \equiv 1/\alpha$ around $\alpha = \infty$ (see Appendix E for a slightly more general derivation of these results, and also [88] for a review on RG). Taking $K_{\tau\tau'} = E_C^{2-\sigma}/(|\tau - \tau'|^\sigma)$ and $n = 2$ Kosterlitz's analysis implies that for small $\varepsilon = 2 - \sigma$

$$\frac{1}{z}\frac{dz}{d\lambda} = (\sigma - 2) + \frac{1}{2\pi^2}z + \mathcal{O}(z^2, (\sigma - 2)z) \tag{2.72}$$

For $\sigma < 2$, z flows back to zero, which corresponds to the strongly interacting limit $\alpha = \infty$ in all the spins are aligned, so the ground state is ordered (ferromagnetic in Kosterlitz's language) in that case. Therefore $\sigma < 2$ means 'decay is slow enough to hold spins (or phases ϕ_τ) aligned'. In particular the case $\sigma = 1$ in eq. (2.71) leads to an ordered ground state, which in its turn reflects in a $\mathcal{G}_{\tau\tau'} \to 1$ at low temperatures, see eq. (2.52).

For kernels decaying even more strongly than $1/|\tau - \tau'|^\sigma$, like the exponential decay case of eq. (2.71), the system is always disordered.

For $\sigma \geq 2$, there is an unstable critical boundary in the $\alpha - \sigma$ plane, $\alpha_c = 1/(2\pi^2(2 - \sigma))$, so that if $\alpha > \alpha_c$ the system orders at low temperatures, and if $\alpha < \alpha_c$ it gets disordered. In the latter case $\mathcal{G}_{\tau\tau'}$ decays at long times, similarly to the dissipationless $\alpha = 0$ case where $\mathcal{G}_{\tau\tau'} = e^{-E_C|\tau-\tau'|}$, [7] although how fast in this case is a more difficult question. Griffith's theorem [42] states that correlation functions such as $\mathcal{G}_{\tau\tau'}$ cannot decay faster than the interaction kernel $K_{\tau\tau'}$. This gives a strict lower bound the decay rate. But actually, in many practical cases the decay law in $K_{\tau\tau'}$ directly translates to $\mathcal{G}_{\tau\tau'}$, as can be seen from Quantum Montecarlo calculations [47]. In particular continuous band grains have a $\mathcal{G} \sim 1/|\tau - \tau'|^2$ decay for long times.

[7] This can be proven by noting that $\mathcal{G}_{\tau\tau'} = \langle \cos(\phi_\tau - \phi_{\tau'}) \rangle = e^{-\frac{1}{2}\langle(\phi_\tau - \phi_{\tau'})^2\rangle}$ if $\alpha = 0$ (cumulant expansion for Gaussian variables again), and then proceeding by usual Fourier expansion, with $\langle \phi_\omega^2 \rangle = 2E_C/\omega^2$. For finite temperatures one gets $G_{\tau\tau'} = e^{-E_C|\tau-\tau'|(1-|\tau-\tau'|/\beta)}$ instead.

Translating this analysis to our phase-only action (2.65) we have following preliminary results for vanishing temperature $\beta \to \infty$ and long times $E_C|\tau - \tau'| \gg 1$

$$\begin{aligned} \text{Infinite continuous band in grain} &\longrightarrow \mathcal{G} \text{ decays algebraically} \\ \text{Finite continuous band in grain} &\longrightarrow \mathcal{G} \text{ decays algebrically} \\ \text{Discrete level away from the Fermi energy} &\longrightarrow \mathcal{G} \text{ decays exponentially} \\ \text{Discrete level at the Fermi energy} &\longrightarrow \mathcal{G} = 1 \\ \text{Repulsive excitonic effects} &\longrightarrow \mathcal{G} = 1 \end{aligned} \tag{2.73}$$

2.5.3 Conductance and phase ordering

So why should one be interested in these imaginary time Green's functions and their long time decay? How are these $\mathcal{G}$ related to transport properties for example? The traditional route for extracting real-time response information is the analytical continuation method, see Appendix A. Indeed, given an imaginary time Green's function $\mathbf{G^d}_{\tau-\tau'}$, see (2.53) and (2.67), it is possible in principle to obtain the corresponding real time one by analytically continuing $\mathbf{G^d}_{i\omega_n}$ to real ω axis. And given $\mathbf{G^d}_{\omega}$ one can use various techniques to obtain linear response information, the most typical of which is the linear conductance, or current response to a small externally applied electric field (using e.g. Meir-Wingreen [69] formula for the case of conductance through an interacting region, see later).

Conductance in terms of $\mathcal{G}_{\bar{\sigma}}$ for some optimal $\bar{\sigma}$

Although this analytical continuation is an (more or less) precise mathematical proposition, its practical aspects make it a very delicate transformation, only doable in cases of relatively smooth spectral function $\mathbf{A}_\omega = -\frac{1}{\pi}\Im[\mathbf{G}^{\mathbf{d}}_\omega]$.

However, some essential features of $\mathbf{G^d}_{\omega}$ can be read directly from $\mathcal{G}_{i\omega_n}$ without going through the process of analytical continuation. In particular, starting from the results of Appendix B we will prove below that the Coulomb Blockade correction to the non-interacting high temperature conductance is merely $\mathcal{G}_{\bar{\tau}} \equiv \mathcal{G}_{\tau-\tau'=\bar{\tau}}$ for a certain optimal value of $\bar{\tau}$ to a good degree of accuracy. The value of $\bar{\tau}$ will depend however on the microscopic details of the grain or quantum dot. In any case the general rule becomes that decaying rotor correlations $\mathcal{G}_{\tau\tau'}$ means tendency towards an insulating regime at low temperatures.

Conductance of the metallic grain

We will now make this general rule more quantitative. The results of Appendix B, and in particular eq. (B.12), relate the linear conductance in the presence of interactions to the rotor correlation function, which essentially contains the interaction effects.

To proceed beyond eq. (B.11) and (B.12) for the linear conductance one must make some assumption about the grain's non-interacting density of states ρ^f_ω. If we are talking about a true metallic grain with a smooth density of states on the scale of temperature, we

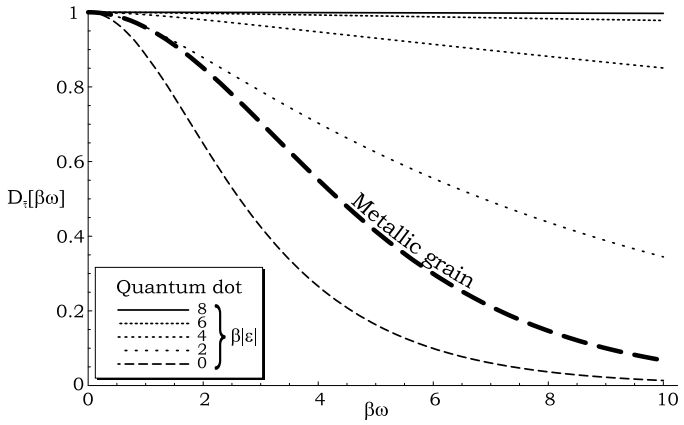

Figure 2.6: The function $D[\beta\omega]$ of equation (B.9) summarizes the microscopical details of the relation between the conductance and the imaginary time rotor correlation function $\mathcal{G}_{\Delta\tau}$. The flatter the curve $D[\beta\omega]$ the better the approximations (2.77) and (2.80) with a truncated series. We plot this curve for the single level quantum dot and for the metallic grain cases.

can approximate $\rho^f_\omega \approx \rho^f(0)$, and choose $\bar{\tau} = \beta/2$ to obtain

$$D_{\beta/2}[\beta\omega] = \frac{\beta\omega/2}{\sinh(\beta\omega/2)} \approx 1 - \frac{1}{24}(\beta\omega)^2 + \frac{7}{5760}(\beta\omega)^4 + \dots \tag{2.74}$$

A different choice of $\bar{\tau}$ other than $\beta/2$ though would introduce a linear term in x of the form $(\bar{\tau} - \beta/2)x$ that would make the series approximation less than optimal. Therefore we can conclude that

$$\bar{\tau} = \beta/2 \tag{2.75}$$

$$g_\infty = \frac{Ne^2}{h}\pi\Gamma\rho^f(0) \tag{2.76}$$

$$g = g_\infty\left(\mathcal{G}_{\bar{\tau}} - \frac{1}{24}\beta^2\mathcal{G}''_{\bar{\tau}} + \frac{7}{5760}\beta^4\mathcal{G}^{(iv)}_{\bar{\tau}} + \dots\right) \tag{2.77}$$

where g_∞ stands for the non interacting conductance of the grain. For small $\beta\omega$, i.e. for large temperatures, this can be approximated by a truncation of the series, see Fig. 2.6 for a pictorial representation.

It has been argued though that this approximation actually holds qualitatively beyond the high temperature limit [14], making even the lowest order in (2.77) a useful interpolation across all temperatures.

Conductance of the single level quantum dot

If one assumes an effective single level quantum dot scenario so that $\rho^f_\omega = \delta(\omega - \epsilon)$, one obtains a variation of the above result (2.77). In this case the value of $\bar{\tau}$ that makes

the first order in $\beta\omega$ vanish is different, and depends of ϵ. The results are as follows

$$\bar{\tau} = \beta(1 - f^+_{|\epsilon|}) \tag{2.78}$$

$$g_\infty = \frac{Ne^2}{h}\pi\Gamma\frac{1}{4}\mathrm{sech}^2(\frac{\epsilon}{2}) \tag{2.79}$$

$$g = g_\infty\left(\mathcal{G}_{\bar{\tau}} - \frac{1}{8}\mathrm{sech}^2(\frac{\epsilon}{2})\beta^2\mathcal{G}''_{\bar{\tau}} + \frac{1}{24}\mathrm{sech}^2(\frac{\epsilon}{2})\mathrm{Tanh}^2(\frac{\epsilon}{2})\beta^2\mathcal{G}^{(iv)}_{\bar{\tau}} + \ldots\right) \tag{2.80}$$

Incidentally, due to the $\mathcal{G}_{\Delta\tau} = \mathcal{G}_{-\Delta\tau}$, $\mathcal{G}_{\Delta\tau+\beta} = \mathcal{G}_{\Delta\tau}$ and $D_{\bar{\tau}}[x] = D_{\bar{\tau}}[-x]$ symmetries, one could also choose $\bar{\tau} = \beta f^+_{|\epsilon|}$ and it would make no difference. The conductance only depends on $\beta|\epsilon|$, not on its sign.

In Fig. 2.6 the reader may find a comparison of different values of $\beta|\epsilon|$. It is clear that the high temperature approximation of truncating the series (2.77) or (2.80) works best for large $|\beta\epsilon|$. In such cases $\mathcal{G}_{\bar{\tau}}$ is quite a good approximation for g/g_∞. How large must $|\beta\epsilon|$ be depends on where is the main weight of $\mathcal{G}^>_\omega$, see (B.11).

2.5.4 Cotunneling and beyond. The limitations of the phase-only approach.

Even in a Coulomb Blockaded grain or dot, in which classical rate equation approaches (sequential tunneling approximations) would give exponentially suppressed conductance of the form $g \sim e^{-\beta E_C}$, more precise quantum mechanical methods like the Quantum Rotor approach allows for the introduction of higher order processes like cotunneling.

Cotunneling consists in transport events from one lead to another via a virtual state of classically forbidden energy in the grain. The amplitude of such processes are suppressed by usual $1/E_C$ factors of perturbation theory plus phase space constraints. In the presence of cotunneling, even in a Coulomb Blockade regime, it can be proven by perturbation theory that conductance at low temperatures goes like $g \sim T^2$ [39]. Incidentally this kind of processes make simple Coulomb Blockade in very small grains ineffective to act as a current valve or switch by gate voltage tuning, since current can seep through despite the blockade.

As we have argued the Quantum Rotor model is exact in the large-N limit of a grain with finite absolute level width $N\Gamma$. In this limit lowest level cotunneling process have a finite amplitude, but any higher order cotunneling events, such as the series that leads to the Kondo effect[8] are suppressed (they involve diagrams of order $Nt^{2n} \to 0$). This is testified by the fact that the $\mathcal{G}_{\Delta\tau}$ is decaying for a single level quantum dot away from the leads' Fermi energy, see (2.73), signaling zero conductance at zero temperature, whereas the exact solution for finite N should be perfect conductance at zero temperature due to the formation of the Kondo resonance [94].

Therefore the Quantum Rotor model, through its dissipation term, captures only the most basic quantum correction to sequential tunneling transport, namely the leading cotunneling processes, but nothing of the higher order effects beyond this for the case of finite N. Several attempts have been made to defeat this limitation by summing up explicitly all the cumulant expansion series [37] which adds a sequence of non-local-in-time

[8]Summing up many coherent cotunneling processes can lead to a divergent perturbative series at zero temperature for transport observables or spectral functions, which signals the onset of the Kondo effect.

terms to the simple dissipative one we have introduced here. Some progress can be made in such direction by the use of sophisticated instanton techniques which cover the finite N case. This precise shortcoming of the phase-only approach inspired the original work on which the next chapter builds [29], where it was found that by including the dynamics of the $\mathbf{f}$ fermions in single level systems within a suitable approximation scheme, the proper Kondo features at and away from the symmetric point were obtained. We will opt by this simpler route and tackle the problem of Kondo physics in the next chapter.

2.6 The spherical limit approximation

For quantitative predictions about these cotunnelling processes one can resort to Quantum Montecarlo calculations of $\mathcal{G}_{\Delta\tau}$ using (2.65), which can be rather costly at low temperatures. For example, using (2.77) one correctly recovers the perturbative result that $g \propto T^2$ in a metallic grain, since $\mathcal{G}_{\Delta\tau} \sim 1/\Delta\tau$ at long $\Delta\tau$'s and low temperatures T.

Some analytical finite temperature attacks are possible on this problem using what is called the 'spherical limit approximation'. The essential difficulty in the phase-only action

$$S = \int \frac{1}{4E_C} (\partial_\tau \phi_\tau)^2 + \alpha \int K_{\tau\tau'} \left[1 - \cos(\phi_\tau - \phi_{\tau'})\right] \tag{2.81}$$

is the nonlinear nature of the dissipation term, the cosine. Therefore the tactic will be to somehow reduce the action to a quadratic form while keeping some flavor of the original cosine (other approaches, each with their own limitations, are also possible, see e.g. [23].) An exact transformation that can be performed is to define the complex field

$$\chi_\tau = e^{i\phi_\tau} \tag{2.82}$$

$$\cos(\phi_\tau - \phi_{\tau'}) = \frac{1}{2}\left(\chi^+_\tau \chi_{\tau'} + \chi^+_{\tau'}\chi_\tau\right) \tag{2.83}$$

$$(\partial_\tau \phi_\tau)^2 = \partial_\tau \chi^+_\tau \partial_\tau \chi_\tau \tag{2.84}$$

and then write

$$\begin{aligned} Z = & \int \mathcal{D}[\chi\chi^+]\delta(|\chi_\tau|^2 - 1) \\ & \times \exp\left\{ - \left[\int \frac{1}{4E_C} |\partial_\tau \chi_\tau|^2 + \alpha \int K_{\tau\tau'}(1-\delta_{\tau\tau'})\left(1 - \Re\{\chi_\tau \chi^+_{\tau'}\}\right) \right] \right\} \end{aligned} \tag{2.85}$$

This kind of model is known as a non-linear sigma model for historical reasons (creatures like these were born in the fires of nuclear physics, when folk used something similar to describe the pi-sigma meson decay). Note the delta function constraint (before the exponential) on the modulus of complex field χ. This makes (2.85) mathematically identical to (2.65), the action looks gaussian, but the constraint is what makes the evaluation of Z just as difficult as before. The constraint enables us also to introduce the $(1 - \delta_{\tau\tau'})$ term in the action for later convenience, since the extra term $K_0|\chi_\tau|$ will be a constant (albeit possibly unbounded).

Despite the ugly aspect of the modulus constraint some progress is possible. Using the functional integral representation of the delta function one can rewrite (2.85) as

$$\int \mathcal{D}[\lambda\chi\chi^+] \exp\left[-S - i\int \lambda_\tau \left(|\chi_\tau|^2 - 1\right)\right] \tag{2.86}$$

and use as a first approximation the saddle point solution for λ_τ, similar to what we did for $\tilde{V_0}$. One must assume a certain path $\lambda_\tau = -i\bar{\lambda}_\tau$ of the field and then minimize the free energy (which now depends on $\bar{\lambda}_\tau$) with respect to fluctuations of that saddle point solution. Therefore the equation for $\bar{\lambda}_\tau$ is

$$\frac{\delta F[\bar{\lambda}_\tau]}{\delta\bar{\lambda}_\tau} = -\frac{1}{\beta Z}\frac{\delta Z}{\delta\bar{\lambda}_\tau} = -\frac{1}{\beta}\langle|\chi_\tau|^2 - 1\rangle_{\bar{\lambda}_\tau} = 0 \tag{2.87}$$

Since S is symmetric under time shifts, $\bar{\lambda}$ will be τ-independent, and real, and will adjust to satisfy $\langle|\chi_\tau|^2\rangle_{\bar{\lambda}_\tau} = 1$. In this approximation then the action, including the Lagrange multiplier, can be approximated as

$$S = \frac{1}{\gamma_{\rm M}}\sum_{\omega_n}\left(\frac{\omega_n^2}{4E_C} + \alpha(K_0 - K_{\omega_n}) + \bar{\lambda}\right)\chi^+_{\omega_n}\chi_{\omega_n} \tag{2.88}$$

where the substraction of $K_0 = K_{\omega_0}$ from K_{ω_n} is a necessary regularization of the otherwise divergent dissipative kernel in the spherical approximation. This is the reason why we introduced the innocuous $(1 - \delta_{\tau\tau'})$ before the saddle point. Another maybe simpler way to do it would have been to redefine $\bar{\lambda}$ by subtracting the constant K_0 from it. Sticking to our formulation, and changing from $\bar{\lambda}$ to simply λ in what follows, λ should be adjusted to satisfy

$$\mathcal{G}_{\Delta\tau=0} = \langle|\chi_\tau|^2\rangle_\lambda = \frac{1}{\beta}\sum_{\omega_n}\frac{\gamma_{\rm M}}{\frac{\omega_n^2}{4E_C} + \alpha(K_0 - K_{\omega_n}) + \lambda} = 1 \tag{2.89}$$

The parameter $\gamma_{\rm M}$ was introduced in (2.88) to correct for the fact that χ is now a complex field with a double amount of degrees of freedom, and should be adjusted to give $\mathcal{G}'_{\Delta\tau=0} = -\beta E_C$, which gives

$$\gamma_{\rm M} = \frac{1}{2} \tag{2.90}$$

See below for details on this correction factor.

To finish note that $\mathcal{G}_{i\omega_n}$ becomes

$$\langle\chi^+_{\omega_n}\chi_{\omega_n}\rangle = \mathcal{G}_{i\omega_n} = \frac{1/2}{\frac{\omega_n^2}{4E_C} + \alpha(K_0 - K_{\omega_n}) + \lambda} \tag{2.91}$$

We will also comment in passing how this picture should be modified in order to include gate voltage effects. For a metallic grain with smooth density of states over scales μ_g, the saddle point solution for $\delta\mu$ as it appears in eq. (2.55) is again derived as in the toy model from (2.35) to give $\delta n = \mathcal{O}(n_G)^2$, or $\delta n = \mathcal{O}(n_G)^3$ if the non-interacting density of

states is particle-hole symmetric. This introduces a new term in $\mathcal{G}_{i\omega_n}$. The modified $\mathcal{G}_{i\omega_n}$ reads, with the corresponding $\gamma_{\rm M}$ correction

$$\langle \chi^+_{\omega_n}\chi_{\omega_n}\rangle = \mathcal{G}_{i\omega_n} = \frac{1/2}{\frac{\omega_n^2}{4E_C} + \alpha(K_0 - K_{\omega_n}) - i\omega(\delta n + n_G) + \lambda} \tag{2.92}$$

This correctly reproduces the position of the poles in the real ω axis for zero α, which denotes the particle and hole excitation energies in the presence of a gate voltage. Two poles appear (one for particle, one for hole excitations) at positions $\omega = E_C(2n_G \pm 1)$, as corresponds to a $E_C(Q - n_g)^2$ dispersion, see (2.1).

The atomic limit and the value of $\gamma_{\rm M}$

Technically speaking, the saddle point approximation becomes exact if one generalizes the non-linear sigma model from one complex scalar field χ_τ of modulus unity to an M-dimensional complex vector field $\vec{\chi}_\tau$, so that $|\vec{\chi}_\tau|^2 = \sum_i^M |\chi_{i\tau}|^2 = 1$, with very large M. Indeed, in this limit the central limit theorem states that fluctuations around $|\vec{\chi}_\tau|^2 = 1$ will vanish as $1/M$, so that fixing the average automatically imposes an exact constraint on the field at all times τ. Some readers however might find this M-component model generalization rather contrived, which is ok, since in reality one should really only worry about the physical $M = 2$ case, for which the 'spherical limit' is just a saddle point approximation, of the same class as the one we performed on $\tilde{V}_0$.

However simply taking $M = 2$ in the model yields a wrong result for various observables in the atomic limit. This is the reason why $\gamma_{\rm M}$ was introduced in (2.85). The criterion is to choose $\gamma_{\rm M}$, together with λ to give the best possible fit at low temperatures of the following exact result in the atomic limit [9]

$$\begin{aligned} G_{\tau-\tau'} &\overset{\alpha=0}{=} e^{-\frac{1}{2}\langle(\phi_\tau - \phi_{\tau'})^2\rangle} = \exp\left[-\frac{2E_C}{\beta}\sum_{\omega_n\neq 0}\frac{1-\cos\omega_n\Delta\tau}{\omega_n^2}\right] \\ &= \exp\left[-E_C|\Delta\tau|\left(1-\frac{|\Delta\tau|}{\beta}\right)\right] \end{aligned} \tag{2.93}$$

which essentially reduces to the following two atomic limit conditions on λ and $\gamma_{\rm M}$

$$\mathcal{G}_{\Delta\tau=0} = 1 \tag{2.94}$$

$$\partial_{\Delta\tau}\mathcal{G}_{\Delta\tau=0} = -E_C \tag{2.95}$$

In the atomic limit the spherical limit $\mathcal{G}_{\Delta\tau}$ evaluates to

$$\mathcal{G}_{\tau-\tau'} \overset{\alpha=0}{=} \frac{\gamma_{\rm M}}{\beta}\sum_{\omega_n}\frac{\cos\omega_n\Delta\tau}{\frac{\omega_n^2}{4E_C} + \frac{E_C}{4}} = 2\gamma_{\rm M}\frac{E_C}{E_C^*}\frac{e^{-\beta E_C^*\frac{|\Delta\tau|}{\beta}} + e^{-\beta E_C^*(1-\frac{|\Delta\tau|}{\beta})}}{1-e^{-\beta E_C^*}} \tag{2.96}$$

[9] The details of this computation involves going over to the zero winding number decomposition eq. (2.21) and then averaging also the winding numbers, which have weight $e^{-\pi^2 m^2/\beta E_C}$. This gives rise to the $\omega_n \neq 0$ constraint. See also footnote in 2.5.2

where E_C^* is defined as $E_C^* = \sqrt{4\lambda E_C}$, but see also later for a more physical discussion of this energy scale. From this and eq. (2.95) it is easy to demonstrate that $\gamma_{\rm M} = 1/2$ for any value of βE_C, as stated in eq. (2.90). While (2.95) is true in the atomic limit, (2.94), or equivalently eq. (2.89), is a completely general constraint, and arises from the definition of $\mathcal{G}$ itself, so it should hold even away from the atomic limit. The particular atomic limit solution for λ in the atomic limit is already non-trivial

$$\frac{\lambda}{E_C} \overset{\alpha=0}{=} \frac{\coth^2\left(\beta E_C\sqrt{\frac{\lambda}{E_C}}\right)}{4} \overset{\beta E_C>2}{\approx} \frac{1}{4} \tag{2.97}$$

but it admits the approximate solution $\lambda = 1/4$, or alternatively $E_C^* = E_C$ for $\beta E_C \gtrsim 2$ in the present $\alpha = 0$ case. See Fig. 2.9 for the $\alpha > 0$ case.

2.6.1 Range of validity of the spherical limit

The extreme spherical limit approximation on the non-linear sigma model breaks several key features of the original model, so that its usefulness gets reduced to a qualitative level. The main feature is the destruction of 'instanton' solutions [16] of the original action (2.85),(2.81). In imaginary time these are closed paths in τ so that the phase winds a finite number of times around the unit circle, while remaining minimal action paths (classical). When the unity constraint in (2.85) is preserved exactly these stable saddle points of the action that can be used as expansion points (quantum fluctuations around instantons) in a semiclassical theory. But within the spherical approximation these are lost, leading to relative unreliability of the approximation for finite values of gate voltage, for example [29] [10]. Furthermore, the fact that even without instanton path contributions, fluctuations can take place out of the unit circle actually leads to only qualitative results for physical quantities, such as spectral properties.

To do a first diagnosis of the range of validity of the spherical limit approximation we can compare the physically meaningful rotor spectral function $\mathcal{A}_\omega$ to the exact one that can be computed in the atomic limit. This quantity contains all the interaction effects of Coulomb blockade in the rotor formulation, as will be shown later, so it is a fundamental object. By making use of the exact result eq. (2.93), and analytically continuing it to the real ω axis we can obtain the exact $\mathcal{A}_\omega = -\frac{1}{\pi}\Im\{\mathcal{G}_\omega^R\}$. Taking into account (2.92), in the spherical and $\alpha = 0$ limits the analytical continuation to the real ω axis is trivial, and we get

$$\mathcal{A}_\omega^{SL} \overset{\alpha=0}{=} \delta(\omega - \sqrt{4E_C\lambda}) - \delta(\omega + \sqrt{4E_C\lambda}) \tag{2.98}$$

where now only λ depends on temperature. Again the scale

$$E_C^* = \sqrt{4E_C\lambda} \tag{2.99}$$

appears. This scale, which is called the 'renormalized charging energy' will remain an essential physical quantity away from the atomic limit, where λ becomes strongly suppressed

[10] A possible improvement in this direction that we have not fully explored, but that seems promising, is to perform a spherical limit approximation only on the fluctuations around instantons, and do an approximate sum over all the winding number sectors. This remains work to be done.

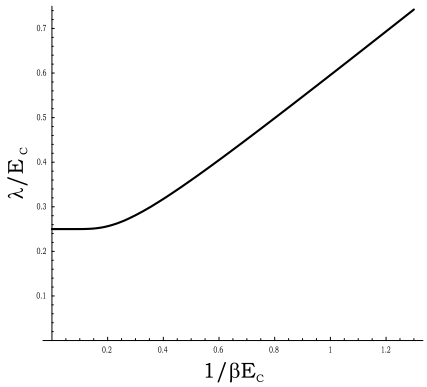

Figure 2.7: Numerical solution for λ in eq. (2.97). The position of the delta peaks in figure 2.8 at different values of βE_C are given by $\sqrt{4\lambda/E_C}$. Only values of $\beta E_C \gg 1$ are meaningful as to the energy of the rotor excitations, since these are widened out for $\beta E_C \sim 1$.

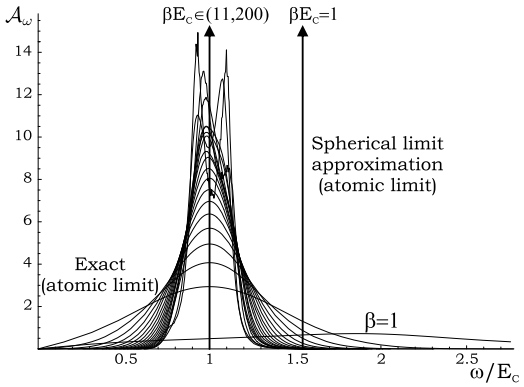

Figure 2.8: By doing a rational interpolation of the exact $\mathcal{G}_{i\omega_n}$ to the real axis we have obtained the exact rotor spectral function $\mathcal{A}_\omega$ in the atomic limit, ranging from $\beta E_C = 1$ to $\beta E_C = 200$ in steps of ten. The spherical limit on the other hand gives a delta function for $\mathcal{A}_\omega$ at a value that is roughly the 'center of mass' of the real spectral function.

from the $\alpha = 0$ value (2.97). This is the basic scale that characterizes interactions in the grain as expressed by the excitation peaks in the rotor spectral function $\mathcal{A}_\omega$. At low temperatures and $\alpha = 0$ we have demonstrated that $E_C^* = E_C$. We will delay the $\alpha > 0$ discussion of E_C^* as the effective charge gap to a later section.

In Fig. 2.8 we can appreciate the difference between the two approaches, the spherical limit and the non-linear sigma model in the $\alpha = 0$ case. We can conclude that the spherical limit is only a good approximation at low enough temperatures, $\beta E_C \gg 1$. Indeed, in the $\beta E_C \to \infty$ limit the spherical approximation in the atomic limit becomes exact, since the difference between (2.93) and (2.96) vanishes at low temperatures. This is only natural since in this limit the contribution of large series of instanton trajectories. [11]

2.6.2 Results for an infinite-band metallic grain

Let us perform some quantitative calculation of the cotunneling corrections within the spherical limit approximation. Beyond the atomic limit the computations with the original action (2.81) becomes untractable unless heavy weight techniques like Montecarlo are brought into play, so this is when the approximate analytical approaches like the spherical limit can be really useful.

Let us then take the case of a metallic grain with an unbounded smooth band.

[11] A warning for the reader familiar with the field: a definition of E_C^* as $E_C^* = \partial_{n_G}^2 F/2$ as is common in the literature is hopeless in the spherical limit approximation, and seems to give a different value from the above definition. We don't fully understand the reason for this inconsistency, but we suspect it is related to the fact that $E_C^* = \partial_{n_G}^2 F/2$ is related to the dispersion of winding numbers, which have vanished in the spherical limit formulation.

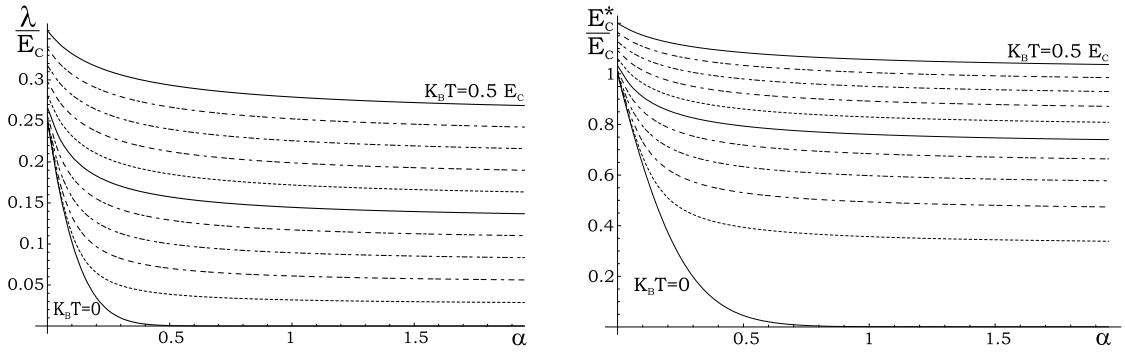

Figure 2.9: To the left, the parameter λ as a function of dimensionless coupling of the grain to the leads within the large-N spherical limit approximation. To the right, the renormalized charging energy $E_C^* = \sqrt{4E_C\lambda}$ is the energy of the rotor excitations for finite coupling α to the leads, which gives information about the full electronic spectral function. This interpretation is meaningful only for $\beta E_C \gg 1$, see Fig. 2.8. The result is essentially non-perturbative, note the exponential decay at zero temperatures, eq. (2.103). The different curves correspond to evenly spaced temperatures from zero to $K_BT = 0.5E_C$.

Using (2.68) at finite temperature we obtain

$$K_0 - K_{\omega_n} = \int_0^\beta d\tau \,(1-\cos(\omega_n\tau))\,\frac{(\pi/\beta)^2}{\sin^2(\pi\tau/\beta)} = \pi|\,\omega_n| \tag{2.100}$$

Now, in the zero temperature limit, equation (2.89) takes the form

$$\begin{aligned}\langle|\chi_\tau|^2\rangle &= \int\frac{d\omega}{2\pi}\frac{1/2}{\frac{\omega^2}{4E_C}+\alpha\pi|\,\omega|+\lambda} = \frac{1}{\pi^2\alpha}\frac{\arctan\sqrt{\frac{\lambda/E_C}{\pi^2\alpha^2}-1}}{\sqrt{\frac{\lambda/E_C}{\pi^2\alpha^2}-1}}\\ &= \frac{1}{2\pi^2\alpha}\log\frac{4\pi^2\alpha^2}{\lambda/E_C}+\mathcal{O}[\frac{1}{\alpha}]^3 = 1\end{aligned} \tag{2.101}$$

From this equation it follows that at zero temperature and strong coupling α one obtains an exponentially suppressed λ

$$\lambda \overset{T=0}{\approx} 4\pi^2\alpha^2 e^{-2\pi^2\alpha}E_C = \frac{1}{4}\frac{{E_C^*}^2}{E_C} \tag{2.102}$$

$$E_C^* \overset{T=0}{\approx} 4\pi\alpha\; e^{-\pi^2\alpha}E_C \tag{2.103}$$

Except for a factor two in the exponential this is the type of result one obtains from various other techniques [43, 87, 96] [12]. At finite temperatures and strong couplings we obtain the asymptotic solution $\lambda \approx 1/\beta$ instead, although as mentioned in the previous section in this limit our approximation is really poor, and λ loses its meaning. An exact numerical solution for the whole range of parameters can be however found in Fig. (2.9).

[12] Although the exponential decay is already a strong non-perturbative result, probably a more careful inclusion of sum over instantons plus spherical limit fluctuations would yield the correct exponent, which (unlike the prefactor) is a well established property. This however remains also work to be done.

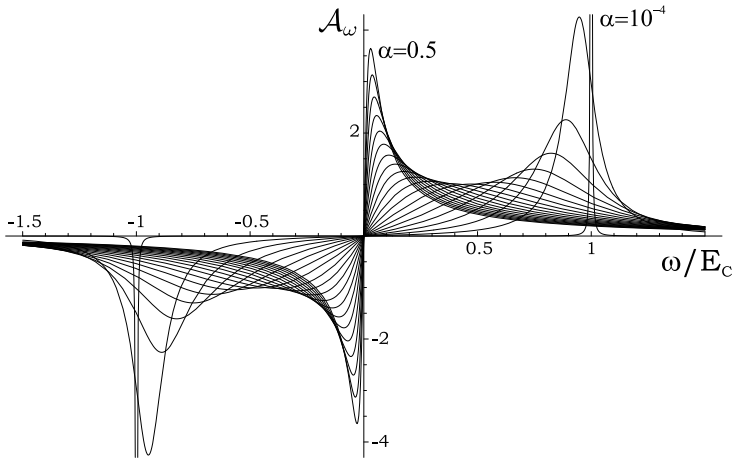

Figure 2.10: The quantum rotor spectral function in the large-N and spherical limit for evenly spaced values of dimensionless conductance α at zero temperature. The position of the peak corresponds to $\pm E_C^*(\alpha)$.

Spectral functions in the real axis. Renormalized charging energy.

We will now return to the analysis of the renormalized charging energy at finite grain-lead coupling α. Such finite rotor dissipation should effectively delocalize electronic charge (and order phase due to finite rotor friction), and therefore reduce effective charging energy E_C^*. This kind of arguments can also be traced by RG analysis, hence the name for E_C^*. To see how E_C^* still holds its meaning as the fundamental interaction scale let us obtain $\mathcal{A}_\omega$ for a finite α. This involves an analytical continuation of $\mathcal{G}_{i\omega_n}$ to the real axis. If we take the upper part of the complex plane and analytically continue $\mathcal{G}_{i\omega_n}$ with $\omega_n > 0$ we will obtain the retarded $\mathcal{G}_\omega^R$, see Appendix (A). Unlike for the case of the exact solution in the atomic limit described earlier, in the spherical limit this continuation is a trivial matter, since

$$\mathcal{G}_{i\omega_n} = \frac{1/2}{\frac{\omega_n^2}{4E_C} + \alpha\pi|\omega| + \lambda} \tag{2.104}$$

is perfectly analytical in the upper complex plane. We obtain

$$\mathcal{A}_\omega = -\frac{1}{\pi}\Im\{\mathcal{G}_\omega\} = \frac{\alpha\omega/2}{(\frac{\omega^2}{4E_C} - \lambda)^2 + (\alpha\pi\omega)^2} \tag{2.105}$$

A pictorial representation of $\mathcal{A}_\omega$ can be found in Fig. 2.10. One can appreciate that $\mathcal{A}_\omega$ will have a pair of peaks roughly at $\omega \approx \pm\sqrt{4E_C\lambda}$, representing rotor excitation energies, or effective interaction contribution to the excitation energy of the grain due to addition or substraction of a unit charge. Note that this value falls exponentially at low temperatures with increasing α, which is also proportional to the width of the peak.

With this it is possible to compute the spectral function of the electronic field

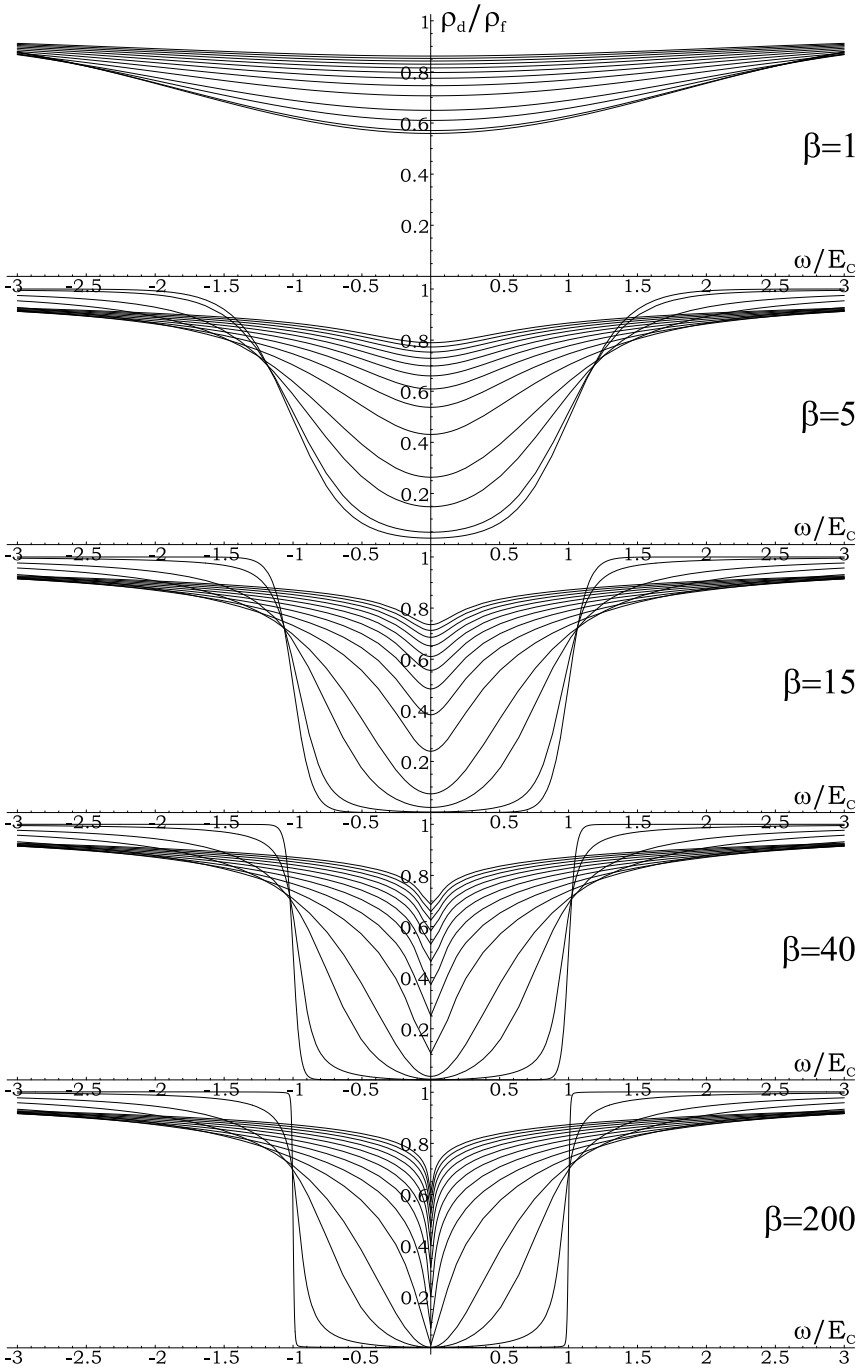

Figure 2.11: Electronic density of states in a metallic grain with charging energy E_C for different temperatures and different values of the grain-lead coupling. From bottom to top, $\alpha = \{0, 0.01, 0.05, 0.1, 0.2, 0.3, 0.4, 0.5, 0.6, 0.7, 0.8, 0.9, 1\}$. The computation was performed in the large-N spherical limit approximation. The density of states is normalized to that of the non-interacting grain, ρ_f. Note that the Coulomb blockade gap gets reduced with increasing α, as suggested by the scale E_C^* in $\mathcal{A}_\omega$, see Fig. 2.10. The validity of the approximation breaks down for $\beta \lesssim 2$.

itself. From (B.4) and (A.17) we can relate $\mathbf{A}^{\mathbf{d}}_{\omega}$ to $\mathbf{A}_{\omega}$ and $\mathcal{A}_{\omega}$,

$$\mathbf{A^d}_{\omega} = \int_{-\infty}^{\infty} d\omega' \frac{1 - f^{+}_{\omega-\omega'}}{1 - f^{+}_{\omega}} \left(1 - f^{-}_{\omega'}\right) \mathbf{A}_{\omega-\omega'} \mathcal{A}_{\omega'} \tag{2.106}$$

which at zero temperature is equal to

$$\mathbf{A^d}_{\omega} = \int_{0}^{\omega} d\omega' \mathbf{A}_{\omega-\omega'} \mathcal{A}_{\omega'} \tag{2.107}$$

Considering, as we are doing in this section, a constant fermionic density of states $\rho_f = \mathrm{Tr}\{\mathbf{A}_{\omega}\}$ we can perform the integral for arbitrary βE_C and coupling α. The results can be found in Fig. 2.11 for the quantity ρ_d/ρ_f at different temperatures and couplings.

Conductance and cotunneling

Our initial motivation in this section was to check if the present model recovers the first quantum correction to the sequential tunneling approach, namely cotunneling conductance, which is known by perturbation theory to go like $g \sim T^2$. One could try to use the results in Appendix B for this. Let us see what we get. In the low temperature, large τ and arbitrary α limit we have

$$\mathcal{G}_{\Delta\tau} = \int_{-\infty}^{\infty} \frac{d\omega}{2\pi} \frac{\cos(\omega\Delta\tau)/2}{\frac{\omega^2}{4E_C} + \alpha\pi|\,\omega| + \lambda} \approx \frac{\alpha/2}{(\lambda\Delta\tau)^2} \tag{2.108}$$

Note that a finite $\lambda = \frac{1}{4}\left(\frac{E_C^*}{E_C}\right)^2 E_C$ is not a conventional mass term in that it is always accompanied by the non-analytical piece $\alpha\pi|\,\omega|$, hence the algebraic instead of exponential decay of $\mathcal{G}_{\Delta\tau}$ for $\Delta\tau \to \infty$.

Let us now try to obtain the conductance. If we simply apply the expansion of $D_{\beta/2}[\beta\partial_{\Delta\tau}]$ on $\mathcal{G}_{\Delta\tau}$ in equation (2.77) we obtain a non-convergent series, so this method proves to be quite useless in this case. However an intermediate step that led to it, eq. (B.11), together with (A.17), will do the trick. For $\bar{\tau} = \beta/2$ (B.11) takes the form

$$g = 2g_{\infty} \int_{0}^{\infty} d\omega \frac{\beta\omega}{\cosh(\beta\omega) - 1} \mathcal{A}_{\omega} \tag{2.109}$$

Since, by (A.23) $\mathcal{A}_{\omega}$ at zero temperature is the inverse Laplace transform of (2.108) we have for small ω that

$$\mathcal{A}_{\omega} = \frac{\alpha\omega}{2\lambda^2} \tag{2.110}$$

see also Fig. 2.10. Therefore we conclude that within this approximation the metallic grain has a low temperature conductance that goes like $\sim T^2$

$$g = g_{\infty} \frac{2\pi^2}{3} \alpha \left(\frac{K_B T}{\lambda}\right)^2 \tag{2.111}$$

The constant g_{∞} is the conductance in the absence of charging effects, i.e. the hight temperature conductance. This result is consistent with the second order perturbation

theory one for cotunneling, except that instead of the bare charging energy E_C we get λ.[13] This result is clearly non-perturbative in the hopping amplitude, i.e. in α, which proves that infinite resummation of perturbation expansions preserves cotunneling, and merely corrects the amplitude of such processes.

Since the features obtained in the case of the single-level quantum dot are quite off the mark, see section 2.5.4, we will delay the discussion of such systems to the next chapter.

2.7 Summary

In this chapter we have given a detailed presentation of the quantum rotor description of charging effects in nanostructures. It can be summarized as the study of the effective dynamics of the total charge of the system, or alternatively of its conjugate, the total phase. Within the large-N approximation, valid in general for metallic grains with many channel contacts, an effective action can be derived governing the system phase without resorting to the details of fermionic excitations. Interestingly enough, the resulting action is closely resembles quantum dissipation models of open systems [24, 62]. Unlike in superconducting system however the gauge symmetry in such action is not broken, but the phase fluctuations encoded in the propagator $\mathcal{G}_{\Delta\tau}$ are still a valuable source of physical information, and they can be employed to derive all necessary physical propagators within the large-N limit. We have shown how this provides a framework to study the renormalization of the Coulomb blockade physics of metallic grains that become strongly coupled to their environment. However this is achieved by the large-N trick, which effectively neglects any contributions from higher-than-cotunneling order in the hopping. Therefore, although proper renormalization of the Coulomb gap and low temperature conductance is achieved, more strongly non-perturbative phenomena relevant to systems with few levels such as Kondo resonance are lost.

We have also discussed an approximate scheme that is useful in performing analytical computations of these phase fluctuations, the spherical approximation method. We have shown how it is enough to recover at least all the major qualitative features of Coulomb blockade, including the renormalization of the charging energy, the conductance, and the real-frequency electronic spectral function. This method is not restricted to the large-N approximation that leads to the phase only approach, and will be fruitfully employed in the following chapters.

[13] Note that cotunneling features (virtual-state mediated processes) seem to be governed by the energy scale λ, which appears as the low frequency scale in $\mathcal{A}_\omega$, while the *real* excitations, given by the high energy peaks in $\mathcal{A}_\omega$, such as the effective Coulomb blockade gap are governed by E_C^*. Both are non-perturbative results, but agree with perturbative analysis when α is small (and therefore $\lambda \approx 2E_C$).

Chapter 3

The Slave Rotor approach to Coulomb Blockade and Kondo

3.1 Joint fermion-phase action and NCA decoupling

The subject of this chapter is a natural extension of the description developed in chapter 2, aimed at improving some of the shortcomings of the quantum rotor description of interacting metallic grains and quantum dots, namely the failure to describe phenomena such as Kondo physics, which is related to spin-flip processes and fermionic character of charge carriers.

It was argued that the N-degenerate fermion fields $\mathbf{f}$ were only relevant as a retarded dissipative bath for the phase of the interacting system if N is very large. In diagrammatic language this can be restated by saying all phase-phase propagator one-particle irreducible diagrams from eq. (2.57) involving $m > 1$ internal sums over channel index will be suppressed at least as $1/N^{m-1}$ due to the necessary number of t^2 fermion-phase vertices involved (recall that $t^2 \sim 1/N$).

In order to retain spin-flip processes we must avoid taking this limit. We will therefore take up (2.57) as our new starting point, which we reproduce here,

$$S = \int -\mathbf{f}_\tau^+ \mathbf{G}^{-\mathbf{1}}_{\mathbf{0}\tau\tau'} \mathbf{f}_{\tau'} + \frac{1}{4E_C} \left(\partial_\tau \phi_\tau\right)^2 + \int \mathbf{f}_\tau^+ \mathbf{\Delta}_{\tau\tau'} \mathbf{f}_{\tau'} \cos(\phi_\tau - \phi_{\tau'}) \tag{3.1}$$

This fermion-phase action will also be denoted by the Slave Rotor model. The reason is that eq. (3.1) is closely reminiscent of the slave boson technique with lead electrons integrated out, whereby a new field b is introduced and coupled to non-interacting pseudofermions $\mathbf{f}$ and lead electrons $\mathbf{c}$, so that creating a boson $b^+|0\rangle$ symbolizes the substraction of one charge unit from the total charge. The 'projection constraint' $b^+b + \mathbf{f}^+\mathbf{f} = 1$ is perfectly analogous to the integration of field $\tilde{V}_0$ as was described in 2.3.3. However the slave boson technique with one slave boson only takes into account the possibility of excitations with extra total charge $|\Delta Q| = \{0, 1\}$, or in other words the asymmetric $E_C \to \infty$ limit. This is a limitation that has been partially addressed in later work, see e.g. [45] introduction of a second slave boson. The slave rotor model does without this limitation by construction, since ϕ is the conjugate variable of the real ΔQ.

3.1.1 Non crossing approximation

To make progress with the non-linear coupled action (3.1) and retain some of its non-perturbative virtues we propose to proceed by a self-consistent decoupling, formally quite similar to mean field approaches, known generally as the Non Crossing Approximation (NCA). In practice it transforms (3.1) into

$$S = \int -\mathbf{f}^+_\tau \mathbf{G}^{-\mathbf{1}}_{\mathbf{0}\tau\tau'} \mathbf{f}_{\tau'} + \frac{1}{4E_C} \left(\partial_\tau \phi_\tau\right)^2 + \int \langle \mathbf{f}^+_\tau \mathbf{\Delta}_{\tau\tau'} \mathbf{f}_{\tau'} \rangle \cos(\phi_\tau - \phi_{\tau'}) + \mathbf{f}^+_\tau \mathbf{\Delta}_{\tau\tau'} \mathbf{f}_{\tau'} \langle \cos(\phi_\tau - \phi_{\tau'}) \rangle \tag{3.2}$$

This approximation goes far beyond the lowest-order perturbative result that led to the phase-only action (2.81) and is the central pivot for the work to follow in the present chapter. Its distinctive feature is the decoupling of fermionic and phase degrees of freedom, whose joint dynamics is nevertheless determined self-consistently. Indeed, the fermionic self-energy obviously depends on the phase-phase correlator $\mathcal{G}_\tau$ and reciprocally. Moreover, the bosonic part of the effective action (3.2) is similar in structure to the phase-only approach (2.81), allowing to use the large body of work on this particular model, including the spherical limit techniques developed in the previous chapter.

As to the formal developments that lead to this kind of approximations (NCA) we will briefly mention that they become exact at least at *subleading* order in the Large-N expansion, which will prove enough to correct the deficiencies of the phase-only approach. Moreover the NCA techniques are founded on very solid developments [15] that were spurred by the need to form a perturbative scheme for many body systems that preserved all sum-rules and conservation laws at each level of approximation. The resulting formalism relies on the Ward-Luttinger potential Φ formed of closed vacuum-vacuum bubble skeleton diagrams, the functional derivatives of which give the self energies one should use to make the perturbative approximation 'conserving'. The present approximation corresponds to the expansion of the Ward-Luttinger potential to lower order, with no vertex corrections, which is generally known by the Non-crossing approximation name.

It is useful to consider the NCA action (3.2) as a the sum of a fermion-only plus a phase only action with self-consistent self energies, as follows

$$S_\phi = \int \frac{1}{4E_C} \left(\partial_\tau \phi_\tau\right)^2 + \alpha K_{\tau\tau'} \left[1 - \cos(\phi_\tau - \phi_{\tau'})\right] \tag{3.3}$$

$$S_f = - \int \mathbf{f}^+_\tau \left(\mathbf{G}_{\mathbf{0}}{}^{-1}_{\tau\tau'} - \mathbf{\Sigma}_{\tau\tau'}\right) \mathbf{f}_{\tau'} \tag{3.4}$$

$$K_{\Delta\tau} = -\frac{1}{\alpha} \mathrm{Tr}\left[\mathbf{\Delta}_{\Delta\tau} \mathbf{G}_{-\Delta\tau}\right] = -\frac{1}{\alpha} \mathrm{Tr}\left[\mathbf{G}_{-\Delta\tau} \mathbf{t} \bar{\mathbf{G}}_{\Delta\tau} \mathbf{t}^+\right] \tag{3.5}$$

$$\mathbf{\Sigma}_{\Delta\tau} = \mathcal{G}_{\Delta\tau} \mathbf{\Delta}_{\Delta\tau} \tag{3.6}$$

We refer the reader back to 2.4 for notation conventions. Looking back at eq. (2.62) and comparing it to eq. (3.5) the reader can appreciate the precise self-consistent nature of the NCA approximation in contrast with the phase-only approach. The NCA dissipative kernel (3.5) for the phase contains the dressed fermionic Green's function, which includes self energy $\mathbf{\Sigma}$, while (2.62) uses the unperturbed $\mathbf{G_0}$ instead. Note that we have changed our notation respect to the previous chapter, where $\mathbf{G}$ stood for the *bare* propagator. The

relation between the two is established by the imaginary time version of Dyson's equation

$$\mathbf{G}_{i\omega_n} = \left(\mathbf{G}^{-1}_{\mathbf{0}i\omega_n} - \mathbf{\Sigma}_{i\omega_n}\right)^{-1} = \mathbf{G_0} + \mathbf{G_0\Sigma G_0} + \mathbf{G_0\Sigma G_0\Sigma G_0} + \ldots|_{i\omega_n} \tag{3.7}$$

$$\mathbf{G}_{\mathbf{0}i\omega_n} = \delta_{ss'}\delta_{\alpha\alpha'}\sum_{\alpha}\frac{1}{i\omega_n - \epsilon_\alpha + \delta\mu - \mu_g} \tag{3.8}$$

Therefore taking $\mathbf{\Sigma} = 0$ here would recover the phase-only action exactly. As expected, this is the case in the large-N limit, in which the Slave Rotor method reduces to the Quantum Rotor method, as we will see below.

The local hopping approximation

Although the computation of $\mathbf{G}$ involves only a matrix inversion for a generic hopping matrix $\mathbf{t} = \delta_{\mathbf{ss'}}\mathbf{t}_{\alpha\mathbf{k}}$, it becomes especially clean in the physically meaningful local hopping approximation that we used all through the phase-only approach, whereby $t_{\alpha k} = t$ is a constant. In such case neither $\mathbf{\Delta} = \delta_{ss'}\Delta$ nor $\mathbf{\Sigma} = \delta_{ss'}\Sigma$ depend on the grain quantum numbers (except on the degenerate channel index s, in which they are diagonal like everything else).

$$\Sigma_{\Delta\tau} = \mathcal{G}_{\Delta\tau}\Delta_{\Delta\tau} \tag{3.9}$$

$$\Delta_{i\omega_n} = L\sum_k \frac{t^2}{i\omega_n - \epsilon_k} \tag{3.10}$$

$$\Delta_{\Delta\tau} = L\rho_l(0)t^2\frac{\pi/\beta}{\sin[\pi\Delta\tau/\beta]} \tag{3.11}$$

(Remember that ϵ_k are the lead energies, and L is the number of identical leads coupled to the grain). In this case (3.5) can be simplified to

$$\alpha K_{\Delta\tau} = -\mathrm{Tr}\left[\mathbf{\Delta}_{\Delta\tau}\mathbf{G}_{-\Delta\tau}\right] = -\Delta_{\Delta\tau}\sum_{\alpha\alpha'}G_{-\Delta\tau\alpha\alpha'} = -NN_L\Delta_{\Delta\tau}G^{\mathrm{loc}}_{-\Delta\tau} \tag{3.12}$$

where the local propagators and self-energies at site position x_0 where electrons hop are defined as follows[1]

$$G^{\mathrm{loc}}_{i\omega_n} = \frac{1}{NN_L}\sum_{s\alpha\alpha'}G_{i\omega_n s\alpha\alpha'} = \left[{G^{\mathrm{loc}}_{0i\omega_n}}^{-1} - \Sigma^{\mathrm{loc}}_{i\omega_n}\right]^{-1} \tag{3.13}$$

$$\begin{aligned} G^{\mathrm{loc}}_{0i\omega_n} &= \frac{1}{NN_L}\sum_{s\alpha\alpha'}G_{0i\omega_n s\alpha\alpha'} = \frac{1}{N_L}\mathrm{Tr}_\alpha[\mathbf{G}_{0i\omega_n}] \\ &= \frac{1}{N_L}\sum_{\alpha}\frac{1}{i\omega_n - \epsilon_\alpha + \delta\mu - \mu_g} \end{aligned} \tag{3.14}$$

$$\Sigma^{\mathrm{loc}}_{\Delta\tau} = N_L\Sigma_{\Delta\tau} = N_L\Delta_{\Delta\tau}\mathcal{G}_{\Delta\tau} \tag{3.15}$$

Equation (3.13) and (3.15) follow from (3.7) in the local hopping approximation, since then, summing in α, α' in the Dyson equation (diagonal in channel index) and dividing by N_L

[1] Note that, unlike $\mathbf{G}$, $\mathbf{G_0}$ is diagonal in index α.

we get $G^{\rm loc}_{i\omega_n} = {\rm Tr}_\alpha[\frac{\mathbf{G}_0}{N_L}] + {\rm Tr}_\alpha[\frac{\mathbf{G}_0}{N_L}](N_L\Sigma){\rm Tr}_\alpha[\frac{\mathbf{G}_0}{N_L}] + \ldots$, where ${\rm Tr}_\alpha$ is the trace over orbital quantum numbers α. The integer N_L stands for the total number of such orbitals in the grain/dot.

Equations (3.11) through (3.15) constitute the self consistent cycle of the Slave Rotor method. Assuming one can calculate $\mathcal{G}_{\Delta\tau}$ for a given kernel $\alpha K_{\Delta\tau}$ one simply starts with an ansatz seed, e.g. $\mathcal{G}_{\Delta\tau} = 1$, plugs it into (3.15), Fourier transforms to $i\omega_n$, calculates $G^{\rm loc}_{i\omega_n}$ with (3.13), Fourier transforms back to $G^{\rm loc}_{\Delta\tau}$, computes the new kernel with (3.12) and finally updates the initial $\mathcal{G}_{\Delta\tau}$ by using the new kernel. Repeating this cycle until (and if) self consistency is reached one obtains all the desired local dressed correlators, which correspond to an infinite resumation of all subleading order diagrams in the large-N perturbative expansion. Non-local matrix correlators like $\mathbf{G}$ can be computed from this solution by means of Dyson's equation (3.7).

3.1.2 General results

Without performing further approximations one can extract valuable conclusions from the slave rotor formalism.

As we mentioned above, in the large-N limit, valid for metallic grains with large contacts with many conserved channels, the present method predicts exactly the same results as the quantum rotor method described in the preceding chapter, i.e. Coulomb blockade at low temperatures with a renormalized charging energy scale E_C^* for the gap that gets exponentially reduced with increasing coupling α. To see this equivalence one must simply recall that the hopping in Δ gets scaled as $t^2 \sim 1/N$, so that $\Sigma^{\rm loc}$ vanishes in (3.13) for $N \to \infty$. Therefore $G^{\rm loc}$ becomes $G_0^{\rm loc}$ and one recovers $\alpha K_{\Delta\tau} = -{\rm Tr}[\mathbf{\Delta}_{\Delta\tau}\mathbf{G}_{\mathbf{0}-\Delta\tau}]$ of equation (2.62). This was expected, since in this $N \to \infty$ limit the phase only approach is exact.

A second conclusion refers to the finite N case, in particular to the case of a quantum dot with interlevel spacing $\delta E < K_B T < E_C$. This is the not-so-small temperature regime for a quantum dot with arbitrary number of channels and per-channel conductances. Previous works [32, 37, 78] found that no matter how open the quantum dot, unless full transparency is reached for a certain channel Coulomb blockade would persist at low temperatures. Their work dealt with $\delta E = 0$ situations, so this is the corresponding regime in our case. Their results are again confirmed by the present method. In this limit the first Matsubara frequency $i\omega_1$ is far enough from the real axis so as to make the following approximation for $G^{\rm loc}_{0i\omega}$ at low frequencies valid

$$G^{\rm loc}_{0i\omega} = \frac{1}{N_L}\sum_\alpha \frac{1}{i\omega_n - \epsilon_\alpha + \delta\mu - \mu_g} \approx -i\pi\rho_g(\delta\mu - \mu_g) \tag{3.16}$$

$\rho_g(\epsilon)$ is the grains average density of states at energy $\epsilon \pm K_B T$. As long as this is finite we have, at low frequencies

$$G^{\rm loc}_{i\omega_n} \approx \left(\frac{i}{\pi\rho_g(\delta\mu - \mu_g)} - \Sigma_{i\omega_n}\right)^{-1} \tag{3.17}$$

The finite imaginary part at $\omega = 0$ dominates the large time behavior in $G^{\rm loc}_{\Delta\tau}$, which becomes $\sim 1/\Delta\tau$ at long times upon Fourier transformation, so that $K_{\Delta\tau}$ on its part will decay as

$1/\Delta\tau^2$ at long times, low temperatures $\delta E < K_B T < E_C$. Kosterlitz RG arguments, as presented in 2.5.2, predict a disordered phase ground state $\mathcal{G}_{\Delta\tau} \sim e^{-E_C^* \Delta\tau}$, and therefore an insulating ground state (see section 2.6.2). In summary, for a quantum dot in the $\delta E < K_B T < E_C$ and arbitrary α, N regime, the slave rotor method predicts insulating ground state, very much like in the large-N limit metallic grain case, with a renormalized charging energy gap. More quantitative computations will be carried out later.

Further results, specifically about the onset of the Kondo resonance, will have to wait until we discuss the last step of the self-consistency cycle more quantitatively, namely the computation of $\mathcal{G}$ from the numerical $\alpha K_{\Delta\tau}$. We will do so in the next section.

3.2 Spherical limit of the slave rotor

As it stands in equations (3.11) through (3.15) the method is most precise, including all non-linear sigma model subtleties such as instanton saddle points, winding numbers, etc. However the computation of $\mathcal{G}$ in (3.11) from the kernel (3.12) requires numerical techniques such as Montecarlo methods. Although these methods are able to deal with the problem down to fairly low temperatures, they become extremely costly if the temperature is lowered too much. For this reason it is interesting to try other less precise methods such as the spherical limit method of section 2.6 in this case. Although the iterative nature of the slave rotor method is necessarily numerical, some analytical results can still be extracted upon taking the spherical limit, in particular non-perturbative Kondo temperature estimations or unitary limit of conductance at zero temperature.

The results of section 2.6 allow us to recast the slave rotor method in the following closed set of equations, which we give in the natural order in which a computer algorithm should make use of them

$$\Sigma^{\text{loc}}_{\Delta\tau} = N_L \Delta_{\Delta\tau} \mathcal{G}_{\Delta\tau} \tag{3.18}$$

$$G^{\text{loc}}_{i\omega_n} = \frac{1}{N_L}\sum_{\alpha\alpha'} G_{i\omega_n s\alpha\alpha'} = \left[\left(\frac{1}{N_L}\sum_{\alpha}\frac{1}{i\omega_n - \epsilon_\alpha}\right)^{-1} - \Sigma^{\text{loc}}_{i\omega_n}\right]^{-1} \tag{3.19}$$

$$\alpha K_{\Delta\tau} = -N N_L \Delta_{\Delta\tau} G^{\text{loc}}_{-\Delta\tau} = N N_L \Delta_{\Delta\tau} G^{\text{loc}}_{\beta-\Delta\tau} \tag{3.20}$$

$$\mathcal{G}_{i\omega_n} = \frac{1/2}{\frac{\omega_n^2}{4E_C} + \lambda + \alpha(K_0 - K_{i\omega_n})} \tag{3.21}$$

$$\mathcal{G}_{\Delta\tau=0} = 1 \quad \text{(fixes } \lambda\text{)} \tag{3.22}$$

In a practical calculation using this algorithm it is necessary also to take into account the large large energy cutoff in the lead electrons (the lead bandwidth W), which in turns cuts off the small $\Delta\tau$ divergence that would otherwise arise in $\Delta_{\Delta\tau}$. Therefore we will substitute (3.11) by the following kernel that corresponds to a elliptical lead density of states of total bandwidth W

$$\Delta_{i\omega_n} = -i\Gamma \frac{2/\omega}{1 + \sqrt{1 + \frac{W^2}{4\omega^2}}} \tag{3.23}$$

$$\Gamma = 2\pi t^2 \rho_l(0) \tag{3.24}$$

For comparison purposes bear in mind that in the case of a grain with a smooth density of states at the Fermi energy the parameter α of previous section is

$$\alpha = \frac{N}{\pi}\Gamma\rho_g(0) \tag{3.25}$$

3.2.1 Numerical implementation of the self-consistency algorithm

We have taken the $\mu_G = 0$ particle-hole symmetric case for simplicity. Otherwise one should have to add to this set the equation for $\delta\mu$, which is zero by symmetry here. These five equations should be supplemented by (3.11). Note also that Matsubara frequencies for $\mathcal{G}_{i\omega_n}$ should of course be bosonic, while for $G^{\rm loc}_{i\omega_n}$ they should be fermionic. The procedure to move between frequency and imaginary time representation involve Fast Fourier Transformations (FFT), but they were modified to take into account the discontinuity in $G^{\rm loc}_{\Delta\tau}$ and $\Delta_{\Delta\tau}$ at $\Delta\tau = 0$. If not dealt with properly this would introduce spurious frequencies in the FFT, which would make the algorithm suboptimal.

The final result of the loop is (luckily) a converged $G^{\rm loc}_{\Delta\tau}$ and $\mathcal{G}_{\Delta\tau}$. By using (2.67), which is still valid here with exactly the same arguments as before, we can obtain $G^{d\rm loc}_{\omega_n}$, which can the be analytically continued numerically to the real ω axis to obtain $G^{\mathbf{d}{\rm loc}R}_{\omega}$, and the local density of states at point x_0, $\rho^{\rm loc}_\omega \equiv A^{\mathbf{d}{\rm loc}}_\omega$. See appendix A for all the necessary relations.

The chosen method for analytical continuation was the symmetrical Padé rational interpolation algorithm, which fits the discrete points $G^{\mathbf{d}{\rm loc}}_{\omega_n}$ on the imaginary axis by a function $P_M(\omega)/Q_M(\omega)$, where P_M and Q_M are M-order polynomials whose coefficients are conveniently fitted by the data. M was taken to range from 10 to about 150 for the most complex cases, although it was found that increasing M very much didn't improve things. The algorithm was however robust enough for all the cases studied.

The convergence was achieved by a controlled annealing of the propagators, i.e. by updating them after each loop with a 'refresh factor' that was increased slowly as convergence was reached, in an adaptative fashion. This sort of 'accelerated convergence' scheme was quite crucial for the efficiency of the method.

The set of physical parameters that can be tuned at will in the algorithm comprise inverse temperature β, charging energy E_C, level width Γ, bath bandwidth W, the number of degenerate channels N and the complete non-interacting spectrum of the grain, the number N_L of levels and their distribution, including the possibility of a continuous band. The output of the algorithm can be set at will to give any of the quantities $\lambda, G^{\rm loc}_d$, the conductance ρ (following e.g. (B.6), or any other correlator in the algorithm.

As to performance and internal parameters, for temperatures as low as $\beta E_C \sim 1000$ the number of Matsubara frequencies that one should take into account is around $2^{14} = 16384$ to be on the safe side. Going down to $\beta E_C \sim 100$ sticking to $2^{12} = 4096$ is more than enough, and at this point the algorithm is very quick on a standard Pentium 4 machine. The algorithm was implemented in C++, and an alternative version of the code was ported to Mathematica with only a small loss in performance. Typical convergence times under Mathematica range from 7 seconds at $\beta E_C \sim 100$ to 26 seconds at $\beta E_C \sim 1000$ for some typical set of parameters.

3.3 Results with the NCA slave rotor method

We will use the NCA slave rotor method in the spherical limit in this section to analyze the effect of grain-lead coupling in metallic grains, the onset of the Kondo effect in single and multiple level quantum dots and the transition from the single level quantum dot regime ($\delta E \gg E_C$) to the metallic grain regime ($\delta E \ll E_C$). Highly non-perturbative physics is involved in these phenomena, although some analytical results exist. It will be a severe test for the present formalism, which as we will demonstrate is nevertheless able to capture all the relevant features one should expect, while providing a valuable interpolation tool between all these regimes.

Keep in mind, in light of the work done in previous sections, that the method becomes increasingly good in large N systems (good to order $1/N$ before spherical limit approximation) and at low temperatures $\beta E_C \gg 1$ (in order for the spherical limit plus saddle point to be precise). We will again restrict our analysis to the particle-hole symmetric case $\delta n = 0$ to simplify the discussion, although introduction of finite gate voltages would in principle be feasible. Despite the above restrictions the method will be able to easily deal temperatures of the order and above the Kondo temperature or the renormalized charging energy, just as slave boson NCA, while preserving the advantage of arbitrary number of charge states (ability to describe the effect of gate voltages) and finite E_C.

3.3.1 Coulomb blockade in a strongly coupled metallic grain

We assume a elliptical band of states in the grain, exactly equal to that of the lead for simplicity. We set both bandwidths to a large value $W = 100E_C$, since they play no role in the low energy physics. The local density of states at point x_0 where hopping occurs is $\rho_f^{\rm loc}(0) = 4/(\pi W)$. We will normalize the interacting density of states to this quantity just as we did in Fig. 2.11 for comparison purposes. The result for the interacting density of states is presented in Fig. 3.1, where a comparison for increasing coupling α with the phase only method is shown.

For very small lead-grain coupling there is virtually no difference in the case of the metallic grain (continuum of levels $N_L \to \infty$) between the self consistent solution and the rotor only (non self consistent) solution for the interacting grain density of states. But for increasing lead-grain coupling, although the gap profile (and therefore the renormalization of the charging energy) is not changed from the phase-only results, we see that at finite $N = 3$ the leads produce a serious modification in the interacting density of states around the gap. Note that some spectral weight is displaced to higher energies for increasing α. The Padé continuation method is not reliable at such high values of ω/E_C, and the result we see in the plot is only a very rough approximation, so the reallocation of these low energy states to energies close to the band edges (at $\omega \sim \pm 50E_C$) should not be quantitatively trusted in the plot. However the spectral function at small energies is correctly interpolated to the real axis, and an evident suppression occurs there. This should imply a decreasing ratio g/α as α is increased (g is the conductance), since such ratio directly probes the low energy electron spectral function, see B.3. Another possible way we can imagine of probing this effect is by doing STM spectroscopy on a strongly coupled grain, since it does not alter the spectral structure of the system at small currents, in the lines of [44] with a tunable

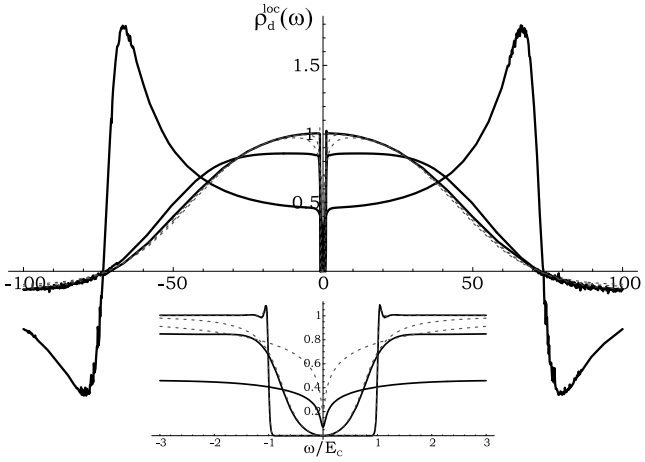

Figure 3.1: In solid lines we present the quantum rotor spectral function in the large-N and spherical limit calculated within the NCA slave rotor method. Dashed lines are the equivalent curves in the phase only approach, see 2.11. Values for α are $0.0001, 0.1, 0.7$. The rest of parameters are $\beta E_C = 100$, $W/E_C = 100$ and $N = 3$.

lead-cluster coupling. We have are not aware of precisely any such experimental study, however.

3.3.2 Kondo effect in single level quantum dot

The method we have presented inherits the ability of NCA slave bosons methods to describe the buildup of the Kondo resonance, with the added benefit of keeping the charging energy finite. In Fig. 3.2 we see how lowering the temperature beyond certain small value T_K produces a resonant state precisely at the Fermi energy. Bear in mind that since the system we are considering in the figure has $\epsilon - \mu = 0$ and $N = 2$, we are dealing with a singly occupied quantum dot level, and therefore Kondo is indeed expected due to spin-flip virtual processes. We will not try to analyze the doubly occupied quantum dot, since that involves going far from the middle of the Coulomb Blockade plateau, and our saddle point for the projection field is no good there, as shown in 2.3.5. Furthermore this very saddle point, as was discussed in 2.3.5, introduces a fictitious and unbounded chain of states of arbitrary charge (related to the unboundedness of the winding numbers). This in itself would allow fictitious 'spin' fluctuations even for the doubly occupied system, since the ceiling for electronic occupation is lost in this saddle point. This remains one of the essential shortcomings of this slave rotor method.

In this discussion we will closely follow the discussion of previous work published in [29, 31].

The main features of the local density of states $\rho_d^{\rm loc}(\omega)$ of the single level particle-hole symmetric quantum dot with spin degeneracy ($N = 2$), see Fig. 3.2, are the following. At all temperatures two 'incoherent' Hubbard bands appear at energies $\omega = \pm E_C$, of width roughly equal to Γ. Fig. 3.2 has been calculated with the slave rotor method, and exhibits a small (upward) shift in the position of these peaks for higher values of Γ that is probably

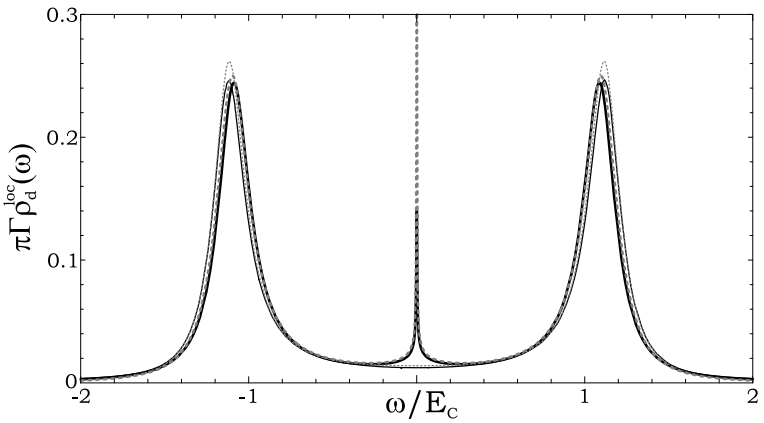

Figure 3.2: Development of Kondo peak at the Fermi energy for the particle-hole symmetric quantum dot with one level and two channels $N = 2$. Thick lines correspond to low temperatures $\beta E_C = 600$, while thin lines are for higher temperatures $\beta E_C = 4$. Solid lines represent the NCA slave rotor result and dashed lines present the phase only result, which as explained at the end of chapter 2 does develop a low energy peak in this particular case but is quantitatively wrong. In particular the strength of the resonance (unitary limit at $T = 0$) is overestimated in the latter case. The rest of parameters are $\Gamma = 0.06E_C$ and $W = 100E_C$. Clearly the analytical continuation yields nonsensical results for large values of ω/E_C, but the small ω region is robust.

an artifact of the method. These are evidently the two single particle levels that correspond to a dot with a hole and the dot with an extra particle above the average, which is of course $N_0 = N/2 = 1$. As temperature is lowered the Kondo peak is developed. Its width should be of order T_K, which is typically a very small energy scale, and it physically represents the energy of the bound system formed by the unpaired spin degree of freedom and the lead electron many body cloud that screens it completely at zero temperature.

Unitary conductance limit

The fact that the spin screening is complete at zero temperature, and that Fermi liquid characteristics are recovered at very low temperatures is well known from classical works of the field [98]. This yields in the present lead-grain-lead setup N completely transparent channels for transport at very low temperatures, so that conductance is expected to be $g = Ne^2/h = 2e^2/h$ in the deep Kondo regime $T \ll T_K$, which imposes an exact 'sum rule' kind of condition on the density of states, according to (B.3),

$$\lim_{T\to 0} \rho_d^{\text{local}}(\omega = 0) = \frac{1}{\pi\Gamma} \tag{3.26}$$

It was shown in [29] that the present method yields the following approximate limiting value, which is only about 10 off for $N = 2$. Nevertheless, the method becomes

exact in the $N \to \infty$ limit as expected.

$$\lim_{T\to 0} \rho_d^{\mathrm{loc}}(\omega = 0) = \frac{1}{\pi\Gamma} \frac{\pi/2}{N+1} \tan\left(\frac{\pi}{2}\frac{N}{N+1}\right) \tag{3.27}$$

We checked this upper bound and found it to be quite a good estimate, although for big enough values of Γ even this ceiling was slightly surpassed, getting even closer than that to the unitary limit (which is, correctly, never surpassed). We have not been able to clear up the reason for this small discrepancy, although perhaps numerical errors are behind this, since the discrepancy is small. This in any case would suggest that the method is doing even better quantitatively than expected by (3.27). The underestimation of the unitary limit has one fundamental physical consequence, namely that the Fermi liquid fixed point is not reached with this method. This implies a non-vanishing imaginary part in the real electron self energy at zero frequency, contrary to the infinite quasiparticle lifetime of Fermi liquids at the Fermi energy. This caveat was already known from [29], however this anomalous quasiparticle decay, which can be tracked to the NCA decoupling, is really quite small even for $N = 2$.

In figure 3.3 we have compared the NCA result to the rotor only one. The latter clearly overshoots this unitary limit. Furthermore the Kondo peak itself was much narrower than in the NCA one. Thinking about the Kondo resonance as a pole in the analytical continuation in the lower complex ω plane from the above one, accross the cut in the real axis, we could say that the rotor only approach predicts a pole that is much closer to the real axis than the NCA one. Since as we stated above, this distance of the pole to the real axis (the width of the resonance) has a physical meaning (it is the values of T_K) it is interesting to compare these results to the exact analytical results for T_K that are known from Renormalization Group studies.

Kondo Temperature

RG analysis yields a Kondo temperature scale which depends exponentially on charging energy and Γ. Similarly to superconductivy transition, no perturbation scheme on the hopping amplitude can recover this result. Renormalization group relies on the flow equation of the 'effective exchange' parameter $J = t^2/E_C$, which under integration of high energy modes of the lead electron fields flows under the following equation (one loop approximation) [48]

$$\frac{\partial J}{\partial \lambda} = \rho_l(0) J^2 \tag{3.28}$$

where the energy cutoff is parametrically reduced as $\Gamma = \Gamma_0 e^{-\lambda}$. The integration of this equation gives $J(\omega) = \left[\rho_l(0) \log \frac{\omega}{\Lambda_0} + \frac{E_C}{t^2}\right]^{-1}$ This one loop approximation to the RG flow breaks down at an energy scale of order

$$T_K = T_0 \exp\left[-\frac{E_C}{t^2 \rho_l(0)}\right] = T_0 \exp\left[-\frac{\pi E_C}{4\Gamma}\right] \tag{3.29}$$

(with $N = 2$ for spin degeneracy) which is the scale at which the one loop $J(\omega)$ solution diverges. The prefactor has also been calculated to be $T_0 = \sqrt{4E_C\Gamma}$ by more sophisticated

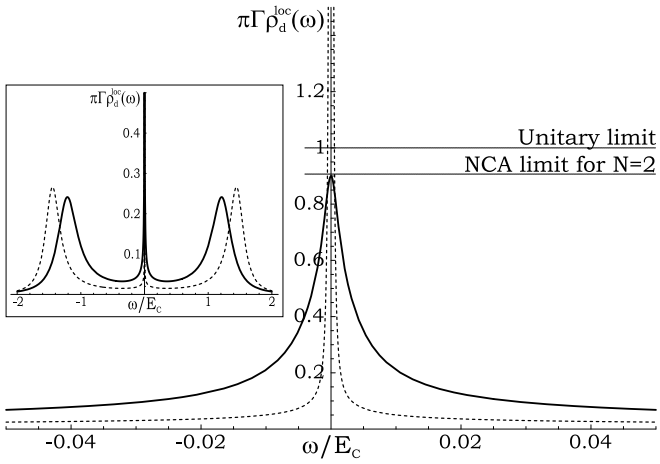

Figure 3.3: The parameters in this plot are $\Gamma = 0.06E_C$, and $\beta E_C = 1000$. We are in the deep Kondo regime. We can see that the NCA slave rotor method (solid line) is quantitatively correct regarding the unitary limit for the conductance, unlike the rotor only method (dashed line). We also notice that the position of the Hubbard bands is closer to the expected value of $\omega = \pm E_C$ in the NCA calculation.

methods. This scale is usually the smallest by far in the system, and in experiments with small quantum dots built in 2DEG's it may range from $1K$ to $\sim 50K$.

An analytical estimation of this scale in our formalism is also possible. Since a Kondo peak implies, by (A.21), a constant $G^{d\mathrm{loc}}_{\Delta\tau}$ for large $\Delta\tau$, and since (2.67) implies that therefore both $G^{\mathrm{loc}}_{\Delta\tau}$ and $\mathcal{G}_{\Delta\tau}$ must likewise saturate to a constant for large $\Delta\tau$, we have the equivalent conditions that $G^{\mathrm{loc}}_{\Delta\tau} \sim \frac{1}{\omega}$ and $G^{\mathrm{loc}}_{\Delta\tau} \sim \frac{1}{|\omega|}$ for small enough ω. Assuming the former (this implies a small value of $\Sigma_{i\omega_1}$ as compared to $(G^{\mathrm{loc}}_{i\omega_1})^{-1}$, which is dominated by the pole of the level at zero energy), we have indeed that $G^{\mathrm{loc}}_{\Delta\tau} \sim -\frac{1}{2N_L}\mathrm{sign}\Delta\tau$. Since this implies $\alpha K_{\Delta\tau} \sim 1/\Delta\tau$ for large $\Delta\tau$ we have the following logarithmic behavior for the rotor self energy at the smallest possible frequency $i\omega_1$, $\alpha(K_0 - K_{i\omega_1}) \sim \frac{2N\Gamma}{\pi}\log\frac{\omega_1}{T_0}$, where T_0 is an undetermined cutoff of order $\sqrt{\Gamma E_C}$ in practice. When this value grows to satisfy $\lambda + \alpha(K_0 - K_{i\omega_1}) \approx 0$, where λ is assumed to be very weakly renormalized (weak coupling to the leads, $\lambda \approx E_C/4$) we obtain the desired saturation of $\mathcal{G}_{\Delta\tau}$ for big $\Delta\tau$, and Kondo resonance sets in. Therefore, since $\omega_1 = 2\pi T$ the condition for this to happen is that the temperature T is smaller than

$$T_K = T_0 \exp\left[-\frac{\pi E_C}{16\Gamma}\right] \tag{3.30}$$

where $N = 2$ and $N_L = 1$ was assumed. This analytical estimate was confirmed by measuring the Kondo peak half-width obtained from the NCA slave rotor method at half-height for increasing E_C, see Fig. 3.4. The exponent of the Kondo temperature dependence is seen to be a factor $1/4$ off respect to the Renormalization Group calculation. We identify this as a quantitative inaccuracy of the method introduced by the spherical limit approximation.

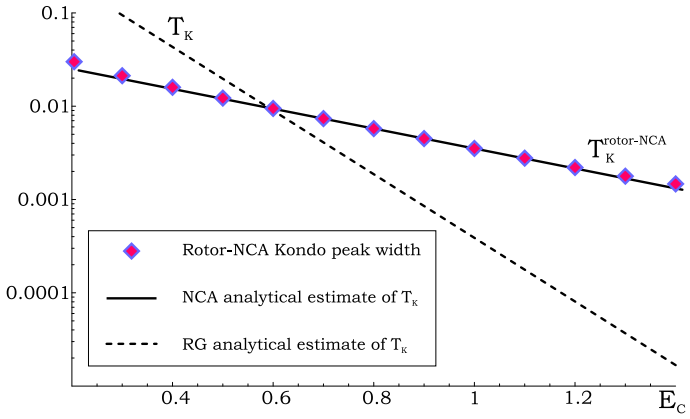

Figure 3.4: The parameters in this plot are $\Gamma = 0.1$, $\beta = 2000$, $N = 2$ and $N_L = 1$ at zero energy. We represent the half-width at half-maximum of the Kondo peak for increasing charging energy E_C. We confirm the exponential dependence of this scale T_K with E_C, as expected from *RG*. We also confirm the exponent of this dependence as derived by analytical arguments from the NCA integral equations, but a factor 1/4 deviation is found respect to the RG prediction.

Comparison to alternative slave-boson techniques

Although the single slave boson technique as initially introduced by Coleman [26] requires an infinite charging energy in the Anderson model (keeping the empty to singly occupied transition within a finite energy) to discard the population of the doubly occupied states, more or less complicated alternatives have been put forth [45], which by applying subsequent generalization of the two-slave-boson NCA approach (known as UNCA and SUNCA) have yielded increasingly reliable descriptions of the Kondo regime at not-so-low temperatures, at the cost of increased computational cost. In Fig. 3.5 we present a comparison of the method developed here within the spherical limit approximation to these other techniques in the symmetrical single level scenario. It is worth noticing that the low energy features of the Kondo resonance are captured with quantitative precision as compared to the most complex (and much more costly) method known as the Symmetrized-U-Non-crossing-approximation (SUNCA). However the incoherent high energy features of the Hubbard bands away from the atomic limit present a systematic deviation of the resonance to higher energies within the rotor-NCA method, but this is most likely due to the spherical limit approximation than to the rotor description. The deviation is however not to important, since only the region close to $\omega = 0$ determines the low temperature-low energy response of the system.

3.3.3 Crossover from Kondo to Coulomb blockade

We have analyzed the extreme cases of both metallic grains and discrete level quantum dots. The former, in which level spacing is neglected, is characterized by a renormalized Coulomb gap E_C^* which makes it an insulator at low temperatures (Coulomb blockade phe-

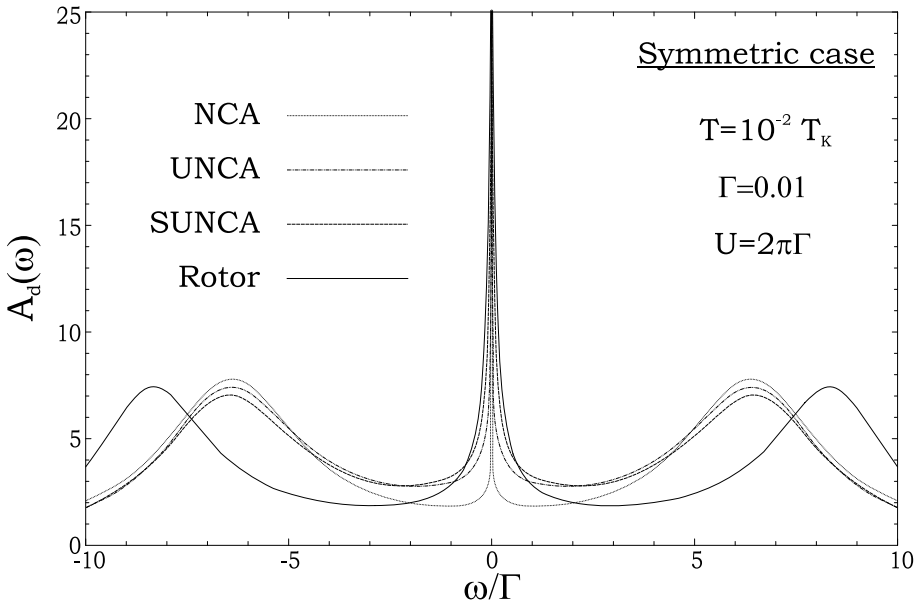

Figure 3.5: We have extracted the results of the spectral density of states of the Anderson impurity model from the work by Haule et al. [45], where a sophisticated skeleton-diagram expansion of the Luttinger Ward functional is employed to give increasingly precise non-perturbative resummation of the processes involved in the not-so-deep Kondo regime (bear in mind that the relevant parameter is $\log(T/T_K)$ which is not very small). The schemes are named (two-boson) NCA, UNCA and SUNCA, and take into account fluctuations between zero, one and two electrons in the impurity, whereas the rotor method does not limit these number fluctuations. We represent also the corresponding spectral density obtained with the spherical limit approximation of the slave-rotor NCA approach. Note that low energy features are quantitatively reproduced, and that a systematic shift of incoherent high energy features is introduced.

nomenon) just as is predicted by simpler sequential tunneling methods. But unlike those perturbative methods, a $\sim T^2$ cotunneling amplitude, a strongly renormalized Coulomb gap and a spectral weight shift to higher energies are predicted for increasing coupling α, all in a unified formalism. On the other hand the Kondo effect of the single level quantum dot is quantitatively described by the same method (in spite of the analyzed inaccuracies in T_K), without any special adaptation. This immediately encourages us to explore how the path in between is covered, the way from Kondo effect to Coulomb blockade, using the NCA slave rotor method as a qualitative interpolation scheme between the two. This, together with the possibility of doing Dynamical Mean Field Theory calculations in granular arrays, is probably the strongest advantage of this formalism.

We will first concentrate on the gradual suppression of the Kondo effect with decreasing values of the single-level coupling Γ. In order to maintain the Coulomb blockade effect, we will keep in this section the total (multilevel) coupling fixed, $\Gamma^{\text{multi}} \equiv N_L\Gamma = 0.25$, and vary the number of levels N_L to allow changes in $\Gamma = \Gamma^{\text{multi}}/N_L$. We will also fix the total bandwidth of the dot, $W = 1$, so that the level spacing δE (assumed to be uniform) is also decreasing, $\delta E = W/(N_L - 1)$. This way of proceeding allows to interpolate from the few, well-separated levels situation relevant for small quantum dots in the Kondo regime to the case of larger dots with small level spacing and many levels N_L, which shows only Coulomb blockade. The scaling of Γ is chosen so that the parameter α of the continuum density of states limit does not scale with N_L, i.e. $t^2\rho_g(0) \propto \Gamma N_L$ in (2.61) is a constant.

Figure 3.6 demonstrates indeed how the low temperature local density of states evolves from $N_L = 1$ (single level: regular Kondo effect) to $N_L = \infty$ (continuum of levels: Coulomb blockade only). In particular the rapid suppression of the Kondo peak for diminishing values of Γ at increasing N_L is in accordance with our previous discussion of the Kondo temperature, equation (3.30).

The temperature dependence of the electronic spectrum is presented for the three level case $N_L = 3$ in figure 3.7. When temperature is lowered, the zero frequency density of states starts diminishing (by Coulomb blockade of states with different charge). One then reaches a minimum, before $\rho_d(0)$ begins shooting up, towards the unitarity limit (Friedel's sum rule) at zero temperature.

It is useful to compare this evolution of the density of states to the variations of the conductance $G(T, N_L)$ with temperatures, figure 3.8. This figure illustrates the reduction of the Kondo temperature with Γ by the downward shifting of the minimum of conductance. The Coulomb blockade is present at higher temperature, as shown by the decrease of $G(T)$ for $T_K < T < E_c^*$ upon lowering T [80]. For the last curve with a continuum of states in the dot, this behavior persists up to zero temperature. The inset in log-scale on the same plot allows to grasp more clearly the saturation of conductance below the Kondo temperature.

3.3.4 Effects due to overlapping resonances in multilevel dots

The analysis in the previous section describes the usual situation where a crossover from the Coulomb blockade regime to the Kondo effect takes place as the temperature is lowered below the interlevel spacing in the dot. A different behavior can be expected when there is a set of overlapping resonances at low energies within the dot, *i.e.* an ensemble of levels of individual width greater than their separation, $\Gamma \gg \delta E$, that act together as a

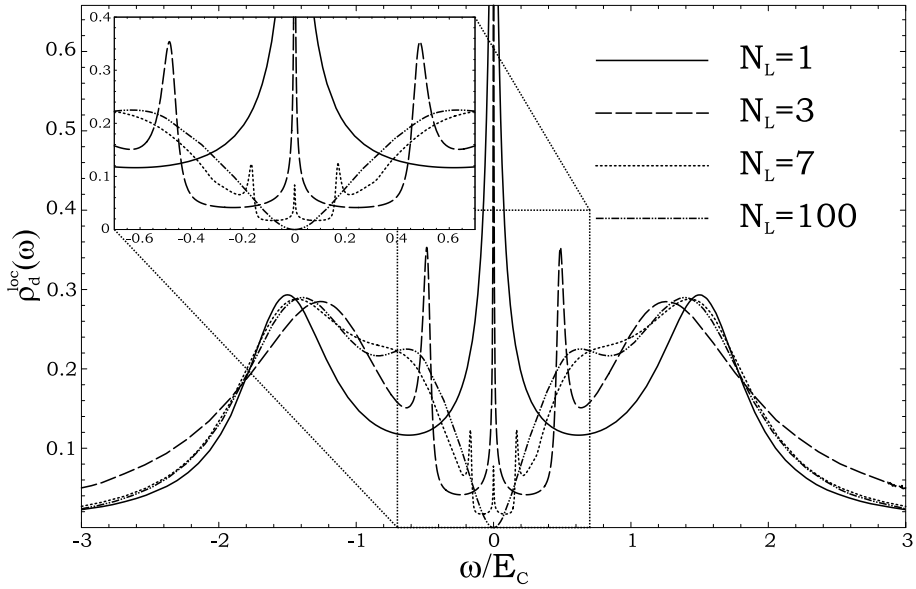

Figure 3.6: Local density of states $\rho_d(\omega)$ at $EC = 1$, $\beta = 800$, and fixed $W = (N_L - 1)\delta E = 1$ and $\Gamma^{\text{multi}} = N_L\Gamma = 0.25$. The four curves correspond to different values of the number of levels in the dot.

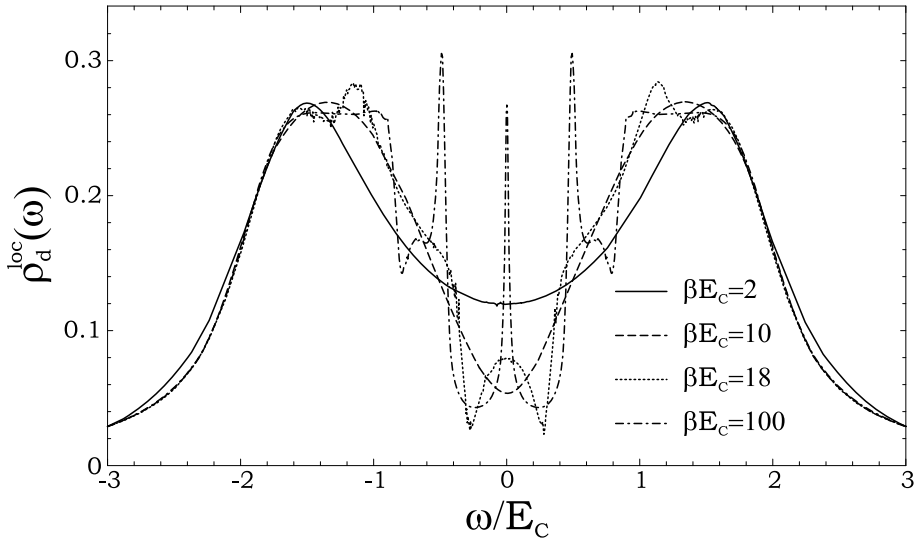

Figure 3.7: Same system as that of Fig. 3.6, but for fixed $N_L = 3$ and various temperatures. The linear conductance between dot and leads is roughly given by the $\omega = 0$ density of states, which presents a minimum before shooting up to the unitary limit.

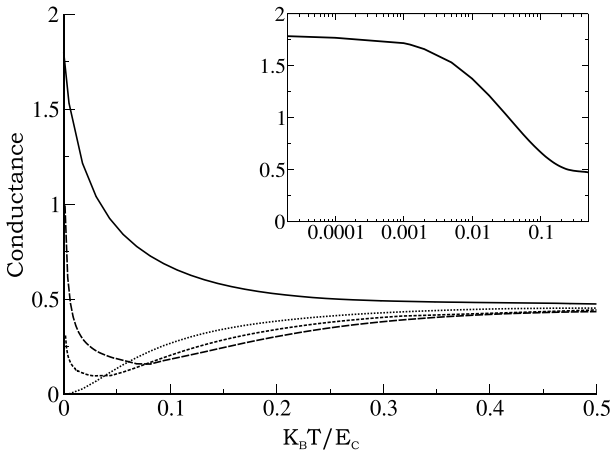

Figure 3.8: Conductance $G(T, N_L)$ in units of e^2/h for the same parameters as in figure 3.7 as a function of temperature; curves with $N_L = 1, 3, 5, \infty$ follow from top to bottom in the extreme left of the plot. Inset: $G(T, N_L = 1)$ in temperature-logarithmic scale.

single effective level with enhanced coupling to the leads (the typical bandwidth of this set of level should also be smaller than the charging energy). The presence of broad resonances near the Fermi level can be relevant to some experimental situations [89, 90]. Note that the conductance distributions for open ballistic quantum dots, estimated from Random Matrix Theory are quite broad [13, 50]. We give first some qualitative arguments in order to describe the new effects expected in this regime, and then present explicit calculations using the integral equations in section 3.2.

Inverse crossover from the Kondo effect to Coulomb blockade

In practical situations encountered in quantum dots, the single-level Kondo temperature T_K is usually much smaller than the level spacing δE (which is typically comparable to E_c). Therefore Coulomb blockade occurs (if it does) inevitably before the Kondo effect sets in, as was shown at length in the previous section. There is however a simple mechanism that allows to obtain Kondo temperatures *greater* than both level spacing and renormalized Coulomb energy E_c^*. The idea is that when the individual level width Γ exceeds the interlevel spacing δE, many levels are involved in the formation of the Kondo resonance. This leads to a "multi-level Kondo temperature" [49, 99]:

$$T_K^{\text{multi}} \sim T_0 \ \exp\left(-\frac{\pi E_c}{2NN_{eff}\Gamma}\right) \tag{3.31}$$

which can be greatly enhanced with respect to the single level estimate, equation (3.30), by the presence of many levels $N_{eff} > 1$ acting together, (increasing the number of channels N might also contributes to this effect). This way of enhancing the Kondo temperature allows to obtain a new regime where $T_K^{\text{multi}} \gg E_c^*, \delta E$, so that the Kondo effect can now occur *before* the Coulomb blockade (when lowering the temperature), in an *inverse* manner as observed traditionally in quantum dots. The fact that the Coulomb energy can be strongly

renormalized to smaller values adds credibility to this idea, see Fig. 2.9. One further notes that, at even lower temperatures, a Kondo peak associated to the formation of a resonance which involves only one electronic state in the dot will ultimately emerge. One therefore has a "two-stage Kondo effect" (if the single-level Kondo temperature is not vanishingly small).

In order to be more precise, we will first give a concrete example with a limiting case that one can understand independently of any approximation scheme. Then, we will illustrate in detail this "inverse crossover" using our integral equations.

Limit of exactly degenerate levels

We consider here the extreme limit in which N_L levels in the dot are simultaneously put to zero: $\epsilon_\alpha = 0$ for all α (the total bandwidth W is therefore also zero). We can formulate the model after a redefinition of the fermionic operators (unitary transformation), as we already implicitly did in section 3.1.1, $\left\{d^\dagger_{\alpha\sigma}\right\} \to \left\{c^\dagger_{x_i\sigma}\right\}$, such that:

$$c^\dagger_{0\sigma} = \frac{1}{\sqrt{N_L}} \sum_{p=1}^{N_L} d^\dagger_{p\sigma} \tag{3.32}$$

This is a kind of real space representation of the electrons in the quantum dot, particularized to position $x_0 = 0$.

In this case, the remaining fermionic degrees of freedom, $c^\dagger_{x_i\sigma}$ for $i > 0$, simply decouple from the problem, leaving an *effective single level* Anderson model describing the fermion $c^\dagger_{0\sigma}$. Actually, a capacitive coupling persists between this fermion and all the other ones, but this influence gets frozen at low temperature. As the conductance through the dot is obtained from the Green's function:

$$G^{loc}_d(\tau) \equiv \frac{1}{N_L} \sum_{\alpha\alpha'} \left\langle d^\dagger_{\alpha\sigma}(0) d_{\alpha'\sigma}(\tau) \right\rangle = \left\langle c^\dagger_{0\sigma}(0) c_{0\sigma}(\tau) \right\rangle \tag{3.33}$$

one gets a full Kondo effect and a complete restoration of unitary conductance at low temperature. Furthermore, the width of this effective level is simply $N_L\Gamma$, as one checks by inserting $c^\dagger_{0\sigma}$ in equation (3.1). This leads then to an enhanced Kondo temperature,

$$T_K^{\text{deg.}} = T_0 \exp\left(-\frac{\pi E_c}{2NN_L\Gamma}\right) \tag{3.34}$$

as discussed in the introductory part of this section (because for this limiting case $\delta E = 0$ one has $N_{eff} = N_L$).

We can easily check that our self-consistent scheme preserves this interesting property of the model. Indeed, when all levels ϵ_α are exactly degenerate ($W = 0$), one gets from equation (3.13) the f-electrons Green's function $G^{\text{loc}}_{i\omega} = [i\omega - \Sigma_{i\omega}]^{-1}$. We obtain therefore the Kondo effect of a single effective level [29].

The following paragraph will allow us to make this discussion more meaningful, by studying the more realistic case of a quantum dot in the regime $\Gamma \gtrsim \delta E$, corresponding to nearly degenerate levels.

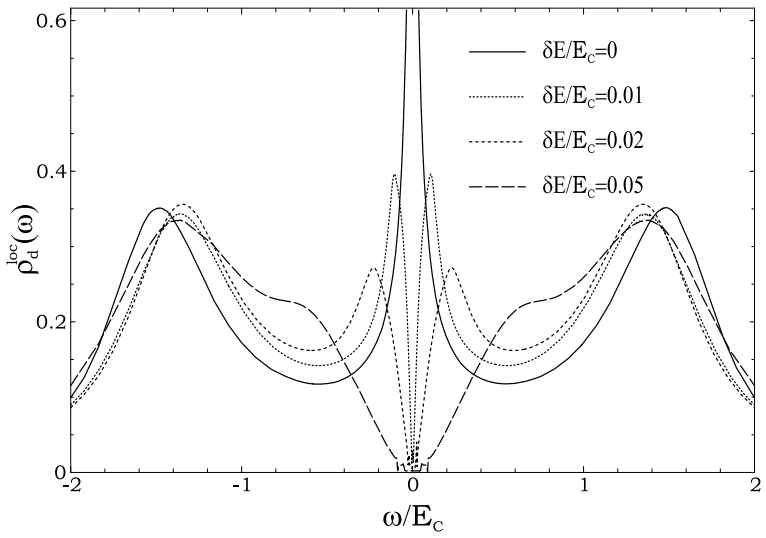

Figure 3.9: Density of states $\rho_d(\omega)$ on the dot for $\Gamma/E_C = 0.01$, inverse temperature $\beta E_C = 1500$, $N_L = 21$ states, and different values of the interlevel spacing: $\delta E/E_C = 0, 0.01, 0.02, 0.05$. Multilevel Kondo temperature becomes big enough to be observed as a N_L-level Kondo resonance, while the single level T_K remains inaccessible. When the total width of the 'microband' surpasses the multilevel T_K, Coulomb blockade features set in.

Inverse crossover: illustration

We now illustrate the inverse crossover discussed qualitatively in paragraph 3.3.4 by solving our integral equations in the regime $\Gamma \gtrsim \delta E$, where multi-level effects play an important role. We will assume here that $\Gamma \ll E_c$ so that one can neglect the single level Kondo effect at low temperature (see however the next paragraph). For this computation, we have fixed $\Gamma = 0.01 E_C$, and taken $N_L = 21$ states in the dot, varying the interlevel spacing from $\delta E = 0$ (exactly degenerate level case considered in the previous paragraph) to $\delta E/E_C = 0.01 = \Gamma/E_C$ (multilevel effect present) to $\delta E/E_C = 0.05 > \Gamma/E_C$ (absence of multilevel effect).

The low-temperature local density of states displayed in figure 3.9 shows the expected multi-level enhanced Kondo peak at $\delta E = 0$ corresponding to formula (3.34). Upon increasing the level spacing to $\delta E = 0.01 E_C$, Coulomb blockade sets in at a scale $E_C^* < T_K^{multi}$, however coherence effects remain around T_K^{multi} (since we are in a regime with $\delta E < \Gamma$). This results in a surprising splitting of the Kondo resonance at low energy. The last curve is taken with $\delta E/E_C = 0.08 > \Gamma/E_C$, so that no multilevel Kondo effect is possible, and only Coulomb blockade is observed. Another interesting consequence of this phenomenon is that the temperature dependance of the conductance is *reversed* with respect to the usual signature of the Kondo effect in quantum dots, *i.e.* to figure 3.8. Indeed, upon lowering the temperature, one notices an initial increase of the conductance (due to the multilevel Kondo effect), *then* a sharp decrease of the conductance because of the Coulomb blockade. This is illustrated by the second curve in figure 3.10.

One can also perform a general evaluation of the multilevel Kondo temperature,

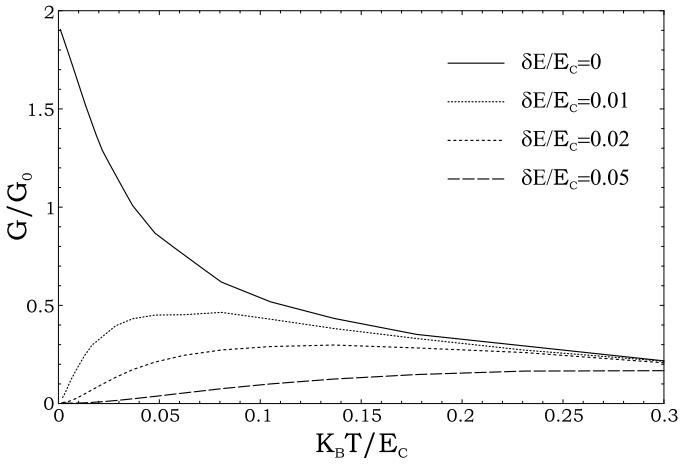

Figure 3.10: Conductance $G(T)$ normalized to $G_0 = e^2/h$ for the same grain described in figure 3.9.

starting from the leading behavior of the f-Green's function at high temperature:

$$G_f^{loc}(i\omega) \simeq \frac{1}{N_L} \sum_p \frac{1}{i\omega - \epsilon_p} \tag{3.35}$$

Equation (3.20) then leads to [2]:

$$\alpha K_{i\omega} = -\frac{N\Gamma}{\pi} \sum_\alpha \log \frac{\omega^2 + |\epsilon_\alpha|^2}{\omega^2 + (|\epsilon_\alpha| + T_0)^2} \tag{3.36}$$

The Kondo temperature is reached when this kernel is of the order of E_C, so that one finds the final equation which determines $T_K^{\rm multi}$:

$$\prod_\alpha \frac{(T_K^{\rm multi})^2 + |\epsilon_\alpha|^2}{(T_K^{\rm multi})^2 + (|\epsilon_\alpha| + T_0)^2} = \left(\frac{T_K}{T_0}\right)^2 \tag{3.37}$$

where T_K is the single level Kondo temperature (3.30). A similar result was obtained previously by a renormalization group argument [99]. The limiting cases studied before are obviously contained in the previous equation: $T_K^{\rm multi}$ reduces to T_K for widely separated levels (δE large) and in the opposite limit of exactly degenerate levels (or if $W \ll T_K^{\rm multi}$), $T_K^{\rm multi} = T_0(T_K/T_0)^{1/N_L}$, consistently with equation (3.34). In general, $T_K^{\rm multi}$ is enhanced with respect to the single level Kondo temperature T_K.

We conclude this paragraph by summing up the physical picture that leads to the observed non-monotonous conductance. In the case of many overlapping resonances, a quantum dot can be described as a small metallic grain dominated by Coulomb blockade at

[2] Naively the cut-off T_0 in this expression should be of order Λ as implied by the regularized expression of the bath $\Delta(\tau) = -N_L\Gamma\ 1 - \exp(-\Lambda|\tau|)\ /(\pi\tau)$. However logarithmic corrections to our approximative derivation imply that $T_0 \sim \sqrt{E_C\Gamma}$.

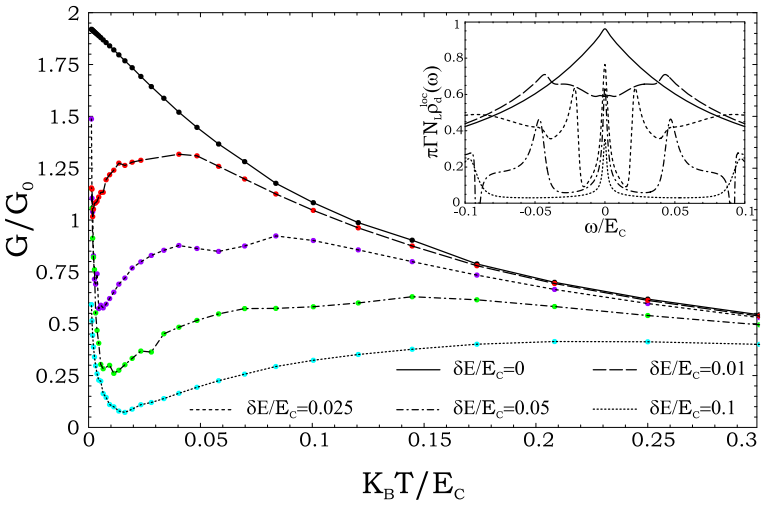

Figure 3.11: Conductance $G(T)$ normalized to $G_0 = e^2/h$ for a grain with $N_L = 9$ levels and $\Gamma/E_C = 0.04$. Note the three phase evolution of the conductance as temperature is lowered: first an increase due to multi-level Kondo effect $T_K^{\rm multi} > E_C*$, then a drop at a scale $T = E_C^*$ and finally an increase due to single level Kondo effect at $T = T_K < E_C^*$. In the inset we represent the corresponding normalized spectral density of the grain at low temperature $\beta E_C = 1000$.

low temperature, which implies a vanishing zero-frequency density of states. Upon raising the temperature, many different charge states become available by the thermal smearing of the Coulomb blockade, and the conductance is rapidly increasing on a scale of the order of E_c^* (which is also the typical size of the dip observed in the split Kondo peak). Due to the large single level width considered in this regime, all these energy levels can then act coherently as a localized spin degree of freedom that undergoes the Kondo effect. This explains the upturn of the conductance when temperature reaches the Kondo energy $T_K^{\rm multi}$.

Two-stage Kondo effect

Finally we consider again a multilevel case, $\delta E \ll \Gamma$, but now with $\Gamma \lesssim E_c$, so that the single-level Kondo resonance is accessible to the low temperature regime. Therefore, one witnesses a further increase of the conductance at low temperature, taking place after the inverse Kondo-to-Coulomb crossover that we discussed previously. The occurence of such a "two-stage Kondo effect" is depicted for the conductances shown in figure 3.11. For this calculation, we have taken $N_L = 9$ levels, $\Gamma/E_C = 0.04$ and various level spacings between zero and 2.5Γ.

The curves with $0 < \delta E < \Gamma$ clearly show this two-stage Kondo effect: a first rise of the conductance at high temperature due to the multilevel resonance at $T \sim T_K^{multi}$, then the Coulomb blockade at $T \sim E_c^*$ and then a further increase at $T \sim T_K$ (smallest scale of the problem). The last two curves, with $\delta E/E_C = 0.05, 0.1$, show the usual crossover that was illustrated on the figure 3.8 in section 3.3.3.

A last point that was checked is that our results are weakly sensitive to the addition

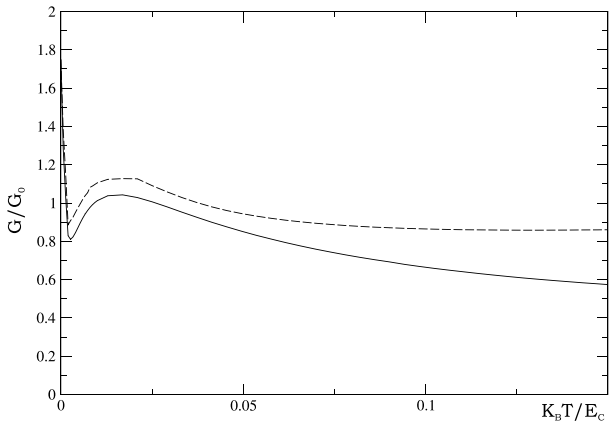

Figure 3.12: Lower curve: conductance $G(T)$ in the case $N_L = 5$, $\Gamma = 0.05$ and $\delta E = 0.015$. Upper curve: similar model, but 10 additional levels (with larger spacing $\delta E' = 0.2$) have been superimposed to the previous ones.

of more levels outside the energy window of width Γ. This calculation is shown in figure 3.12.

3.3.5 Summary of the different regimes of transport

A sketch of the different regimes analyzed in this paper is given in figure 3.13, as a function of the level spacing, δE, and single level width, Γ. We assume that the number of electrons in the dot is odd, so that the ground state, in the absence of the coupling to the leads is degenerate.[3] The transition between different regimes is a smooth crossover.

The occurrence of Kondo effect is signaled by a non monotonous temperature dependance of the conductance, and is observable at experimentally accessible temperatures as long as $\Gamma \lesssim E_C$. The Kondo temperature given by the method is given by equation (3.30), although the precise coefficient in the exponent seems to be a factor 4 off. This is the usual single-level Kondo effect, and it is a resolvable feature as long as $\delta E \gg \Gamma$. Additional levels are seen to develop satellite Kondo resonances around the single-level one at the Fermi energy, the width of which is typically T_K also for non-overlapping levels.

If $\Gamma \gtrsim \delta E$, and at the same time the dot's 'bandwith' $W = N_L \delta E$ is smaller than the charging energy, or in other words, if $\delta E/E_C < 1/N_L$, a multi-level type of Kondo effect can dominate at not-so-low temperatures, $T < T_K^{\rm multi} \approx T_0 (T_K/T_0)^{1/N_{\rm eff}}$, where the new scale $T_K^{\rm multi}$ can be orders of magnitude larger than T_K. At temperatures $T_K < T < T_K^{\rm multi}$ all the satellite single-level Kondo resonances fuse into a much wider multi-level Kondo resonance.

Coulomb blockade is manifested, loosely speaking, as a suppression of zero frequency spectral weight due to Coulomb repulsion. Away from the multi-level Kondo region this happens whenever $T > T_K$. If $\delta E/E_C > 1$ however the situation is not usually called

[3] Actually, our formalism is exact, as already mentioned many times, when such degeneracy is very large (i.e. large N)

Coulomb blockade, since although transport is blocked due to Coulomb interactions, the hallmark of metallic Coulomb blockade, which is the more or less periodic dependence of conductance with gate voltage is dramatically altered by the sizable energy shifts imposed by the energy differences between levels, so that such periodic modulation is completely scrambled into spectral peaks. We will therefore denote that regime simply by the (single level) Kondo regime in Fig. 3.13. As for the usual Coulomb blockade, it sets in in general already at finite energy scales below E_C^*, which can be typically much smaller than the bare E_C for more or less open quantum dots. It is the inverse decay time in the imaginary time axis of the phase-phase correlator $\mathcal{G}_{\Delta\tau}$. If such long-time correlations are decaying, the low energy density of states will be suppressed for $\omega < E_C^*$. The formation of the Kondo resonance is manifested in imaginary time by the saturation of this decay when temperature is low enough, see A.23, so that Coulomb blockade is eventually suppressed by the opening of a transparent transport channel (the region denoted as "Coulomb blockade + Kondo" in Fig. 3.13.

As explained above, the energy scale at which this happens can be increased to T_K^{multi} when several overlapping energy levels are accumulated below E_C, so that $\delta E/E_C < 1/N_L$ and $\Gamma \gg \delta E$. But unlike the single level Kondo resonance, this multi-level resonance has an inherent finite energy scale (when the levels involved have a finite separation) that aborts the upward renormalization flow of the multi-level Kondo coupling, so that the resonance can be split in two around $\omega = 0$ as Coulomb blockade sets back in (before the single level Kondo effect finally takes over at very low temperatures). This scale, that might be intuitively written as $W_{\text{eff}} = N_{\text{eff}}\delta E$, (where N_{eff} is the number of levels effectively involved in the formation of the Kondo resonance) is in rigor E_C^*, since it is the actual system's gap. Therefore, under imminent multilevel Kondo conditions, when the level spacing is however not very low, $\delta E \sim \Gamma$, we can find an inverse crossover as energy is lowered, from multi-level Kondo, to Coulomb blockade (and back to single level Kondo if the temperature is low enough).

We emphasize that if Γ is much smaller than E_C the (single level) Kondo temperature is extremely small and the Kondo effect unobservable in practice; this corresponds to weakly coupled dots, and this situation shows only Coulomb blockade at low energies. Note that the Kondo effect involving many levels can also occur in dots with an even number of electrons, in a similar manner to the Kondo resonance which arises at a singlet-triplet crossing in an applied magnetic field [35]. Finally, the region $\Gamma \gg E_c$ of the diagram (denoted "Coherent") is associated with large conductances that are weakly modulated with temperature or applied gate voltage. This discussion has been schematically summarized in Fig. 3.13.

3.4 Summary and outlook

We have demonstrated how the spherical limit approximation on the NCA equations of fermionic plus slave rotor auxiliary field can provide a powerful yet technically simple framework to explore the transport features of interacting nanostructures, which we have described within a thermal equilibrium formalism. Still the technique is by no means limited to equilibrium situations, and could be extended to include Keldysh propagator

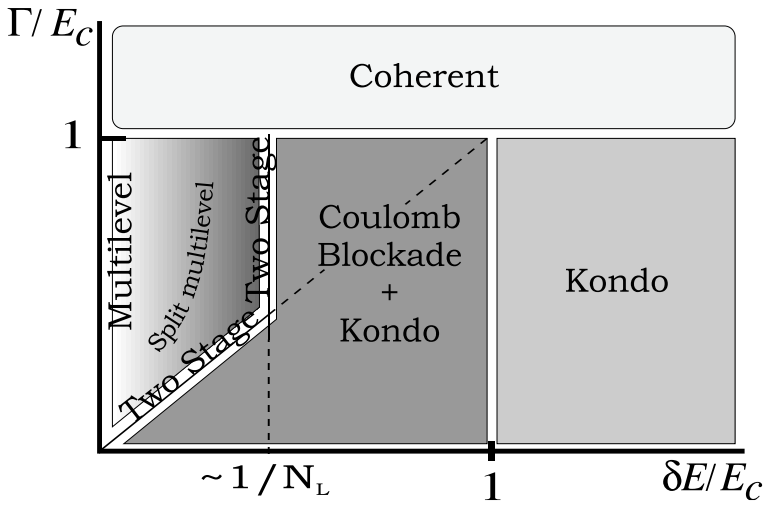

Figure 3.13: Sketch of the the different regimes discussed in the paper, as function of the charging energy, E_C, level spacing within the dot, δE, and level widths, Γ, with a constant number of levels. The notation "Kondo" corresponds to a single-level Kondo effect. The region "Kondo + Coulomb-Blockade" is the usual situation in quantum dots. The "Multilevel" region is also associated to the Kondo effect, but with important renormalization of the Kondo temperature, as discussed in the text. The "Coherent" regime stands for a temperature independant conductance.

techniques. Another interesting road for improvement towards a more quantitatively exact description of these phenomena involves the introduction of instanton saddle points before the spherical approximation is taken as we have suggested in the previous chapter. Furthermore, the analysis of behavior with off-symmetry gate voltages could easily be implemented, more so if instanton-series summation is taken into account.

The possibilities described in this chapter around single and multi level Kondo effects could be interesting from both fundamental and technological points of view. In particular, for example, the fact the single-particle level structure is reproduced as narrow satellite structures around the Kondo resonance, replicating all the level positions but with a much more narrow profile $\sim T_K$ could prove to be a spectroscopic tool to probe an otherwise blurred spectral density, since typically $T_K \ll \Gamma$. Other possibilities could make use of the complex-Kondo features such as the abrupt and extremely temperature sensitivity of conductance depicted in Fig. 3.10. Temperature dependent valves or highly non-linear transport devices could perhaps make use of these features in some way.

Chapter 4

Spin blockade in magnetic grains

In this chapter we will show how spin dynamics can be included in the discussion of interacting transport. This is interesting in the context of transport through magnetic nanostructures in which exchange interactions can play a role together with standard electrostatic effects. Such interactions arise from the fact that the Fermi exclusion principle imposes total antisymmetry of the many-body electronic wave function. For repulsive Coulomb interactions, making the spin sector symmetric (as in triplets formed from two spins) reduces the potential energy of electron pairs, since antisymmetric spatial wavefunctions have a lower Coulomb interaction that the symmetric case (lower overlap of spatial wavefunctions). This is the intuitive idea behind the familiar Hund rules, which in normal metals state that the lower energy configuration for a given set of electronic orbitals tends to have parallel alignment of spins. When the energy gained by aligning the spins of many electrons surpasses (in average) the energy required to put those electrons in different levels (which is a requirement to have parallel spins), the system can undergo a transition to a ferromagnetic state. This simple idea is known as the Stoner criterion [91] which states that the condition to reach the Stoner ferromagnetic instability is $J > \delta E$, where J is the typical exchange energy and δE is the typical level spacing. [1]

In the case of a superconducting metal electronic interactions are attractive below some energy scale, usually due to phonon-exchange. Such a system is unstable and undergoes a superconducting transition at temperature T_C, breaking the Fermi liquid and opening a gap in the excitation spectrum. Either below or above this transition, however, Hund's rules are reversed due to the attractive interactions. This is one way to understand the fact that usual BCS-type superconducting pairing favors singlets, since they correspond to a symmetric spatial wave-function for electron pairs, and therefore lower energy.

Such spin dependence of the system's energy is modeled by a simple dipole-like interaction, involving the energy scale $J_{\alpha\alpha'}$, known as 'exchange'

$$H_{ex} = \sum_{\alpha,\alpha'} J_{\alpha\alpha'} \vec{S}_\alpha \vec{S}_{\alpha'} \tag{4.1}$$

where here α contains purely spatial quantum number, not spin, and the operator $\vec{S}_\alpha = \frac{1}{2}\sum_{ss'} d^+_{\alpha s}\vec{\sigma}_{ss'}d_{\alpha s'}$ is the spin of electron in orbital α.

[1] For realistic distributions of these scales the criterion must be elaborated further.

Random Matrix Theory (RMT) arguments parallel to those that lead to the orthodox model of Coulomb blockade [4], in which all electrostatic interactions between electrons where modeled by a capacitor-type charging energy term $H_C = E_C Q^2$, Q being the total charge in the system, were used to study exchange interactions at low energies in chaotic dots with large dimensionless conductance (strongly chaotic systems). These interactions where found to be described by a simplified total-spin coupling term with constant $J_{\alpha\alpha'} = J$

$$H_{ex} = J\vec{S}^2 = J\left(\sum_{\alpha}\vec{S}_{\alpha}\right)^2 \tag{4.2}$$

The value of the single exchange energy scale involved, J, was also studied under RMT in the case of metallic dots, and unlike the geometrically related charging energy E_C, J was found to be smaller than (but of the same order as) the level spacing, so that in such chaotic nanostructures no ferromagnetic instability was in general predicted.

The case of superconducting quantum dots was also analyzed [59], by studying the universal properties of a pairing interaction term. Although the pairing interaction in the universal Hamiltonian description starts out as a small scale, also of the order of the level spacing in the dot, it logarithmically renormalized to higher values for attractive interactions, which leads to the opening of a gap below the critical temperature. Early papers on the subject [74] already computed the magnetic susceptibility χ (which is directly related to J, namely $J = 1/2\chi$) in this superconducting phase by means of Ginzburg-Landau type arguments, resulting in a greatly enhanced value of J below the superconducting critical temperature. Indeed, J should also grow under RG in superconducting systems in parallel with the pairing interaction, since it represents the energy gap that should have to be overcome to create a triplet spin excitation from a singlet ground state, which is the superconducting gap itself.

Therefore, to summarize, the most standard results in the field of universal description of chaotic nanostructures state that either the exchange interaction is negative and of the order of the level spacing (in normal nanostructures) or positive and possibly much larger that the level spacing in the presence of attractive interactions (superconducting grains), in which case the system has an electronic gap below certain critical temperature.

The main idea underlying this chapter is that in either case the form of the exchange term is very similar to the charging energy term, and might be tractable with techniques similar to the ones discussed in the previous chapters [2]. There is one important caveat however, since while E_C is always positive, J can have either sign. A negative J is analogous to attractive electronic interactions. In such case the formal development that will follow should be modified in the lines of [7], where the Hubbard - Strattonovich decoupling used to absorb the interaction term should be anomalous, introducing a Cooper channel-like field $\Delta^* d^+_\alpha d^+_{\alpha'}$ instead of a normal one $V d^+_\alpha d_{\alpha'}$ as we have done in the previous chapters. For simplicity we will consider the simpler case $J > 0$ to illustrate the possibility

[2] Although spin in this case has dynamics, recall that the large-N requirement that the channels be degenerate only concerned the hopping amplitudes, that had to be channel-conserving, so that the validity of the large-N arguments with $N = 2$ used to integrate out the fermions in chapter 2 remain valid even in the presence of exchange interactions. In any case, apart from the spin degeneracy, further degeneracy can exist in magnetic grains with large enough interfaces to the leads.

of building a rotor description for spin, but we will leave for future work the possibility of implementing a negative J and the analysis of ferromagnetic transitions.

4.1 Rotor description of a superconducting grain

The type of system we are going to analyze is a small grain or quantum dot with attractive interactions between electrons, possibly mediated by phonons or any other mechanism. We will not discuss the microscopic aspects of this interaction but will rather focus on the resulting total-spin positive exchange interactions that arise because of them. Electrostatic effects of the usual $E_C Q^2$ type are in general present in these small systems, since even though the effective screened electron-electron interactions are attractive, the boundaries of the system always induce a capacitive energy term [4].

The transport properties of such systems below their critical temperature when coupled to normal leads through tunnel junctions are largely suppressed by the superconducting gap Δ^{BCS}. Andreev processes in which electrons tunnel in pairs into or out of the grain become important for more or less transparent contacts. Additional effects due to Coulomb blockade impose an additional gap without pairing effect that tends to suppress the Andreev processes, specially when $E_C > \Delta^{\mathrm{BCS}}$. The microscopic derivation of the BCS theory that accounts for all this was clarified in precisely the context of non-linear sigma models and Hubbard - Strattonovich transformations [7] which serves as inspiration for the present work.

Let us leave aside for a while the exchange interaction. We will add and analyze that ingredient later. The novelty introduced by attractive interactions is a term in the Hamiltonian (or in the imaginary time action) of the form

$$H_{\mathrm{pairing}} = -g \int dx d\tau \psi^+_\sigma(\vec{x}) \psi^+_{-\sigma}(\vec{x}) \psi_\sigma(\vec{x}) \psi_{-\sigma}(\vec{x}) \tag{4.3}$$

where g is assumed a positive pairing energy representing the strength of the attractive interactions. As was shown by Bardeen, Cooper and Schrieffer the correct Hubbard - Strattonovich decoupling of this quartic term is of the form

$$\int \Delta^{\mathrm{BCS}}_\tau(\vec{x}) \psi_{\sigma\tau}(\vec{x}) \psi_{-\sigma\tau}(\vec{x}) + H.c. \tag{4.4}$$

where the kinetic term is of the form $\int |\Delta^{\mathrm{BCS}}_\tau(\vec{x})|^2/4g$. This complex Hubbard - Strattonovich field $\Delta^{\mathrm{BCS}}_\tau(\vec{x})$ was introduced in a very similar way to the V_τ field in [7]. Only when it is approximated in a mean field (saddle point) fashion $\Delta^{\mathrm{BCS}}_\tau(\vec{x}) = \langle \psi^+_{\sigma\tau}(\vec{x}) \psi^+_{-\sigma\tau}(\vec{x}) \rangle$ does one recover the BCS form of the theory of superconductivity. A finite value of this amplitude (given by the gap equation above) signals the spontaneous breaking of the local gauge symmetry, which is the hallmark of a superconducting state. Note however that even if one is above the critical temperature and $\Delta^{\mathrm{BCS}}(\vec{x}) = 0$ in mean field, that doesn't mean that attractive interactions are not present. Indeed, the bare value of g can be assumed to be roughly temperature independent (at least much below the Debye temperature), but it is not enough to 'bind' Cooper pairs above T_C.

Fine, so we have two Hubbard - Strattonovich fields, V_τ and $\Delta_\tau^{\rm BCS}(\vec{x})$. The strategy is similar as in the Coulomb blockade problem: do a local gauge transformation on the electrons that reabsorbs the biggest possible part of these coupling terms, and treat the rest in a saddle point fashion, see 2.3.5. One (sometimes hidden) approximation is that the phase of both Hubbard - Strattonovich fields may be identified and treated as a single degree of freedom, so that a single local gauge transformation can reabsorb both V_τ and the global phase of $\Delta_\tau^{\rm BCS}(\vec{x})$, which gets pinned at $e^{2i\phi_\tau}$. Physically this means that the voltage drop in the junction instantly follows the fluctuations of the superconducting phase. The modulus $|\Delta_\tau^{\rm BCS}(\vec{x})| = \Delta^{\rm BCS}$ is indeed approximated at a saddle point level,

$$\begin{aligned} \mathbf{\Delta}^{\rm BCS} &= \langle \mathbf{f}^+_{\uparrow\tau}\mathbf{f}^+_{\downarrow\tau}\rangle & (4.5)\\ \Delta^{\rm BCS}_{\alpha\alpha'} &= \langle f^+_{\uparrow\alpha\tau}f^+_{\downarrow\alpha\tau}\rangle\delta_{\alpha\alpha'} = \Delta^{\rm BCS}_\alpha\delta_{\alpha\alpha'} & (4.6)\end{aligned}$$

Recall that s is the spin index. A very natural notation to implement the $\uparrow\leftrightarrow\downarrow$ pairing is Nambu space [77], which redefines the vectors of creation and annihilation operators in eq. (2.39) in a convenient pairing fashion

$$\begin{aligned} \vec{\mathbf{f}}_\tau &= \begin{pmatrix} f_{\uparrow\alpha\tau} \\ f^+_{\downarrow\alpha\tau}\end{pmatrix} \equiv \begin{pmatrix} \mathbf{f}_{\uparrow\tau} \\ \mathbf{f}^+_{\downarrow\tau}\end{pmatrix} & (4.7)\\ \vec{\mathbf{f}}^+_\tau &= \left(f^+_{\uparrow\alpha\tau}, f_{\downarrow\alpha\tau}\right) \equiv \left(\mathbf{f}^+_{\uparrow\tau}, \mathbf{f}_{\downarrow\tau}\right) & (4.8)\end{aligned}$$

and equivalently for $\vec{\mathbf{d}}_\tau$. This vector construct substitutes the implicit sum over spin index we have been using so far, and furthermore allows us to write the superconducting action in exactly the same form as the metallic grain

$$S = \int -\vec{\mathbf{f}}^+_\tau \hat{\mathbf{G}}^{-1}_{0\tau\tau'}\vec{\mathbf{f}}_{\tau'} + \frac{1}{4E_C}\left(\partial_\tau\phi_\tau\right)^2 + \int \vec{\mathbf{f}}^+_\tau \hat{\mathbf{\Delta}}_{\tau\tau'}\vec{\mathbf{f}}_{\tau'}\cos(\phi_\tau - \phi_{\tau'}) \qquad (4.9)$$

by merely defining the Nambu bath function

$$\hat{\mathbf{\Delta}}_{\tau\tau'} = \begin{pmatrix} \Delta_{\alpha\tau\alpha'\tau'} & 0 \\ 0 & -\Delta_{\alpha'\tau'\alpha\tau}\end{pmatrix} \qquad (4.10)$$

and the inverse Green's function in the Nambu space notation

$$\hat{\mathbf{G}}^{-1}_{0\tau\tau'} = \begin{pmatrix} -(\partial_\tau + \epsilon_\alpha - \mu - \delta\mu) & \Delta^{\rm BCS}_\alpha \\ \Delta^{\rm BCS}_\alpha & -(\partial_\tau - \epsilon_\alpha + \mu + \delta\mu)\end{pmatrix}\delta_{\tau\tau'}\delta_{\alpha\alpha'} \qquad (4.11)$$

so that a finite (and real) saddle point value of $\Delta^{\rm BCS}$ implements the anomalous vertex (4.4). The change of sign in the lower right elements comes from anti-commuting the Grassmann variables, e.g. $\epsilon_\alpha f_{\downarrow\alpha\tau}f^+_{\downarrow\alpha\tau} = -\epsilon_\alpha f^+_{\downarrow\alpha\tau}f_{\downarrow\alpha\tau}$. Note also that the gauge transformation (2.13) that introduces the phase description should honor the new Nambu definition of $\vec{\mathbf{f}}$ and $\vec{\mathbf{d}}$

$$\vec{\mathbf{f}}_\tau = \begin{pmatrix} e^{i\phi_\tau} & 0 \\ 0 & e^{-i\phi_\tau}\end{pmatrix}\vec{\mathbf{d}}_\tau \qquad (4.12)$$

Note that the Green's function is now composed of a normal part in the diagonal, and an anomalous one out of the diagonal

$$\hat{\mathbf{G}}_{0\tau\tau'} = \begin{pmatrix} -\langle \mathbf{f}_{\uparrow\tau}\mathbf{f}^+_{\uparrow\tau'}\rangle & -\langle \mathbf{f}_{\uparrow\tau}\mathbf{f}_{\downarrow\tau'}\rangle \\ -\langle \mathbf{f}^+_{\downarrow\tau}\mathbf{f}^+_{\uparrow\tau'}\rangle & -\langle \mathbf{f}^+_{\downarrow\tau}\mathbf{f}_{\downarrow\tau'}\rangle \end{pmatrix} = \begin{pmatrix} \mathbf{G_0}_{\uparrow\tau\uparrow\tau'} & \mathbf{F_0}_{\uparrow\tau\downarrow\tau'} \\ -\mathbf{F_0}^*_{\uparrow\tau'\downarrow\tau} & -\mathbf{G_0}_{\downarrow\tau'\downarrow\tau} \end{pmatrix} \tag{4.13}$$

The second equality relates the Nambu propagator to the propagators of previous chapter (note for example that the lower right one is the *hole* causal propagator in imaginary time) and also defines the anomalous propagators $\mathbf{F_0}_{s\tau s'\tau'} = -\langle \mathbf{f}_{s\tau}\mathbf{f}_{s'\tau'}\rangle$. In the frequency domain we have

$$\hat{\mathbf{G}}_{0i\omega_n} = \begin{pmatrix} -\frac{i\omega_n+\epsilon_\alpha}{\omega_n^2+\epsilon_\alpha^2+\Delta_\alpha^{\mathrm{BCS}2}} & \frac{\Delta_\alpha^{\mathrm{BCS}}}{\omega_n^2+\epsilon_\alpha^2+\Delta_\alpha^{\mathrm{BCS}2}} \\ \frac{\Delta_\alpha^{\mathrm{BCS}}}{\omega_n^2+\epsilon_\alpha^2+\Delta_\alpha^{\mathrm{BCS}2}} & \frac{i\omega_n-\epsilon_\alpha}{\omega_n^2+\epsilon_\alpha^2+\Delta_\alpha^{\mathrm{BCS}2}} \end{pmatrix} \delta_{\alpha\alpha'} \tag{4.14}$$

By continuing to the real ω axis we immediately appreciate that the poles of the normal part of the retarded Green's function are located at $\pm\sqrt{\epsilon_\alpha^2+\Delta_\alpha^{\mathrm{BCS}2}}$, i.e. the available particle and hole excitation energies acquire a gap $|\Delta_\alpha^{\mathrm{BCS}}|$. Using e.g. (A.23) we can conclude that whatever the spectrum ϵ_α, we will get an long time exponential decay in the imaginary time normal Green's function $\mathbf{G_0}_{s\tau s\tau'}$ of the type

$$\mathrm{Tr}\{\mathbf{G_0}_{s\tau s\tau'}\} \sim e^{-\sqrt{\min_\alpha\left\{\Delta_\alpha^{\mathrm{BCS}2}+\epsilon_\alpha^2\right\}}|\tau-\tau'|} \sim e^{-\min_\alpha\{|\Delta_\alpha^{\mathrm{BCS}}|\}|\tau-\tau'|} \tag{4.15}$$

Incidentally it should be noted that a point-interaction as the one presented in (4.3) leads to a constant $\Delta_\alpha^{\mathrm{BCS}} = \Delta^{\mathrm{BCS}}$. We will proceed with this assumption in the following.

The last equation has direct consequences in the resulting phase only action, which as before takes on the form (2.65)

$$S = \int \frac{1}{4E_C}\left(\partial_\tau\phi_\tau\right)^2 + \alpha\int K_{\tau\tau'}\left[1-\cos(\phi_\tau-\phi_{\tau'})\right] \tag{4.16}$$

since using (2.62)

$$\alpha = LNt^2\rho_l(0)\rho_g(0) \tag{4.17}$$

$$K_{\tau\tau'} = -\frac{1}{\alpha}\mathrm{Tr}\left[\mathbf{G_0}_{\tau'\tau}\mathbf{t}\bar{\mathbf{G}}_{\mathbf{0}\tau\tau'}\mathbf{t}^+\right] = -\frac{LNt^2}{\alpha}\mathrm{Tr}\left[\mathbf{G_0}_{\tau'\tau}\right]\mathrm{Tr}\left[\bar{\mathbf{G}}_{\mathbf{0}\tau\tau'}\right] \tag{4.18}$$

we can see that $K_{\tau\tau'}$ is now exponentially decaying with the gap. [3] According to previous discussion this implies that phase-phase correlator $\mathcal{G}_{\tau\tau'}$ will decay exponentially at long times if Δ^{BCS} is finite, which speaks as expected of activated conductance (no cotunneling) in the superconducting phase. Let us note in passing that if the leads had been superconducting, an extra term would have arisen upon the integration of the lead fermions of the form $\mathbf{f}^+_\tau\bar{\mathbf{F}}_{\tau\tau'}\mathbf{f}^+_{\tau'}e^{-i(\phi_\tau+\phi_{\tau'})}$ that would yield a $\cos(\phi_\tau+\phi_{\tau'})$ type of term in the phase only action. This new term describes the Josephson coupling between grain and leads.

[3] Note that definition of α in (2.62) convenient for this context contains the normal-state density of states at the Fermi energy, not the interacting (gapped) one.

4.2 Rotor description of exchange interactions

We have shown that by the convenient Nambu notation the description of a superconducting grain takes on a form that is totally analogue to the metallic case (2.1), albeit with a finite order parameter Δ^{BCS}. Let us build on that by adding also an extra exchange term to the model

$$H_{\mathrm{ex}} = J(\vec{S} - \vec{S}_{\mathrm{ext}})^2 \tag{4.19}$$

where we have introduced the possibility of an offset spin $\vec{S}_{\mathrm{ext}} = \frac{1}{2J}\vec{H}_{\mathrm{ext}}$ induced by an external magnetic field $\vec{H}_{\mathrm{ext}}$. We will retain for the moment the usual definition $\vec{S} = \frac{1}{2}\sum_{ss'\alpha} d^+_{\alpha s}\vec{\sigma}_{ss'}d_{\alpha s'}$ without turning to Nambu space for the spin yet. The idea now, as with the charge, is to use a Hubbard - Strattonovich decoupling on this quartic interaction term

$$e^{-J(\vec{S}-\vec{S}_{\mathrm{ext}})^2} \propto \int \mathcal{D}\vec{H} e^{-\frac{1}{4J}\vec{H}^2 - i(\vec{S}-\vec{S}_{\mathrm{ext}})\vec{H}} \tag{4.20}$$

The new vectorial field $\vec{H}_\tau$ plays the role of a fluctuating magnetic field, much in the same way as V_τ plays the role of a fluctuating voltage in the grain that mediates the electron's interactions. With this decoupling we have the following model

$$\begin{aligned} S &= S_{\mathrm{lead}} + S_{\mathrm{grain}} + S_{\mathrm{hop}} + S_0 + S_1 \\ S_0 &= \int d\tau \left(\frac{1}{4E_C}V^2 + \frac{1}{4J}\vec{H}^2 + iVn_D + i\vec{H}\vec{S}_{\mathrm{ext}} \right) \\ S_1 &= \int d\tau \left(iVQ + i\vec{H}\vec{S} \right) \end{aligned} \tag{4.21}$$

We introduce a unitary $\mathrm{U}(1)\otimes\mathrm{SU}(2)$ transformation on the $\mathbf{d}$ fields that reabsorbs as much as possible of the coupling S_1. In normal (spin-space) notation we write

$$\mathbf{f}_\tau = U_\tau \mathbf{d}_\tau \tag{4.22}$$

$$U_\tau = e^{i\phi_\tau} e^{\frac{i}{2}\xi_\tau \hat{n}_\tau \vec{\sigma}} \tag{4.23}$$

where both ϕ_τ and ξ_τ live in the unit circle, and $\hat{n}_\tau$ is a 3D unit vector. $\vec{\sigma}$ acts on the spin index of the fermions. Since the old $\mathbf{d}_\tau$'s and also the new fields $\mathbf{f}_\tau$ must be β-antiperiodic (they are fermions), one must have $U_\tau = U_{\tau+\beta}$, and therefore the three fields ϕ_τ, ξ_τ and $\hat{n}_\tau$ must obey

$$\begin{aligned} \phi_{\tau+\beta} &= \phi_\tau + 2\pi m, \quad \text{where } m \in \text{Integers} \\ \xi_{\tau+\beta} &= \xi_\tau + 2\pi k, \quad \text{where } k \in \text{Integers} \\ \hat{n}_{\tau+\beta} &= \hat{n}_\tau \end{aligned} \tag{4.24}$$

The condition that the most part of S_1 be reabsorbed by this transformation leads to the condition

$$(\partial_\tau U^+)U = -i\left[\mathbb{1}(V - \tilde{V}_0) + \frac{1}{2}\vec{\sigma}(\vec{H} - \vec{\tilde{H}}_0) \right] \tag{4.25}$$

which after some algebra that we summarize in the following equation

$$
\begin{aligned}
(\partial_\tau U^+)U &= -i\int_0^1 d\nu e^{-i\nu(\phi\mathbb{1}+\frac{1}{2}\xi\hat{n}\vec{\sigma})}(\mathbb{1}\dot{\phi}+\frac{1}{2}\dot{\xi}\hat{n}\vec{\sigma}+\frac{1}{2}\xi\dot{\hat{n}})e^{i\nu(\phi\mathbb{1}+\frac{1}{2}\xi\hat{n}\vec{\sigma})} && (4.26)\\
&= -i\left[\dot{\phi}\mathbb{1}+\frac{1}{2}\dot{\xi}\hat{n}\vec{\sigma}+\frac{1}{2}\xi\int d\nu e^{-\frac{i}{2}\nu\xi\hat{n}\vec{\sigma}}\dot{\hat{n}}\vec{\sigma}e^{\frac{i}{2}\nu\xi\hat{n}\vec{\sigma}}\right]\\
&= -i\left[\dot{\phi}\mathbb{1}+\frac{1}{2}\dot{\xi}\hat{n}\vec{\sigma}+\frac{1}{2}\xi\vec{\sigma}\int d\nu\left(\cos(\nu\xi)\dot{\hat{n}}+\sin(\nu\xi)\dot{\hat{n}}\times\hat{n}\right)\right] && (4.27)\\
&= -i\left[\dot{\phi}\mathbb{1}+\frac{1}{2}\vec{\sigma}\left(\dot{\xi}\hat{n}+\sin\xi\dot{\hat{n}}+(1-\cos\xi)\dot{\hat{n}}\times\hat{n}\right)\right]\\
&= -i\left[\mathbb{1}(V-\tilde{V}_0)+\frac{1}{2}\vec{\sigma}(\vec{H}-\vec{\tilde{H}}_0)\right] && (4.28)
\end{aligned}
$$

leads to the identification[4]

$$
\begin{aligned}
V_\tau-\tilde{V}_0 &\equiv L_{\hat{u}}=\dot{\phi} && (4.29)\\
\vec{H}_\tau-\vec{\tilde{H}}_0 &\equiv \vec{L}_{\hat{v}}=\dot{\xi}\hat{n}+\sin\xi\dot{\hat{n}}+(1-\cos\xi)\dot{\hat{n}}\times\hat{n} && (4.30)
\end{aligned}
$$

Since this calculation runs very parallel to the one performed in chapter 2 the reader might have already guessed that the time independent $\tilde{V}_0$ and $\vec{\tilde{H}}_0$ in the last equations are the (minimum) projection fields that must be subtracted from the auxiliary fields V_τ and $\vec{H}_\tau$ to relate them to the β-periodic phases. Indeed, since no periodicity constraint exists on the auxiliary fields while the phases must obey (4.24), it is impossible to satisfy equations (4.29) and (4.30) for a general path of the auxiliary fields, see section 2.3.3.

As before, the integration of the 'projection fields' would impose the instantaneous all-times constraint by which $\xi_\tau\hat{n}_\tau$ is the conjugate of $\vec{S}=\frac{1}{2}\sum_{ss'\alpha}d^+_{\alpha s}\vec{\sigma}_{ss'}d_{\alpha s'}$ and ϕ_τ the conjugate of $\sum_{s\alpha}d^+_{\alpha s}d_{\alpha s}-N_0$. However, while the functional $\tilde{V}_0[V_\tau]=\frac{1}{\beta}\int_0^\beta V_\tau d\tau \bmod 2\pi$ was straightforward to obtain from the first equation of (4.24) and (4.29) (so that $V_\tau-\tilde{V}_0$ has zero average, see 2.3.3), an explicit expression and intuition of $\vec{\tilde{H}}_0$ will prove a bit more involved. We refer the reader to Appendix C for a detailed description of the geometrical meaning of $\vec{\tilde{H}}_0$, and a justification of why it is time-independent. The philosophy however will be again to treat $\vec{\tilde{H}}_0$ in a saddle point manner instead of doing a sum over all values, a treatment which becomes exact in the large-N limit. And just as before, in absence of external fields $\vec{S}_{\text{ext}}=0$ the saddle point value of $\vec{\tilde{H}}_0$ will be zero due to the manifest rotation invariance of the system. Otherwise it will contribute as a shift to the external field,

$$
\delta\vec{H}_{\text{ext}}=2J\delta\vec{S}_{\text{ext}}\equiv -i\,\vec{\tilde{H}}_0\Big|_{\text{saddle}} \qquad (4.31)
$$

just as for $\delta\mu=2E_C\delta n\equiv -i\tilde{V}_0\Big|_{\text{saddle}}$. We again refer the reader to Appendix C for details.

[4]The reason for the notation $L_{\hat{u}}$ and $\vec{L}_{\hat{v}}$ will become clear later when we define $\hat{u}$ and $\hat{v}$.

The resulting rotor parametrization of the effective action for a superconducting grain takes the form $S = S_{\text{lead}} + S_{\text{grain}} + S_{\text{hop}} + S_{\text{rotor}} + S_{\text{fields}}$, with

$$S_{\text{lead}} = -\int \mathbf{c}_\tau^+ \bar{\mathbf{G}}^{-1}_{0\tau\tau'} \mathbf{c}_{\tau'} \tag{4.32}$$

$$S_{\text{grain}} = -\int \vec{\mathbf{f}}_\tau^+ \hat{\mathbf{G}}^{-1}_{0\tau\tau'} \vec{\mathbf{f}}_{\tau'} - \delta\mu Q - \delta\vec{H}_{\text{ext}}\vec{S} \quad \text{(Nambu notation)} \tag{4.33}$$

$$S_{\text{hop}} = \int \mathbf{f}_\tau^+ U_\tau \mathbf{t} \mathbf{c}_\tau \tag{4.34}$$

$$S_{\text{rotor}} = \int \frac{1}{4E_C}\dot{\phi}^2 + \frac{1}{4J}\left(\dot{\xi}^2 + \dot{\hat{n}}^2 \sin^2\xi\right) \tag{4.35}$$

$$\begin{aligned} S_{\text{fields}} = & -iL_{\hat{u}}(n_G + N_0 - \delta n) + 2E_C\delta n(N_0 + n_G - \frac{1}{2}\delta n) \\ & -i\vec{L}_{\hat{v}}\left(\vec{S}_{\text{ext}} - \delta\vec{S}_{\text{ext}}\right) + 2J\delta\vec{S}_{\text{ext}}\left(\vec{S}_{\text{ext}} - \frac{1}{2}\delta\vec{S}_{\text{ext}}\right) \end{aligned} \tag{4.36}$$

The different contributions have been reordered so that in the absence of external fields or gate voltages (particle-hole symmetry preserved) and in the saddle point approximation for the projection fields, all of S_{fields} will vanish (plus the last two terms in S_{grain}).

An interesting point to note is the form that the observable for the total spin takes in this formulation. While the total charge was given by

$$\langle Q \rangle = n_G - \delta n + i\langle\dot{\phi}\rangle/2E_C = n_G - \delta n + i\langle L_{\hat{u}}\rangle/2E_C \tag{4.37}$$

cf. eq. (2.36), in the case of the spin we have

$$\langle\vec{S}\rangle = \vec{S}_{\text{ext}} - \delta\vec{S}_{\text{ext}} + i\langle\vec{L}_{\hat{v}}\rangle/2J. \tag{4.38}$$

While the case for the charge can be familiar for some readers (time derivative of the phase of the system having the meaning the voltage drop through a junction, which is in turn related to the charge accumulated in the junction by $V = Q/C$) the analogous result for the total spin will be new and much more complex. We will develop the natural description of eq. (4.38) in the next sections, so that a perfect analogy will become apparent relating the 'polarization drop' as the time derivative of a 'generalized phase' given by a point on a 4D spherical surface (as opposed to 2D for ϕ).

Integration of the leads

The integration of the lead degrees of freedom is straightforward (see sec. 2.4), and yields $S = S_{\text{grain}} + S_{\text{rotor}} + S_{\text{dis}} + S_{\text{fields}}$ with the dissipative action S_{dis} arising from $\langle S_{\text{hop}}\rangle^2$

$$S_{\text{dis}} = \int \mathbf{f}_\tau^+ \mathbf{\Delta}_{\tau\tau'} \frac{U_\tau U_{\tau'}^+ + U_{\tau'} U_\tau^+}{2} \mathbf{f}_{\tau'} \tag{4.39}$$

and $\mathbf{\Delta}_{\tau\tau'}$ given by (2.58) as usual.

Large-N integration of the fermions

The phase-only model is obtained just as in section 2.5 by the integration of the **f** fermions to leading order in the $1/N$ expansion. One arrives at the simple model

$$S = \int \left(\frac{{L_{\hat{u}}}^2}{4E_C} + \frac{\vec{L}_{\hat{v}}^2}{4J} \right) + \alpha \int K_{\tau-\tau'} \mathrm{Tr} \frac{U_\tau U_{\tau'}^+ + U_{\tau'} U_\tau^+}{4} + S_{\text{fields}} \tag{4.40}$$

The term in the parenthesis is just another way of writing S_{rotor} of eq. 4.35. The extra factor 2 in the denominator of the trace comes from the inclusion of the $N = 2$ channels in the definition of α, eq. (2.61). The kernel $K_{\Delta\tau}$ will in general be given by the results of section 4.1, and will be 'gapped' (exponentially decaying) below the superconducting temperature.

The $U(1) \otimes SU(2)$ group element U_τ in the $N = 2$ representation, see eq. (4.23), can be expanded in terms of Lie parameters by using $\exp[\frac{i}{2}\xi\hat{n}\vec{\sigma}] = \mathbb{1}\cos\frac{\xi}{2} + i\vec{\sigma}\sin\frac{\xi}{2}$ and $\mathrm{Tr}[\vec{k}\vec{\sigma}\vec{l}\vec{\sigma}] = 2\vec{k}\vec{l}$, to give

$$\mathrm{Tr}\frac{U_\tau U_{\tau'}^+ + U_{\tau'} U_\tau^+}{4} = \cos(\phi_\tau - \phi_{\tau'}) \times \left(\cos\frac{\xi_\tau}{2}\cos\frac{\xi_{\tau'}}{2} + \hat{n}_\tau \cdot \hat{n}_{\tau'} \sin\frac{\xi_\tau}{2}\sin\frac{\xi_{\tau'}}{2} \right)$$

It becomes apparent that the type of non-local in time dissipative contribution to the phase dynamics (representing the exit of an electron at one time and the return of an electron at another time) becomes inextricably mixed with an analogous form of dissipation on the spin-phase $(\xi_\tau, \hat{n}_\tau)$, that represents the simultaneous exit and return of a spin of modulus 1/2 but arbitrary orientation (with proper angular momentum composition rules).

4.3 A grain or a rotating sphere?

The reader might have been somewhat surprised in the course of the first chapter to see how the dynamics of the charge in a grain obeys the same dynamical equations as quantum 2D rotor, such as a disc with fixed axis of rotation, subject to some manner of dissipative effects such as might be produced by a surrounding fluid with some kind of memory effect depending on the spectral properties of the grain and the leads. This striking analogy goes even further in the case of the spin dynamics as we will show in what follows. Much like coordinate ϕ_τ describes the orientation of the charge $2D$ rotor, the coordinates $\xi_\tau, \hat{n}_\tau$ parameterize the orientation of a 3D sphere, and the dynamics of these phases is precisely that of such a rotor and sphere plus a dissipation of some kind. This analogy has its root in the isomorphism between $U(1)$ and the 2D rotations, and between $SU(2)$ and the 3D rotations, as explained in the following section.

4.3.1 The SU(2) - SO(3) Isomorphism

It is well known that a certain element of Lie group SO(3), say $e^{i\xi\hat{n}\vec{A}}$ (where $\vec{A}$ are the generators of SO(3)) has a one to *two* correspondence to a couple of elements of SU(2). The precise mapping is

$$e^{i\xi\hat{n}\vec{A}} \longrightarrow \left\{ e^{\frac{i}{2}\xi\hat{n}\vec{\sigma}}, e^{\frac{i}{2}(\xi+2\pi)\hat{n}\vec{\sigma}} \right\} = \left\{ \pm e^{\frac{i}{2}\xi\hat{n}\vec{\sigma}} \right\} \tag{4.41}$$

This correspondence is sometimes quite obscurely stated by saying that SU(2) is the 'square root' of SO(3). Alternatively it is said that particles with spin 1/2 have to be turned 4π radians to return to their previous state. All this means nothing more than the isomorphism stated above.

Within the path integral approach, and recalling that matrix $M = e^{i\xi\hat{n}\vec{A}}$ acts on three-dimensional bodies by rotating them an angle ξ around axis $\hat{n}$, one can think of the possible paths $(\xi_\tau, \hat{n}_\tau)$ in U_τ as *orientation paths of a 3D solid* that becomes rotated about to different positions respect to the initial one (choosing paths so that $U_{\tau=0} = \mathbb{1}_{2\times 2}$) as τ goes from 0 to β. The orientation of the sphere at time τ corresponds to rotating a fixed reference sphere by an angle ξ_τ around axis $\hat{n}_\tau$.

The bosonic cyclical condition $U_\tau = U_{\tau+\beta}$ in this language implies that in the 3D solid follows a periodic rotation in τ. This and the fact that the action is invariant under the transformation $U(\tau) \to -U(\tau)$ tells us that the descriptions of paths within SO(3), without taking into account the peculiar duality of the isomorphism (except for a counting factor, see below), is perfectly correct. The total spin that is governed by our action proves to be equivalent to a regular SO(3) angular momentum.

This discussion has a relevant payoff for our intuition. The vector that appears in equation (4.30)

$$\vec{L}_{\hat{v}} = \dot{\xi}\hat{n} + \sin\xi\dot{\hat{n}} + (1-\cos\xi)\dot{\hat{n}} \times \hat{n} \tag{4.42}$$

happens to be the angular momentum of certain rotating 3D sphere that turns around according to the SO(3) matrix $M(\tau) = e^{i\xi(\tau)\hat{n}(\tau)\vec{A}}$. Although this statement is far from trivial, and since it provides a very useful intuitive picture of the problem, we will briefly sketch how one can work this out analytically. One easy way is to calculate the kernel of matrix $\partial_t M$. Since the columns of $M(\tau)$ are the coordinates of the sphere's reference system at time τ, the kernel of $\dot{M}(\tau)$ is essentially the instantaneous axis of rotation, i.e. the axis of the sphere that remains instantly still at time τ. For a sphere the angular momentum lies precisely in that axis. Its modulus in eq. (4.42) can be checked to be correct too. To make this plausible without carrying out the calculation note that for static $\hat{n}$, the modulus is $\dot{\xi}$, which is what one expects for a rotating sphere with fixed axis of rotation.

Furthermore, the kinetic energy $\frac{\vec{L}_{\hat{v}}^2}{4J} = \frac{1}{4J}\left(\dot{\xi}^2 + \dot{\hat{n}}^2\sin^2\xi\right)$ corresponds precisely to the rotation energy of such a sphere of orientation path $\xi_\tau, \hat{n}_\tau$.

4.3.2 4D sphere representation

We are now ready to discuss a subtle point that was bypassed in the derivation of the rotor action: what is the Jacobian for the path coordinates $\{\xi, \hat{n}\}$? Since we have changed variables of integration from the cartesian coordinates of field $\vec{H}_\tau$ to the conjugate coordinates of total spin, a Jacobian could be expected to appear in the transformation. It seems quite reasonable to expect that at least for $\hat{n}$ the Jacobian be that of a 3D sphere surface, but what about ξ? Let us work this out. [5]

To do this we must return to the starting point where we introduced field $\vec{H} = \{H_x, H_y, H_z\}$. The Jacobian for this $\vec{H}$ should be one in cartesian coordinates, that is,

[5] The case of ϕ is trivial, the Jacobian being 1 as in polar coordinates.

$\vec{L}_{\hat{v}} = \vec{H} - \vec{\tilde{H}}_0$ should also be uniformly distributed across 3D space, with cartesian Jacobian $J = 1$. So if we define in cartesian coordinates $\hat{n} = (n_x, n_y, n_z)$ as

$$\hat{n} = (\sin\theta\cos\varphi, \sin\theta\sin\varphi, \cos\theta) \tag{4.43}$$

what does this $J = 1$ imply for the Jacobian of $\{\xi, \theta, \varphi\}$? By working on eq. (4.42) we find that we can alternatively write

$$\vec{L}_{\hat{v}} dt = \hat{n}_\xi d\xi + \hat{n}_\theta \sin\frac{\xi}{2} d\theta + \hat{n}_\varphi \sin\frac{\xi}{2}\sin\theta d\varphi \tag{4.44}$$

where the $\hat{n}$'s are three orthogonal unit vectors that are functions of $\{\xi, \hat{n}\}$ (in particular $\hat{n}_\xi = \hat{n}$). Since this $\vec{L}_{\hat{v}}$ must be distributed uniformly in 3D with density 1, and therefore its coordinates in the $\{\hat{n}_\xi, \hat{n}_\theta, \hat{n}_\varphi\}$ reference frame must be uniform, we conclude that the Jacobian in the new angle coordinates should be

$$J(\xi, \theta, \varphi) = \sin^2\frac{\xi}{2}\sin\theta \tag{4.45}$$

This corresponds precisely to the Jacobian for the generalized spherical coordinates $\{\xi/2, \theta, \varphi\}$ in 4D.

One can therefore visualize the total state of the system (or alternatively the orientation of the 3D sphere and the 2D rotor) at imaginary time τ by a certain point $\hat{m}_\tau$ on the 4D spherical surface plus another point on the 2D spherical 'surface' $\hat{u}_\tau$

$$\hat{u}_\tau = (\cos\phi_\tau, \sin\phi_\tau) \tag{4.46}$$

$$\hat{v}_\tau = \left(\cos\frac{\xi_\tau}{2}, \sin\frac{\xi_\tau}{2}\hat{n}_\tau\right) \tag{4.47}$$

What is remarkable is that action (4.40) can be cast into a very compact generalized form of the usual 2D rotor action in this notation

$$S = \frac{1}{2}\int\left(\frac{\dot{\hat{u}}^2}{4E_C} + \frac{\dot{\hat{v}}^2}{4J}\right) + \alpha\int K_{\tau-\tau'}\left(1 - \hat{u}_\tau\hat{u}_{\tau'}\hat{v}_\tau\hat{v}_{\tau'}\right) + S_{\text{fields}} \tag{4.48}$$

The complicated form of the kinetic energy of the spin-phase is expressed in a very simple fashion when one realizes that the natural degree of freedom for the conjugate of the total spin lives in a 4D sphere manifold. An even more compact and elegant form of this phase action, mainly in what concerns the coupling to an external field, can be obtained by the use of Quaternion algebra. We refer the interested reader to appendix D for details.

4.4 Discussion

Abundant conclusions can be drawn before doing any calculations from staring at the form of the action (4.48). First of all, we should note that the system without spin gap $J = 0$ is described by exactly the same model as before (2.65), since in this limit $\hat{v}_\tau$ becomes infinitely rigid (like the position coordinate for a particle of infinite mass), and we have $\hat{v}_\tau \cdot \hat{v}_{\tau'} = 1$.

As J is increased however, the fluctuations of $\hat{v}_\tau$ grow, giving typically $\hat{v}_\tau \cdot \hat{v}_{\tau'} < 1$ for any path with high weight, and actually this dot product will tend to decay with $\tau - \tau'$. Therefore, regardless of the decay law of $K_{\Delta\tau}$ we can conclude that the disordering of charge-phase (charge localization) is reinforced by the disordering of spin-phase (spin localization), which is favored by a finite spin gap J. This is a manifestation of the fact that charge and spin hop together in and out of the grain.

4.4.1 General comments

Indeed, if we were to expect a given value of the large-α exponentially renormalized charging energy cf. (2.103) (neglecting the superconducting gap as $\Delta^{\mathrm{BCS}} \ll E_C$)

$$E_C^* = 4\pi^2 \alpha^2 E_C e^{-2\pi^2 \alpha} \tag{4.49}$$

in the absence of spin gap J [43, 87], it is reasonable to expect that this suppression will be reduced by an amount roughly equivalent to substituting α by $\alpha\langle|\hat{v}|^2\rangle < \alpha$. For a rough evaluation of $\langle|\hat{v}|^2\rangle$ we can neglect dissipation for $\hat{v}$ for frequencies higher that E_C, and assume small harmonic fluctuations in that region, which would yield

$$\langle|\hat{v}|^2\rangle = 1 - \int_{E_C}^{\infty} \frac{d\omega}{\omega^2/2J} = 1 - 2J/E_C \tag{4.50}$$

and roughly

$$E_C^* = 4\pi^2 \alpha^2 E_C e^{-2\pi^2 \alpha(1-2J/E_C)} \tag{4.51}$$

which would be valid for small J/E_C. This would mean an exponential dependence of charge fluctuations with the spin gap. The physical picture is that although charge fluctuations can be greatly facilitated by a strong coupling to the leads, the fact that charge and spin are inseparable would tend to re-localize charge if there is a spin gap. This is only a qualitative discussion but we will show some Monte-Carlo calculations later that confirm this strong J dependence of the effective charging energy.

Another conclusion that can be drawn pertains systems without a developed superconducting gap (for example for $T > T_C$). An extension of Kosterlitz arguments [58] on spin chains which can be found in appendix E can be employed to ensure that in the absence of excitonic effects (see the beginning of chapter 2 and the discussion of parameter ϵ) all systems obeying the present model will be insulating at very low temperatures, even in the limit of strong coupling to the leads $\alpha \gg 1$. This comes as no surprise however, since the system without a spin gap already shows this behavior, so an additional energy gap should not alter the picture.

4.4.2 Parameter regimes and results for a regular superconducting grain

For the case of a system with a finite superconducting gap Δ^{BCS} we can do a qualitative analysis by neglecting the charge-phase and spin-phase path correlations, and doing $\hat{u}_\tau \hat{u}_{\tau'} \hat{v}_\tau \hat{v}_{\tau'} \approx \langle \hat{u}_\tau \hat{u}_{\tau'} \rangle \hat{v}_\tau \hat{v}_{\tau'} + \hat{u}_\tau \hat{u}_{\tau'} \langle \hat{v}_\tau \hat{v}_{\tau'} \rangle$. Using this decoupling and assuming a self consistent decay law of $\langle \hat{u}_\tau \hat{u}_{\tau'} \rangle \sim e^{-\lambda_v \Delta\tau}$ and $\langle \hat{v}_\tau \hat{v}_{\tau'} \rangle \sim e^{-\lambda_u \Delta\tau}$ for certain energy scales

λ_u and λ_v, we can establish two conditions on these energy scales, which correspond to the effective charge and spin energy gaps: on the one hand

$$\lambda_u^{-1} > E_C^{-1} \tag{4.52}$$
$$\lambda_v^{-1} > J^{-1} \tag{4.53}$$

since the phase rigidity given by the kinetic energy in (4.48) forbids variations of correlations below these typical times; on the other we can argue that if the decoupling above is valid both $\hat{u}_\tau$ and $\hat{v}_\tau$ will experience an effective exponentially decaying static kernel with inverse decay times $\Delta^{\mathrm{BCS}} + \lambda_v$ and $\Delta^{\mathrm{BCS}} + \lambda_u$ respectively. Using Griffith's theorem from section 2.5.2 we can establish the following inequalities

$$\lambda_u^{-1} > (\Delta^{\mathrm{BCS}} + \lambda_v)^{-1} \tag{4.54}$$
$$\lambda_v^{-1} > (\Delta^{\mathrm{BCS}} + \lambda_u)^{-1} \tag{4.55}$$

This leads to the solution depicted in Fig. 4.1. Recall that in the absence of grain-lead coupling the exact solution is $\lambda_u = E_C$ and $\lambda_v = J$, see footnote in 2.5.2. For arbitrarily small α, and always assuming that the correlationless decoupling explained above is approximately valid (true at least for small α), Griffith's theorem is enough to set a non trivial upper bound for the energy gap of charge and spin fluctuation, in terms of the values of $\Delta^{\mathrm{BCS}}, E_C$ and J. The total energy gap for single electron transport will simply be $E_{\mathrm{gap}} \equiv \lambda_u + \lambda_v$, since the physical electron propagator within this approximation will be (see eq. (2.67))

$$\mathbf{G}_{\mathbf{d}\,\Delta\tau} = \langle \mathbf{f}_\tau^+ \mathbf{f}_{\tau'} \rangle \langle \hat{u}_\tau \hat{u}_{\tau'} \hat{v}_\tau \hat{v}_{\tau'} \rangle \approx \langle \mathbf{f}_\tau^+ \mathbf{f}_{\tau'} \rangle \langle \hat{u}_\tau \hat{u}_{\tau'} \rangle \langle \hat{v}_\tau \hat{v}_{\tau'} \rangle \tag{4.56}$$

From this simple arguments we can conclude that

- **Case** $J \ll E_C, \Delta^{\mathrm{BCS}}$: If either J is very small as compared with the other energy scales E_C and Δ^{BCS} we see that $\lambda_v \approx 0$ and the energy gap is

  $$E_{\mathrm{gap}} < \min\{E_C, \Delta^{\mathrm{BCS}}\} \text{ for } J \ll E_C, \Delta^{\mathrm{BCS}} \tag{4.57}$$

  This is illustrated schematically on the left side of Fig. 4.1.

  - **Case** $J \ll \Delta^{\mathrm{BCS}} \ll E_C$: This is nothing but the case of the metallic grain we have studied in depth in chapter 2. The result $E_{\mathrm{gap}} < \Delta^{\mathrm{BCS}} \approx 0$ is indeed consistent with our previous analysis of metallic grains, since by construction E_{gap} is truly a spectral gap, unlike E_C^*, i.e. a zero interacting density of states for $\omega < E_{\mathrm{gap}}$, or alternatively a finite timescale *exponential* decay of phase correlations. Therefore the $\Delta^{\mathrm{BCS}} \approx 0$ limit gives $E_{\mathrm{gap}} \approx 0$. This means there is no exponential decay, but rather a power-law one, which was precisely the result we obtained for metallic grains and which was the manifestation of cotunneling. On the other hand we see that an arbitrarily small lead-grain coupling with a small but *finite* $\Delta^{\mathrm{BCS}} < E_C$ superconducting gap in the grain breaks cotunneling at low temperatures, and a finite $E_{\mathrm{gap}} \lesssim \Delta^{\mathrm{BCS}}$ *can* develop, probably superimposed on the $\sim \omega^2$-type density of states of the cotunneling regime, as a small

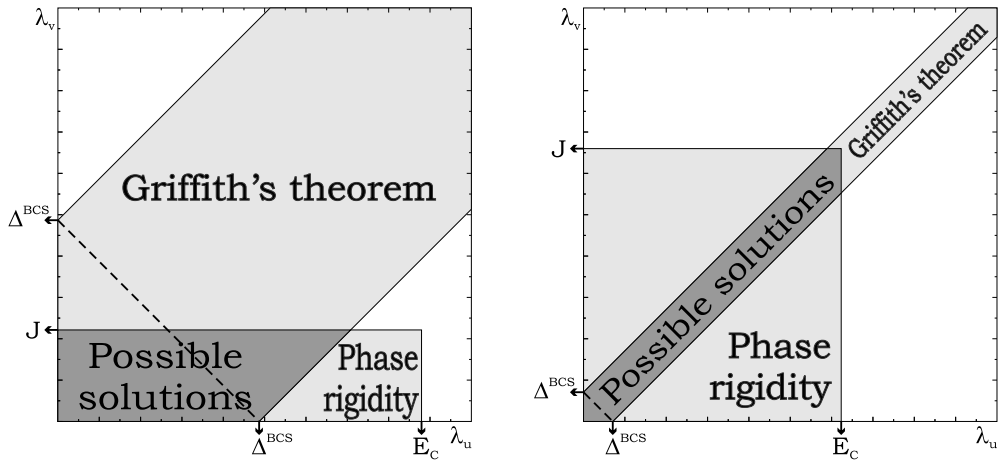

Figure 4.1: The two sets of inequalities on the inverse decay time of charge and spin phases, λ_u and λ_v arising from phase rigidity and Griffith's theorem constraints are represented in light gray. The overlap of both regions give the possible solutions consistent with such constraints, in darker grey. Note that this is enough to identify an upper bound for the charge and spin gaps that is non-trivial in the presence of coupling to the leads. The physical electronic gap is $\lambda_u + \lambda_v$. An additional upper bound can be identified by another application of Griffith's theorem, see text, so that only solutions below the dashed line $\lambda_u + \lambda_v < \Delta^{\mathrm{BCS}}$ are valid.

and sharp E_{gap} gap opening in the low temperature curves of Fig. 2.11. Note that this result completely neglects the effect of Andreev processes (because they vanish in the large N limit). These would be the next dominant contributions below E_{gap}, but to describe them we would have to remain in the subleading $1/N$ approximation of our formalism, as we did in chapter 3. This is left for future work.

- **Case** $J \ll E_C \ll \Delta^{\mathrm{BCS}}$: Interestingly enough the effect of a large superconducting gap is to recover a definite spectral gap $E_{\mathrm{gap}} \lesssim E_C$. This also makes sense, since the $\sim 1/\tau^2$ decay of $\mathcal{G}$ in (2.108) should no longer be valid, as cotunneling processes are killed by the superconducting gap. Therefore the algebraic $\sim T^2$ temperature dependence of conductance will turn into $\sim e^{-E_{\mathrm{gap}}/K_B T}$ behavior, but the scale E_{gap} is expected to be roughly independent of Δ^{BCS}. This is markedly different from the sequential tunneling result whereby the conductance would behave as $\sim e^{-\Delta^{\mathrm{BCS}}/K_B T}$. We restate that the experimental regime where we expect to find this non-trivial behavior is that of a grain with a large number of conduction channels and dimensionless conductance but a small value of per-channel transmission. The present qualitative arguments are unable to say what kind of spectral profile we would find above E_{gap} in this case.

- **Case** $E_C \ll J, \Delta^{\mathrm{BCS}}$: Since the system is symmetric between charge and spin (except for the dimension of the manifold where the phases belong) a behavior analogous to the previous one should be expected in this case. For $\Delta^{\mathrm{BCS}} < J$ cotunneling transport

through the spin gapped state would be suppressed at energies below the effective superconducting gap $E_{\rm gap} \lesssim \Delta^{\rm BCS}$ whereas above it a power-law spectral profile will be expected. If $J < \Delta^{\rm BCS}$ the situation is reversed but no particular power-law is expected above $E_{\rm gap} \lesssim J$. As in the last case, the present qualitative arguments do not provide any insight as to the typical spectral profile above $E_{\rm gap}$ in the latter case.

- **Case $\Delta^{\rm BCS} \ll E_C, J$**: If $\Delta^{\rm BCS}$ is the smallest energy scale of the three the best upper bound we can give for the energy gap will be

$$E_{\rm gap} < 2\min[J, E_C] \tag{4.58}$$

There is however a problem hidden here. It is possible to argue that in this case the decoupling of charge and spin leads to a wrong result. The correct one can be quite simply derived by applying Griffith's theorem again in a slightly different manner, which leads to $E_{\rm gap} = 0$, i.e. cotunneling is restored in this regime. This is what one should physically expect, since the perturbative arguments for cotunneling in the absence of superconductivity hold exactly the same in the presence of a finite spin gap. The reasoning goes as follows: if we don't decouple $\hat{u}_\tau \hat{u}_{\tau'} \hat{v}_\tau \hat{v}_{\tau'}$ and argue that it is the correlation function of the joint degree of freedom $\hat{u}_\tau \hat{v}_\tau$ which is experimenting a long range $1/\tau^2$ retarded interaction ($\Delta^{\rm BCS} \approx 0$), Griffith's theorem states that $G(\Delta\tau) \equiv \langle \hat{u}_\tau \hat{u}_{\tau'} \hat{v}_\tau \hat{v}_{\tau'} \rangle$ cannot decay exponentially, since interactions decay more slowly than that. Therefore $E_{\rm gap} \lesssim \Delta^{\rm BCS} \approx 0$. The simple decoupling of previous sections is seen to be incorrect in this case even for small α. A Quantum Monte Carlo computation was performed to verify this result, see Fig. 4.2, and surprisingly enough, while charge-only and spin-only correlators $G_u(\Delta\tau) \equiv \langle \hat{u}_\tau \hat{u}_{\tau'} \rangle$ and $G_v(\Delta\tau) \equiv \langle \hat{v}_\tau \hat{v}_{\tau'} \rangle$ where found to be both exponentially decaying, the joint charge-spin propagator $G(\Delta\tau)$ was found to decay algebraically as predicted by Griffith's theorem. This is a singular situation in which the approximate decoupling $G(\Delta\tau) \approx G_u(\Delta\tau) G_v(\Delta\tau)$ gives a totally unphysical result (i.e. absence of cotunneling with a charge and spin gap). 'Vertex corrections' are essential in this decoupling, as is demonstrated by the Quantum Monte Carlo results. Some more attention will be payed to this case in the next section.

4.4.3 Monte Carlo calculations in the small $\Delta^{\rm BCS}$ limit

The peculiar charge and spin correlation in the last case $\Delta^{\rm BCS} \ll E_C, J$ give rise to a similar kind of physics as in an exotic metallic grain, in which $\Delta^{\rm BCS}$ can be ignored and we take a small non-interacting level spacing, but in which exchange interactions are not negligible. This regime could be a reasonable description in a gapless superconductor, in which one finds a strong spin paramagnetism but a finite density of states at the Fermi energy due to an undeveloped superconducting gap. This more or less exotic type of behavior can be found in thin superconducting films [70] or granular arrays [60], or in superconducting systems with a finite density of magnetic impurities [65, 84], a superconducting grain with a large supercurrent driven through it, etc. We will however stay at this level of qualitative description and leave a more microscopic study for future work. We wish here to analyze what the effect of this positive exchange in the case of a continuous gapless spectrum would be on the renormalized charging energy E_C^* (see chapter 2). This is an

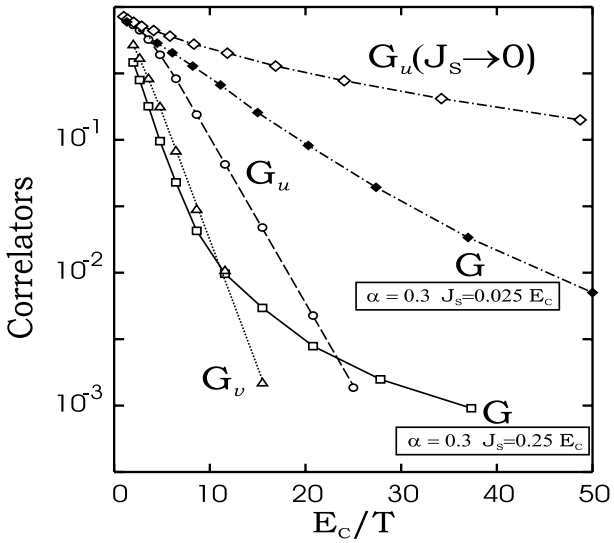

Figure 4.2: For very small Δ^{BCS}, if one neglects vertex corrections and assumes a $G(\Delta\tau) \approx G_u(\Delta\tau)G_v(\Delta\tau)$ decoupling, an exponential decay is predicted in $G(\Delta\tau)$, and therefore the incorrect result that there is no cotunneling through the system. A detailed Quantum Monte Carlo computation reveals strong correlations between $\hat{u}_\tau$ and $\hat{v}_\tau$ phase fluctuations, which lead to an algebraic decay of $G(\Delta\tau)$ consistent with Griffith's theorem and physical intuition.

important quantity mostly to characterize the strength of charge fluctuations in the system and more importantly the thermodynamic response of the free energy to the variation of an external gate, i.e. the effective capacitance of the grain in the presence of paramagnetic spin exchange.

Various Monte Carlo computations where performed in which it became evident that a finite positive exchange J indeed increases the value of E_C^* linearly with small J/E_C, consistently with (4.51), see Fig. 4.3. For larger values of J/E_C, E_C^* is seen to behave qualitatively as in (4.51) but changing $(1 - 2J/E_C)$ by something like $1/(1 + 2J/E_C)$, although we did not manage to perform a more analytical validation of this.

As to the α dependence of E_C^* in the present case, it was qualitatively confirmed to also obey (4.51) for large α and small J/E_C, although it is hard to reach convergence for large values of α within Monte Carlo algorithms. However a peculiar small α dependence was found for large values of J/E_C that deviates from (4.51), see Fig. 4.4. $E_C^*(\alpha)$ appears to have a negative second derivative for small α that does not occur for $J = 0$. This is one feature that could in principle be measured directly that could identify spin-blockade contributions. When interpreting these Quantum Monte Carlo results however bear in mind that values for E_C^* have an increasing error for smaller values of E_C^* due to cancelation errors.

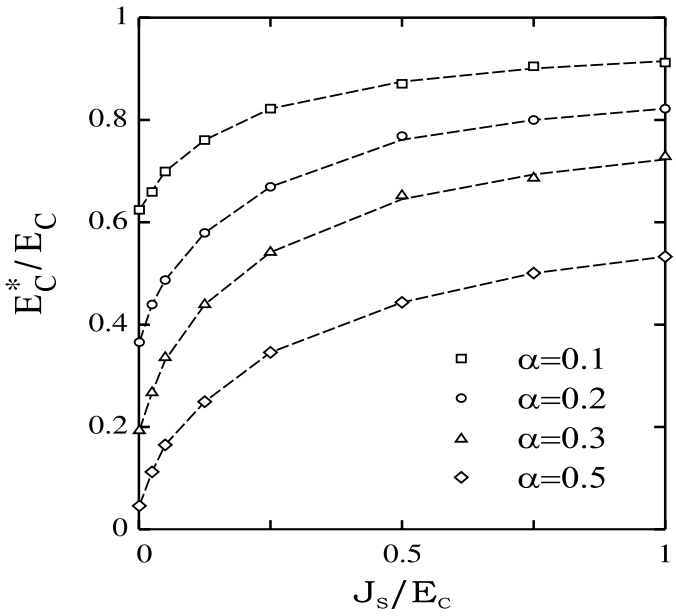

Figure 4.3: Monte Carlo result for the renormalized charging energy of the grain E_C^* in the presence of a finite spin gap J_S, versus the value of the spin gap J_S. Note the saturation for large J_S. This corresponds to the small $\Delta^{\rm BCS}$ regime, as explained in the text.

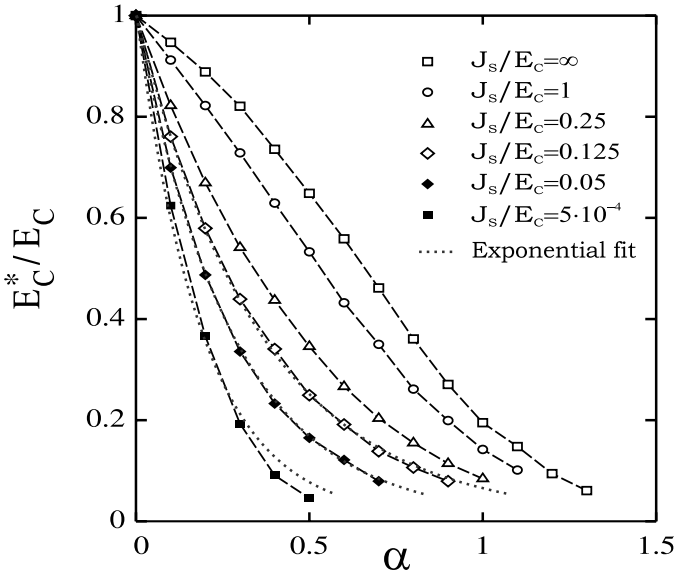

Figure 4.4: Renormalized charging energy of the grain in the presence of a finite spin gap J_S, versus the non-dimensional grain-lead coupling α. Note that the decay becomes less pronounced for growing spin gap, and departs from the purely exponential behavior at small α's.

4.4.4 External fields

In the present formalism the coupling of the spin-phase to an external magnetic field $\vec{S}_{\text{ext}}$ in (4.36) takes on a similar form as the coupling of the charge-phase to an external gate potential, i.e. through a time derivative of the phase. However, while in the case of the charge-phase it is an exact derivative ($-in_G \int L_{\hat{u}} = \int \dot{\phi}$ does not depend on the specific path, only on the topological winding number, which is the equivalent of the integer total charge Q), it is not the case for the spin-phase $-i\vec{S}_{\text{ext}} \int \vec{L}_{\hat{v}}$. The periodicity of the Coulomb blockade peaks (conductance versus dimensionless gate voltage n_G) can be traced back to the existence of winding numbers in the phase[6], since the system is symmetric under a shift of n_G of one unit and the addition of a uniform winding number of one unit to all paths. This invariance is not shared by the spin degree of freedom, since close paths on SU(2) cannot be classified into distinct non-trivial topological sectors.

The fact that all paths on the $4D$ sphere can be continuously deformed to a point (there are no loopholes in a $4D$ sphere) makes the concept of winding numbers invalid in the case of the spin phase, and therefore the usual instanton approaches based on these topological sector decomposition are probably bound to be fruitless in the case of spin dynamics. However it is a matter of physical intuition that a similar effect as the Coulomb Blockade periodicity should be expected for high magnetic fields, since in such limit spin fluctuations away from the external field directions should be suppressed (only spins aligned with $\vec{S}_{\text{ext}}$ can enter the grain), and the SU(2) degree of freedom becomes an effective U(1) phase like for charge. In other words, in the presence of a large $\vec{S}_{\text{ext}}$ the directionality of spin addition should get frozen, $\hat{n}_\tau$ should then get fixed and only the phase ξ_τ should fluctuate exactly in the same way as ϕ_τ, with effective winding numbers that would result in a perfectly periodic dependence of conductance on external field. How does this happen in our formalism?

To answer this question we must make use of the geometrical interpretation of $\vec{L}_{\hat{v}}$ and $\int \vec{L}_{\hat{v}}$ explained in Appendix C. It was shown there that $\vec{L}_{\hat{v}}$ is the velocity on the tangent space of the 4D spherical surface where $\hat{v}_\tau$ lives. The 'rolling SU(2)' picture for $\int \vec{L}_{\hat{v}}$ is enough to show that the set of paths for which $\int \vec{L}_{\hat{v}}$ is an extremum (i.e. linear deviations for these paths result in quadratic deviations on $\int \vec{L}_{\hat{v}}$) correspond to straight lines on the tangent space, and therefore to maximum circles around the 4D sphere (constant $\hat{n}_\tau$). If the term

$$-i\vec{S}_{\text{ext}} \int \vec{L}_{\hat{v}} \tag{4.59}$$

is present in the imaginary time actio and $\vec{S}_{\text{ext}}$ is very large, it is clear that only the paths with extremal $\int \vec{L}_{\hat{v}}$ will have a sizeable probability, since the rest will experience a random phase cancelation. This is a semiclassical-type of argument. Therefore the $\vec{S}_{\text{ext}} \gg 1$ limit transforms the model into an effective two-rotor system, being ξ_τ the new rotor coordinate, with effective topological winding numbers imposed by the semiclassical constraint $\hat{n}_\tau =$

[6]The usual approximation $\delta n \approx 0$ is assumed here for simplicity of the argument, although it can be shown not to be essential

$\hat{n} = \vec{S}/|\vec{S}|$. Furthermore, by doing a transformation of the type

$$\psi = \phi + \xi \tag{4.60}$$
$$\bar{\phi} = \phi - \xi \tag{4.61}$$

the dissipative dynamics of $S_{\rm dis}$ will decouple from $\bar{\psi}$ and we will end up with an effective one-rotor model, with kinetic energy $\int(\frac{1}{4E_C} + \frac{1}{4J})\dot{\psi}^2$ and external field coupling $-i\int(n_G + |\vec{S}_{\rm ext}|)\dot{\psi}$.

This would result in a coupled spin-charge Coulomb blockade type of conductance oscillations that would depend only on the external field combination $\frac{V_G}{2E_C} + \frac{|\vec{H}_{\rm ext}}{2J}|$. A deviation from this rule should be expected as soon as the semiclassical limit breaks down, i.e. if $|\vec{S}_{\rm ext}| = \frac{|\vec{H}_{\rm ext}|}{2J} \sim 1$.

4.5 Summary and outlook

In this chapter we have extended the concept of slave field to include the total-spin dynamics in an analogous way to the total charge dynamics described by usual slave fields. The complications of spin composition are cleanly dealt with by building such slave field as an object living in the $SU(2)$ group. A very simple modification of the phase-only description of metallic or superconducting grains is enough to include the large paramagnetic spin susceptibility of such systems, namely by a simple extension of the dissipation terms. The new formulation, although not accessible to simple spherical limit approximations or NCA decouplings of charge and spin, remains tractable by Quantum Monte Carlo simulations. We have shown how such a spin gap exponentially suppresses the renormalized charging energy in a superconducting grain, how cotunneling is preserved in the formalism whenever the BCS gap is negligible as compared to E_C, J, and how the system is expected to respond to both electrostatic or magnetic external fields. An analogous route is suggested to treat spin diamagnetism of normal metals that could perhaps lead to an interesting description of ferromagnetic transitions that formally mirrors superconducting transitions. This idea is left as an open possibility for future work.

Chapter 5

Metal-Insulator transition in granular arrays

5.1 Preliminary concepts

We step in this chapter through the outer fringes of the complex world of material science. While synthetic mesoscopic systems such as metallic nanograins or lateral quantum dots are the perfect playground for the study of quantum correlations and controlled interactions, and have a a very real interest also from a technological point of view, there is an even more fascinating field from the point of view of the author that deals with the addition of many such quantum components to constitute what could be loosely called a 'material'. While usual materials are composed of atoms as their basic constituent it is also possible to conceive and synthesize materials composed of atomic clusters or metallic grains, which are conveniently described by the type of models we have been discussing here. The study of such 'bulk systems' opens the path to very interesting phenomena associated to concepts like dimensionality, coordination, percolation, phase transitions, phase separation, etc. In this chapter we will concentrate on one simple idea put forth a long time ago by Mott [72, 73] concerning the effect on transport of local interactions in materials, namely the Mott-Hubbard metal-insulator phase transition. We will also look into the problem of metal-insulator transitions under non-equilibrium conditions, by which we understand transport where quasiparticles do not have time to fully develop, and interactions screening is not complete between electron transfer events.

5.1.1 Mott-Hubbard transition

It was argued in the late 40's [72] that strong enough local interactions in solids would break up the Fermi liquid behavior. The argument was rather simple. Imagine a hypothetical one-dimensional periodic array of atoms (or n-dimensional for that matter) such that no intra-atomic electron-electron interactions are present, and whose independent orbitals have a finite overlap integral equivalent to a certain hopping amplitude t from atom to atom. As is well known from basic quantum mechanics, quantum coherence has the striking effect of opening up a window of energies wherein electrons can traverse the

array without any scattering, what is called a 'band'. From a classical point of view this is certainly surprising, since it would be like saying that an injected electron of energy within the band will always follow a perfectly periodic orbit across the infinite array, zig-zagging around the nuclei say, without ever being backscattered by one. In classical mechanics such stable orbits are much less robust than in classical mechanics. It is in general enough to slightly change the energy of the electron or introduce a very small amount of disorder in the array to destabilize such orbits. Quantum mechanics tends to make all these phenomena much more robust, which is why it is sometimes said that the stability of solid matter is a direct macroscopic manifestation of quantum coherence.

As we know from Fermi liquid theory a small amount of electron-electron interaction does not change things much, merely changing the meaning of 'particle' to a composite entity called 'quasiparticle'. But Mott intuitively argued that if a fixed repulsion energy E_C is induced by the addition of one electron to any site of the array, and then one starts to take the atom-atom spacing to increasingly large distances, the concept of coherent transport through the array should break down for large enough spacing, since individual real atoms separated one mile apart should not form delocalized bands. He argued that there should be a condition for the formation of transport bands, and that the criterion should be that the kinetic energy of electrons in the band surpasses the repulsion on-site energy, i.e. $t > E_C$. This happens to be a similar criterion to that of the breakdown of the Fermi Liquid at low densities, and the formation of a Wigner Lattice (see Introduction), although the interactions here are associated to the atomic sites in the material. Therefore it was argued that a transition from a metallic to an insulating type of behavior was expected to occur in a wide variety of materials whenever $t \sim E_C$. Since the hopping amplitude t depends exponentially on the inter-atom distance, it was further argued that at least some insulators at atmospheric temperature should become metallic under pressure, which was readily confirmed in many materials, e.g. the time-honored experiments on Cr-doped V_2O_3, see Fig. 5.1 [66–68].

This was christened as the 'Mott-Hubbard metal-insulator phase transition'. The order of the transition is still under debate. Some authors [63] find that the jump between the two phases is first order, even giving rise to phase coexistence close to the transition, although careful Monte Carlo studies by other authors shed some doubt on those claims [86]. Complicate situations are predicted when magnetism or frustration are involved [25, 100].

5.1.2 Non-equilibrium effects

Another ingredient in this chapter is the effect of incomplete dressing of quasiparticles upon electron tunneling. The history of this type of effects go back to predictions in 1967 by Mahan about the expected absorption spectrum of X-ray in metals. It was argued that the dominant contribution to X-ray absorption comes from the promotion of deep lying core electrons to the conduction band. A naïve guess would predict an absorption spectrum proportional to the density of states of empty states, therefore presenting a jump from zero to a finite value when the energy of the X-rays are enough to promote the core electron to just above the Fermi energy. The caveat of this reasoning is that interactions between the electrons in the metal and the core hole left by the promotion make this transition forbidden in first order of perturbation theory. To first order in the electromagnetic perturbation the

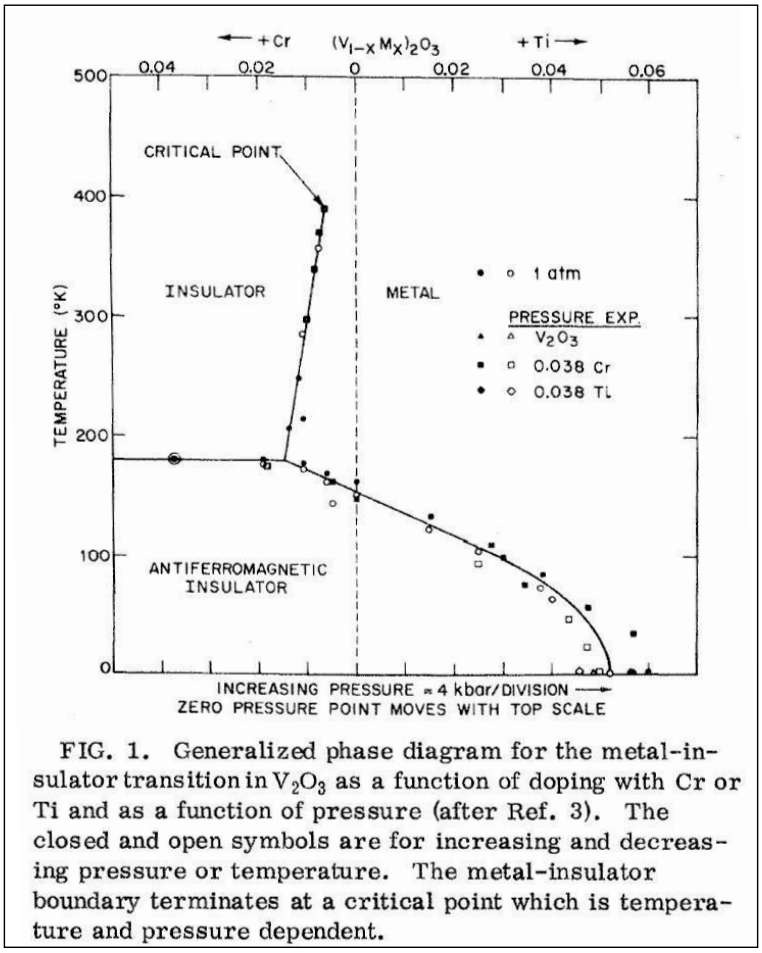

FIG. 1. Generalized phase diagram for the metal-insulator transition in V_2O_3 as a function of doping with Cr or Ti and as a function of pressure (after Ref. 3). The closed and open symbols are for increasing and decreasing pressure or temperature. The metal-insulator boundary terminates at a critical point which is temperature and pressure dependent.

Figure 5.1: Famous experimental results on the Mott transition in Cr-doped V_2O_3 by McWhan *et al.* [66].

absorption amplitude is proportional to the scalar product of the system's state with the core electron promoted to an empty conduction state and the minimum energy state with that same core electron promoted, i.e. between the unrelaxed and the relaxed states with a core hole. Now, in the presence of electron-electron interaction it was first proved by Anderson (1967) that the unscreened state (sudden core hole potential) is orthogonal, in the thermodynamic limit, to the screened one, which therefore is a complex superposition of many one-particle excited states of the initial system. This is called the 'orthogonality catastrophe'. Its origin can be traced back (following Anderson) to the phase shift δ by which all the original single-electron states in the metal are displaced by the action of the core hole potential. The scalar product is then computed to be $S = N^{-\delta^2/\pi^2}$ which goes to zero in the thermodynamic limit $N \to 0$. Therefore the transition amplitude has to be computed beyond first order (including polarization diagrams), and it turns out to give a spectral absorption profile that is power-law

$$P_A(\omega) = (\omega - \omega_{\text{thresh}})^g \tag{5.1}$$

(with $g > 0$) instead of step-like.

The whole problem of X-ray absorption revolves around the effect of a sudden localized potential (produced by an injected particle or hole) on the delocalized electrons. Even if each of them readjusts it's wave-function slightly the whole many electron state gets strongly altered, becoming orthogonal to the unrelaxed one when many particles are involved.

What is the relation of this story to the problem at hand of metallic grains and the metal-insulator transition of granular arrays? If one considers that what we call electrons in the grain are in fact quasi-electrons (screened particles) and that tunneling events however can only transfer single real electrons, we realize that in our formalism there is one propagator missing when calculating the dissipative kernel that acts on the phase of the system in the phase-only model, i.e. the propagator from particle to quasiparticle, or in other words the transition amplitude from an unscreened localized electron+grain state to a screened (quasi)electron state. If the electron is very localized after the tunneling event and it is not very close to the lead the orthogonality effect will be strong, and tunneling will be suppressed. However if the electron tunnels to a region in the grain that is not far from the leads an opposite contribution can dominate, known as the excitonic effect, whereby tunneling is enhanced by the formation of a bound state between the hole that is left behind and the electron that just tunneled. The computation of these effect has been performed in the literature for various metallic grain geometries [14, 93] in the lines of Anderson's arguments, and it was found to change the power-law decay of $K_{\Delta\tau}$ from eq. (2.68) to (2.70)

$$K_{\tau\tau'} = E_C^{\varepsilon} \left[\frac{\pi/\beta}{\sin\left(\pi(\tau - \tau')/\beta\right)} \right]^{2-\varepsilon} \overset{\beta\to\infty}{\longrightarrow} \frac{E_C^{\varepsilon}}{|\tau - \tau'|^{2-\varepsilon}} \tag{5.2}$$

The parameter ε, which is a function of the g above, is negative when orthogonality catastrophe effects dominate and positive for dominant excitonic effects, which are possibly the most frequent and also the most interesting since the oppose Coulomb blockade. We will mostly assume $\varepsilon > 0$ in the following pages. ε can be expressed also in terms of Anderson's phase

shift δ, see [14], and describes the dominant contribution of non-equilibrium effects beyond the orthodox theory of Coulomb blockade (see footnote just before eq. (2.70)).

This simple change can bring about important physical predictions as explained in section 2.5.2. To summarize Kosterlitz' results from our previous discussion he found that a metallic grain was expected to be insulating for $\varepsilon \leq 0$ and exhibit a metallic (finite zero temperature conductance) or insulating phase for $\varepsilon > 0$ in the following parameter range

$$\alpha > \frac{1}{2\pi^2 \varepsilon} \quad \Rightarrow \quad \text{metallic phase} \tag{5.3}$$

$$\alpha < \frac{1}{2\pi^2 \varepsilon} \quad \Rightarrow \quad \text{insulating phase} \tag{5.4}$$

where, recall eq. (2.61), α was associated to the coupling strength of the grain to the leads (in fact $4\pi^2\alpha$ is precisely the total dimensionless high temperature conductance of the junction, see Appendix B). These results are exact for the phase only model of chapter 2, and speak of a different type of metal-insulator transition associated to non-equilibrium effects, instead of merely interactions.

Conductance in terms of phase correlators

It has been shown in section 2.5.3 that linear conductance at low temperatures can be obtained from the imaginary time phase correlation function $\mathcal{G}_{\bar{\tau}}$ for $\bar{\tau} = \beta/2$ in the case of metallic grains (recall definition (2.52)). When excitonic or orthogonality effects are present the analysis leading to the above result must be modified by the introduction of vertex corrections in the expression of $\mathbf{G^d}$, and the calculation in Appendix B loses validity. Qualitative arguments were given in [14] for the modification of the $g = g_\infty \mathcal{G}_{\beta/2}$ result in the presence of non-equilibrium effects, which would become

$$g = g_\infty \left(\beta E_C\right)^\varepsilon \mathcal{G}_{\beta/2} \tag{5.5}$$

5.1.3 Dynamical Mean Field Theory

The study of many coupled impurities or grains or atoms with intra-site interactions has been the subject of many efforts to understand the properties of real materials. The most famous paradigm for the modeling of correlated materials is perhaps the Hubbard model, whereby a certain material is simplified as a set of single-orbital constituents with an internal electron-electron interaction term and coupled by tunneling amplitudes with each other. Such an extremely simplified model however exhibits an extraordinary complexity, and is nowadays still the subject of many studies. We are going to concentrate instead in a slightly more general case, in which each site hosts an arbitrary non-interacting spectrum of levels (such as in the grains of chapters 2 and 5) and electronic interaction within the grains are modeled by a charging energy-type of term with a given E_C. We will denote this generic model as a 'granular array', although it could apply to an array of other components, such as atoms with several levels packed close together around the Fermi energy.

One sort of approach that is specially powerful in this kind of problems is known as Dynamical Mean Field Theory (DMFT). Instead of making progress by the usual path of perturbation theory, it manages to write an approximation for the propagators in a

generic n-dimensional array of self-interacting sites that becomes exact when the dimension n is taken to infinity. It consists in reducing the problem of N sites to an effective self consistent action of the electrons in one site, and build propagators among different sites by employing the self consistent single-site self energy result. The essential idea on which this large-dimension approximation works is that a certain class of diagrams for the self energy can be disregarded in this limit, particularly the irreducible diagrams for intra-site (local) self energy in which two propagators are dressed by interactions in different sites. Neglecting this diagrams (which are suppressed at least like $1/n$ because the electron must exit into one of the $L \sim n$ possible neighboring sites and come back to precisely the original one) leads to the effective single site self consistent action of DMFT. There are excellent reviews on this technique [34], so we will simply sketch the most relevant result for the work to follow.

In the case of a granular array model with site connectivity as in an n-dimensional Bethe lattice[1], or an arbitrary lattice with an elliptic non-interacting density of states, which is a reasonable first approximation for a disordered granular material with complete magnetic frustration, DMFT gives a strikingly simple result for the effective one-site action. It is actually almost identical to our eq. (3.1), in the sense that it includes the usual intra-site interaction, the non-interacting level spectrum plus a last term coming from the coupling of that site to the rest of the system. In our case the integration of the lead electrons was an exact operation since they where non-interacting, thus yielding the bath function Δ, eq. (2.58), in terms of the non-interacting lead propagator $\bar{\mathbf{G}}$. According to DMFT the substitution of the leads around our site A by an n-dimensional Bethe lattice environment of interacting sites only leads to changing $\bar{\mathbf{G}}$ by the full electron propagator of the site A itself, $\mathbf{G^d}$, eq. (2.53), and changing the number of leads L in (2.61) by the connectivity of the lattice $L \sim n$ (or alternatively change the resulting Lt^2 by $\sum_i^L t_i^2$ if the coupling to the L neighboring grains are not all equal). Making use of eq. (2.67) once more, and assuming zero gate voltage we have

$$\begin{aligned} S &= \int -\mathbf{f}_\tau^+ \mathbf{G}^{-\mathbf{1}}_{\mathbf{0}\tau\tau'} \mathbf{f}_{\tau'} + \frac{1}{4E_C}\left(\partial_\tau \phi_\tau\right)^2 + Lt^2 \int \mathbf{f}_\tau^+ \mathbf{G^d}_{\tau\tau'} \mathbf{f}_{\tau'} \cos(\phi_\tau - \phi_{\tau'}) \qquad (5.6) \\ &= \int -\mathbf{f}_\tau^+ \mathbf{G}^{-\mathbf{1}}_{\mathbf{0}\tau\tau'} \mathbf{f}_{\tau'} + \frac{1}{4E_C}\left(\partial_\tau \phi_\tau\right)^2 + Lt^2 \int \langle \mathbf{f}_{\tau'}^+ \mathbf{f}_\tau \rangle \langle \cos(\phi_\tau - \phi_{\tau'}) \rangle \mathbf{f}_\tau^+ \mathbf{f}_{\tau'} \cos(\phi_\tau - \phi_{\tau'}) \end{aligned}$$

That is all. This simple result gets somewhat more elaborate if the density of states is not elliptic, although it is also easy to implement. We refer the reader to [34] for details.

The self consistency of the bath function therefore requires one to loop over the computation of $\mathbf{G^d}$ conveniently updating the bath function $\mathbf{\Delta}_{\Delta\tau}$ at each step until convergence is reached. This in general requires one to be able to compute an interacting propagator $\mathbf{G^d}$ in any DMFT loop with a certain 'impurity solver', the choice of which is left to the user. The theory developed in chapters 2 and 3 is just what we need, a convenient impurity solver for DMFT with the convenience of capturing Coulomb blockade, Kondo and excitonic effects on the same footing, without imposing limitations on the spectral properties of the grains. We just need to modify the equations where the bath function

[1] An n-dimensional Bethe lattice is a network of nodes with a disposition similar to a tree, so that a given node is coupled to n sub-nodes (branches), and each of those are only coupled to n corresponding sub-subnodes, but never to any higher level node. It exhibits an elliptic non-interacting density of states.

$\Delta_{\Delta\tau} = \mathbf{t}\bar{\mathbf{G}}_{\mathbf{\Delta}\tau}\mathbf{t}$ appears, e.g. in section 3.2, by

$$\Delta_{\Delta\tau} = \mathbf{t}\mathbf{G}^{\mathbf{d}}_{\mathbf{\Delta}\tau}\mathbf{t} = Lt^2 N_L G^{\mathrm{loc}}_{\Delta\tau}\mathcal{G}_{\Delta\tau} \tag{5.7}$$

We have used (2.67) here again [2].

5.2 Non-equilibrium effects and the metal-insulator transition in metallic grain arrays

The first question that we are going to analyze is an extension of the discussion of section 5.1.2.[3] We have seen that excitonic effects (i.e. incomplete screening of quasiparticles, or orthogonality catastrophe due to sudden potential switching induced by tunneling) lead to a metallic behavior of isolated metallic grains with strong enough coupling $\alpha > 1/\varepsilon$, where ε characterizes the strength of these non-equilibrium effects. Now we want to see if this has any consequence in the context of granular arrays, which can be considered an extreme case of a disordered metal[4]

Since in the absence of excitonic effects a single grain (with a finite density of states at the Fermi energy) is always insulating at zero temperature, it is correct to assume that a granular material will also be. This statement, that is derived from the results of chapter 2 is submitted to that approximations used therin, i.e. that all of the N transport channels have a low dimensionless conductance $\sim \alpha/N$, although the total conductance α can be large. This is compatible with the intuitive Mott criterion that systems with $t < E_C$ will be insulating, since t in our approximation is $\sim 1/\sqrt{N}$, which is small. The results in chapter 3 are precise enough to hint at a metallic phase (labeled as 'coherent' in Fig. 3.13) for $\Gamma > E_C$, where Γ is the single level width $\sim 1/N$. The phase-only approach of chapter 2 cannot therefore capture Mott's transition as-is. It is enough however to study how excitonic effects can cause also a transition to a metallic phase even if the system is far from the Mott's condition, like in the case of arrays of large metallic grains, in which the Large-N approximation holds. We will therefore start our analysis of these effects within the phase-only model, which within DMFT gets modified to the following action

$$S = \frac{1}{4E_C}\left(\partial_\tau \phi_\tau\right)^2 + \alpha \int K_{\tau-\tau'}\langle\cos(\phi_\tau - \phi_{\tau'})\rangle\left[1 - \cos(\phi_\tau - \phi_{\tau'})\right] \tag{5.8}$$

where this time $K_{\tau\tau'} = -\frac{1}{\alpha}\mathrm{Tr}\left[\mathbf{G}_{\mathbf{0}\tau'\tau}\mathbf{t}\mathbf{G}_{\mathbf{0}\tau\tau'}\mathbf{t}^+\right]$, cf. (2.68), and $\mathbf{G}_{\mathbf{0}\tau\tau'} = -\langle\mathbf{f}_\tau\mathbf{f}^+_{\tau'}\rangle$ given in section 2.4. Assuming a constant density of non-interacting fermions in the grain and

[2] In the phase-only approach, $G^{\mathrm{loc}}_{0\Delta\tau}$ should be used as explained in chapter 2.

[3] Most of the results in this section have been published in [10]. Note however that there are some notational differences between that work and the present text. In particular the charging energy here is twice that in the article. Similarly λ in the article should be scaled by $1/4$, and and the value of α by $1/2^{1+\varepsilon}$ to match the definitions given here.

[4] The discussion that follows neglects a possibly important feature of granular arrays, since it becomes quite cumbersome in the present formalism: the inter-grain capacitance. As in the simple Hubbard model, interaction terms of the form $C_{ij}n_i n_j$ with sites $i \neq j$ are neglected. Otherwise, terms of the form $\dot{\phi}_i\dot{\phi}_j$ would have to be included in the model, and the simple DMFT results extended. Moreover we neglect the effect of disorder in the charging energy and in the strength of the excitonic effect, neglecting their dispersions and simply using the average for E_C and ε.

including excitonic effects in the kernel decay as in [93] we have simply eq. (2.70) again

$$K_{\tau\tau'} = E_C^{\varepsilon}\left[\frac{\pi/\beta}{\sin\left(\pi(\tau-\tau')/\beta\right)}\right]^{2-\varepsilon} \overset{\beta\to\infty}{\longrightarrow} \frac{E_C^{\varepsilon}}{|\tau-\tau'|^{2-\varepsilon}} \tag{5.9}$$

Note that the effective single-site DMFT action is essentially identical to the one of the single grain coupled to Fermi liquids, only that the kernel is effectively changed to

$$K^{\text{eff}}_{\tau-\tau'} \equiv K_{\tau-\tau'}\langle\cos(\phi_\tau - \phi_{\tau'})\rangle \tag{5.10}$$

self consistently.

5.2.1 Results

As in previous chapters quite a bit of information can be obtained before performing any computation by examining the action (5.8). The most striking result is that in the case $\varepsilon = 0$ there is no self-consistent solution in which $\mathcal{G}_{\Delta\tau}$ decays algebraically, that is as we discussed in previous chapters the signature of cotunneling processes. Indeed, although $K_{\Delta\tau} \sim 1/\Delta\tau^2$, we would get $K^{\text{eff}} \sim 1/\Delta\tau^4$ in the first iteration loop, and an exponentially decaying $\mathcal{G}_{\Delta\tau}$ thereafter due to Kosterlitz's arguments, section 2.5.2.

This was to be expected. Cotunneling through the whole system is forbidden, since the lattice is assumed unbounded by DMFT, and the amplitude for such processes would therefore be of the order of $(\Gamma/E_C)^M$, with the number M of grains across the system is very large. This amplitude is zero in the Coulomb blockade regime $\Gamma < E_C$. This was confirmed by using Monte Carlo simulation as an impurity solver, and plotting the low temperature conductance cf. section 5.1.2. The results are presented in Fig. 5.2 in logarithmic scale. The exponential decay of the conductance with βE_C is a signature of a truly gapped system (activated transport), and the absence of cotunneling. Such kind of definite gap has been recently observed in granular Aluminium thin films [40], where a very clear direct observation of the corresponding $G \sim e^{-E_C^*/K_BT}$ low temperature conductance has been reported, see Fig. 5.3 as compared to 5.2. This result is in contrast to the pioneering model for transport in granular metals proposed in [46], which predicted rather that $G \sim e^{-\sqrt{E_C/K_BT}}$.

The $\varepsilon = 0$ case is not a critical system anymore in the first order Renormalization Group sense, and the general trend imposed by the DMFT self-consistency is to drive the system towards a gapped insulator. In this sense a negative value of ε representing orthogonality catastrophe phenomena is not very interesting, since it pushes the system further towards the insulating regime, and nothing peculiar happens.

The case of a finite value of $\epsilon > 0$ is however more interesting. It certainly pushes the system in the opposite direction, since the phase tends to order due to the longer range dissipative kernel, and therefore charge fluctuations and conductance tend to grow. Does a critical value of the intergrain coupling α_c^{DMFT} exist for a finite value of ε as in the single junction case?

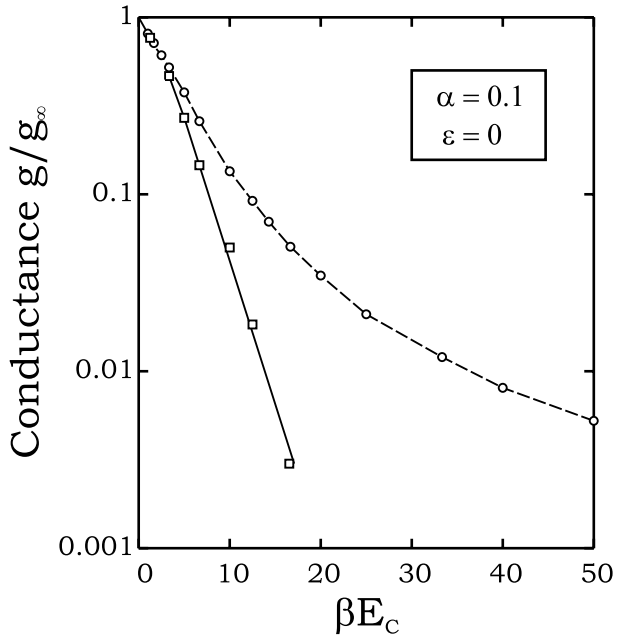

Figure 5.2: Temperature dependence of the normalized conductance $g/g\infty$, as derived from path-integral Monte Carlo simulations for a granular system (squares) and for a single tunnel junction (circles) with the same parameters: $\alpha = 0.1, \varepsilon = 0$.

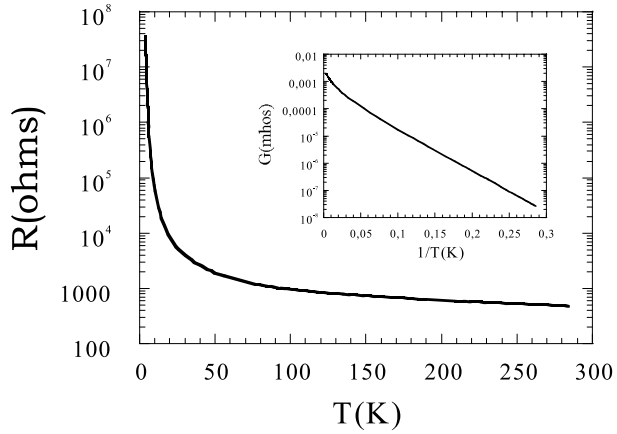

Figure 5.3: Experimental temperature dependence of the resistance and conductance of a granular Aluminium thin film, reproduced with the kind permission of T. Grenet. A clean observation of the gapped nature of the system is obtained, whereby $G \sim e^{-E_C^*/T}$.

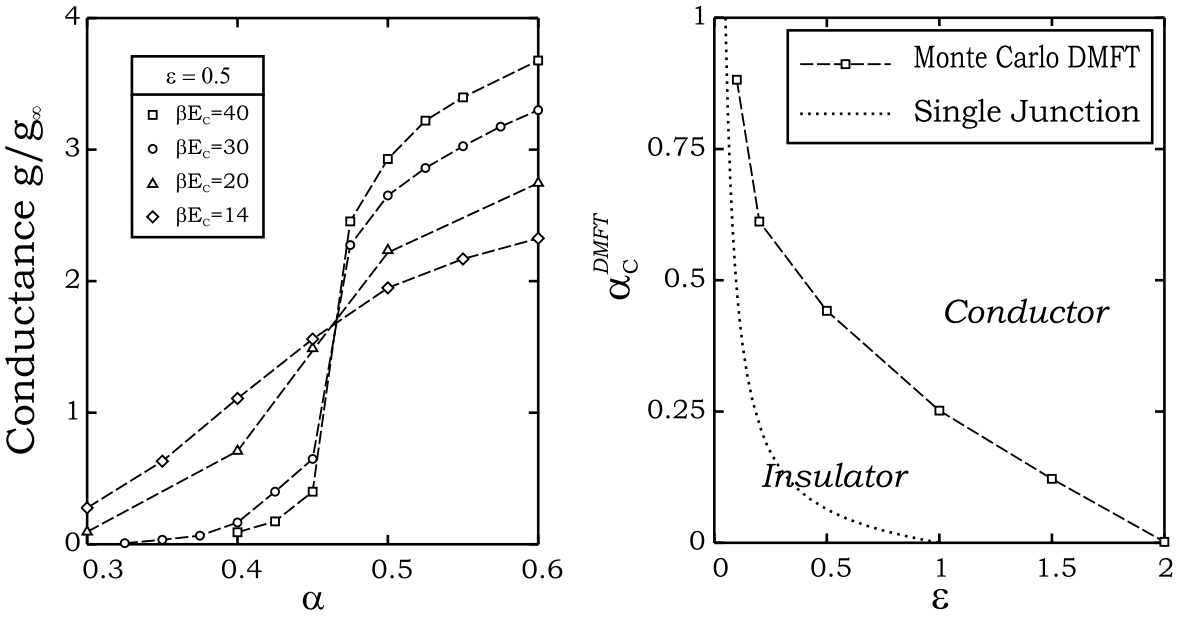

Figure 5.4: To the left we have plotted the conductance approximated by eq. 5.5 for fixed $\varepsilon = 0$ using a Monte Carlo impurity solver for the DMFT of an array of metallic grains. We find a critical value of intergrain coupling strength α in the granular array, α_c^{DMFT}, such that conductance jumps from a low to a high value, signaling a metal-insulator transition. To the right we compare the $\alpha_c^{DMFT}(\varepsilon)$ profile to the single-junction case $\alpha_c = 1/2\pi^2\varepsilon$.

5.2.2 Monte Carlo simulations

We performed a Monte Carlo simulation to check this, and indeed, a finite value α_c^{DMFT} was found such that at low temperatures when $\alpha > \alpha_c^{DMFT}(\varepsilon)$ the conductance of the system jumps up to a finite value, see Fig. 5.4. The precision on the value of α_c^{DMFT} depends on how low in temperature one can go with the Monte Carlo simulation. We have also plotted in Fig. 5.4 the value of α_c^{DMFT} for various values of ε and compared those results with the single junction value $\alpha_c = 1/2\pi^2\varepsilon$, see Appendix E. The trend is similar to the single junction case, but in the granular system the critical α is systematically above the former. This means that in general the insulating phase is more robust in the granular system than for a single grain. The reason for this is quite physical, since for non-equilibrium effects to drive an initially Coulomb blockaded grain into a metallic phase for a single junction it is only necessary to beat the Coulomb gap of the grain, since the environment is already metallic. In a granular system the environment is itself an insulator to start with. What might be striking is that a metallic phase can indeed be reached for a strong enough grain-grain coupling. To better understand the features of the transition we will make use later of the methods described in chapter 2, which are much less costly computationally than Quantum Monte Carlo. But before that let us make some more general analytical argumentation around the structure of the DMFT equations.

5.2.3 Analytical arguments

The mere self consistency requirement together with Kosterlitz's RG results, Appendix E, are enough to predict a fair amount of results expected to hold within the DMFT approximation.

The first of them is the fact that the non-equilibrium metal-insulator transition in granular arrays requires a larger critical coupling α_c^{DMFT} than in the single junction case, as pointed out in the previous section. To see this simply note that if one assumes a non-decaying $\mathcal{G}_{\Delta\tau}$, or even an algebraically decaying $\mathcal{G}_{\Delta\tau} \sim 1/\Delta\tau^\sigma$ in the region $\alpha < \alpha_c = 2/(\pi^2\varepsilon)$, one arrives at a contradiction. Indeed, the effective kernel (5.10) in the first DMFT loop would result in a stronger-than-critically decaying kernel in the Kosterlitz sense, since $\mathcal{G}_{\Delta\tau} \leq 1$, which would therefore result in an exponentially decaying $\mathcal{G}_{\Delta\tau}$ in the next step of the loop. Therefore, the DMFT loop reinforces decaying phase correlators, as already seen in Fig. 5.2 in the $\varepsilon = 0$ case, so that any system below $\alpha = 1/2\pi^2\varepsilon$ will remain insulating at zero temperature (actually gapped).

Another exact result is 'hysteresis'. This is a very generic feature of the DMFT method, although it does not mean that hysteresis should be expected in finite-dimensional systems, of course, since there DMFT is only an approximation. By hysteresis we mean the following. Mathematically, a self consistency loop result can depend on the initial 'seed' chosen for $\mathcal{G}_{\Delta\tau}$. In our case, close to the critical value α_c^{DMFT} the converged result for $\mathcal{G}$ can be insulating (decaying) for an insulating seed, or otherwise conducting (saturating at long times) for a conducting seed. When this happens for a finite range of a parameter, such as α, we say that the system is hysteretic, and therefore there is not one but two critical values α_c^{DMFT}. If the result is correct, it has the obvious physical consequence of hysteretic behavior, whereby the phase of the system depends on its past history, on the way the system has approached that parameter point, which therefore determines at which of the two critical α_c^{DMFT} the transition occurs. It could also give way to an inhomogeneous phase where both phases coexist in 'phase separation' in the region $\alpha_c^{DMFT(1)} < \alpha < \alpha_c^{DMFT(2)}$.

To see why DMFT can show this feature let us choose α slightly above the single-junction boundary $\alpha \gtrsim \alpha_c = 1/2\pi^2\varepsilon$ *with a non decaying initial seed* $\mathcal{G}_{\Delta\tau} = 1$. By Kosterlitz's RG results, the first loop will yield a non-decaying correlation function, i.e. $\lim_{\Delta\tau\to\infty} \mathcal{G}_{\Delta\tau} = \mathcal{G}_\infty$, with $\mathcal{G}_\infty = F(\alpha - \alpha_c)$ for certain (monotonous) function $F(x)$ characteristic of the single-junction such that $0 < F(x) \leq 1$ for $x > 0$, see left of Fig. 5.5. This is for the first loop. The effective kernel in the next loop will be

$$K_{\Delta\tau}^{\text{eff}} = K_{\Delta\tau}(\mathcal{G}_\infty + \Delta\mathcal{G}_{\Delta\tau}) \tag{5.11}$$

where $\Delta\mathcal{G}_{\Delta\tau} \equiv \mathcal{G}_{\Delta\tau} - \mathcal{G}_\infty$ is decaying with some unknown law, although 'probably' positive. Doing the (extreme) simplification of neglecting the effect of $\Delta\mathcal{G}_{\Delta\tau}$, we are left in this second loop with a calculation identical to the first, although with αG_∞ instead of α. Doing this simplification in every loop, we are left with the self consistency condition $G_\infty = F(\alpha G_\infty - \alpha_c)$, see right of Fig. 5.5. By inspecting the figure it is evident that a non-zero solution for $\mathcal{G}_\infty$ requires α greater that a critical value $\alpha > \alpha_c^{DMFT(1)} > \alpha_c$. Note that we are in the case favorable to a conducting solution due to the non-decaying seed for $\mathcal{G}$. We can therefore conclude that the insulating region of the granular system is greater than

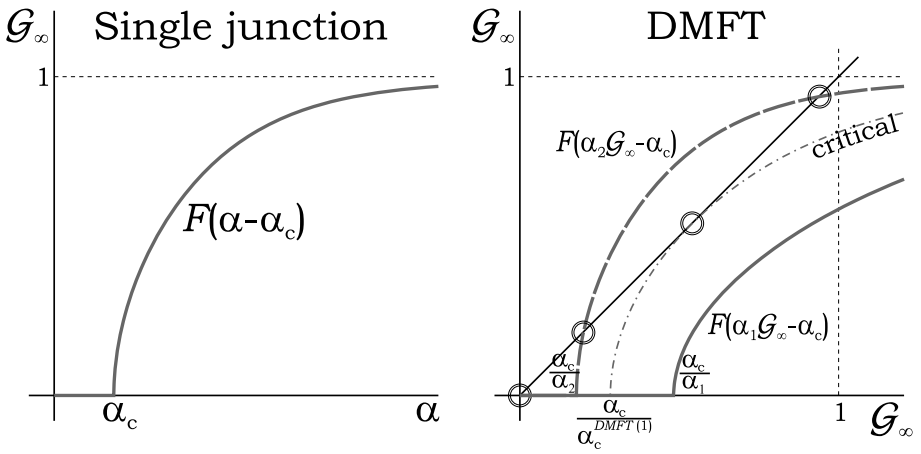

Figure 5.5: To the left we depict the essential shape of function $F(x)$ that relates the asymptotic $\mathcal{G}_\infty = \lim_{\Delta\tau\to\infty} \mathcal{G}_{\Delta\tau}$ to the junction dimensionless conductance α. The solution of $\mathcal{G}_\infty$ for the single junction is finite whenever $\alpha > \alpha_c$. The right figure shows the analytical approximate solution for $\mathcal{G}_\infty$ within DMFT (circled intersections), which is non-zero only if $\alpha > \alpha_c^{DMFT(1)} > \alpha_c$. Incidentally, of the two solutions of the α_2 curve, the upper one should be chosen, since it is closer to the original seed $\mathcal{G} = 1$. The solid line has only zero solution, $\alpha_c^{DMFT(1)} > \alpha_1 > \alpha_c$, while the dashed line (α_2) has at least one finite solution.

that of the corresponding single junction, and the (lower) critical value $\alpha_c^{DMFT(1)}$ is shifted upward from α_c.

Now let us analyze the case with a insulating seed, i.e. an initially decaying correlator $\mathcal{G}_{\Delta\tau}$. The strongest decay that makes sense as a seed is the $\alpha = 0$ solution, which has a typical decay type E_C^{-1} (see footnote in section 2.5.3). Neither Kosterlitz' arguments nor Griffith's theorem can tell us how big should α be for a given ε before this seed results in a metallic solution, but it is reasonable to expect this value to be above $\alpha_c^{DMFT(1)}$, since an initially exponential decay effectively disables any long-range ordering tendency that could originally be expected until a very strong α is reached. This hand-waving arguments need confirmation by specific calculations. To see how far above $\alpha_c^{DMFT(1)}$ does this $\alpha_c^{DMFT(2)}$ become we will now use the spherical limit approach which makes fast calculations accessible, while keeping in touch with the Monte Carlo results of previous section to have some insight into the validity of the approximation.

5.2.4 Spherical limit approximation

Let us pick up the techniques used in chapter 2 to proceed in the analysis of the non-equilibrium metal-insulator transition. In the spherical limit of the quantum rotor

language, the DMFT self consistent equation read at zero temperature

$$\mathcal{K}^{\rm eff}_{\Delta\tau} = K_{\Delta\tau}\mathcal{G}_{\Delta\tau} = \frac{E_C^{\varepsilon}}{|\Delta\tau|^{2-\varepsilon}}\mathcal{G}_{\Delta\tau} \tag{5.12}$$

$$G_{\Delta\tau} = \int_{-\infty}^{\infty}\frac{d\omega}{2\pi}\frac{\cos(\omega\Delta\tau)/2}{\frac{\omega^2}{4E_C}+\alpha(K_0^{\rm eff}-K_\omega^{\rm eff})+\lambda} \tag{5.13}$$

$$G_{\Delta\tau=0} = 1 \tag{5.14}$$

Before plunging into any calculations to confirm the arguments of previous sections, let us tarry a little by looking into the mathematical properties we can expect from this method. First of all, what is the mathematical manifestation of a gapped solution in this language? Let us first look at the case of a single grain with $\varepsilon \neq 0$. In such case we have, cf. eq. (F.3)

$$K_0 - K_\omega = \frac{\pi}{\Gamma(2-\varepsilon)\cos(\pi\varepsilon/2)}E_C^{\varepsilon}|\omega|^{1-\varepsilon} \tag{5.15}$$

As shown in Appendix F, the spherical method gives a good result for the critical α_c in a single grain (in agreement with renormalization group results) for the Kosterlitz metal-insulator transition. The transition is characterized by a zero renormalized Coulomb gap E_C^*, i.e. by the vanishing of λ. This happens for $\alpha > \alpha_c$ given in Appendix F. As argued also in the appendix, beyond that point eq. $G_{\Delta\tau=0} = 1$ has no possible solution in λ within the spherical limit approximation, and we must drop this description and assume a solution with long range order in the phase, i.e. $\mathcal{G}_\infty = \lim_{\Delta\tau\to\infty}\mathcal{G}_{\Delta\tau} > 0$. This was assumed in the arguments of the preceding section.

This vanishing of λ as a sign of the transition should be expected to happen also in the granular array described by the self consistent DMFT equations above, although at a different value of $\alpha = \alpha_c^{DMFT(2)}$ as discussed in the preceding sections. In other words, if we begin sweeping α from zero to increasing values, and at each α initialize the DMFT loop by assuming a decaying trial seed e.g. $G_{\Delta\tau} \sim 1/\Delta\tau^2$, λ will drop to zero at a certain point $\alpha = \alpha_c^{DMFT(2)}$. Beyond that point only the ordered solution exists, and we have reached the higher critical coupling. If we now reverse the sweep direction by reducing α but at each value initializing the loop with an ordered seed $\mathcal{G}_{\Delta\tau} = 1$, we should expect by the hysteresis arguments given above to remain in the saturated $\mathcal{G}_\infty > 0$ solution for a longer interval than before, until we reach down to $\alpha = \alpha_c^{DMFT(1)} < \alpha_c^{DMFT(2)}$. The precise value of $\alpha_c^{DMFT(1)}$ is obtained as the value of α for which the DMFT equations (5.12) trough (5.14) acquire a non-negative solution for λ with an ordered seed.

This behavior is indeed observed as represented in Fig. 5.6. Note that the transition is discontinuous is λ which points to a first order-type character, unlike in the single-grain case where the renormalized charging energy falls continuously to zero at $\alpha = \alpha_c$. Note also that the hysteretic loop grows in amplitude as α increases, although for ε narrowing on the limiting $\varepsilon = 2$ this tendency is slowly reversed. A detailed sweep of this computation in parameter ε is presented in Fig. 5.7, in black and white circles. We can appreciate in the latter plot that that there is an almost quantitative agreement between the results obtained with the extremely economical spherical limit approximation and the costly Quantum Monte Carlo computation. It should also be noted that the introduction

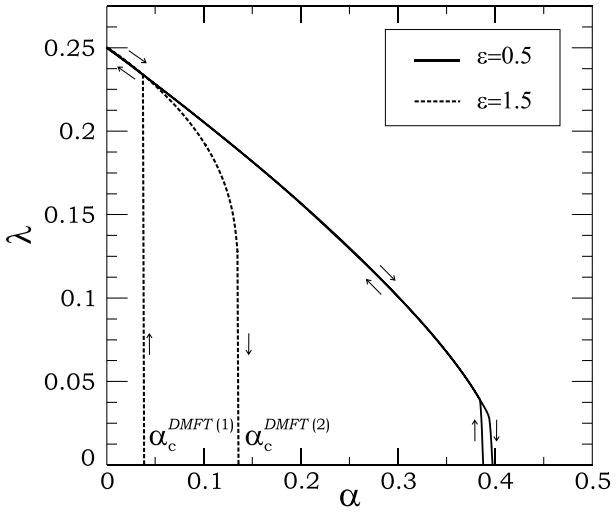

Figure 5.6: Parameter λ as an order parameter of the metal-insulator transition driven by excitonic effects. The two curves correspond to two different values of parameter ε which measures the non-equilibrium effects. Note the hysteretic and first order character of the transition (the jump in λ appears discontinuous).

of heuristic parameter γ_M in the definition of the spherical limit, eq. (2.90) is essential to obtain quantitative accuracy, as is also demonstrated in the single grain case, Appendix F.

5.2.5 Variational approach

It is possible go one more step beyond the spherical limit approximation towards an analytical characterization of the transition by making a variational ansatz about the effective kernel $K^{\rm eff}_{\Delta\tau}$ at criticality $\alpha = \alpha_c^{DMFT}$. The argument relies on the large and small τ properties of any self consistent solution of the DMFT equations given above. First of all, since $\mathcal{G}_{\Delta\tau=0} = 1$ we can read off from eq. (5.12) that at small times $K^{\rm eff}\tau \approx E_C^2/|E_C\tau|^{2-\varepsilon}$. On the other hand, at criticality we can assume that correlations decay algebraically, so that at long times

$$K^{\rm eff}_{\tau} \approx E_C^2 \frac{A}{|\tau|^{2-\delta}} \tag{5.16}$$

$$K^{\rm eff}_{0} - K^{\rm eff}_{\omega} = E_C^2 \pi A \frac{|\omega|^{1-\delta}}{\Gamma(2-\varepsilon)\cos(\pi\varepsilon/2)} \tag{5.17}$$

We can find the self consistent values of A and δ by combining (5.12) and (5.13) at $\lambda = 0$ and neglecting the $\sim \omega^2$ term in the denominator of (5.13) to obtain the large τ behavior of the integral

$$\frac{K^{\rm eff}_{E_C\tau\gg 1}}{E_C^2} \approx \frac{1}{|E_C\tau|^{2-\varepsilon}} \int_{-\infty}^{\infty} \frac{d\omega}{2\pi} \frac{\cos(\omega\tau)/2}{\alpha_c \pi A \frac{|\omega|^{1-\delta}}{\Gamma(2-\varepsilon)\cos(\pi\varepsilon/2)}} = \frac{A}{|\tau|^{2-\delta}} \tag{5.18}$$

The following solution is indeed found at criticality,

$$\delta = \frac{\varepsilon}{2} \tag{5.19}$$

$$A = \sqrt{\frac{(2-\varepsilon)\cot\left[\frac{\pi\varepsilon}{4}\right]}{8\pi\alpha_c}} \tag{5.20}$$

The idea is now obviously to make an ansatz on the function $K_\tau^{\rm eff}/E_C^2$ that interpolates from the small τ behavior $1/|E_C\tau|^{2-\varepsilon}$ and the large τ behavior $A/|E_C\tau|^{2-\varepsilon/2}$. One possibility that gives interesting results is the following[5]

$$\tilde{K}^{\rm eff}_{\tilde{\tau}}[\eta] \equiv \frac{K_\tau^{\rm eff}}{E_C^2} = \frac{e^{-\eta\tilde{\tau}}}{|\tilde{\tau}|^{2-\varepsilon}} + A\frac{\left(1-e^{-\eta\tilde{\tau}}\right)^2}{|\tilde{\tau}|^{2-\varepsilon/2}} \tag{5.21}$$

$$\tilde{K}^{\rm eff}_{\tilde{\omega}}[\eta] = \frac{K_\omega^{\rm eff}}{E_C} \tag{5.22}$$

where we have switched to dimensionless coordinates $\tilde{\tau} = E_C\tau$ and $\tilde{\omega} = \omega/E_C$ for convenience. Obviously this is not the only possibility and as we will see its validity is restricted to certain range of ε values. This trial function sets the blending point between the two behaviors at ηE_C, where η is our variational parameter. We intend to find the value of η that better meets the self consistency condition on $\mathcal{G}_{\Delta\tau}$, eqs. (5.12) and (5.13)

$$\mathcal{G}_{\Delta\tau} = \int_{-\infty}^{\infty}\frac{d\tilde{\omega}}{2\pi}\frac{\cos(\tilde{\omega}\Delta\tilde{\tau})/2}{\frac{\tilde{\omega}^2}{4}+\alpha_c(\tilde{K}_0^{\rm eff}-\tilde{K}_{\tilde{\omega}}^{\rm eff})} = |\Delta\tilde{\tau}|^{2-\varepsilon}\tilde{K}^{\rm eff}_{\Delta\tilde{\tau}} \tag{5.23}$$

At the same time $\alpha_c = \alpha_c[\eta]$ for a given value of η is computed as in Appendix F by the criticality criterion

$$\mathcal{G}_{\Delta\tau=0} = \int_{-\infty}^{\infty}\frac{d\tilde{\omega}}{2\pi}\frac{1/2}{\frac{\tilde{\omega}^2}{4}+\alpha_c(\tilde{K}_0^{\rm eff}-\tilde{K}_{\tilde{\omega}}^{\rm eff})} = 1 \tag{5.24}$$

Performing this set of calculations for a variety of values of η it becomes clear by comparing the two sides of eq. (5.23) (middle and right expressions) as a function of $\Delta\tau$ that the best fit is achieved by choosing $\eta = 1$. We plot in Fig. 5.8 the two sides of the latter equations for $\eta = 1$ and various values of ε. The agreement is very good for intermediate values of ε, but sizeable deviations occur for $\varepsilon < 0.5$ and $\varepsilon > 1.5$. In this regions a different ansatz would be necessary to approach an analytical self-consistent solution.

We can compare the values of α_c thus obtained to the ones calculated by doing the full DMFT iterative procedure. The value of α_c within the variational approach closely follows that of $\alpha_c^{DMFT(2)}$ in the validity interval $\varepsilon \in [0.5, 1.5]$, see Fig. 5.7. Out of that interval the deviations again reveal the ansatz is not good for those values.

By its very nature the variational approach does not reveal anything about the possible hysteresis of the system. However it seems the properties implicit in the variational ansatz we have used give a closer description of the critical α with an insulating seed, $\alpha_c^{DMFT(2)}$, see Fig. 5.7. This is obviously due to the fact that the ansatz we have made is actually decaying at long times.

[5]The reason for the square in the second term is to ensure that $\mathcal{G}_{\Delta\tau} = |E_C\tau|^{2-\varepsilon}\tilde{K}^{\rm eff} \leq 1$.

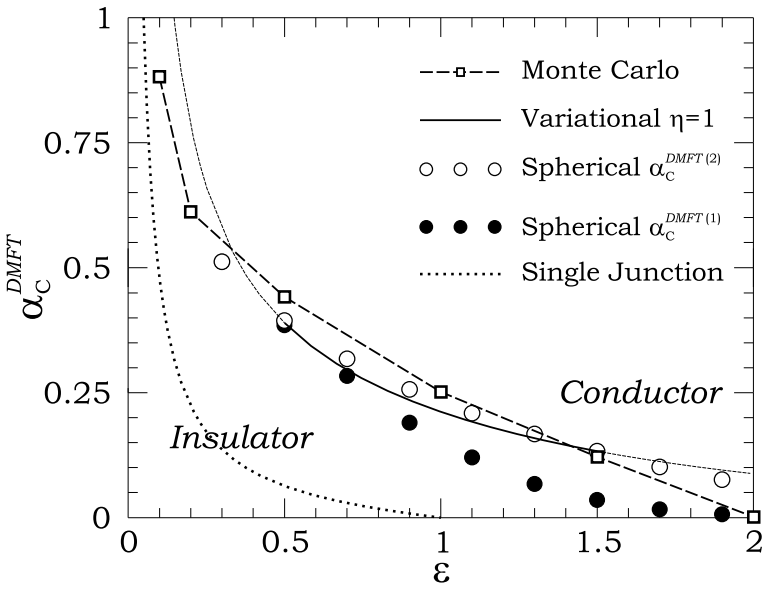

Figure 5.7: Comparative of the results obtained for the critical coupling α_c in the Kosterlitz metal-insulator transition of granular arrays by several methods: Quantum Monte Carlo simulation, spherical limit, and variational approach.

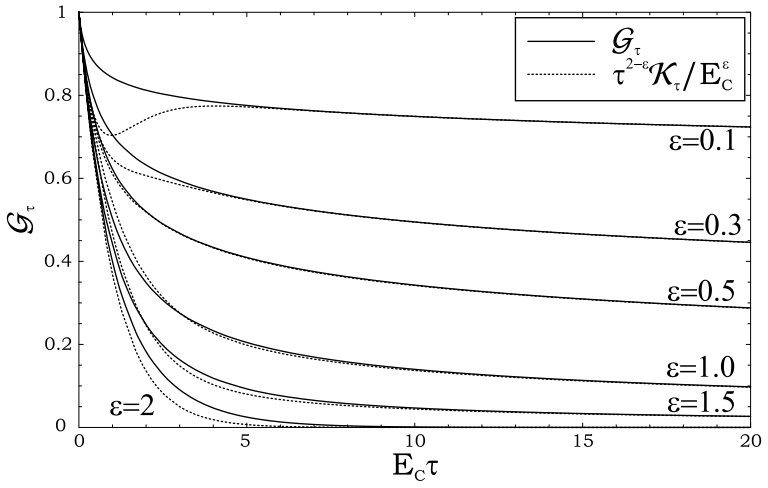

Figure 5.8: Comparison of the two definitions of propagator $\mathcal{G}_{\Delta\tau}$. Parameter $\eta = 1$ is chosen to provide the best visual fit of the trial effective kernel with the spherical limit $\mathcal{G}$.

5.2.6 Summary

We have described a metal-insulator transition in metallic grains of a different nature to the one discussed by Mott and Hubbard. The underlying mechanism is tunneling enhancement due to non-perturbative excitonic effects, of a similar origin as the X-ray emission anomalies in metals. It is also reached by increasing pressure (α), but the critical value is not related to the ratio t/E_C, but to α/ε, or conductance over excitonic phase shift of plane waves by the sudden potential switch, in Anderson's language of the X-ray absorption problem.

The possible descriptions of this transition are varied. The RG method is valid for small values of ε (large coupling limit, large α_c). The DMFT plus Monte Carlo impurity solver method is temperature limited and is costly, but it is in principle numerically exact at infinite dimensions. It predicts an exponential decay of phase correlations in the insulating phase, and therefore exponential suppression of conductance at low temperatures, in contrast with the algebraic dependence in the single junction case. Hence cotunneling transport is forbidden in the (infinite) granular array, which was obviously expected due to the charging energy at every site.

The DMFT plus spherical limit impurity solver approach is a powerful and semi-analytical path, that is computationally cheap and quantitatively accurate, as exposed by Fig. 5.7. One of the features revealed by the latter method is the existence of a hysteretic effect on the transition, whereby the exact value of α_c depends on whether we approach it from the insulating phase or the conducting phase. It remains to be seen if this hysteretic feature is a characteristic of infinite dimensional systems only, or if it shows up also in finite dimensions. Further variational ansatz attacks on the DMFT plus spherical solver method can give analytical insight on the correlation decay at criticality, which at the upper value of α_c (coming from the insulating phase) predict a precise $\sim 1/|\tau|^{2-\varepsilon/2}$ decay law for phase-phase correlations, that would yield a $g \propto T^{2-\varepsilon/2}$ temperature dependence of the conductance at low temperature just at the transition. Therefore, coming from the insulating phase we predict an evolution of the temperature dependence of the conductance from exponential, to algebraic (at criticality) to constant. Unfortunately the spherical limit approach is unable to describe the metallic phase, since it cannot account for a non-decaying $\mathcal{G}_{\Delta\tau}$, but it is good enough to describe the evolution up to the transition.

Another prediction of the DMFT plus spherical solver method is that the transition appears to be first order, giving a discontinuous jump for the renormalized charging energy at the transition of the granular system. In contrast in the single junction case the charging energy E_C^* is continuous across the transition, which occurs at a lower coupling strength α_c (the transition to the metallic phase is much more favorable since the environment for a single grain is already metallic). Yet another difference to the single junction case is that the system can exhibit an insulating phase all the way up to the maximum value of $\varepsilon = 2$, while in the single junction, renormalization group arguments, see Fig. 5.7, seem to suggest a maximum of $\varepsilon \sim 1$ (although of course at those values RG as presented here is not reliable anymore, since it is only valid for $\alpha_c \gg 1$, i.e. $\varepsilon \ll 1$).

5.3 Mott-Hubbard metal insulator transition in granular arrays

On second thought it might seem striking that in the absence of excitonic effects $\varepsilon = 0$ the methods described in the previous section predict no transition whatsoever of a granular system to a metallic state. In fact it completely fails to describe Mott's original arguments which had nothing to do with excitonic effects but predicted a transition for $t \sim E_C$, t being the inter-site hopping amplitude of a given transport channel. The DMFT in the phase only approach predicts for $\varepsilon = 0$ an strictly gapped phase (even more strongly insulating than the single junction scenario) up to an arbitrary large value of $\alpha \sim t^2$.

The answer to this apparent inconsistence must be found a long way back, around chapter 2. Recall that the phase-only description of metallic grains by the system dissipative action we have employed was correct only in the large-N limit, N being the number of degenerate transport channels through each junction, and recall that α was in fact proportional to Nt^2. While N was taken to infinity, α was held constant (although it could be arbitrarily large), and this was key to the derivation. This implies that t should actually be vanishingly small, in fact t had to scale as $t/\sqrt{N}$ for the large-N limit to make any sense. Therefore the phase-only model (at least with the simple dissipative action, although see also [37, 78]) is unable to describe any regime such as Mott described, with $t \sim E_C$.

However the phase-fermion method described in chapter 3 is free from this requirement, being in fact able to reach finite values of t/E_C, or Γ/E_C, where $\Gamma \sim t^2$ is the single level width. Therefore it should be expected that the Mott transition be described to some extent by a DMFT plus fermion-phase impurity solver approach. This will be the subject of this section.

5.3.1 DMFT equations with slave rotor impurity solver

Taking up equation (5.7) and its discussion we can straightforwardly transforms the spherical limit slave rotor integral equations in section 3.2 by their DMFT form

$$\Sigma^{\rm loc}_{\Delta\tau} = \frac{\Gamma^2}{4} G^{\rm loc}_{\Delta\tau} \mathcal{G}^2_{\Delta\tau} \tag{5.25}$$

$$G^{\rm loc}_{i\omega_n} = \left[\left(\frac{1}{N_L} \sum_\alpha \frac{1}{i\omega_n - \epsilon_\alpha} \right)^{-1} - \Sigma^{\rm loc}_{i\omega_n} \right]^{-1} \tag{5.26}$$

$$\alpha K_{\Delta\tau} = -N \frac{\Gamma^2}{4} \mathcal{G}_{\Delta\tau} G^{\rm loc}_{\Delta\tau} G^{\rm loc}_{-\Delta\tau} \tag{5.27}$$

$$\mathcal{G}_{i\omega_n} = \frac{1/2}{\frac{\omega_n^2}{4E_C} + \lambda + \alpha(K_0 - K_{i\omega_n})} \tag{5.28}$$

$$\mathcal{G}_{\Delta\tau=0} = 1 \quad \text{(fixes } \lambda\text{)} \tag{5.29}$$

In this context the single level width $\Gamma = L\pi t^2 \rho(0)$, cf. eq. (B.2), is quite simply

$$\Gamma = 2\sqrt{L} N_L t \tag{5.30}$$

since $\rho(0)$ is now the non-interacting density of states of the Bethe lattice of grains itself at the Fermi energy, since it has substituted the L metallic leads of chapter 3. Such density of states is a half-ellipse of width $2t\sqrt{L}$ when L is large, as explained e.g. in Appendix A of reference [34], so that $\rho(0) = 2N_L/(\pi t\sqrt{L})$.[6] Note that Γ is also the non-interacting bandwidth of the system,[7] which is commonly taken as the energy reference unit in the DMFT literature. We will follow suit and write all energies in units of Γ, as in W/Γ, E_C/Γ and K_BT/Γ.

The above modified slave rotor algorithm in the spherical limit approximation will be used to investigate the Mott transition and its dependence on spectral properties of the single grains. We focus in the particular case in which the non-interacting density of states in the grains is a smooth half-ellipse of full width W, i.e. the non-interacting fermionic Green's function is

$$G^{\mathrm{loc}}_{0i\omega} = \frac{1}{N_L}\sum_{\alpha}\frac{1}{i\omega - \epsilon_\alpha} = -i\frac{2/\omega}{1+\sqrt{1+\frac{W^2}{4\omega^2}}} \tag{5.31}$$

We neglect completely the effects of disorder in W, E_C or Γ.

5.3.2 Preliminary discussion

The case in which $W = 0$ was analyzed in the initial work by S. Florens and A. Georges [29], although their method differs slightly from the one presented here due to their different implementation of parameter γ_M in 2.90. We believe the approach presented here is more adequate, since it allows to recover various analytical results in the context of the phase-only approach to excitonic effects in granular arrays, as explained in the preceding sections of this chapter. Regarding the metal-insulator transition in particular, Florens and Georges indeed found a transition at zero temperature in qualitative agreement with Mott's arguments. To be precise the critical value of the charging energy they obtained was something close to $E_C/\Gamma = 1.25$ (note that Γ is proportional to t). However the details of the transition revealed an hysteretic behavior at low temperatures, similar to the ones we have encountered in the excitonic transition problem, see their Fig. 7 (note that $U = 2E_C$). Therefore in reality the system at $W = 0$ exhibits two critical values of E_C, which are, according to their work, $E_{C1}/\Gamma = 1.15$ and $E_{C2}/\Gamma = 1.45$. These two values are obtained by previously tuning the value of N (number of channels) to $N = 3$ so that E_{C2}/Γ agrees with previous results that predicted precisely $E_{C2}/\Gamma \approx 1.45$ for a two channel system [71] using a different approximation. Our implementation of the spherical limit would yield the same curve at $W = 0$ by hand tuning N to 1.5. We have opted however for a non-tuned computation, leaving $N = 2$, since in our opinion artificial tuning of parameters unnecessarily detracts from any result one might obtain, and we prefer to study the possible biases as well as the virtues of the present description. Reproducing Florens' and Georges' computation with our equations yields $E_{C1} \approx 1.4$ and $E_{C2} \approx 2.1$.

[6] Note that the condition $L \gg 1$ is not necessary for equation (5.30) to be verified, but simply that the density of states be semielliptic of width $\sqrt{L}t$, which is simply something different from the Bethe lattice for finite coordination L.

[7] The bandwidth of the system with $N_L = 1$ is simply $D = 2\sqrt{L}t$. Introducing N_L simply amounts to substituting t by $N_L t$ and restrict to the 'local hopping' base which decouples all the other sites.

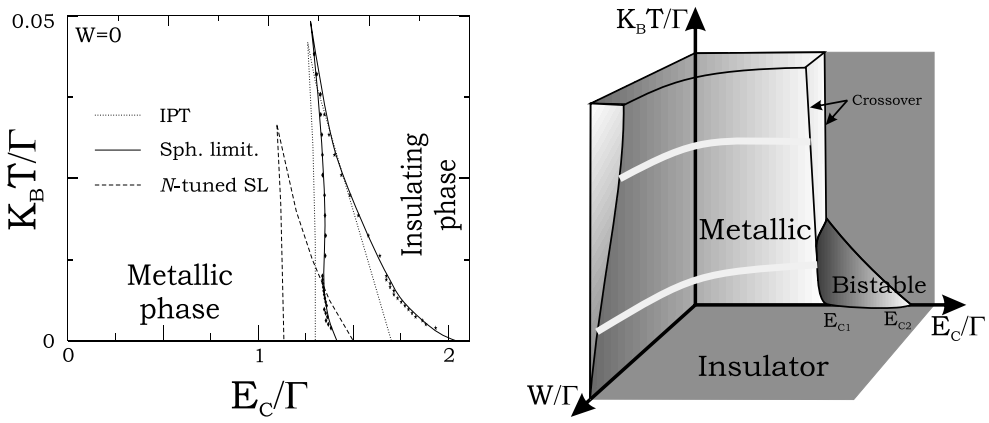

Figure 5.9: To the left we represent the results found in [29] for the $W = 0$ metal-insulator transition by a slight modification of the method presented here with a hand-tuned value $N = 3$. We also plot the corresponding results of our implementation together with the curve derived by Iterated Perturbation Theory (IPT), [33]. To the right we represent a working hypothesis for the phase diagram of the granular material based on the arguments in the text. We represent the bistable or coexistence region where both metallic and insulating solutions are satisfied as a small pocket near $W = 0$.

Independently of the precise values of these two critical E_C's it is clear that the DMFT method again suggests that there exists a region in parameter space in which the system can be either metallic or insulating depending of its previous history. This 'coexistence region' was found in [29] to extend only up to a small temperature $K_B T^* \approx 0.04\Gamma$, see Fig. 5.9, beyond which the crossover from metal to insulator occurs in a smooth fashion without a phase transition. In our case we obtain $K_B T^* \approx 0.05\Gamma$.

Our method allows us to go beyond the $W = 0$ case. For a finite W we can argue that at zero temperature $K_B T \ll W$ and finite E_C the system should remain a gapped insulator. The reason for this is analogous to the discussion around eq. (3.16), which ensure that $G^{\rm loc}_{\Delta\tau} \sim 1/\Delta\tau$ at long times. At finite W we should therefore expect a long time decay of $\alpha K_{\Delta\tau} = -N\frac{\Gamma^2}{4}\mathcal{G}_{\Delta\tau}G^{\rm loc}_{\Delta\tau}G^{\rm loc}_{-\Delta\tau}$ of *at least* $1/\Delta\tau^2$. This points to a Coulomb blockaded grain, which implies a decaying $\mathcal{G}_{\Delta\tau}$, and therefore $\alpha K_{\Delta\tau}$ actually decays faster than $1/\Delta\tau^2$, and there is a well formed gap.

At finite temperatures we can expect the preceding argument to break down, specially close to the region $E_C < E_{C1}$ which is metallic at $W = 0$. We need to perform a more quantitative analysis of the DMFT equations to clear up the precise details of the $T \sim W \sim E_{C1}$ region, although by continuity from the $W = 0$ solution and the $E_C = 0$ solution (which is of course metallic) we expect to find something in the lines of Fig. 5.9 (right side). In particular we expect the coexistence region to extend out to a maximum value W^*. We will perform some detailed analysis of the various features of this phase diagram in the following sections.

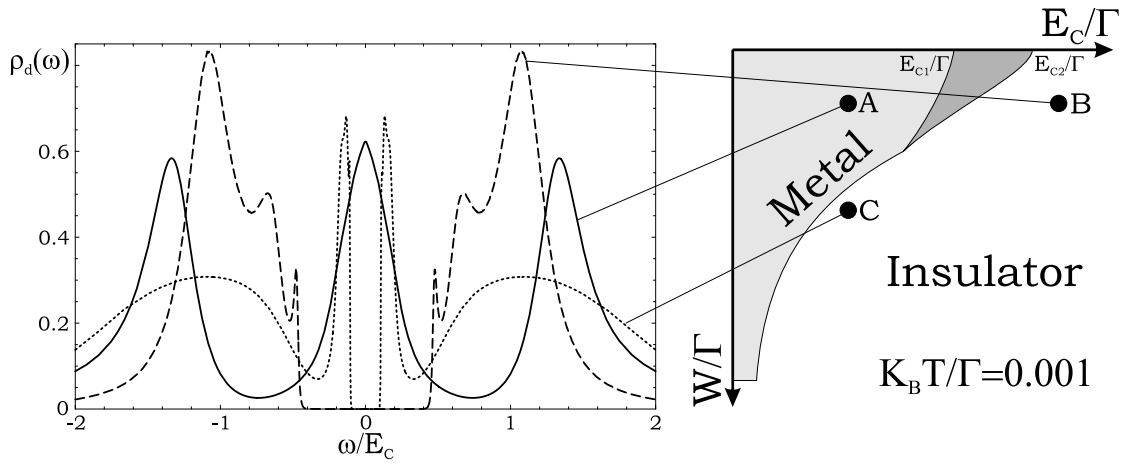

Figure 5.10: Typical density of states obtained for various points in the $E_C/\Gamma - W/\Gamma$ plane for fixed K_BT/Γ. From the point of view of a single junction point A corresponds to Kondo regime, point B to Coulomb blockade, and point C to split-Kondo regime, where an inverse crossover from Kondo to Coulomb blockade has appeared.

Kondo effect-Coulomb blockade competition vs. the metal-insulator transition

Within DMFT the metallic phase can be viewed as single grain coupled to certain environmental density of states such that the grain acquires a finite zero energy interacting spectral density, which in turns leads to certain ohmic conductance when a small bias is applied through the junction between the grain and the self consistent environment. One might wonder what is the kind of physics that can yield such a low energy spectral density for a given grain coupled to certain environment. The answer is of course no other than the Kondo effect. Therefore, from the point of view of DMFT a metallic bulk state, where coherent transport can be established through the sample at vanishing bias, is simply due to an overlap of the Kondo resonances at each grain arising from the interaction between that grain and its resulting environment. Similarly the insulating phase is seen from the point of view of the single grain as a gapped environment with zero spectral weight at zero energy, which together with the charging energy of the grain itself gives a gapped interacting density of states at zero energy for the grain (since cotunneling is forbidden by the self-consistent environment's gap).

Therefore it is the same competition between Coulomb blockade and Kondo effect which determines the phase of the granular system within the DMFT description. If the single junction system has not reached the parameter regime for Kondo effect, so that it remains in the Coulomb blockade+cotunneling state, the DMFT loop will reinforce the insulating behavior (by making the bath function more and more rapidly decaying), until a definite gap is opened of order E_C^* between the two Hubbard bands. However if the single junction system is deep into the Kondo regime, the finite density of states of the grain at $\omega = 0$ (Kondo peak) guarantees self-consistency, since the environment also retains a finite density of states at zero energy, which is essential for the formation of the Kondo resonance in the first place. See 5.10 for a typical converged solution in both extreme

cases. In the region between both extremes, i.e. close to the critical values of E_C/Γ both phenomena compete, which is what makes the state close to the transition so far from trivial. Indeed, even the DMFT equations suffers from the critical slowing down typical of most self-consistent algorithms close to phase transitions, and thousands of iterations and careful tuning becomes necessary to reach self consistency. Curiously enough this difficulty remains at temperatures even above the critical point T^* at $W = 0$, see previous section, where the phase transition has vanished but fluctuations around the converged solution become pretty wild.

Another scenario also present in the analysis of chapter 3 is also relevant in the bulk system, namely the inverse crossover from Kondo to Coulomb blockade. We saw that if we set up a single grain with a very thin band around the Fermi energy, and a large enough coupling to the leads the scale T_K could become greater than E_C^*, so that the resulting density of states at low energies would consist of a wide Kondo resonance split in two in the middle at scales E_C^*. This kind of crossover is what we find when we start in point A and move over to point C in 5.10, which shows the typical split-Kondo density of states.

5.3.3 Charging energy driven transition

We are going to analyze in more detail the coexistence region which separates the metallic and the insulating regions to the left and right of E_{C1} and E_{C2} respectively. First of all we compare the $W = 0$ result obtained by the hand-tuned method in [29] to the $W = 0$ case with $N = 2$ in our case. The result is presented on the left panel of Fig. 5.9. Incidentally, the present treatment agrees better with a different technique called 'iterated perturbation theory' (IPT) [33], which we also represent in the plot. However the qualitative features of the transition are obviously the same in the three approaches. Compared to the implementation of [29] we obtain a shift to higher critical charging energies of about 40%. The value of the critical temperature below which coexistence exists is found to exist is $K_B T^*/\Gamma \approx 0.05$, in approximate agreement with the other two methods.

This coexistence region was obtained by fixing temperature and doing a sweep of increasing values of E_C from the metallic phase up to the insulating phase, and always using as seed the solution obtained in the previous step. We recorded the converged solution for the imaginary frequency true electron propagator at each value of E_C and then began to sweep back from the insulating to the metallic phase. The absolute difference from the solutions at a given E_C in the upward and in the downward sweep (which had different seed of course) was in general zero, except in an interval of E_C's, in which hysteretic behavior appeared, giving rise to simultaneously valid insulating and a metallic solutions. Close to this region we observed a severe critical slowing down of convergence that had to be dealt with carefully. In particular we had to anneal the propagators more and more slowly, adding more friction to the update of the rotor propagator when approaching the transition from the metallic side (charge fluctuations grow) and to the fermion propagator when approaching it from the insulating side.

The next question that arises is, can this type of Mott-Hubbard transition persist with a finite value of the grain's bandwidth around the Fermi level? According to the discussion in 5.3.2 as soon as $W \gg T$ the system should systematically show an insulating behavior, so we expect to have at most a maximum value of W such that the transition

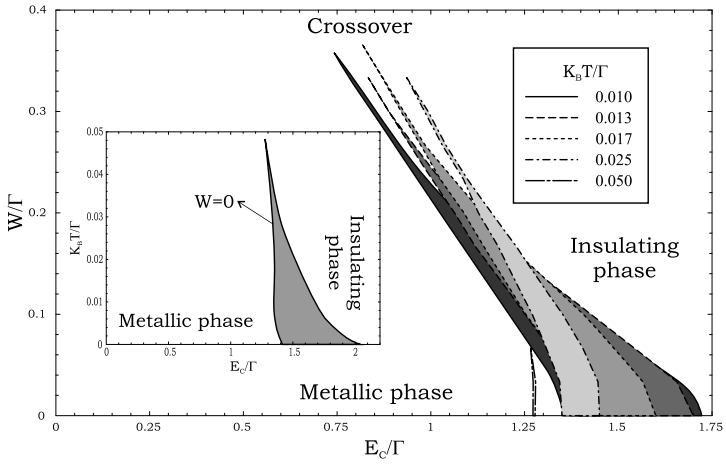

Figure 5.11: On the main plot we represent the parameter regions where metallic and insulating solutions coexists at finite W for various values of temperature. As we get closer to the critical temperature T^*/Γ the strip of finite W that can harbor the two phases narrows down to a thin finger. The section of this plot at $W = 0$ can be found in the inset.

still occurs. We have repeated the procedure of the above paragraph by sweeping W/Γ instead of temperature, and we have confirmed the existence of a finite maximum value of $W/\Gamma \approx 0.4$, such that the coexistence region survives for values smaller than this in an increasingly thin strip of E_C values, as represented in Fig. 5.11 (note that the charging energies required for the transition to occur are reduced when W is increased, as is the size of the coexistence window). As the bandwidth is increased however the strength of the hysteretic effect rapidly declines, although the fluctuations of the propagators do not. We have tried to represent how this happens in Fig. 5.12. Up to a critical value $W^* \approx 0.4\Gamma$ the upward and downward sweeps showed definite hysteresis, and the high and low E_C transitions was systematically accompanied by a sharp rise in the number of DMFT loop iterations required for convergence. However this strong critical slowing down persisted well above the maximum critical value of W^*. This could physically mean that the system will probably feel the vicinity of the instability for $W > W^*$, which would be manifested in the behavior of correlation functions and observable fluctuations. We have not analyzed this point further, however.

5.3.4 Bandwidth driven transition

Let us analyze in some more detail the transition induced by the widening of the single grain band, or the inverse crossover in the language of section 5.3.2 and chapter 3. Starting from a $W = 0$ case, analogous to the usual Hubbard model (albeit in the large-N [level degeneracy] limit) the system becomes metallic for $E_C < E_{C1}$. This reflects the Kondo mechanism that a single grain experiences due to its effective environment. In the single grain case, a widening of the grain's band is expected to spoil such mechanism as soon as $E_C^* \sim T_K$. We expect something similar to happen in the granular case, at least at non-vanishing temperatures, since in that case any $W \gg K_B T$ is enough to make the

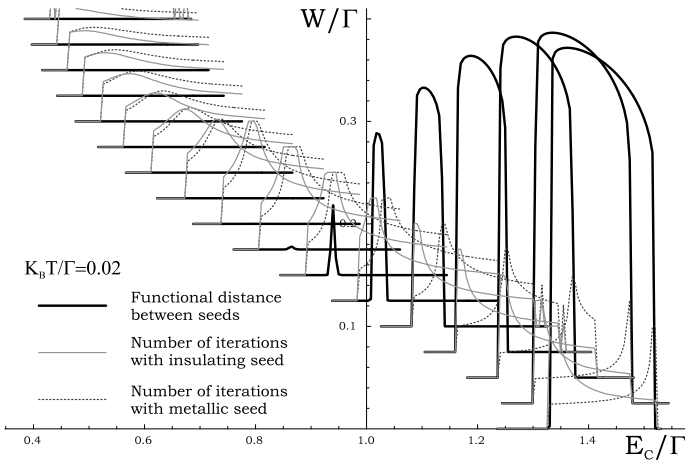

Figure 5.12: In thick solid lines we have the absolute distance between the converged solutions starting with metal and insulating seeds for several values of W/Γ. Note the rapid decline of the hysteretic effect as W/Γ increases. In thin solid lines the relative number of iterations of the DMFT loop with an insulating seed, and in thin dashed lines the one corresponding a metallic seed. Each shoots up at one side of the coexistence region. Note that the instability of the loop extends up to values of W/Γ far greater than the maximum critical value.

system insulating, as explained in the previous section. A rough estimate of the critical W at which $E_C^* \sim T_K$ is satisfied can be performed by using 3.25, with $\rho_g(0) = 4/\pi W$, and making further use of (3.34), (2.103) and (2.99) we can establish the following criterion for the maximum value of W before we cross over to an insulating material

$$\frac{W}{\Gamma} = a + b\left(\frac{E_C}{\Gamma}\right)^{-1} \tag{5.32}$$

for certain constants a and b.

We can check this qualitative law against the solution obtained by iteration of the DMFT loop in the desired region of small E_C. What we do is we fix the temperature to a small value and set a small threshold conductance as the criterion for metallic phase. We then do a sweep over increasing E/Γ and iterate the loop until convergence at each step. This allows us to obtain the precise boundary according to our method, which we expect to look like the light lines on the right side of Fig. 5.10. We have done this for three different temperatures, and the result is presented in Fig. 5.13. The log-log in the inset and the fits in the main plot give a good confirmation of the above estimate up to E_C/Γ close to the Mott transition. Moreover, the asymptotic value of $W/\Gamma \approx 0.4$ at $E_C \sim E_{C1}$ seems to support the fact that this bandwidth-driven metal-insulator crossover stems from the tip of the finite W coexistence pockets, as sketched on the right side of Fig. 5.10. Therefore the slave rotor DMFT method satisfies all the features sketched in the phase diagram proposed in 5.9.

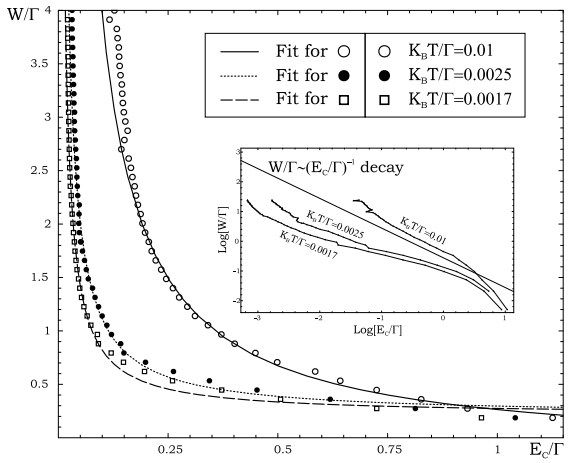

Figure 5.13: Maximum value of the grain bandwidth for the dimensionless conductance of the system to remain above a threshold value of 10^-4. Three different temperatures were considered. A log-log plot is represented in the inset.

5.3.5 Summary and Outlook

We have employed the slave rotor technique in the spherical limit approximation to trace the different regions and boundaries in the phase space of a granular system where each grain has a spectral density peak around the Fermi energy with finite bandwidth W. We have found that such system inherits in one way or another the corresponding features of single grains, albeit qualitatively transformed by the DMFT self-consistency. We have traced the metallic low W region and its direct relation with Kondo effect. The crossover to an insulating phase for larger W has been related to the inverse-crossover from Kondo to Coulomb blockade regimes. The crossover boundary curve was computed. Moreover it was shown that the Mott transition into the large-E_C insulating region, which is related with simple Coulomb blockade in the single junction case, occurs by first order transitions across a finite bistability pocket. The two corresponding critical values for E_C were given, with a fair agreement to previous works.

The present method could naturally be used to analyze more complex scenarios, like non particle-hole symmetric systems, or quantum dot arrays with discrete spectra, in which the two-stage Kondo effect described in chapter 3 is expected to offer interesting possibilities. The addition of disorder to the scheme remains a challenge that could be interesting to pursue in future works, e.g. attempting tactics in the line of [28]. Also the implementation of improvements of the DMFT method, such as in [54] could prove a valuable strategy to advance in the clarification of more delicate questions such as the true order of the Mott transition and the existence of a bistable region in truly 3D systems. As it stands however the present approach has proven to be simple and powerful enough to gain insight on the main features of these systems, and further exploration of the Mott transition using this technique has been carried out in some very recent works [30].

Appendix A

Different Green's functions and properties

The path integral technique translates the time-ordered operator expectation values of traditional quantum mechanics into average of fields, for example

$$\mathbf{G}_{tt'} = -i\langle T\hat{\mathbf{f}}_t\hat{\mathbf{f}}^+_{t'}\rangle = -i\langle \mathbf{f}_t\mathbf{f}^+_{t'}\rangle \tag{A.1}$$

Here T stands for a time ordering operator. The second equality, although deceptively similar in notation, is formally very different from the first. It is the average of the *number* $\mathbf{f}_t\mathbf{f}^+_{t'}$ when performing a functional integration of the fields $\mathbf{f}_t$ and $\mathbf{f}^+_{t'}$ with weight $e^{iS[\mathbf{f}^+_t,\mathbf{f}_t]}$. However both expressions yield identical result, even though $\mathbf{f},\mathbf{f}^+$ are usual numbers, or Grassman variables in the case of fermions. How does one obtain the other types of Green's functions in the path integral formalism? And furthermore, how does one obtain all these real time Green's functions from the imaginary time path integral formalism? We will give a brief overview of these problems in this appendix. Throughout we will denote the bosonic case with the upper sign, and the fermionic case with the lower sign.

Definition of real time Green's functions

One might want to compute other correlation functions that are straightforwardly expressed in the operator notation, such as

$$G^{>}_{gt,g't'} = -i\langle \hat{f}_{gt}\hat{f}^+_{g't'}\rangle \tag{A.2}$$
$$G^{<}_{gt,g't'} = \mp i\langle \hat{f}^+_{g't'}\hat{f}_{gt}\rangle \tag{A.3}$$

In terms of these elementary functions, and setting $\Delta t \equiv t - t'$, the other most usual Green's functions (causal, retarded, advanced) are defined as

$$\mathbf{G}_{\Delta t} = \theta_{\Delta t}\mathbf{G}^{>}_{\Delta t} + \theta_{-\Delta t}\mathbf{G}^{<}_{\Delta t} \tag{A.4}$$
$$\mathbf{G}^{R}_{\Delta t} = \theta_{\Delta t}\left(\mathbf{G}^{>}_{\Delta t} - \mathbf{G}^{<}_{\Delta t}\right) \tag{A.5}$$
$$\mathbf{G}^{A}_{\Delta t} = -\theta_{-\Delta t}\left(\mathbf{G}^{>}_{\Delta t} - \mathbf{G}^{<}_{\Delta t}\right) \tag{A.6}$$

The natural definition of these in the path integral formalism requires the Keldysh contour, whereby the time axis is doubled into two distinct forward and backward branches $t_\pm$, and the fields are correspondingly doubled into two $\mathbf{f}_{t_\pm}$. Although this technique is very powerful and interesting we will follow the philosophy of the main text and stick to the Matsubara formalism, which is sufficient in equilibrium situations. This works by defining the imaginary time Green's functions, which in operator language are defined simply by

$$\mathbf{G}_{\tau\tau'} = -\langle T\hat{\mathbf{f}}_\tau \hat{\mathbf{f}}^+_{\tau'}\rangle = -\langle \mathbf{f}_\tau \mathbf{f}^+_{\tau'}\rangle \tag{A.7}$$

where T now orders times τ along the imaginary time interval, $\tau \in (-\beta, 0]$, and the second equality is the path integral version. The cornerstone of the Matsubara formalism is that the Fourier transform of $\mathbf{G}_{\tau\tau'} = \mathbf{G}_{\tau-\tau'}$, denoted by $\mathbf{G}_{i\omega_n}$ can be analytically continued to the real ω axis to give the physical Green's function $\mathbf{G}_\omega$, $\mathbf{G}^R_\omega$ or $\mathbf{G}^A_\omega$ by following appropriate limit prescriptions.

Going from imaginary time to real time Green's functions

The precise statement underlying the Matsubara formalism is that if one defines

$$\mathbf{G}(z) = \int_{-\infty}^{\infty} d\omega \frac{\mathbf{A}_\omega}{z-\omega} \tag{A.8}$$

$$-2\pi i \mathbf{A}_\omega = \mathbf{G}^>_\omega - \mathbf{G}^<_\omega \tag{A.9}$$

with z a general complex number, one can demonstrate that $\mathbf{G}(z = i\omega)$ is precisely the Matsubara Green's function (A.7),

$$\mathbf{G}(z = i\omega_n) = \mathbf{G}_{i\omega_n} \tag{A.10}$$

Furthermore, it is also straightforward to establish that the real-time Green function in ω space satisfy

$$\mathbf{G}^R_\omega = \mathbf{G}(\omega + i\epsilon) \tag{A.11}$$

$$\mathbf{G}^A_\omega = \mathbf{G}(\omega - i\epsilon) = \left(\mathbf{G}^R_\omega\right)^* \tag{A.12}$$

$$\mathbf{A}_\omega = -\frac{1}{\pi}\Im[\mathbf{G}^R_\omega] = \frac{1}{\pi}\Im[\mathbf{G}^A_\omega] \tag{A.13}$$

for vanishing positive ϵ, and finally

$$\mathbf{G}_\omega = i\int_{-\infty}^{\infty} \frac{d\omega}{2\pi}\left(\frac{\mathbf{G}^<_{\omega'}}{\omega + i\epsilon - \omega'} - \frac{\mathbf{G}^>_{\omega'}}{\omega - i\epsilon - \omega'}\right) \Rightarrow$$

$$\Re[\mathbf{G}_\omega] = \Re[\mathbf{G}(\omega)] \tag{A.14}$$

$$\Im[\mathbf{G}_\omega] = \mathbf{A}_\omega\left(1 \pm 2f^\mp_\omega\right) = \mathbf{A}_\omega \times \begin{cases} \coth\frac{\beta(\omega-\mu)}{2} \\ \tanh\frac{\beta(\omega-\mu)}{2} \end{cases} \tag{A.15}$$

where the last equation follows from the Fluctuation-Dissipation theorem, which holds in thermal equilibrium, and that can be summarized in the following general relation

$$\mathbf{G}^>_\omega = \pm e^{\beta(\omega-\mu)}\mathbf{G}^<_\omega \tag{A.16}$$

so that

$$-2\pi i \mathbf{A}_\omega = \pm \frac{\mathbf{G}^<_\omega}{f^\mp_\omega} = \frac{\mathbf{G}^>_\omega}{1 \pm f^\mp_\omega} \tag{A.17}$$

with

$$f^\mp_\omega = 1/(e^{\beta(\omega-\mu)} \mp 1) \tag{A.18}$$

the Bose/Fermi distribution.

Therefore the link between the two representations is found. As long as one can extend $\mathbf{G}_{i\omega}$ analytically to find $\mathbf{G}(z)$, one can obtain all other real-time response functions, first obtaining $\mathbf{G}^R_\omega$, then $\mathbf{A}_\omega$ and from there the rest of the Green's functions.

Spectral representation of the imaginary time Green's function

Since $\mathbf{G}_{\Delta\tau}$ is the inverse Fourier expansion of $\mathbf{G}_{i\omega_n}$, we can write using (A.9)

$$\mathbf{G}_{\Delta\tau} = \int_{-\infty}^{\infty} d\omega' \frac{1}{\beta} \sum_{\omega_n} \frac{\mathbf{A}_\omega}{i\omega_n - \omega'} e^{-i\omega_n \Delta\tau} \tag{A.19}$$

To evaluate this we will introduce a very useful relation for imaginary time fermionic Green's function calculations at finite temperature

$$\frac{1}{\beta} \sum_{\omega_n} \frac{e^{-i\omega_n\Delta\tau}}{i\omega_n - \omega} = -\frac{e^{-\omega\Delta\tau}}{e^{\beta\omega} \mp 1} \left(e^{\beta\omega}\theta_{\Delta\tau} \pm \theta_{-\Delta\tau} \right) = -e^{-\omega\Delta\tau} \left[(1 \pm f^\mp_\omega)\theta_{\Delta\tau} \pm f^\mp_\omega \theta_{-\Delta\tau} \right] \tag{A.20}$$

where the Bose/Fermi distributions in the last equality correspond to $\mu = 0$.

Making use of (A.20) we evaluate (A.19) to get

$$\mathbf{G}_{\Delta\tau} = -\int_{-\infty}^{\infty} d\omega \left[(1 \pm f^\mp_\omega)\theta_{\Delta\tau} \pm f^\mp_\omega \theta_{-\Delta\tau} \right] \mathbf{A}_\omega e^{-\omega\Delta\tau} \tag{A.21}$$

Making further use of (A.17) this simplifies to

$$\mathbf{G}_{\Delta\tau} = \int_{-\infty}^{\infty} \frac{d\omega}{2\pi i} \left[\mathbf{G}^>{}_\omega \theta_{\Delta\tau} + \mathbf{G}^<{}_\omega \theta_{-\Delta\tau} \right] e^{-\omega\Delta\tau} \tag{A.22}$$

At vanishing temperature this reduces to

$$\mathbf{G}_{\Delta\tau>0} = -\int_0^{\infty} d\omega A_\omega e^{-\omega\Delta\tau} \tag{A.23}$$

$$\mathbf{G}_{\Delta\tau<0} = \int_{-\infty}^{0} d\omega A_\omega e^{-\omega\Delta\tau} \tag{A.24}$$

Equations (A.21 and (A.22) are sometimes referred to the spectral representation of the Matsubara Green functions.

Other properties

Let us take the particular case of bosonic degree of freedom whose imaginary time action is real and symmetrical under time inversion, one has real and even Matsubara Green's function in imaginary time, so that

$$\mathbf{G}_{\Delta\tau} = \mathbf{G}_{-\Delta\tau} \tag{A.25}$$
$$\Im\mathbf{G}_{\Delta\tau} = 0 \tag{A.26}$$

This is the case of the rotor Green's function $\mathcal{G}_{\Delta\tau}$ defined in the text (2.52). Now, such function has the property

$$\mathbf{G}_{i\omega_n} = \mathbf{G}_{-i\omega_n} \tag{A.27}$$
$$\Im\mathbf{G}_{i\omega_n} = 0 \tag{A.28}$$

which by virtue of (A.9) and (A.10) implies

$$\mathbf{A}_\omega = -\mathbf{A}_{-\omega} \tag{A.29}$$

so that, by (A.17),

$$\mathbf{G}^{>}_{-\omega} = e^{-\beta\omega}\mathbf{G}^{>}_{\omega} \tag{A.30}$$
$$\mathbf{G}^{<}_{-\omega} = e^{\beta\omega}\mathbf{G}^{<}_{\omega} \tag{A.31}$$

In this case then, and for $\Delta\tau > 0$, equation (A.22) takes the particular form

$$\mathbf{G}_{\Delta\tau>0} = \int_0^\infty \frac{d\omega}{2\pi}\left(e^{-\omega\Delta\tau} + e^{-\omega(\beta-\Delta\tau)}\right) i\mathbf{G}^{>}{}_{\omega} \tag{A.32}$$

This form will be used in Appendix B

Appendix B

Linear conductance and imaginary time Green's functions

In this appendix we will establish the relation between linear conductance in thermal equilibrium and the imaginary time rotor-rotor correlation function (2.52). We take as a starting point the generalized interacting Landauer formula for the linear conductance g [69] in a $L = 2$ equal lead setup

$$g = -\frac{Ne^2}{h}\pi \int_{-\infty}^{\infty} d\omega \mathrm{Tr}\left[\mathbf{\Gamma^d}_\omega \mathbf{A^d}_\omega\right] \frac{\partial f_\omega}{\partial \omega} \tag{B.1}$$

Here as usual N stands for number of independent channels, and $\rho^d_\omega = \mathrm{Tr}[\mathbf{A^d}_\omega]$ is the density of states *per channel* corresponding to grain electrons $\mathbf{d}$ (the trace is done only over the other quantum numbers), and $\mathbf{\Gamma} = \pi \mathbf{t}\bar{\mathbf{A}}\mathbf{t}^+$ is the inverse mean lifetime of a grain electron of energy ω per lead. $\bar{\mathbf{A}}_\omega$ is the spectral function of the lead electrons, see 2.4. Using the local hopping approximation for $\mathbf{t}$ and a smooth density of states in the leads this is a c-number,

$$\Gamma = L\pi t^2 \rho_l(0) \tag{B.2}$$

(where L is the number of leads, two in the usual setup) and since therefore $\mathrm{Tr}\left[\mathbf{\Gamma^d}_\omega \mathbf{A^d}_\omega\right] = N_L \Gamma \mathrm{Tr}\left[\mathbf{A^d}_\omega\right]$ (N_L is the number of orbitals or levels in the grain) we get

$$g = -\frac{Ne^2}{h}\pi N_L \Gamma \int_{-\infty}^{\infty} d\omega \rho^d_\omega \frac{\partial f_\omega}{\partial \omega} = -\frac{Ne^2}{h}\pi N_L \Gamma \int_{-\infty}^{\infty} \frac{d\omega}{2\pi} \frac{\mathrm{Tr}\left[i\mathbf{G^d}^{>}{}_\omega\right]}{1 - f^+_\omega} \frac{\partial f_\omega}{\partial \omega} \tag{B.3}$$

see (A.17).

Now, the grain density of states must be computed in the presence of interactions $\rho^d_\omega = \mathrm{Tr}[\mathbf{A^d}_\omega] = -\frac{1}{\pi}\mathrm{Tr}\{\mathrm{Im}[\mathbf{G^d}_\omega]\}$, as opposed to the non-interacting density of states $\rho^f_\omega = \mathrm{Tr}[\mathbf{A}_\omega] = -\frac{1}{\pi}\mathrm{Tr}\{\mathrm{Im}[\mathbf{G}_\omega]\}$ that appears in the more common version of the Landauer formula, see section 2.4 in the main text. We will do so using the results of chapter 2.

Given that $\mathbf{G^d_{\Delta_\tau}}$ factorizes in imaginary time, eq. (2.67), and repeatedly employing

properties of Appendix A, one can prove that also $\mathbf{G^d}^>$ factorizes in *real* time

$$i\mathbf{G^d}^>{}_{\Delta t} = i\mathbf{G}^>{}_{\Delta t}\, i\mathcal{G}^>{}_{\Delta t} \tag{B.4}$$

$$i\mathbf{G^d}^>{}_{\omega} = \int_{-\infty}^{\infty} \frac{d\omega'}{2\pi} i\mathbf{G}^>{}_{\omega-\omega'} i\mathcal{G}^>{}_{\omega'} \tag{B.5}$$

Recall that $\mathbf{G}^<{}_{\Delta t}$ corresponds to non-interacting fermions $\mathbf{f}$ in the grain. Therefore, after some algebra

$$g = \frac{Ne^2}{h}\pi N_L \Gamma \int_{-\infty}^{\infty} \frac{d\omega'}{2\pi} i\mathcal{G}^>_{\omega'} \int_{-\infty}^{\infty} d\omega \beta f^+_{\omega} f^+_{\omega'-\omega} \rho^f_{\omega-\omega'} \tag{B.6}$$

This equation reduces to the non-interacting Landauer formula in the case of $E_C \to 0$, i.e. when $i\mathcal{G}^>_{\Delta t} = 1 \Rightarrow i\mathcal{G}^>_{\omega} = 2\pi\delta(\omega)$, to give to familiar Landauer result for the non-interacting linear conductance

$$g_\infty = \frac{Ne^2}{h}\pi N_L \Gamma \int_{-\infty}^{\infty} d\omega \beta f^+_{\omega} f^+_{-\omega} \rho^f_{\omega} \tag{B.7}$$

Defining the functions

$$\tilde{D}[\beta\omega] = \int_{-\infty}^{\infty} d\omega' \beta f^+_{\omega'} f^+_{\omega-\omega'} \rho^f_{\omega'-\omega} \tag{B.8}$$

$$D_{\bar\tau}[\beta\omega] = \frac{\tilde{D}[\beta\omega]}{\tilde{D}[0]} e^{\bar\tau\omega} \tag{B.9}$$

where $\bar\tau$ is an arbitrary positive imaginary time $\bar\tau \in [0, \beta)$, we can rewrite (B.6) and (B.7) exactly as

$$g_\infty = \frac{Ne^2}{h}\pi N_L \Gamma \tilde{D}[0] \tag{B.10}$$

$$g = g_\infty \int_0^{\infty} \frac{d\omega}{2\pi} \left(D_{\bar\tau}[\beta\omega] e^{-\bar\tau\omega} + D_{\bar\tau}[-\beta\omega] e^{-(1-\bar\tau)\omega} \right) i\mathcal{G}^>_{\omega} \tag{B.11}$$

And finally, recalling the result (A.32), we can write the formal expression

$$g = g_\infty \; D_{\bar\tau}[\beta\partial_{\Delta\tau}] i\mathcal{G}^>_{\Delta\tau}\big|_{\Delta\tau=\bar\tau} \tag{B.12}$$

It should be emphasized that this result is exact. The particular choice of $\bar\tau$ is free, and one will usually like choose a value that makes $D_{\bar\tau}[x]$ particularly convenient for approximations as is discussed in section 2.5.3.

Appendix C

Spin constraint field and its geometrical meaning

In this appendix we will give a close expression for the value of the constraint field $\vec{\tilde{H}}_0$ in terms of $\vec{H}$ that appear in equations (4.30), based on the condition that the transformation U_τ in eq. (4.23) must obey the periodicity constrain (4.24) and also the gauge relation (4.25). We will also give a geometrical meaning to the constraint field and to the angular momentum $\vec{L}_{\hat{v}}$.

Defining for convenience the spin part of $U_\tau = e^{i\phi_\tau} Q_\tau$ as

$$Q_\tau = e^{\frac{i}{2}\xi_\tau \hat{n}_\tau \vec{\sigma}} \tag{C.1}$$

$$(\partial_\tau Q_\tau^+) Q_\tau = -i\frac{1}{2}\vec{\sigma}(\vec{H}_\tau - \vec{\tilde{H}}_0) = -i\frac{1}{2}\vec{\sigma}\vec{L}_{\hat{v}} \tag{C.2}$$

we can use the properties of operator time ordering to write

$$Q_\tau = \mathcal{T}\exp\left[\frac{i}{2}\int_0^\tau \vec{\sigma}(\vec{H} - \vec{\tilde{H}}_0)\right] = \mathcal{T}\exp\left[\frac{i}{2}\int_0^\tau \vec{\sigma}\vec{L}_{\hat{v}}\right] \tag{C.3}$$

Indeed, the last equation is equivalent to (C.2) as can be checked by differentiation taking into account that $\mathcal{T}$ orders all matrices in the expansion of the exponential by time, so that for example

$$\mathcal{T}\exp\left[\int_0^\tau A_{\tau'} d\tau'\right] = \mathcal{T}\exp\left[\int_0^{\tilde{\tau}} A_{\tau'} d\tau'\right] \mathcal{T}\exp\left[\int_{\tilde{\tau}}^\tau A_{\tau'} d\tau'\right] \tag{C.4}$$

for any matrix $A_{\tau'}$ and time $0 \leq \tilde{\tau} \leq \tau$. It is implicit in this redefinition that $Q_0 = 1$. This is always possible since the essential condition that must be fulfilled is (C.2) that does not include any particular boundary condition for Q_0.

Now, we wish to analyze the periodicity condition (4.24) that can be rewritten as

$$Q_0 = Q_\beta = 1 \tag{C.5}$$

While the periodicity constraint is very transparent in the $\xi_\tau, \hat{n}_\tau$ and in the 4D sphere $\hat{v}_\tau$ representations (eq. (4.47)), it is not straightforward in the $\vec{H}$ representation, i.e. there is

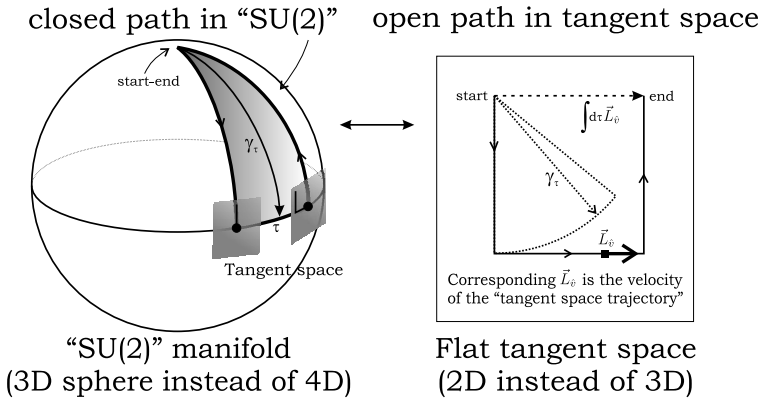

Figure C.1: Tangent space trajectory versus SU(2) trajectory and the geometrical meaning of $\vec{L}_{\hat{v}}$ as a 'tangent velocity'. Note how the path on the right gets drawn on the small tangent plane on the left as the point $\hat{v}_\tau$ moves around a closed trajectory on the 4D sphere (isomorphous to SU(2)).

no evident way to define $\vec{\tilde{H}}_0$ in terms of $\vec{H}$ so that the corresponding $\hat{v}_\tau$ satisfies $\hat{v}_\beta = \hat{v}_0$. If we picture the 4D sphere on which $\hat{v}_\tau$ lives (isomorphous to SU(2)) as a regular 3D sphere in our heads we can draw $\hat{v}_\tau$ as a closed path on its 2D surface representing the β-periodic gauge transformation, see Fig. C.1. Considering (C.3) and (C.2) it is easy to convince oneself that $\vec{L}_{\hat{v}}$ merely represents the projection of the velocity of point $\hat{v}_\tau$ onto the 'tangent space', represented in C.1 as a small 2D flat surface tangent to the (curved) sphere at point $\hat{v}_\tau$ that gets carried along the path $\hat{v}_\tau$ in a parallel-transport fashion. This tangent velocity $\vec{L}_{\hat{v}}$ can plot a path on the tangent space that is not closed even if $\hat{v}_\tau$ is closed for a generic path on the sphere. This is why it is not straightforward to find a definition $\vec{\tilde{H}}_0[\vec{H}]$ that makes $\vec{L}_{\hat{v}} = \vec{H} - \vec{\tilde{H}}_0$ correspond to a closed path on the sphere.

A useful geometrical intuition can be constructed however if we now do a change of our point of view, and think of point $\hat{v}$ not as a point moving on the surface, but as the point of contact of the 3D sphere with a flat surface (a table) on which the sphere is rolling. The velocity of the rolling sphere on the table will be equal to the vector $\vec{L}_{\hat{v}}$, while the periodicity condition (C.2) is equivalent to saying that the sphere must end in the same orientation as it started, see Fig. C.2 This geometrical picture derives quite trivially from the 'tangent space arguments' and will be useful when dealing with the response of a magnetic grain to external magnetic fields, see section 4.4.4.

Definition of $\vec{\tilde{H}}_0[\vec{H}_\tau]$

Now imagine we have a certain $\vec{H}_\tau$ and define

$$\tilde{Q}_\tau = \mathcal{T}\exp\left[\frac{i}{2}\int_0^\tau \vec{\sigma}\vec{H}\right] \equiv e^{\frac{i}{2}\tilde{\xi}_\tau \tilde{\hat{n}}_\tau \vec{\sigma}} \tag{C.6}$$

This transformation $\tilde{Q}_\tau$ does not satisfy (C.5) for an arbitrary path $\vec{H}_\tau$, i.e. $\tilde{\xi}_\tau, \tilde{\hat{n}}_\tau$ do no satisfy (4.24). Using the 4D sphere representation (4.47) we can also build the path on the

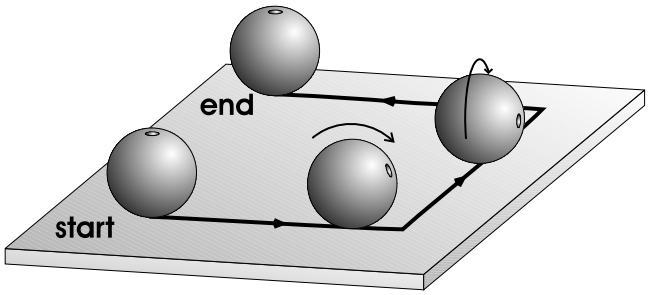

Figure C.2: Geometrical criterion for the β-periodicity condition $C.5$ in terms of a 'rolling SU(2)'. The path on the tangent space (horizontal plane) corresponds to that of Figure C.1.

4D sphere $\tilde{v}_\tau$ that will *not* satisfy $\tilde{v}_\beta = \tilde{v}_0$, i.e. the sphere rolling on the table with velocity $\vec{H}$ will not end up in the same position as it started. However, we can easily relate $\tilde{Q}_\tau$ to Q_τ using (C.4). We can restore the sphere given by $\tilde{Q}_\beta$ to its upright initial position by adding to $\vec{H}_\tau$ a final instantaneous velocity kick $\int_0^\beta \vec{H}_\tau \to \int_0^\beta \vec{\sigma}\left[\vec{H}_\tau - \beta\delta(\tau-\beta)\vec{\tilde{H}}_0\right] = \int_0^\beta \vec{\sigma}\left[\vec{H}_\tau - \vec{\tilde{H}}_0\right]$ and use (C.4) to write

$$Q_\beta = \tilde{Q}_\beta e^{-\frac{i}{2}\beta\vec{\sigma}\vec{\tilde{H}}_0} \tag{C.7}$$

Using (C.5) we can write $\vec{\tilde{H}}_0[\vec{H}_\tau]$ in a simple close form

$$e^{-\frac{i}{2}\beta\vec{\sigma}\vec{\tilde{H}}_0} = \tilde{Q}_\beta = \mathcal{T}\exp\left[\frac{i}{2}\int_0^\beta \vec{\sigma}\vec{H}\right] \tag{C.8}$$

which is analogous to the simpler form of $\tilde{V}_0[V_\tau]$ introduced in (2.15).

Appendix D

Quaternion description of spin dynamics

The description we have developed in chapter 4 of the fluctuating spin degrees of freedom of the metallic grain, or alternatively of the degrees of freedom of the equivalent spherical rotor, relies on a compact object $\hat{v}_\tau$ (a point on a 4D spherical surface) which represents an element of the group of rotations. As is discussed in [5], this representation of the rotation group is a quaternion, an object invented by Hamilton which belongs to an extension of the complex number algebra, and which contains four units $(1, i, j, k)$ instead of two $(1, i)$. For quaternions we also have $i^2 = j^2 = k^2 = -1$, but in this case the internal product is non-commutative, so that $ij = -ji = k, jk = -kj = i, ki = -ik = j$. This immediately reminds of the vector cross product in 3D space.

We can write a quaternion $a + b_x i + b_y j + b_z k$ as (a, b_x, b_y, b_z), or even as $(a, \vec{b})$.[1] In this notation, $v = \left(\cos\frac{\xi}{2}, \sin\frac{\xi}{2}\hat{n}\right)$ is a unit quaternion that represents a rotation (all unit quaternions represent certain rotation in 3D). Indeed, if a normal 3D vector $\vec{w}$ is promoted to a quaternion with the rule $w_c = (0, \vec{w})$, then $w'_c = v w_c \bar{v}$ is the 'quaternionised' version of vector w rotated an angle ξ around axis $\hat{n}$ [12]. We have used quaternion conjugation $\bar{v} = \left(\cos\frac{\xi}{2}, -\sin\frac{\xi}{2}\hat{n}\right)$, and the quaternion internal product defined above. Rotation composition is easily carried out by quaternion multiplication $v_{tot} = v_1 v_2$.

This powerful algebra simplifies our representation even further, since one can work out the following important restatement of equation (4.30)

$$L_{\hat{v}} \equiv (0, \vec{L}_{\hat{v}}) = \bar{v}_\tau \dot{v}_\tau \tag{D.1}$$

Promoting the external magnetic field $\vec{H}_{\rm ext} - \delta\vec{H}_{\rm ext}$ to a quaternion, $H_{\rm ext} - \delta H_{\rm ext} \equiv (0, \vec{H}_{\rm ext} - \delta\vec{H}_{\rm ext})$, and writing $\vec{u}$ as a 'quaternionized' complex number $u = e^{i\phi} = (\cos\phi, \sin\phi, 0, 0)$, we could rewrite the total action fully in terms of quaternions for the spin sector and complex

[1] One useful relation in this notation is $(s_1, \vec{v}_1) * (s_2, \vec{v}_2) = (s_1 s_2 - \vec{v}_1 \cdot \vec{v}_2, s_1\vec{v}_2 + s_2\vec{v}_1 + \vec{v}_1 \times \vec{v}_2)$.

numbers for the charge sector as follows[2],

$$\begin{aligned} S &= \int \frac{|\dot{u}|^2}{4E_C} + \frac{|\dot{v}|^2}{4J} + \alpha \int K_{\tau-\tau'} \left[1 - \Re(\bar{u}_\tau u_{\tau'})\Re(\bar{v}_\tau v_{\tau'})\right] \\ &\quad + i\Re\left[\left(\overline{H}_{\text{ext}} - \overline{\delta H}_{\text{ext}}\right)\bar{v}\dot{v}\right] + \delta\vec{S}_{\text{ext}}\left(\vec{H}_{\text{ext}} - \frac{1}{2}\delta\vec{H}_{\text{ext}}\right) \end{aligned} \tag{D.2}$$

The second line belongs to S_{fields} and describes the effect of an external field.

[2]The real part of a quaternion $Q = (q, \vec{q})$ is defined simply as $\Re(Q) = (Q + \bar{Q})/2 = q$.

Appendix E

Kosterlitz Renormalization Group criterion for the metal-insulator transition in presence of magnetism

The model described in chapter 4 for the effective action in a magnetic grain can be written as follows, in terms of charge-phase 2D unit vector $\hat{u}_\tau \equiv (\cos\phi, \sin\phi)$ and 'spin-phase' 4D unit vector $\hat{v}_\tau$:

$$S = \int d\tau \left(\frac{\dot{\hat{u}}^2}{4E_C} + \frac{\dot{\hat{v}}^2}{4J} \right) + \alpha \int d\tau d\tau' K_{\tau-\tau'} \left[1 - (\hat{u}_\tau \cdot \hat{u}_{\tau'})(\hat{v}_\tau \cdot \hat{v}_{\tau'}) \right] \tag{E.1}$$

Now we assume large βE_C and βJ. Also we assume that α is very *large*. This yields a model equivalent to that of two spin chains with very strong non-local exchange interaction, similar to that studied by Kosterlitz in 1976 [58], but with two types of spins instead of one.

$$S = \alpha \int d\tau d\tau' K_{\tau-\tau'} \left[1 - (\hat{u}_\tau \cdot \hat{u}_{\tau'})(\hat{v}_\tau \cdot \hat{v}_{\tau'}) \right] \tag{E.2}$$

In Kosterlitz case β was roughly the equivalent to our α. There is not such a simple spin-spin interaction picture as he used, since our interaction is now quartic, not quadratic.

As in Kosterlitz's original work we wish to know what is the effective low energy α in the renormalization group (RG) sense, and if the system can exhibit an insulating (vanishing renormalized α) for certain (large) initial values of bare α. Therefore we proceed by calculating the RG flow of α, which is done by introducing a Matsubara frequency cutoff Λ and integrating a shell of modes below such cutoff. We will work in a path integral picture. Also, we will assume dimensionless fields, since it doesn't make sense to scale anything that must remain on a unit sphere. To do RG we need to work in terms of the ω components of the path, which will serve to differentiate between 'fast' and 'slow' contributions. But what coordinates should we Fourier transform? The proper way to do this is to establish a coordinate system in the 2D and 4D unit spheres (for $\hat{u}$ and $\hat{v}$ respectively). It seems

natural to choose spherical coordinates, and describe $\hat{u}$ by ϕ_τ and $\hat{v}$ by $\{\xi_\tau/2, \theta_\tau, \varphi_\tau\}$ (see eq. (4.47)). Now we Fourier transform these coordinates, and separate the contribution to $\hat{u}_\tau$ and $\hat{v}_\tau$ due to ω in $[0, \Lambda']$ (slow), and in $[\Lambda', \Lambda]$ (fast, to be integrated out). We will also make Λ' infinitely close to Λ (expansion parameter $= d\lambda = \frac{\Lambda - \Lambda'}{\Lambda}$) so that the fast component of the vector is very small, and we expand $\hat{u}[\phi_\tau^{slow} + \delta\phi_\tau^{fast}] \approx \hat{u}^s[\phi_\tau^{slow}] + \delta\hat{u}[\delta\phi_\tau^{fast}] + \mathcal{O}(d\lambda^2)$. If we impose that both $\hat{u}^s$ and $\hat{u}$ be unitary (the expansion in the previous equation should never leave the unit sphere at any order), we obtain that $\delta\hat{u}_\tau \cdot \hat{u}_\tau^s = 0$, and that the second order expansion must be

$$\hat{u}_\tau = \frac{\hat{u}_\tau^s + \delta\hat{u}}{\sqrt{1 + \delta\hat{u}_\tau^2}} \approx \hat{u}_\tau^s + \delta\hat{u}_\tau - \frac{1}{2}\hat{u}_\tau^s \delta\hat{u}_\tau^2 \tag{E.3}$$

(and equivalently for $\hat{v}$). Here, as stated, $\hat{u}^s$ is already unitary. We could have guessed the form of this expansion by geometrical reasoning.

We wish now to re-write the action in terms of these slow and fast components up to second order in $d\lambda$, in order to integrate out the fast components. We will use the fact that, neglecting terms linear in $d\lambda$ (which would integrate to zero, since the action is even in the fields), we can write

$$\begin{aligned}
\hat{u}_\tau \hat{u}_{\tau'} &= \hat{u}_\tau^s \hat{u}_{\tau'}^s + \delta\hat{u}_\tau \delta\hat{u}_{\tau'} - \frac{1}{2}\hat{u}_\tau^s \hat{u}_{\tau'}^s (\delta\hat{u}_\tau^2 + \delta\hat{u}_{\tau'}^2) \\
\hat{v}_\tau \hat{v}_{\tau'} &= \hat{v}_\tau^s \hat{v}_{\tau'}^s + \delta\hat{v}_\tau \delta\hat{v}_{\tau'} - \frac{1}{2}\hat{v}_\tau^s \hat{v}_{\tau'}^s (\delta\hat{v}_\tau^2 + \delta\hat{v}_{\tau'}^2)
\end{aligned}$$

Now some subtlety pertaining the case of $\hat{v}$. For a given (τ, τ'), the unit vectors $\{\hat{v}_\tau^s, \hat{v}_{\tau'}^s\}$, which are in general different, span a 2D plane in 4D space. The fast vector components $\{\delta\hat{v}_\tau, \delta\hat{v}_{\tau'}\}$ can be further decomposed as a sum of two subcomponents, the one within the aforementioned plane, which we will call $\{\delta\hat{v}_\tau^{\parallel}, \delta\hat{v}_{\tau'}^{\parallel}\}$ (a c-number), and the one perpendicular to that plane $\{\delta\hat{v}_\tau^{\perp}, \delta\hat{v}_{\tau'}^{\perp}\}$ (a 2D vector). In the case of $\hat{u}$ only the 'parallel' component exists. Now, in terms of these two components, we have the relations

$$\delta\hat{u}_\tau \delta\hat{u}_{\tau'} = \hat{u}_\tau^s \hat{u}_{\tau'}^s \delta\hat{u}_\tau^{\parallel} \delta\hat{u}_{\tau'}^{\parallel} \tag{E.4}$$

$$\delta\hat{v}_\tau \delta\hat{v}_{\tau'} = \hat{v}_\tau^s \hat{v}_{\tau'}^s \delta\hat{v}_\tau^{\parallel} \delta\hat{v}_{\tau'}^{\parallel} + \delta\hat{v}_\tau^{\perp} \delta\hat{v}_{\tau'}^{\perp} \tag{E.5}$$

With this in mind the action (E.2) can be recast into $S = S^{fast} + S^{slow} + S^{int}$, where

$$S^{slow} = \alpha \int_K (1 - \hat{u}_\tau^s \hat{u}_{\tau'}^s \hat{v}_\tau^s \hat{v}_{\tau'}^s) \tag{E.6}$$

$$S^{fast} = \frac{1}{2}\alpha \int_K (\delta\hat{u}_\tau - \delta\hat{u}_{\tau'})^2 + (\delta\hat{v}_\tau - \delta\hat{v}_{\tau'})^2 \tag{E.7}$$

$$\begin{aligned}
S^{int} = &-\frac{1}{2}\alpha \int_K (1 - \hat{u}_\tau^s \hat{u}_{\tau'}^s \hat{v}_\tau^s \hat{v}_{\tau'}^s) \times (\Delta\delta\hat{u}^2 + \Delta\delta\hat{v}^{\parallel 2} + \delta\hat{v}_\tau^{\perp 2} + \delta\hat{v}_{\tau'}^{\perp 2}) \\
&-\alpha \int_K (1 - \hat{u}_\tau^s \hat{u}_{\tau'}^s) \delta\hat{v}_\tau^{\perp} \delta\hat{v}_{\tau'}^{\perp}
\end{aligned} \tag{E.8}$$

Notation here is $\int_K \equiv \int d\tau d\tau' K(\tau - \tau')$ and $\Delta\delta\hat{u} \equiv \delta\hat{u}_\tau - \delta\hat{u}_{\tau'}$. This requires some attention, but there is nothing difficult here really. One thing to remember though, is that the paths

$\delta\hat{u}_\tau$ and $\delta\hat{v}_\tau$ over which we are integrating correspond only to fast harmonics, so that, expressed in ω components, S^{fast} would only contain $\Lambda' < \omega < \Lambda$ terms.

Now the 'large α' reasoning. If $\alpha \gg 1$ only paths with unit vectors quite well aligned for all τ will have a reasonably high weight, and the rest can be neglected. In such case S^{int} will be small with respect to S^{fast}, and we can integrate out the fast modes using the first order cumulant expansion $\langle e^{-S^{int}}\rangle_{fast} \approx e^{-\langle S^{int}\rangle_{fast}}$. We can already see in (E.8) that α will be renormalized with a negative contribution due to S^{int}, and that, in principle, a new term could appear proportional to $1 - \hat{u}^s_\tau \hat{u}^s_{\tau'}$. It will turn out that this contribution is negligible.

Moreover, if we work in the limit of zero temperature and assume Fermi liquid-type

$$K_\tau = E_C^\epsilon \frac{(\pi T)^{2-\epsilon}}{\sin^{2-\epsilon}(\pi T \tau)} \approx \frac{E_C^\epsilon}{\tau^{2-\epsilon}} \tag{E.9}$$

we can calculate the ω-space Green function for the fast components $\frac{1}{\beta}\langle \delta\hat{v}_{i\omega}\delta\hat{v}_{j\omega'}\rangle_{fast} = \delta_{ij}\delta_{\omega',-\omega}G(\omega)$, which gives[1]

$$G(\omega) = \left[\alpha \int_{-\infty}^{\infty} d\tau 2\left(1-\cos(\omega\tau)\right)\frac{E_C^\epsilon}{\tau^{2-\epsilon}}\right]^{-1} = \frac{1}{2\pi\alpha}\left(\frac{|\omega|}{E_C}\right)^\epsilon \frac{\Gamma(2-\epsilon)\cos(\frac{\pi}{2}\epsilon)}{|\omega|} \tag{E.10}$$

Remember that this applies only to values $\Lambda' < \omega < \Lambda$ of ω. We have used here the Fourier series expansion $\delta\hat{v}_\tau = \frac{1}{\beta}\sum_\omega e^{i\omega\tau}\delta\hat{v}_\omega$, and assumed $\beta \to \infty$. Note that $\delta\hat{v}_\tau$ no longer lies on a unit sphere, so that a component-by-component Fourier series can be performed, corresponding to the fourier series of displacement spherical coordinates around point $\hat{v}^s_\tau$.

Parameterizing the reduction of the cutoff by $\Lambda = \Lambda_0 e^{-\lambda} \Rightarrow -d\Lambda = \Lambda d\lambda$ ($\lambda \in [0,\infty]$), we can write

$$\begin{aligned}\langle \delta\hat{v}_{i\tau}\delta\hat{v}_{i\tau'}\rangle &= \frac{1}{\beta^2}\sum_{|\omega|,|\omega'|=\Lambda'}^{\Lambda} e^{i(\tau\omega+\tau'\omega')}\langle \delta\hat{v}_{i\omega}\delta\hat{v}_{i\omega'}\rangle = \\ &= d\lambda\frac{\Lambda}{\pi}\cos\left(\Lambda(\tau-\tau')\right)\frac{\langle \delta\hat{v}_{i\Lambda}\delta\hat{v}_{i,-\Lambda}\rangle}{\beta}\end{aligned} \tag{E.11}$$

(and equivalently for $\hat{u}$) which finally allows us to integrate out the fast modes in (E.8). Note though, that in the previous equation, if $\tau \neq \tau'$ like in the last term of S^{int} for example, the average gains a Λ frequency phase, that would give zero if τ-integrated together with any 'slow' path, which only contains smaller-than-Λ frequencies. Therefore only α suffers renormalization (from the $\tau = \tau'$ terms in S_int), and as mentioned earlier no other terms arise.

We end up with the following flow equation for α (the ϵ term is the bare scaling) by identifying $d\alpha = \epsilon\alpha d\lambda - \alpha\left(\langle \delta\hat{u}_\tau\delta\hat{u}_\tau\rangle + \sum_i\langle \delta\hat{v}_{i\tau}\delta\hat{v}_{i\tau}\rangle\right)$

$$\frac{1}{\alpha}\frac{d\alpha}{d\lambda} = \epsilon - \frac{4}{\pi}\Lambda G(\Lambda) = \tag{E.12}$$

[1]Bear in mind that the correct way to take the zero temperature limit is to change from $\int_{-\beta/2}^{\beta/2}$ to $\int_{-\infty}^{\infty}$, and not from $\int_0^\beta$ to $\int_0^\infty$, since the β-periodicity of the integrand gives a contribution at $\tau \lesssim \beta$ equivalent to $\tau \gtrsim 0$. Note also the factor 1/2 in the exponent of S_{fast} that should be excluded from G^{-1} since we are dealing with gaussian integrals of real variables.

The flow of $z \equiv 1/\alpha$, more appropriate since the whole scheme is valid for $\alpha \to \infty$, is

$$\begin{aligned} \frac{1}{z}\frac{dz}{d\lambda} &= -\epsilon + \frac{4}{\pi}\Lambda G(\Lambda) = \\ &= -\epsilon + 4z\frac{1}{2\pi^2}\left(\frac{\Lambda}{E_C}\right)^{\epsilon}\Gamma(2-\epsilon)\cos(\frac{\pi}{2}\epsilon) \approx \\ &\approx -\epsilon + 4z\frac{1}{2\pi^2} + \mathcal{O}(z^2, \epsilon z) \end{aligned} \tag{E.13}$$

which suggests a critical value of

$$\alpha_c = \frac{2}{\pi^2\epsilon}\left(\frac{\Lambda_0}{E_C}\right)^{\epsilon}\Gamma(2-\epsilon)\cos(\frac{\pi}{2}\epsilon) \approx \frac{2}{\pi^2\epsilon} + \mathcal{O}[\epsilon] \tag{E.14}$$

If $\alpha > \alpha_c$ the system will remain metallic (infinite α fixed point is stable) at low energuies/temperatures, and if $\alpha < \alpha_c$ it will start to flow away from $\alpha = \infty$ as we lower the cutoff, eventually escaping the strong coupling fixed point towards the $\alpha = 0$ one, which is always stable (attractive). In such case one would effectively have an insulating system at zero temperature with a finite renormalized charging energy E_C^* as soon as $\alpha < \alpha_c$.

Note that this whole calculation is also valid for the spinless case by simply removing the $\sum_i \langle \delta\hat{v}_{i\tau}\delta\hat{v}_{i\tau}\rangle$ term contributing to the flow of α, which therefore becomes

$$\frac{1}{z}\frac{dz}{d\lambda} = -\epsilon + z\frac{1}{2\pi^2}\left(\frac{\Lambda}{E_C}\right)^{\epsilon}\Gamma(2-\epsilon)\cos(\frac{\pi}{2}\epsilon) \approx -\epsilon + z\frac{1}{2\pi^2} + \mathcal{O}(z^2, \epsilon z) \tag{E.15}$$

in the non-magnetic case, yielding

$$\alpha_c = \frac{1}{2\pi^2\epsilon}\left(\frac{\Lambda_0}{E_C}\right)^{\epsilon}\Gamma(2-\epsilon)\cos(\frac{\pi}{2}\epsilon) \approx \frac{1}{2\pi^2\epsilon} + \mathcal{O}[\epsilon] \tag{E.16}$$

The natural cutoff Λ_0 is actually of the order of E_C, since this is the inverse time of the fastest allowed components of the rotor fields. This doesn't arise explicitly since we have neglected the kinetic energy $\sim \dot{\hat{u}}/4E_C$ terms in the initial action, which would begin being important if α gets renormalized to a small enough value. Indeed, assuming cartain $\Lambda_0 > E_C$ one can expect equations (E.14) and (E.16) even for non-small ϵ.

Appendix F

Kosterlitz transition in the spherical limit

We have shown by renormalization group arguments around the $\alpha = \infty$ fixed point in Appendix E that a single Coulomb blockaded non-magnetic metallic grain can experience a transition to a conducting state in the presence of excitonic effects if the coupling strength to the leads is greater than

$$\alpha_c = \frac{1}{2\pi^2\epsilon}\left(\frac{\Lambda_0}{E_C}\right)^{\epsilon}\Gamma(2-\epsilon)\cos(\frac{\pi}{2}\epsilon) \approx \frac{1}{2\pi^2\epsilon} + \mathcal{O}[\epsilon] \tag{F.1}$$

being α the dimensionless conductance of the junction and $\varepsilon > 0$ the parameter describing the enhance tunneling produced by an excitonic resonance around the junction, see section 5.2.

The question arises as to whether the spherical limit approach employed throughout this text can hope to capture this transition in a quantitative manner. In the presence of $\varepsilon \neq 0$ in a metallic grain low temperatures $\beta E_C \gg 1$ the spherical limit constraint on λ reads, according to (2.89)

$$\mathcal{G}_{\Delta\tau=0} = \int_{-\infty}^{\infty}\frac{d\omega}{2\pi}\frac{1/2}{\frac{\omega^2}{4E_C} + \alpha(K_0 - K_\omega) + \lambda} = 1 \tag{F.2}$$

The metallic kernel K_ω with excitonic effects is

$$K_0 - K_\omega = \int_{-\infty}^{\infty} d\tau\,(1-\cos(\omega\tau))\,\frac{E_C^{\epsilon}}{\tau^{2-\epsilon}} = \pi E_C^{\varepsilon}\frac{|\omega|^{1-\varepsilon}}{\Gamma(2-\varepsilon)\cos(\pi\varepsilon/2)} \tag{F.3}$$

With this kernel we the integral (F.2) can be performed exactly if $\lambda = 0$. Since $\lambda = 0$ means a vanishing value of the renormalized Coulomb gap $E_C^* = \sqrt{4\lambda E_C}$, taking $\lambda = 0$ in (F.2) and solving for α can give us the low temperature value of the critical α_c according to the spherical limit. Doing just that we obtain the criticality condition

$$\alpha_c = \frac{\Gamma(2-\varepsilon)\cos(\pi\varepsilon/2)}{2\pi^2\varepsilon}\left[\frac{2}{\pi}\right]^{\varepsilon}\left[\Gamma\left(\frac{2+\varepsilon}{1+\varepsilon}\right)\Gamma\left(\frac{\varepsilon}{1+\varepsilon}\right)\right]^{1+\varepsilon}\varepsilon \tag{F.4}$$

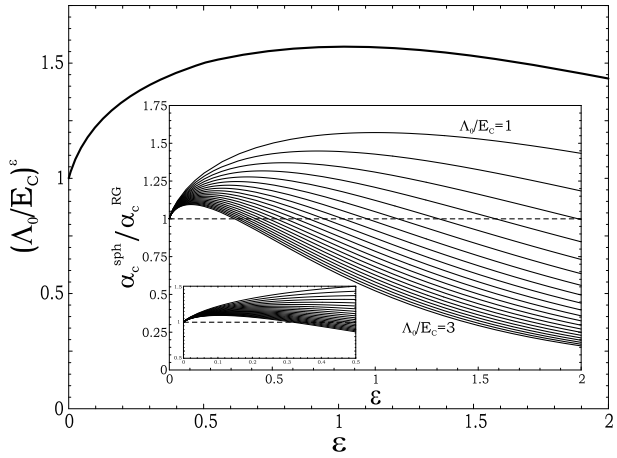

Figure F.1: In the main plot we see the behavior of the optimal cutoff correction of eq. (F.5), which satisfies $\left(\frac{\Lambda_0}{E_C}\right)^{\varepsilon} \gtrsim 1$. In the inset we plot a comparison of the critical α_c of the single non-magnetic metallic grain obtained by renormalization group around the strong coupling limit and the spherical limit approximation for a range of values of non-equilibrium parameter ε. The different curves are obtained by choosing a different initial cutoff in the RG result $\Lambda_0/E_C = 1, 1.1, 1.2, \ldots, 3$, starting from the top curve. Both approaches coincide close to $\varepsilon = 0$, where they give $\alpha_c = 1/(2\pi^2\varepsilon)$. The agreement is quite reasonable up to $\varepsilon \approx 0.5$.

If we allow for an ε dependent cutoff (which is not very physical however, since the cutoff stems from the ε-independent kinetic term) the latter expression would allow us to identify the optimum kinetic cutoff correction that should be used in the Kosterlitz arguments for finite ε in order to agree identically with the spherical limit approximation,

$$\left(\frac{\Lambda_0}{E_C}\right)^{\varepsilon} = \left[\frac{2}{\pi}\right]^{\varepsilon} \left[\Gamma\left(\frac{2+\varepsilon}{1+\varepsilon}\right)\Gamma\left(\frac{\varepsilon}{1+\varepsilon}\right)\right]^{1+\varepsilon} \varepsilon \approx 1 - \varepsilon(\log\left[\frac{1}{\varepsilon}\right] - 0.45) + \mathcal{O}[\varepsilon^2] \qquad \text{(F.5)}$$

This correction factor has several appealing features, i.e. it is identically one for $\varepsilon = 0$, so both renormalization group and spherical limit predict the same transition point in this limit. Furthermore, the correction is $\frac{\Lambda_0}{E_C} \gtrsim 1$ as stated by physical arguments at the end of Appendix E.

If Λ_0/E_C is assumed a constant one can still get a reasonable agreement between renormalization group and spherical limit predictions of α_c by taking $\Lambda_0/E_C \sim 2$, and again an *exact* agreement around $\varepsilon = 0$. The comparison in depicted in Fig. F.1, together with a plot of the optimal cutoff correction of eq. (F.5).

The question remains as to what is the behavior of the spherical limit approach beyond the transition $\alpha > \alpha_c$. In such case there exists no solution for equation (F.2). A negative λ is not adequate, since the integral acquires poles at low ω's. Therefore we have to conclude that the spherical limit approach is good up to the metallic transition or below, but cannot describe the metallic grain above the transition, in the conducting regime. We can assume by continuity however that since the system has become gapless the real solution

acquires a finite asymptotic value $\mathcal{G}_\infty = \lim_{\Delta\tau\to\infty} \mathcal{G}_{\Delta\tau} > 0$, i.e. a sudden long range rigid ordering of the phase of the system appears, much like in the superconducting transition. In the insulating regime, since the low ω behavior of $\mathcal{G}_{i\omega}$ is $\mathcal{G}_{i\omega} \sim 1/|\omega|^{1-\varepsilon}$, a modified cotunneling law for the conductance is to be expected, in particular $g \propto T^{2-\varepsilon}$.

Appendix G

Rate equation techniques

To solve the problem of transport through a grain, one usually employs a 'rate equation' type of approach, expressing the total current as a sum over transfer rates of electrons entering and exiting the grain. To begin write the steady-state current flowing through junction r, $I_r = \langle \hat{I}_r \rangle$ as follows

$$I = \langle \dot{Q}_r(t) \rangle = \partial_t \sum_i \rho_i \langle i|Q_r(t)|i\rangle, \text{with t}\to\infty \tag{G.1}$$

where ρ_i is the occupation probability of a global state $|i\rangle$ (depends on temperature). In equilibrium (small current limit) we have $\rho_i = \langle i|e^{-\beta H}|i\rangle/Z$.

We will now use Schrödinger's picture to write $|i(t)\rangle = e^{-iH(t-t_0)/\hbar}|i\rangle$ ($|i\rangle$ is the initial state at $t = t_0 \to -\infty$ before connecting the hopping). Inserting a complete set of eigenstates of Q_r, $Q_r|f\rangle = q_f|f\rangle$ we have

$$I = \partial_t \sum_{f,i} \langle i(t)|f\rangle\langle f|Q_r|i(t)\rangle = \sum_{f,i} q_f \rho_i \Gamma_{i\to f} \tag{G.2}$$

where $\Gamma_{i\to f} \equiv \partial_t |\langle i(t)|f\rangle|^2$ in the steady state. This matrix element is a transfer rate of q_f electrons across junction r, associated with the transition from the initial state $|i\rangle$ to $|f\rangle$. This rate can be computed in a variety of ways, the most natural of which usually involves perturbation theory.

With some work one can demonstrate that

$$\Gamma_{i\to f} = \frac{1}{h}\delta(\epsilon_i - \epsilon_f)\left|\langle i|\hat{T}(\epsilon_i)|f\rangle\right|^2 \tag{G.3}$$

where $\hat{T}(\omega) = H_T\left[1 - G_0(\omega)H_T\right]^{-1} = H_T + H_T G_0(\omega) H_T + \ldots$ is the T-matrix operator, while $G_0(\omega) = 1/(\omega - H_0 + i0)$ is the unperturbed retarded resolvent operator (whose 1-particle matrix elements are the usual 1-particle unperturbed retarded Green's functions in the ω domain). Also ϵ_i and ϵ_f are the eigenvalues of $|i\rangle$ and $|f\rangle$ under H_0 respectively.

To demonstrate (G.3) we proceed as follows. Using now the interaction picture we

compute

$$\begin{aligned}\langle f|i(t)\rangle &= \langle f|T\exp\left[-\frac{i}{\hbar}\int_{t_0}^{t}H_T(t')dt'\right]|i\rangle \qquad \text{(G.4)}\\ &= \sum_{n=0}^{\infty}\left(\frac{-i}{\hbar}\right)^n\int_{t_0}^{t}dt_1\int_{t_0}^{t_1}dt_2\ldots\int_{t_0}^{t_{n-1}}dt_n\langle f|H_T(t_1)\ldots H_T(t_n)|i\rangle = \\ &= \sum_{n=0}^{\infty}\left(\frac{-i}{\hbar}\right)^n\int_{t_0}^{t}dt_1\int_{t_0}^{t_1}dt_2\ldots \\ &\quad \ldots\int_{t_0}^{t_{n-1}}dt_n\langle f|e^{-iH_0(t_0-t_1)}H_Te^{-iH_0(t_1-t_2)}H_T\ldots e^{-iH_0(t_{n-1}-t_n)}H_Te^{-iH_0(t_n-t_0)}|i\rangle\end{aligned}$$

Note that the outer evolution operators give a factor $e^{-\epsilon_f(t_1-t_0)}e^{-\epsilon_i(t_n-t_0)}$, and that we have set $\hbar=1$ in these expressions. We proceed by integrating all times in order, from the highest t_n down to t_1, and using

$$\begin{aligned}\int_{t_0}^{t_{m-1}}dt_m e^{-i\frac{H_0}{\hbar}(t_{m-1}-t_m)}e^{-i\frac{\epsilon_i+i0}{\hbar}t_m} \\ = \frac{\hbar}{-i}\frac{e^{-i\frac{\epsilon_i+i0}{\hbar}t_{m-1}}}{\epsilon_i-H_0+i0} \qquad \text{(G.5)}\end{aligned}$$

We obtain after some easy algebra

$$\begin{aligned}\langle f|i(t)\rangle = \langle f|i\rangle + \sum_{n=1}^{\infty}\langle f|H_T\left[G_0(\epsilon_i)H_T\right]^{n-1}|i\rangle \\ \times\frac{e^{-i\frac{\epsilon_i-\epsilon_f}{\hbar}t}}{\epsilon_i-\epsilon_f-i0} \qquad \text{(G.6)}\end{aligned}$$

Using $\Gamma_{i\to f}=2\Re\left\{\langle i(t)|f\rangle\partial_t\langle f|i(t)\rangle\right\}$, dropping out the first term (which is zero unless $q_f=0$, so it never contributes to the current) and recalling that $2\Re\left[-i\frac{1}{\epsilon_i-\epsilon_f+i0}\right]=2\pi\delta(\epsilon_i-\epsilon_f)$, we finally recover equation (G.3).

One last note. When summing over all states $|f\rangle$ one must be careful not to include repetitions. In particular, since something like $c_i^+c_j^+|0\rangle$ and $c_j^+c_i^+|0\rangle$ differ only by a phase, they should only be included once. Recall that the sum over $|f\rangle$ comes from the insertion of an identity operator, which in Fock space is something as follows

$$\begin{aligned}\mathbf{1} &= |0\rangle\langle 0| + \sum_a c_a^+|0\rangle\langle 0|_a^c + \sum_{a<b}c_a^+c_b^+|0\rangle\langle 0|c_ac_b + \ldots = \\ &= |0\rangle\langle 0| + \sum_a c_a^+|0\rangle\langle 0|_a^c + \frac{1}{2!}\sum_{a,b}c_a^+c_b^+|0\rangle\langle 0|c_ac_b + \ldots\end{aligned}$$

Note the $1/n!$ in the n-body term!

The evaluation of eq. (G.3) can be performed rigorously in equilibrium or non-equilibrium situations using e.g. the real-time diagrammatic approach developed by Schoeller,

Schön and König [57]. This technique provides a powerful path to follow in many cases, given its generality, and it is very interesting in itself. However many physical effects, such as Kondo or excitonic effects require a summation of infinite series of diagrams, which can become quite intractable. Another technique that is well suited to deal with the present problem is the 'Symmetrized-U Non-crossing approximation' (SUNCA) developed by Haule and Kroha [45] from the NCA approximation to slave bosons. In this case non-perturbative results are more easily accessible, but it relies on technical tricks as the concept of slave bosons. In the particular case of SUNCA the formal side also remains quite tough.

The quantum rotor and slave rotor methods, which are kind of brothers to the slave boson techniques, and the extensions we describe in the main body of this work have the advantage of being non-perturbative (in a controlled manner, as NCA is) quite tractable numerically, and formally (and intuitively) quite simple too.

Appendix H

Determinants of continuous differential operators

We will give the details that lead to the following relation for differential fermionic operator $\hat{D} = \partial_\tau - \epsilon$

$$Z = \int \mathcal{D}[c^+ c] e^{-\int c^+_\tau \hat{D}_{\tau,\tau'} c_{\tau'}} = \det\left[\hat{D}\right] = \det\left[\partial_\tau - \epsilon\right] = 1 + e^{-\beta\epsilon} \tag{H.1}$$

which is used to evaluate gaussian integrals of fermions. We will present a non-rigorous derivation, overlooking precise mathematical definitions and Hilbert space subtleties.

The definition of the determinant of an differential operator can be extended from that of a discrete matrix by taking a finite discretization of time (or space) coordinates. In such case there is no difference between a differential operator or an everyday matrix. In particular if the operator is hermitian it will have a set of eigenvalues d_n and its eigenvectors will form a base. Since the determinants is invariant under unitary transformations we should have

$$\det\left[\hat{D}\right] = C_1 \prod_n d_n = C_1 \exp\left[\sum_n \log(d_n)\right] \tag{H.2}$$

which is the form of the determinant of the diagonal matrix $\hat{D}$ in the base of its eigenvectors. Prefactor C_1 was introduced in this (special) definition of the determinant to account for the condition that $Z = \mathrm{Tr}\left[e^{-\beta H}\right]$ of equation (H.1) satisfy the third principle of thermodynamics, i.e. that the zero temperature entropy is zero, or that the ground state of any well mannered system is non-degenerate. In other words, C_1 should be chosen so that $Z \to 1$ when $\beta \to \infty$.

Let us proceed with eq. (H.2). For an unbounded matrix as we would have in the limit of a continuous τ this expression could (and does) diverge. For example, for our particular $\hat{D}$, whose fermionic eigenvectors in the β imaginary time ring are simply $e^{i\omega_n \tau}$ functions, has eigenvalues $d_n = i\omega_n - \epsilon$, so that the above expression in the continuum limit involves the divergent sum $\sum_{n=-\infty}^{\infty} \log(i\omega_n - \epsilon) = \sum_{n=0}^{\infty} \log(\omega_n^2 + \epsilon^2)$. We can however formally extract an ϵ-independent pre-factor $C_2 = \exp\left[\sum_{n=0}^{\infty} \log(\omega_n^2)\right]$ out of $\det\left[\hat{D}\right]$, and

write

$$\det\left[\hat{D}\right] = C_1 C_2 \exp\left[\sum_{n=0}^{\infty} \log(1 + \frac{\epsilon^2}{\omega_n^2})\right] = C\cosh(\frac{\beta\epsilon}{2}) \tag{H.3}$$

The last equality holds for fermionic Matsubara frequencies $\omega_n = (2n+1)\pi/\beta$. We can finally write

$$\det\left[\hat{D}\right] = C_1 C_2 \frac{e^{\beta\epsilon/2}}{2}\left(1 + e^{-\beta\epsilon}\right) \tag{H.4}$$

Imposing the zero temperature $Z = 1$ condition on the prefactors we recover eq. (H.1).

A more general and elegant derivation of this type of relations can be found in the inspiring book by

Appendix I

Cumulant expansion theorem

The cumulant expansion theorem states that for a certain random variable x of arbitrary distribution $P(x)$, the average of $\exp(x)$ can be expressed as the exponential of an infinite series of cumulants of $P(x)$[1]

$$\langle \exp(x) \rangle = \exp \sum_{n=0}^{\infty} \frac{1}{n!} \langle\langle x^n \rangle\rangle \tag{I.1}$$

The definition of the n-th order cumulant $\langle\langle x^n \rangle\rangle$ of $P(x)$ is a certain combination of momenta of $P(x)$ of order less or equal to n. One of the possible general definition of cumulants makes use of the so-called characteristic function $\chi(p)$, which is the Fourier transform of $P(x)$,

$$\chi(p) = \int_{-\infty}^{\infty} dx e^{ipx} P(x) \tag{I.2}$$

The n-th cumulant is then defined as

$$\langle\langle x^n \rangle\rangle \equiv \left. \frac{d^n \log \chi(p)}{dp^n} \right|_{p=0} \tag{I.3}$$

It is easy to evaluate the above expression by derivating the log of $\chi(p)$ repeatedly by the chain rule, and using its definition to obtain the general expressions

$$\begin{aligned}
\langle\langle x \rangle\rangle &= \langle x \rangle & \text{(I.4)} \\
\langle\langle x^2 \rangle\rangle &= \langle x^2 \rangle - \langle x \rangle^2 & \text{(I.5)} \\
\langle\langle x^3 \rangle\rangle &= \langle x^3 \rangle - 3\langle x^2 \rangle \langle x \rangle + 2\langle x \rangle^3 & \text{(I.6)} \\
\langle\langle x^4 \rangle\rangle &= \langle x^4 \rangle - 4\langle x^3 \rangle \langle x \rangle + 12\langle x^2 \rangle \langle x \rangle^2 - 6\langle x \rangle^4 & \text{(I.7)}
\end{aligned}$$

and so on.

Several general conclusions can be immediately drawn from this theorem. For a gaussian distribution $P(x) = \frac{1}{\sqrt{2\pi}\sigma} \exp\left[-\frac{(x-x_0)^2}{2\sigma}\right]$ one has an equally gaussian $\chi(p) =$

[1] We will stick to one dimensional distribution of an unbounded variable, although the generalization is very straightforward. We will not present any demonstration, which can be found in most text books on statistics.

$e^{2p^2\sigma}e^{ix_0p}$, since that is one of the important properties of such function. Therefore $\log\chi(p)$ will be a second order polynomial, so that only first and second order cumulants of the gaussian distribution are non-zero. For a centered gaussian $P(x)$ only the second cumulant is non-zero, and equal to the dispersion σ, so that in such case

$$\langle e^x\rangle = e^{\frac{1}{2}\langle x^2\rangle} \tag{I.8}$$

$$\langle e^{ix}\rangle = \langle\cos(x)\rangle = e^{-\frac{1}{2}\langle x^2\rangle} \tag{I.9}$$

Another conclusion which we use in the main text pertains the cumulants of a degenerate set of N uncorrelated random variables x_i, all with the same probability function $P(x_i)$ and characteristic function $\chi(p_i)$, so that $P(\vec{x}) = \prod_i^N P(x_i)$. If we want to find the cumulants of the 'total x variable', $\bar{x} \equiv \sum_i^N x_i$ in order to average $\exp(\bar{x})$ we can proceed as follows. First compute $\chi(\bar{p})$ by realizing that the distribution for $\bar{x}$ is

$$\bar{P}(\bar{x}) = \int dx_1dx_2\ldots dx_{N-1}P(x_1)P(x_2)\ldots P(\bar{x}-x_1-\ldots-x_{N-1}) \tag{I.10}$$

so that

$$\chi(\bar{p}) = \int dx_1dx_2\ldots dx_N e^{i\bar{p}\bar{x}}P(x_1)P(x_2)\ldots P(\bar{x}-x_1-\ldots-x_{N-1}) \tag{I.11}$$

The above expression is the Fourier transform of the *convolution* of N distribution function $\bar{P}(\bar{x}) = P\star P\star\ldots P(\bar{x})$, which by the properties of Fourier transforms equates to

$$\bar{\chi}(\bar{p}) = \chi(\bar{p})^N \tag{I.12}$$

This implies by (I.3) the general property

$$\langle\langle\bar{x}^n\rangle\rangle = N\langle\langle x_i^n\rangle\rangle \tag{I.13}$$

which can be employed as an essential tool in the large-N expansion schemes as demonstrated in the main text.

Appendix J

Anexo en castellano

Incluimos a continuación una traducción de la introducción y de las conclusiones de cada capítulo, lo cual constituye el resumen global de este trabajo, como parte de los requisitos de presentación de tesis doctorales de la Universidad Autónoma de Madrid.

J.1 Introducción: Interacciones en la física del estado sólido

La modelización de los sistemas física forma parte de las raíces de la Física tal y como la conocemos. Hay todo un universo de suposiciones implícitas sobre la realidad que debemos aceptar antes de llegar a esta forma de pensar, que es el substrato sobre el que se funda la Física. En este proceso el mundo físico es objetivizado (separado del pensador), ordenado y descompuesto en ciertos ingredientes, como las partículas elementales o los campos, a los que se les atribuyen un conjunto de propiedades y relaciones mutuas. De esta manera se construye un marco conceptual, y a los físicos nos resta la tarea de jugar con los ingredientes, de averiguar las relaciones 'correctas' y las manifestaciones fenomenológicas que pueden surgir de ellas de acuerdo con las reglas del juego. A los filósofos se les deja la descomunal tarea de encontrar sentido al mundo sin todas estas suposiciones previas. Por suerte para nosotros (¡y para mí!) a los físicos se nos está oficialmente permitido ignorar preguntas tales como "¿Qué *es* un campo?", o "¿Qué *son* las interacciones?". ¡Ya es un buen peso que nos quitamos de encima! En esta introducción nos concentraremos en su lugar meramente en ilustrar el papel de las interacciones electrónicas en la materia en estado sólido, que constituye el tema principal del presente trabajo, y en clasificar algunas de los diferentes fenómenos de los que estas interacciones son directamente responsables.

Encerrémonos pues en nuestras mentes durante un rato, y demos un paseo empezando en uno de los sistemas más simples del juego conocido por 'Mecánica Cuántica no relativista', el Gas de Fermi Ideal, o en otras palabras un conjunto dado de fermiones (tales como los electrones) no interactuantes en una caja. Podemos pensar en este sistema como uno de los *ingredientes* del juego, no relacionado aún por ninguna interacción. Es un punto de partida conveniente, ya que el presente trabajo versa precisamente sobre algunas de las situaciones donde un modelo casi igual de simple, el Líquido de Fermi, deja de ser válido para describir a un sistema electrónico.

El Líquido de Fermi

Uno esperaría que este modelo de Gas de Fermi no interactuante fuera bastante inútil en sistemas electrónicos del mundo real, ya que sabemos que una de las propiedades esenciales de los electrones es que interaccionan con cualquier otra partícula cargada a través de campos electromagnéticos. Y esta interacción es muy fuerte. En cualquier instante un electron típico de la banda de conducción del oro sufre una aceleración veinte órdenes de magnitud mayor que la de la gravedad terrestre debido a sus interacciones electromagnéticas con los electrones vecinos. Incluso si se le pudiese seguir la pista como si fuese una partícula clásica distinguible su trayectoria sería muy distinta de la de un electron no interactuante en vuelo libre. Sin embargo su naturaleza fermiónica is responsable de un resultado muy llamativo aplicable a muchos sistemas electrónicos realistas en ausencia de desorden fuerte y de densidades razonablemente altas: un electron extra inyectado en un metal a baja temperatura, si es considerado junto con la nube de carga positiva de fondo que excita en torno a sí debito a la repulsión electrón-electrón, puede cuantizarse y resulta ser una entidad casi no interactuante perfectamente análoga a un electrón libre[1]. Se la conoce como cuasipartícula. Esta es desde luego una forma de hablar un tanto imprecisa para un lector de orientación matemática, pero el hecho preciso es que expresado en cierta base de estados (ya no de partículas individuales, sino de superposiciones de muchas, la cuasipartícula), el Hamiltoniano de un sistema electrónico realista a menudo se asemeja (al menos en lo relativo al espectro de excitaciones de energía asintóticamente pequeñas) aquel del Gas de Fermi a pesar de las fuertes interacciones electrónicas, aunque con un valor distinto de la masa de las nuevas partículas tal y como aparece en su relación de dispersión conocida como masa efectiva m^*. Esa 'trivialidad de las interacciones' resulta estar estrechamente relacionada con la estadística fermiónica de los electrones, y con el hecho de que estos forman un 'mar de Fermi' con el fin de satisfacer el principio de exclusión de Pauli. Para las excitaciones de energía finita E sin embargo, sus interacciones mutuas efectivas crecen como E^2 dentro de la teoría del Líquido de Fermi.

Esta es la vase de lo que se conoce como teoría del Líquido de Fermi para metales, que fue concebida por la genial intuición del físico ruso y premio Nobel Lev Davidovich Landau en los años cincuenta [61]. Una derivación muy elegante de su teoría y de sus correcciones dominantes puede realizarse mediante técnicas del Grupo de Renormalización, véase por ejemplo [88].

Este trabajo de tesis trata sobre algunos de los casos más relevantes donde el paradigma del Líquido de Fermi falla, y las interacciones aparecen como un ingrediente esencial de la mecánica del sistema. Procederemos ahora a dar un resumen rápido de algunos de los mecanismo responsables de que dicha teoría deje de ser válida.

Apantallamiento

Desde un punto de vista microscópico una explicación intuitiva del carácter irrelevante de las interacciones electrón-electrón en metales es el mecanismo del 'apantallamiento', que subyace a la teoría del Liquido de Fermi. Se dice que la nube electrónica que men-

[1] 'Casi' significa aquí que conserva una fuerza de interacción entre dos tales entidades que desaparece al reducir a cero sus escalas de energías típicas.

cionamos más arriba que 'viste' al electrón desnudo inyectado en el metal apantalla el potencial electrostático que el electrón crea mediante una disminución de la densidad electrónica circundante. Si uno calcula, dentro de ciertas aproximaciones, el potencial que siente cualquier otro electrón inducido por el nuevo electrón una vez apantallado, resulta ser de la forma $V(r) \sim e^{-r/\xi}/r$ en lugar de $V(r) \sim 1/r$, de forma que queda suprimido a distancias mayores que cierta distancia de apantallamiento ξ.

De manera que, ¿por qué no son las interacciones totalmente irrelevantes en la práctica? Bueno, este apantallamiento sólo es efectivo en condiciones apropiadas. Por ejemplo, el apantallamiento sólo sería eficiente si la energía típica de interacción es más pequeña que la energía cinética típica, de manera que los electrones permanezcan móviles a pesar de las interacciones. De otro modo los electrones quedarían localizados en posiciones fijas (cristalización de Wigner), lo cual es de hecho una predicción para sistemas con una densidad electrónica extremadamente baja y en ausencia de una modulación de carga de fondo apreciable (véase más abajo). Otro requisito es que el sistema debe ser lo suficientemente grande para que la relajación de los electrones del sistema causada por el nuevo electrón inyectado es más o menos completa. Si el sistema es pequeño la relajación de sus electrones por la presencia del nuevo no es completa debido a las restricciones cinemáticas impuestas por las fronteras, que impiden el apantallamiento total del potencial electrostático. Por tanto la presencia de fronteras o la baja dimensionalidad pueden hacer de las interacciones un ingrediente muy relevante en la física de un sistema, incluso (¡especialmente!) a bajas energías.

Sistemas de cero dimensiones

Un caso típico de este efecto de frontera es una pequeña isla metálica o un punto cuántico. Una isla metálica es básicamente una gotita de metal, quizás acoplada electrostáticamente a un electrodo de puerta, y conectada mediante uniones túnel de óxido a un metal masivo. Un punto cuántico es generalmente una pequeña región en un gas electrónico bidimensional (2DEG) donde los electrones se confinan mediante electrodos litografiados encima de la heterounion, y que pueden hacer túnel desde y hacia el 2DEG a través de barreras sintonizables. Otras realizaciones equivalentes son también posibles.

Ambos sistemas se clasifican como 'cero-dimensionales' en contraste con los hilos, láminas o sistemas masivos, y cada uno tiene características específicas que les hacen especialmente adecuados para estudiar diferentes efectos de las interacciones. En una primera aproximación ambos pueden verse como una pequeña región espacial, conectada (o no) de alguna manera a un metal masivo, y donde los electrones quedan confinados por ciertas fronteras. La energía electrostática asociada a la adición de un electrón en dicha región es mayor cuanto menor es el tamaño de la misma. Esto no es sino el concepto de capacidad C. Un trozo de metal pequeño tiene menor capacidad, de forma que un pequeño incremento de la carga genera una gran variación de la energía potencial electrostática. Como consecuencia se requiere una energía de carga finita $E_C = e^2/(2C)$ para añadir la mínima cantidad posible de carga e, un sólo electrón [2], que puede rondar en torno a los $10 - 100mK$ para

[2]Existe una importante suposición que se esconde en la simplicación de suponer que C es una constante independiente del número total de electrones del sistema, aunque es suficientemente buena en todos salvo los regímenes más extremos, y continuaremos usando esta simplificación en el resto de esta memoria.

$C \lesssim 10^{-15}F$, que en puntos cuánticos 2D supone tamaños del orden de los $100nm$. Tal proeza técnica de microfabricación empezó a ser posible a principios de los noventa [36, 51]. Para los granos metálicos tridimensionales el tamaño necesario es un orden de magnitud menor, pero también esto fue logrado a mediados de los noventa [81]. En sistemas mayores la temperatura requerida para que estos efectos de la discretitud de la carga no queden enmascarados por efectos térmicos se escapan más allá de las posibilidades experimentales actuales, de manera que los electrones que atraviesan el sistema pueden considerarse (una vez apantallados) como cuasipartículas libres a todos los efectos prácticos sin más complicaciones mientras que el resto de los requisitos del Líquido de Fermi se satisfagan.

Sistemas unidimensionales

Otro caso típico de apantallamiento ineficiente y constitución de cuasipartículas es el del sistema electrónico unidimensional. El problema en este caso es que el concepto mismo de cuasipartícula deja de tener sentido en un sistema puramente unidimensional, ya que dos cuasipartículas nunca podrían evitar una colisión y por tanto aparentar ser no interactuante. El espacio de fases disponible para el evento de dispersión resulta ser demasiado pequeño en una dimensión. Intuitivamente, dos cuasipartículas que se propaguen en sentidos opuestos siempre chocarían frontalmente con probabilidad 100% y las nubes electrónicas se invadirían mutuamente, y por tanto interactuando directamente como electrones libres a distancias cortas, aún teniendo en cuenta su naturaleza cuántica. Más aún, puede argumentarse que puesto que el potencial electrostático desnudo en una dimensión es lineal con la distancia no puede haber un apantallamiento completo por mucho que los otros electrones reajusten sus estados. La dinámica de baja energía es por tanto muy distinta de la del Gas de Fermi. Se conoce más bien como el Líquido de Luttinger.

Otros escenarios comunes no descritos por la teoría del Líquido de Fermi.

Las suposiciones básicas de la teoría del Líquido de Fermi para sistemas metálicos son las siguientes

- Existe una correspondencia biunívoca entre excitaciones con y sin interacciones.
- El sistema no sufre ninguna transición de fase si conectásemos adiabáticamente las interacciones (no hay 'cruce de niveles').
- El estado fundamental es no degenerado.

Tanto el sistema electrónico en cero y una dimensiones incumple la primera suposición, pero hay otros sistemas muy comunes que no se comportan como un Líquido de Fermi por otras razones. Damos una lista sin pretensiones de completitud de algunas de estas situaciones, como resumen de contexto

- **Sistemas en cero y una dimensiones.**

  Como ya hemos explicado, estos dos tipos de sistemas tienen un espectro de excitaciones que no fluye de manera continua a partir de las excitaciones del sistema sin interacciones. En su lugar hay que emplear una familia de numeros cuánticos distinta para clasificar las excitaciones.

- **Sistemas desordenados.**

  La teoría de Localización de Anderson nos muestra cómo una cierta cantidad de desorden (tal como las dislocaciones de la red cristalina u otros defectos) en un sistema tridimensional inicialmente metálico pueden conducirlo a un estado aislante incluso en ausencia de interacciones. Los autoestados inicialmente extendidos de las partículas o cuasipartículas (como los de las bandas de conducción) se localizan debido a la competición entre la energía cinética y la diferencia de energía entre sitios diferentes. En dos dimensiones un sistema no interactuante se vuelve aislante con una densidad de defectos arbitrariamente baja [1]. La cuestión de los defectos con interacciones en 2D sigue siendo una problema abierto. En tres dimensiones la situación se vuelve bastante complicada en la medida en que ciertas porciones de una banda (separadas por ciertos 'bordes de movilidad') se localizan mientras que el resto no lo hacen, pero existe una teoría satisfactoria para este caso. En una dimensión incluso la corrección de localización débil a la conductancia (que introduce en general correcciones de alta temperatura con cualquier densidad de desorden) llevaría a una fase aislante mientras que la longitud de coherencia de las cuasipartículas exceda al tamaño del sistema.

  Aunque el desorden puede invalidar el Líquido de Fermi es un tipo de complicación fundamentalmente distinta de las interacciones. No involucra efectos de muchos cuerpos, es más bien una supresión del transporte coherente de partículas individuales, debido a la interferencia no constructiva de caminos extendidos en la muestra, cuya interferencia constructiva es el motivo mismo de la formación de las bandas de transporte en los sólidos. Cierta aleatoriedad en la red cristalina destruye esta formación de bandas coherentes, lo cual hace que las excitaciones de baja energía dejen de estar conectadas una a una con las del Gas de Fermi.

  En este trabajo meramente apuntaremos a las posibilidades de aplicar los formalismos desarrollados al problema del desorden en metales, ya que un análisis más profundo de estos problemas escaparía totalmente el ámbito de esta tesis.

- **Superconductividad**

  Puede demostrarse que cualquier tipo de interacción atractiva efectiva entre electrones, ya sea por intercambio retardado de fonones o a procesos colectivos más complicados, desestabilizan el estado fundamental de un Líquido de Fermi, y conducen a una ruptura espontanea de la simetría gauge local que posee inicialmente tal teoría. Esto no es sino una transición de fase superconductora. En sistemas de tamaño finito el estado fundamental sufre un cruce de niveles con las primeras excitaciones, más allá del cual la continuidad biunívoca respecto del Gas de Fermi queda rota. Se desarrolla un gap y surgen nuevas propiedades físicas. En cualquier caso, al menos en superconductores BCS, se puede recuperar una situación análoga al del Líquido de Fermi en cierta base un tanto exótica de 'Bogolones', o 'cuasipartículas BCS', aunque con una relación de dispersion distinta (con gap).

  Muchas de las técnicas presentadas en este trabajo tienen su origen en la teoría microscópica de uniones Josephson (uniones débiles entre superconductores), y por tanto son muy apropiadas para incluir superconductores BCS en el análisis. Trataremos de esto en el capítulo 4.

- **Transición metal-aislante de Mott-Hubbard**

  Otro escenario muy corriente para la no aplicabilidad del paradigma del Líquido de Fermi es la transición metal-aislante de Mott-Hubbard. Es una transición predicha pen particular para el modelo de Hubbard, que se diseño como un modelo extremadamente simplificado para los metales reales que preservara efectos no triviales de muchos cuerpos. Esencialmente sustituye la tremenda variedad de orbitales electrónicas en un átomo de un metal real por un solo orbital, capaz de albergar hasta dos electrones con spin opuesto. El Hamiltoniano está compuesto de una interacción de hopping entre átomos vecinos, más una interacción intra-atómica que penaliza ocupaciones distintas de cierto promedio fijo N_0[3]. La formulación general toma la forma

  $$H = E_C \sum_i (n_i - N_0)^2 + t \sum_i c_i^+ c_{i+1} + H.c \tag{J.1}$$

  donde $n_i = c_i^+ c_i$.

  Como veremos en más detalle en el capítulo 5, este modelo tiene una fase de tipo Líquido de Fermi para valores suficientemente pequeños de E_C/t. Recuérdese que en el límite del continuo t toma el significado de una energía cinética típica. E_C representa las interacciones de Coulomb entre electrones, incluida solamente dentro del mismo átomo por simplicidad (otras generalizaciones también han sido analizadas, tales como el model de Hubbard extendido [9, 27, 92]). Si la temperatura normalizada $K_B T/E_C$ cae por debajo de cierto valor, aparece una frontera crítica en ciertos valores de E_C/t que separa una fase tipo Líquido de Fermi de otra aislante, en la cual el concepto de cuasipartícula coherente deja de tener sentido. Esta transición de fase, que de acuerdo con nuestros resultados resulta ser de primer orden, tiene mucho sentido físico, ya que meramente pone de manifiesto el hecho de que hace falta una cierta cantidad mínima de energía cinética para que el estado de la cuasipartícula adquiera un carácter extendido propio del estado conductor, ya que la repulsión Coulomb intra-atómica debe ser superada para permitir las fluctuaciones locales de carga que implica un estado extendido. Si t es es demasiado pequeña, los electrones permanecerán en estados localizados en torno a cierto átomo, dando lugar a una fase aislante (que requiere un voltaje finito para provocar una corriente finita). Para temperaturas suficientemente altas esta transición de fase se convierte en una transición suave (crossover). Esta transición de fase es el mecanismo fundamental que explica las características principales de diversos materiales de electrones correlacionados tales como los Vanadatos $(V_{1-x}Cr_x)_2O_3$ [66–68] o los compuestos orgánicos quasi-bidimensionales de la familia $\kappa - BEDT$ [52, 55].

- **Cristalización de Wigner**

  La cristalización de Wigner es el análogo de la transición de fase del apartado anterior pero aplicado al modelo de electrones libres (en el sentido de que no existe una modulación de fondo favoreciendo ciertos puntos del espacio) interaccionando mutuamente mediante potenciales de Coulomb de largo alcance. También en este modelo,

[3] El valor de equilibrio N_0 es ajustable por potenciales externos.

cuando la densidad de electrones es suficientemente baja de forma que la energía cinética típica E_F no es capaz de superar la repulsión de Coulomb, los conceptos de apantallamiento y cuasipartícula pierden validez, dando paso a una fase peculiar en la que los electrones permanecen localizados como en un cristal [97] en un patrón triangular (en 2D). La densidad a la cual se predice que se produzca esta transición es extremadamente baja, y es tal que la distancia media entre electrones es del orden de unos 40 radios de Bohr $a_0 \approx 0.53$Å), lo cual está hasta donde tengo noticia aún bastante lejos de la tecnología actual en sistemas electrónicos. Ciertas observaciones en la superficie del Helio líquido hace un par de décadas sí apuntaron a una posible medida directa de esta fase [79].

Aunque este tema es tremendamente interesante en sí mismo y está directamente relacionado con los efectos no triviales de las interacciones en hipotéticos sistemas metálicos, no ahondaremos en este tema en el resto de este trabajo.

- **Interacciones de intercambio y el Efecto Kondo**

  No hemos mencionado aún el tema de las propiedades magnéticas del Líquido de Fermi. En ausencia de interacciones y en el caso de un número par de electrones, el estado fundamental de un sistema electrónico es un singlete, ya que cada estado queda ocupado por un singlete de dos electrones. Este resultado también se aplica al Líquido de Fermi por el argumento de continuidad. Sin embargo cuando las interacciones empiezan a dominar surge toda una nueva gama de posibilidades en las propiedades magnéticas. En cualquier caso el mecanismo dominante responsable de un estado fundamental magnético no es las interacciones dipolares magnéticas entre electrones o las interacciones spin-órbita [11]. Resulta que las interacciones de Coulomb añadidas a la estadística fermiónica son suficientes para generar efectos magnéticos no triviales como el orden magnético. Este mecanismo se conoce por el nombre genérico de interacciones de intercambio (o sus variaciones como superintercambio) y es lo que hay detrás de las reglas de Hund, según las cuales la repulsión electrónica tiende a maximizar el spin total, el momento orbital y el momento total en una configuración de electrones dada. ¿Por qué hace esto la repulsión Coulomb? Dos electrones en general tenderán a disminuir esta energía de Coulomb minimizando el solape de sus funciones de onda, en particular haciendo que el valor esperado $\Psi(\mathbf{r_1} \approx \mathbf{r_2})$ sea mínimo. La estadística fermiónica por su lado requiere que la función de onda total sea antisimétrica. Esto implica que la mínima energía se logrará en una configuración triplete (spines paralelos), ya que un triplete es simétrico en el sector de spin, y por tanto la función de onda espacial Ψ será asimétrica, con un solape mutuo mucho menor que en la configuración espacialmente simétrica (singlete de spin). En resumen, las interacciones repulsivas empujan al sistema hacia un estado fundamental ferromagnético, mientras que las atractivas lo empujan hacia un estado de spin total cero. Estos razonamientos se mantienen en el caso de muchos electrones, y las propiedades magnéticas resultantes no se pueden describir de manera natural dentro de la teoría del Líquido de Fermi estándar.

  Un caso especialmente célebre de efectos de intercambio no triviales se conoce como el problema de Kondo. Discutiremos extensamente este efecto en el transcurso de este

trabajo, de manera que por ahora baste notar que la física de Kondo debida a una concentración finita de impurezas magnéticas en un metal, junto con la "suposición multicanal" (por la cual un cierto número cuántico aparte del spin - por ejemplo el momento angular en la dirección $\hat{z}$ - se conserva en el proceso de dispersión electrónica contra las impurezas) es suficiente para garantizar rigurosamente que el estado fundamental del sistema ya no será un Líquido de Fermi, y fuertes correlaciones sobrevivirán entre electrones debido a las interacciónes residuales de intercambio.

J.2 Conclusiones al capítulo 2

En este capítulo hemos dado una presentación detallada de la descripción mediante un rotor cuántico de los efectos de carga en nanoestructuras. Puede resumirse como el estudio de la dinámica efectiva de la carga total del sistema, o alternativamente de su conjugado, la fase. Dentro de la aproximación de N grande, válida en general para granos metálicos con contactos anchos de muchos canales, se puede derivar una acción efectiva que gobierna la fase del sistema sin recurrir a los detalles de las excitaciones fermiónicas. Como resultado interesante, la acción obtenida se asemeja estrechamente a la de los sistemas cuánticos abiertos con disipación [24, 62]. A diferencia de de los sistemas superconductores sin embargo la simetría gauge no está rota, aunque las fluctuaciones de fase codificadas en el propagador $\mathcal{G}_{\Delta\tau}$ siguen siendo una gran fuente de información física, y pueden emplearse para derivar todas los propagadores físicos dentro del límite de N grande. Hemos mostrado de qué manera esto constituye un marco sencillo y potente para el estudio de la renormalización de la física del bloqueo de Coulomb en granos metálicos fuertemente acoplados a su entorno. Sin embargo esto se logra mediante el límite de N grande, lo cual deja fuera toda contribución de procesos cuánticos a órdenes superiores al cotunneling en el hopping. Por tanto, aunque se recupera la renormalización correcta del gap de Coulomb y la conductancia lineal de baja temperatura, se pierden otros fenómenos más fuertemente no perturbativos relevantes en sistemas de pocos niveles, como la formación de resonancias Kondo.

También hemos discutido un método aproximado que es útil para calcular las fluctuaciones de esta fase, el método del límite esférico. Hemos mostrado que es suficiente para recuperar al menos cualitativamente todas las propiedades del bloqueo de Coulomb, incluida la renormalización de la energía de carga con acoplos fuertes al entorno, la conductancia, y la densidad de estados electrónica. Este método no se restringe a la aproximación de N grande que nos condujo a la descripción del rotor cuántico, y será empleado fructíferamente en los siguientes capítulos más allá de esta aproximación.

J.3 Conclusiones al capítulo 3

Hemos demostrado cómo la aproximación del límite esférico aplicado a las ecuaciones NCA de campos fermionicos más un rotor esclavo auxiliar proporcionan un marco potente aunque técnicamente sencillo para explorar las propiedades de transporte de nanoestructuras con interacciones. Para ello hemos empleado un formalismo para sistemas en equilibrio térmico. Aún así la técnica no se limita en absoluto a situaciones de equilibrio, y

podría ser empleada dentro de técnicas de Keldysh. Otra línea interesante de desarrollo hacia resultados cuantitativamente más precisos consistiría en la adición de contribuciones de los puntos silla instantónicos antes de pasar al límite esférico, como se sugirió en el capítulo anterior. Más aún, de esta manera el análisis del comportamiento con potenciales de puerta fuera del punto de simetría podría realizarse fácilmente.

Las posibilidades descritas en este capítulo en torno al efecto Kondo de un nivel y multinivel podría resultar interesantes tanto desde un punto de vista fundamental como tecnológico. En particular por ejemplo el hecho de que la estructura de niveles sin interacción se reproduce en forma de estrechos satélites alrededor de la resonancia Kondo principal, replicando todas las posiciones de niveles pero con un perfil mucho más estrecho $\sim T_K$ podría resultar ser una herramienta espectroscópica para discernir una densidad espectral que de otra forma aparecería completamente emborronada por el acoplo finito del sistema con su entorno, ya que típicamente $T_K \ll \Gamma$. Otras posibilidades incluyen el uso con fines experimentales del las características de este efecto Kondo complejo, tales como el carácter abrupto y la extrema sensibilidad ante la temperatura de la conductancia representada en la Fig. 3.10. Hipotéticas válvulas o diodos dependientes de la temperatura o componentes de transporte muy no lineales podrían quizás hacer uso de estas peculiaridades de diversas maneras.

J.4 Conclusiones al capítulo 4

En este capítulo hemos extendido el concepto del campo esclavo para incluir la dinámica del spin total en forma análoga a la de la carga total que tratan los campos esclavos habituales. Las complicaciones de las reglas de composicion de spines quedan limpiamente resueltas mediante la construcción de dicho campo auxiliar dentro del grupo $SU(2)$. Una modificación muy simple de la descripción en términos únicamente de la fase de granos metálicos y superconductores es suficiente para incluir la gran susceptibilidad paramagnética de spin de estos últimos sistemas. En concreto basta con generalizar la forma del término de acoplo disipativo. La nueva formulación, aunque no es accesible a un tratamiento sencillo del tipo límite esférico o desacoplos NCA de la carga y el spin, sigue siendo tratable mediante simulaciones Monte Carlo cuánticas. Hemos mostrado cómo el mencionado gap de spin suprime exponencialmente la energía de carga renormalizada en un grano superconductor, la manera en que el cotunneling sobrevive al gap de spin siempre que el gap BCS sea despreciable respecto de E_C, J, y cómo se espera que responda el sistema a campos externos electrostáticos o magnéticos. Sugerimos una ruta análoga a la ejemplificada aquí apta para tratar diamagnetismo de spin propio de los metales normales, lo cual podría probablemente conducir a una interesante descripción de las transiciones ferromagnéticas que sea formalmente análoga a las transiciones superconductoras. Esta idea queda abierta como una posibilidad para trabajo futuro.

J.5 Conclusiones al capítulo 5

Empleando las técnicas de rotores esclavos en límite esférico hemos localizado y caracterizado las diferentes regiones y fronteras en el diagrama de fases de un sistema gran-

ular donde cada grano posee una banda centrada en la energía de Fermi de anchura W. Nos hemos encontrado con que este tipo de sistema hereda de alguna manera las características correspondientes de los granos individuales, aunque cualitativamente transformadas por el requisito de autoconsistencia del campo medio dinámico (DMFT). Hemos localizado la conexión de un régimen metálico para W pequeña con el efecto Kondo de granos aislados. La transición suave a una fase aislante para valores mayores de W se ha relacionado con la transición inversa de Kondo a bloqueo de Coulomb descrita en el capítulo 3. Se ha calculado la frontera entre ambas fases. Por otro lado hemos demostrado que la transición de Mott hacia la región aislante de E_C grande, que se relaciona con el bloqueo de Coulomb en el caso de granos individuales, ocurre a través de una transición de primer orden atravesando una pequeña zona de biestabilidad. Calculamos los dos valores críticos de E_C de la transición, con un acuerdo razonable con trabajos anteriores.

El método empleado podría naturalmente usarse para analizar escenarios más complejos como sistemas sin simetría partícula-agujero, o redes de puntos cuánticos con espectro discreto, en el que es de esperar que el efecto Kondo en dos etapas descrito en el capítulo 3 ofrezca posibilidades interesantes. La inclusión de desorden en el método sigue constituyendo un desafío que podría tener interés para futuros trabajos, por ejemplo mediante el empleo de tácticas en la línea de [28]. También la implementación de mejoras en el método DMFT, como en [54] podrían ayudarnos para avanzar en cuestiones sutiles como el verdadero orden de la transición de Mott o la existencia de una región biestable en sistemas realmente tridimensionales. En su versión actual sin embargo el formalismo presentado ha demostrado ser una herramienta lo suficientemente simple y potente para arrojar luz sobre las características principales de estos sistemas. Trabajos muy recientes han avanzado en otras facetas del problema de la transición de Mott con estas mismas técnicas.

Bibliography

[1] E. Abrahams, P. W. Anderson, D. C. Licciardello, and T. V. Ramakrishnan. Scaling theory of localization - absence of quantum diffusion in 2 dimensions. *Phys. Rev. Lett.*, 42(10):673–676, 1979.

[2] O. Agam, B. L. Altshuler, and A. V. Andreev. Spectral statistics - from disordered to chaotic systems. *Phys. Rev. Lett.*, 75(24):4389–4392, 1995.

[3] R. Aguado and D. C. Langreth. Kondo effect in coupled quantum dots: A noncrossing approximation study. *Phys. Rev. B*, 67(24), 2003.

[4] Brouwer P. W. Aleiner I. L. and Glazman L. I. Quantum effects in coulomb blockade. *Phys. Rep.*, 358(5-6):309–440, 2002.

[5] S.L. Altmann, editor. *Rotations, Quaternions, and Double Groups.* Clarendon Press, Oxford, 1986.

[6] B. L. Altshuler, Y. Gefen, A. Kamenev, and L. S. Levitov. Quasiparticle lifetime in a finite system: A nonperturbative approach. *Phys. Rev. Lett.*, 78(14):2803–2806, 1997.

[7] V. Ambegaokar, U. Eckern, and G. Schön. Quantum dynamics of tunneling between superconductors. *Phys. Rev. Lett.*, 48(25):1745–1748, 1982.

[8] P. W. Anderson. Infrared catastrophe in fermi gases with local scattering potentials. *Phys. Rev. Lett.*, 18(24):1049, 1967.

[9] L. D. Anh, H. A. Tuan, and N. T. Thang. Charge ordering under a magnetic field in the extended hubbard model. *Modern Physics Letters B*, 17(20-21):1103–1110, 2003.

[10] D. P. Arovas, F. Guinea, C. P. Herrero, and P. San-Jose. Granular systems in the coulomb blockade regime. *Phys. Rev. B*, 68:085306, 2003.

[11] N. W. Ashcroft and N. D. Mermin, editors. *Solid State Physics.* Harcourt College Publishers, 1976.

[12] A.L. Baker, editor. *Quaternions as the Result of Algebraic Operations.* Van Nostrand, New York, 1911.

[13] H. U. Baranger and P. A. Mello. Mesoscopic transport through chaotic cavities - a random s-matrix theory approach. *Phys. Rev. Lett.*, 73(1):142–145, 1994.

[14] E. Bascones, C. P. Herrero, F. Guinea, and G. Schön. Nonequilibrium effects in transport through quantum dots. *Phys. Rev. B*, 61(24):16778–16786, 2000.

[15] G. Baym and Kadanoff.Lp. Conservation laws and correlation functions. *Physical Review*, 124(2):287, 1961.

[16] A. A. Belavin and A. M. Polyakov. Quantum fluctuations of pseudoparticles. *Nuclear Physics B*, 123(3):429–444, 1977.

[17] E. Ben-Jacob, E. Mottola, and G. Schön. Quantum shot noise in tunnel junctions. *Phys. Rev. Lett.*, 51:2064, 1983.

[18] N. E. Bickers. Review of techniques in the large-n expansion for dilute magnetic-alloys. *Rev. Mod. Phys.*, 59(4):845–939, 1987.

[19] C. T. Black, D. C. Ralph, and M. Tinkham. Spectroscopy of the superconducting gap in individual nanometer-scale aluminum particles. *Phys. Rev. Lett.*, 76(4):688–691, 1996.

[20] Y. M. Blanter. Electron-electron scattering rate in disordered mesoscopic systems. *Phys. Rev. B*, 54(18):12807–12819, 1996.

[21] Y. M. Blanter and A. D. Mirlin. Correlations of eigenfunctions in disordered systems. *Physical Review E*, 55(6):6514–6518, 1997.

[22] Y. M. Blanter, A. D. Mirlin, and B. A. Muzykantskii. Fluctuations of conductance peak spacings in the coulomb blockade regime: Role of electron-electron interaction. *Phys. Rev. Lett.*, 78(12):2449–2452, 1997.

[23] R. Brown and E. Simanek. Transition to ohmic conduction in ultrasmall tunnel-junctions. *Phys. Rev. B*, 34(4):2957–2959, 1986.

[24] A. O. Caldeira and A. J. Leggett. Influence of dissipation on quantum tunneling in macroscopic systems. *Phys. Rev. Lett.*, 46(4):211–214, 1981.

[25] R. Chitra and G. Kotliar. Dynamical mean field theory of the antiferromagnetic metal to antiferromagnetic insulator transition. *Phys. Rev. Lett.*, 83(12):2386–2389, 1999.

[26] P. Coleman. New approach to the mixed-valence problem. *Phys. Rev. B*, 29(6):3035–3044, 1984.

[27] G. H. Ding, F. Ye, and B. W. Xu. Charge gap in one-dimensional extended hubbard model. *Communications in Theoretical Physics*, 39(1):105–108, 2003.

[28] M. Fabrizio and C. Castellani. Anderson localization in bipartite lattices. *Nuclear Physics B*, 583(3):542–583, 2000.

[29] S. Florens and A. Georges. Quantum impurity solvers using a slave rotor representation. *Phys. Rev. B*, 66(16), 2002.

[30] S. Florens and A. Georges. Slave-rotor mean-field theories of strongly correlated systems and the mott transition in finite dimensions. *Phys. Rev. B*, 70(3), 2004.

[31] S. Florens, P. San-Jose, F. Guinea, and A. Georges. Coherence and coulomb blockade in single-electron devices: A unified treatment of interaction effects. *Phys. Rev. B*, 68(24), 2003.

[32] A. Furusaki and K. A. Matveev. Theory of strong inelastic cotunneling. *Phys. Rev. B*, 52(23):16676–16695, 1995.

[33] A. Georges and G. Kotliar. Hubbard-model in infinite dimensions. *Phys. Rev. B*, 45(12):6479–6483, 1992.

[34] A. Georges, G. Kotliar, W. Krauth, and M. J. Rozenberg. Dynamical mean-field theory of strongly correlated fermion systems and the limit of infinite dimensions. *Rev. Mod. Phys.*, 68(1):13–125, 1996.

[35] D. Giuliano, B. Jouault, and A. Tagliacozzo. Kondo ground state in a quantum dot with an even number of electrons in a magnetic field. *Physical Review B*, 63(12):art. no.–125318, 2001.

[36] V. J. Goldman, B. Su, and J. E. Cunningham. Single-electron tunneling in double-barrier nanostructures. *Int. Nat. J. Mod. Phys. B*, 6(13):2321–2343, 1992.

[37] D. S. Golubev and A. D. Zaikin. Coulomb blockade and insulator-to-metal quantum phase transition. *Europhys. Lett.*, 60(1):113–119, 2002.

[38] G. Goppert and H. Grabert. Single electron tunneling at large conductance: The semiclassical approach. *European Physical Journal B*, 16(4):687–704, 2000.

[39] H. Grabert and M. H. Devoret, editors. *Single Electron Tunneling.* Plenum, New York, 1992.

[40] T. Grenet. Symmetrical field effect and slow electron relaxation in granular aluminium. *European Physical Journal B*, 32(3):275–278, 2003.

[41] N. Grewe and H. Keiter. Diagrammatic approach to the intermediate-valence compounds. *Phys. Rev. B*, 24(8):4420–4444, 1981.

[42] R. B. Griffiths. Correlations in ising ferromagnets. *J. Math. Phys.*, 8:478, 1967.

[43] F. Guinea and G. Schön. *J. Low Temp. Phys.*, 69:219, 1986.

[44] L. Gurevich, L. Canali, and L. P. Kouwenhoven. Scanning gate spectroscopy on nanoclusters. *App. Phys. Lett.*, 76(3):384–386, 2000.

[45] K. Haule, S. Kirchner, J. Kroha, and P. Wolfle. Anderson impurity model at finite coulomb interaction u: Generalized noncrossing approximation. *Phys. Rev. B*, 6415(15), 2001.

[46] J. S. Helman and B. Abeles. Tunneling of spin-polarized electrons and magnetoresistance in granular ni films. *Phys. Rev. Lett.*, 37(21):1429–1432, 1976.

[47] C. P. Herrero, G. Schön, and A. D. Zaikin. Strong charge fluctuations in the single-electron box: A quantum monte carlo analysis. *Phys. Rev. B*, 59:5728, 1999.

[48] A.C. Hewson. *The Kondo Problem to Heavy Fermions*. Cambridge University Press, 1997.

[49] T. Inoshita, A. Shimizu, Y. Kuramoto, and H. Sakaki. Correlated electron-transport through a quantum-dot - the multiple-level effect. *Phys. Rev. B*, 48(19):14725–14728, 1993.

[50] R. A. Jalabert, J. L. Pichard, and C. W. J. Beenakker. Universal quantum signatures of chaos in ballistic transport. *Europhys. Lett.*, 27(4):255–260, 1994.

[51] A. T. Johnson, L. P. Kouwenhoven, W. Dejong, N. C. Vandervaart, Cjpm Harmans, and C. T. Foxon. Zero-dimensional states and single electron charging in quantum dots. *Phys. Rev. Lett.*, 69(10):1592–1595, 1992.

[52] K. Kanoda. Electron correlation, metal-insulator transition and superconductivity in quasi-2d organic systems, (et)(2)x. *Physica C*, 282:299–302, 1997.

[53] H. Keiter and J. C. Kimball. Diagrammatic approach to anderson model for dilute alloys. *Journal of Applied Physics*, 42(4):1460, 1971.

[54] H. Keiter and D. Otto. Generalizations of dynamical mean field theory by the lace expansion. *Journal of Magnetism and Magnetic Materials*, 226:63–65, 2001.

[55] H. Kobayashi, H. Tomita, T. Naito, A. Kobayashi, F. Sakai, T. Watanabe, and P. Cassoux. New bets conductors with magnetic anions (bets equivalent to bis(ethylenedithio)tetraselenafulvalene). *Journal of the American Chemical Society*, 118(2):368–377, 1996.

[56] J. Kondo. Resistance minimum in dilute magnetic alloys. *Progress of Theoretical Physics*, 32(1):37, 1964.

[57] J. Konig and H. Schoeller. Strong tunneling in the single-electron box. *Physical Review Letters*, 81(16):3511–3514, 1998.

[58] J. M. Kosterlitz. Phase-transitions in long-range ferromagnetic chains. *Phys. Rev. Lett.*, 37(23):1577–1580, 1976.

[59] I. L. Kurland, I. L. Aleiner, and B. L. Altshuler. Mesoscopic magnetization fluctuations for metallic grains close to the stoner instability. *Phys. Rev. B*, 62(22):14886, 2000.

[60] G. Lamura, J. C. Villegier, A. Gauzzi, J. Le Cochec, J. Y. Laval, B. Placais, N. Hadacek, and J. Bok. Granularity-induced gapless superconductivity in nbn films: Evidence of thermal phase fluctuations. *Phys. Rev. B*, 65(10), 2002.

[61] L. D. Landau. The theory of a fermi liquid. *Soviet Physics Jetp-Ussr*, 3(6):920–925, 1957.

[62] A. J. Leggett, S. Chakravarty, A. T. Dorsey, M. P. A. Fisher, A. Garg, and W. Zwerger. Dynamics of the dissipative 2-state system. *Rev. Mod. Phys.*, 59(1):1–85, 1987.

[63] Q. Li, K. E. Gray, A. Berger, and J. F. Mitchell. Electronically driven first-order metal-insulator transition in layered manganite la1.04sr1.96mn2o7 single crystals. *Phys. Rev. B*, 67(18), 2003.

[64] G. D. Mahan. Excitons in degenerate semiconductors. *Physical Review*, 153(3):882, 1967.

[65] T. E. Mason, G. Aeppli, S. M. Hayden, A. P. Ramirez, and H. A. Mook. Low-energy excitations in superconducting la1.86sr0.14cuo4. *Phys. Rev. Lett.*, 71(6):919–922, 1993.

[66] D. B. McWhan, A. Menth, W. F. Brinkman, and J. P. Remeika. Metal-insulator transitions in titanium doped v2o3. *Bulletin of the American Physical Society*, 16(3):425, 1971.

[67] D. B. McWhan, A. Menth, and J. P. Remeika. Metal-insulator transitions in zr and mg doped v2o3. *Bulletin of the American Physical Society*, 16(1):103, 1971.

[68] D. B. McWhan, J. P. Remeika, T. M. Rice, W. F. Brinkman, J. P. Maita, and A. Menth. Electronic specific heat of metallic ti-doped v2o3. *Phys. Rev. Lett.*, 27(14):941, 1971.

[69] Y. Meir and N. S. Wingreen. Landauer formula for the current through an interacting electron region. *Phys. Rev. Lett.*, 68(16):2512–2515, 1992.

[70] J. S. Meyer and B. D. Simons. Phase coherence phenomena in superconducting films. *Phys. Rev. B*, 65(14), 2002.

[71] G. Moeller, Q. M. Si, G. Kotliar, and M. Rozenberg. Critical-behavior near the mott transition in the hubbard-model. *Phys. Rev. Lett.*, 74(11):2082–2085, 1995.

[72] N. F. Mott. The basis of the electron theory of metals, with special reference to the transition metals. *Proceedings of the Physical Society of London Section A*, 62(355):416–422, 1949.

[73] N. F. Mott. Metal-insulator transition. *Rev. Mod. Phys.*, 40(4):677, 1968.

[74] B. Mühlschlegel, D. J. Scalapino, and R. Denton. Thermodynamic properties of small superconducting particles. *Phys. Rev. B*, 6(5):1767, 1972.

[75] E. Mullerhartmann. Self-consistent perturbation-theory of the anderson model - ground-state properties. *Zeit. Phys. B*, 57(4):281–287, 1984.

[76] G. Murthy, R. Shankar, D. Herman, and H. Mathur. Solvable regime of disorder and interactions in ballistic nanostructures: Consequences for coulomb blockade. *Phys. Rev. B*, 69(7), 2004.

[77] Y. Nambu. Quasi-particles and gauge invariance in the theory of superconductivity. *Physical Review*, 117(3):648–663, 1960.

[78] Y. V. Nazarov. Coulomb blockade without tunnel junctions. *Phys. Rev. Lett.*, 82(6):1245–1248, 1999.

[79] F. M. Peeters. Two-dimensional wigner crystal of electrons on a helium film - static and dynamic properties. *Phys. Rev. B*, 30(1):159–165, 1984.

[80] M. Pustilnik and L. Glazman. Kondo effect in quantum dots. *Journal of Physics-Condensed Matter*, 16(16):R513–R537, 2004.

[81] D. C. Ralph, C. T. Black, and M. Tinkham. Spectroscopic measurements of discrete electronic states in single metal particles. *Phys. Rev. Lett.*, 74(16):3241–3244, 1995.

[82] D. C. Ralph, C. T. Black, and M. Tinkham. Nano-particle transistors and energy-level spectroscopy in metals. *Superlattices and Microstructures*, 20(3):389–394, 1996.

[83] D. C. Ralph, C. T. Black, and M. Tinkham. Studies of electron energy levels in single metal particles. *Physica B*, 218(1-4):258–261, 1996.

[84] A. I. Rusinov. On theory of gapless superconductivity in alloys containing paramagnetic impurities. *Soviet Physics Jetp-Ussr*, 29(6):1101, 1969.

[85] P. San-Jose, C. P. Herrero, F. Guinea, and D. P. Arovas. Interplay between exchange interactions and charging effects in metallic grains. *cond-mat/0401557, to apear in PRB*, 2004.

[86] J. Schlipf, M. Jarrell, P. G. J. van Dongen, M. Blumer, S. Kehrein, T. Pruschke, and D. Vollhardt. Absence of hysteresis at the mott-hubbard metal-insulator transition in infinite dimensions. *Phys. Rev. Lett.*, 82(24):4890–4893, 1999.

[87] G. Schön and A. D. Zaikin. *Phys. Rep.*, 198:238, 1990.

[88] R. Shankar. Renormalization-group approach to interacting fermions. *Rev. Mod. Phys.*, 66(1):129–192, 1994.

[89] P. G. Silvestrov and Y. Imry. Towards an explanation of the mesoscopic double-slit experiment: A new model for charging of a quantum dot. *Phys. Rev. Lett.*, 85(12):2565–2568, 2000.

[90] P. G. Silvestrov and Y. Imry. Spin effects and transport in quantum dots with overlapping resonances. *Phys. Rev. B*, 65(3), 2002.

[91] E. C. Stoner. *Proc. R. Soc. London*, 169:339, 1939.

[92] M. Tsuchiizu and A. Furusaki. Ground-state phase diagram of the one-dimensional half-filled extended hubbard model. *Phys. Rev. B*, 69(3), 2004.

[93] M. Ueda and F. Guinea. Conductance anomalies of small tunnel-junctions inside the coulomb gap. *Zeit. Phys. B*, 85(3):413–419, 1991.

[94] W. G. van der Wiel, S. De Franceschi, T. Fujisawa, J. M. Elzerman, S. Tarucha, and L. P. Kouwenhoven. The kondo effect in the unitary limit. *Science*, 289(5487):2105–2108, 2000.

[95] J. von Delft and D. C. Ralph. Spectroscopy of discrete energy levels in ultrasmall metallic grains. *Phys. Rep.*, 345(2-3):62–173, 2001.

[96] X. H. Wang and H. Grabert. Coulomb charging at large conduction. *Phys. Rev. B*, 53(19):12621–12624, 1996.

[97] E.P. Wigner. *T. Faraday Soc.*, 34:678, 1938.

[98] K. G. Wilson. Renormalization group - critical phenomena and kondo problem. *Rev. Mod. Phys.*, 47(4):773–840, 1975.

[99] K. Yamada, K. Yosida, and K. Hanzawa. Comments on the dense kondo state. *Prog. of Theor. Phys.*, 71(3):450–457, 1984.

[100] I. Yang, E. Lange, and G. Kotliar. Impact of magnetic frustration on the mott transition within a slave-boson mean-field theory. *Phys. Rev. B*, 61(4):2521–2524, 2000.